UMCEE 99-13 January 2000

DEVELOPMENT OF A GUIDE FOR EVALUATION OF EXISTING BRIDGES PHASE 2

PROJECT 98-1219 DIR

Final Report submitted to the Michigan Department of Transportation

Andrzej S. Nowak, Ahmet Sanli, and Junsik Eom

Department of Civil and Environmental Engineering
University of Michigan
Ann Arbor, Michigan 48109-2125

Testing and Research Section
Construction and Technology Division
Research Project No. RC -1378

DISCLAIMER

The contents of this report reflect the views of the authors, who are responsible for the facts and the accuracy of the information presented herein. This document is disseminated under the sponsorship of the Michigan Department of Transportation and Great Lakes Center for Truck and Transit Research at the University of Michigan Transportation Research Institute, in the interest of information exchange. The Michigan Department of Transportation assumes no liability for the contents or use thereof.

Executive Summary

The test program documented in this report covered simply supported, steel girder bridges with spans from 20 to 30 m. The objective of the tests was to verify girder distribution factors (GDF) for interior girders, dynamic load factors (DLF), and load carrying capacity for the bridges selected. In addition, the tests were to check the efficiency of two new equipment systems: wireless transmitters to replace the cables, and an optical deflection measurement device.

Six bridges were instrumented and loaded with heavy 11-axle trucks. The results were obtained for one truck and two trucks side-by-side. The vehicles were moving at crawling speed for the static load measurement and at a regular speed for the dynamic load measurement. Two truck positions were considered for each case: close to the curb and center of the traffic lane. The strains for both trucks when placed in same lane position are practically the same, which confirms the repeatability of the results. The measured maximum static strains were also the same for crawling speed and a regular speed.

The tested bridges were simply supported structures, however one of them was continuous over the piers with pin-hangers in the adjacent spans. The maximum measured strain was less than 210 με, except of the bridge with pin-hangers for which the strains were less than 348 με. Lower than expected strain values were due to partial fixity of supports, and flexural stiffness of the deck slab, sidewalks, parapets and curbs.

The field tests confirmed that the code specified GDF's, for a single lane and for two lane traffic, are conservative, for both AASHTO LRFD (1998) and AASHTO Standard (1996). For evaluation of existing

steel girder bridges, it is recommended to use AASHTO LRFD (1998) GDF's. For low traffic volume bridges (ADTT < 1000), GDF's specified for a single lane can be used for two lane structures, because of a reduced probability of a simultaneous occurrence of two heavy trucks side-by-side.

The dynamic load factors (DLF) obtained from the tests for a single truck is about 0.20. For two trucks side-by-side, DLF is less than 0.10 for all the bridges except of bridge B01-59041 for which it is about 0.14. However, in case of the latter bridge, the value of DLF is overestimated. Therefore, for evaluation of existing steel girder bridges it is recommended to use DLF = 0.10 for two lane loading, and DLF = 0.20 for a single truck load case.

An advanced finite element analysis was performed and the results are compared with the test results. It was observed that the most important and difficult task is the selection of the boundary conditions (in particular support conditions). The actual bridge behavior was modeled by assuming a partial fixity of the supports (fixed hinges and restrained rotation).

There were some problems with wireless transmitters (interference, poor connections, range), and there is a need for further field trials. The measurement of deflection using the optical device by Noptel provided good results. However, there is a need to purchase additional units to measure the deflection at several points simultaneously (only one unit was available for this project).

TABLE OF CONTENTS

Note:

Intentionally left blank

Acknowledgments

The presented research has been sponsored by the Michigan Department of Transportation, and the Great Lakes Center for Truck and Transit Research (GLCTTR) at the University of Michigan which is gratefully acknowledged. The authors thank the technical staff of the Michigan DOT, Roger Till, Steve Beck, Glen Bukoski, Robert Kelley, Sudhakar Kulkarni, David Juntunen and Mark Vanportfleet, for their useful comments, discussions and support, and Thomas Gillespie, of the University of Michigan Transportation Research Institute (UMTRI) for his support.

The project team received help from other researchers, current and former students and staff of the University of Michigan. In particular, thanks are due to Chris Eamon, Dr. Maria Szerszen, Dr. Leslaw Kwasniewski, Arnaud Chenal, Joe Way, Ken Maschke, Krystyna Grzbiela, and Maria Mariner. They were involved in field instrumentation, measurements, and processing of the results.

Thanks are due to the Michigan State Police for their cooperation. Proof load test was carried out using military tanks provided by the Michigan National Guard represented by General Robert Taylor and Major Stanley Monroe, which is gratefully acknowledged.

The realization of the research program would not be possible without in kind support of the Michigan DOT and the University of Michigan. Measurements were taken using equipment purchased by the University of Michigan.

Note:

Intentionally left blank

1. Introduction and Literature Survey

1.1 Introduction

A rational bridge management requires a good knowledge of the actual loads, load distribution, load effects and structural condition (load carrying capacity). Therefore, evaluation of existing structures is very important. Efficient management of bridges will depend even more on reliable data on loads and resistance. Yet, there is a considerable number of bridges which are very difficult, if not impossible, to evaluate using traditional inspection methods and analysis. For example, this applies to many deteriorated structures (severe corrosion, cracking), and those for which the documentation is missing. It also may apply to structures showing difficult to explain behavior (excessive vibration, deflection, accelerated deterioration, and so on).

There is a growing need for developing efficient procedures for evaluation of the actual load spectra, load distribution, actual strength and predict the remaining life of the structure. There is a need to verify if the currently used girder distribution factors are too conservative. The research work carried out in 1997-98 focused on short span (about 10-18 m) steel girder bridges. Therefore, this project is focused on medium span girder bridges (20-30 m), with the objective to develop efficient procedures for bridge evaluation and diagnostics, including both analytical methods and field testing.

Field testing is an increasingly important topic in the effort to deal with the deteriorating infrastructure, in particular bridges and pavements. There is a need for accurate and inexpensive methods for diagnostics, verification of load distribution and determination of the actual load carrying capacity.

Recent studies indicate that 40 percent of the national bridges are deficient. The major factors that have contributed to the present situation are: the age, inadequate maintenance, increasing load spectra and environmental contamination. The deficient bridges are posted, repaired or replaced. The disposition of bridges involves clear economical and safety implications. To avoid high costs of replacement or repair, the evaluation must accurately reveal the present load carrying capacity of the structure and predict loads and any further changes in the capacity (deterioration) in the applicable time span.

Accuracy of bridge evaluation can be improved by using the recent developments in bridge diagnostics, structural tests, material tests, and structural analysis. Advanced diagnostic procedures can be applied to evaluation of the current capacity of the structure, monitoring of load and resistance history and evaluation of the accumulated damage. Full scale bridge tests provide very useful information about the structural behavior. There is a need for significantly more test data, covering various bridge types. However, extensive test programs are very costly. Therefore, a considerable effort should be directed towards evaluation and improvement of the current analytical methods, on the basis of available test data.

A considerable number of Michigan bridges were constructed in 1950's and 1960's. Many of them show signs of deterioration. In particular, there is severe corrosion on many steel and concrete structures. By analytical methods, some of these bridges are not adequate to carry normal highway traffic. However, the actual load carrying capacity is often much higher than what can be determined by conventional analysis, due to more favorable load sharing, effect of non-structural components (parapets, railing, sidewalks), and other difficult to quantify factors. Field testing, in particular proof load

testing can reveal the hidden strength reserve and thus verify the adequacy of the bridge.

An important consideration in field testing is traffic control. There is a need for testing methods which do not require closure of the bridge or even a lane. Therefore, in the study, we also employed remote sensing techniques, in particular infrared beam-based deflection measurement system by Noptel Oy, and wireless transfer of the signal from strain transducers to the data acquisition system.

The Michigan Guide for Evaluation of Existing Bridges has been developed as a result of Phase 1 of this project. The Guide includes analytical procedures for evaluation, selection criteria for field tests, and procedures for field tests (diagnostic, weigh-in-motion, and proof load). This study focuses on the girder distribution factors for medium span bridges (spans of 20-30 m) and it involves diagnostic field testing to verify the load distribution factors, development of practical proof load procedures using remote sensing, and efficient interpretation of the results.

1.2 Literature Review

The new available literature was reviewed for the period since the Phase I report was completed. No new publications were found dealing with field tests to verify the girder distribution factors and dynamic load factors. The only new related papers were dealing with the finite element analysis.

Extensive research using analytical methods has been conducted to improve the techniques used in the analysis and the design of slab-on-beam bridges. Available theoretical methods vary with regard to the procedure, assumptions, and accuracy. Bridge superstructures can

be idealized for theoretical analysis in many different ways. Various assumptions and simplifications used in the idealization of the bridge can have a significant effect on how closely the calculated results match the actual behavior.

A wheel load distribution formula was developed by Tarhini and Frederick (1992) based on the results of three dimensional finite element analysis for common type of steel I-girder bridges. The concrete slab was modeled as an isotrophic, eight node brick element, with three degrees of freedom at each node. The girder flanges and web were modeled using three-dimensional, quadrilateral, four node shell element with five degrees of freedom at each node. The parameters considered in this study were: the size and spacing of steel girders, presence of transverse diaphragms, concrete slab thickness, span length, single and continuous spans, and so on. The maximum girder distribution factors were determined by dividing the maximum girder moment in the actual bridge using finite element analysis by the maximum moment calculated due to the wheel load.

Mabsout, Tarhini, Frederick, and Tayar (1997) applied finite element method (FEM) to investigate the wheel load distribution factors for typical bridges with one span, simply supported, two traffic lanes, and composite steel girders. They used four different finite element techniques and the results were compared with the American Association of State Highway and Transportation Officials (AASHTO) Code distribution factors (1996 and 1998). The first FEM model was based on research performed by Hayes et al. (1986). The concrete slab was idealized as quadrilateral shell elements with five degrees of freedom at each node and the steel girders were idealized as space frame member with six degrees of freedom at each node. The centroid of each girder coincided with the centroid of concrete slab. The second FEM model was based on research reported by Imbsen

and Nutt (1978). The concrete slab was idealized as quadrilateral shell elements and eccentrically connected space frame members representing the girders. This model was similar to the approach by Hayes et al. (1986), but rigid links were imposed to accommodate for the eccentricity of the girders with regard to the slab. The third FEM model was based on the research reported by Brockenbrouh (1986). The concrete slab and steel girder web were idealized as quadrilateral shell elements, girder flanges were modeled as space frame members, while flange to deck eccentricity was modeled by imposing a rigid link. The fourth FEM model was based on the research reported by Tarhini and Frederick (1992). The first and the fourth finite element analysis results were similar to the girder distribution factors from the AASHTO LRFD (1998) but less than the AASHTO Standard (1996). AASHTO code specified girder distribution factors are explained in Chapter 5. Therefore, they suggested that concrete slab be modeled as quadrilateral shell element and the girders as concentric space frame elements to reduce the input data preparation and computing time.

Note:

Intentionally left blank

2. Questionnaire on Girder Distribution Factors.

A questionnaire was prepared and sent to all 50 state DOT's, as shown in Table 2.1. The objective was to compare the current practice with regard to girder distribution factors (GDF's). The responses are summarized in Table 2.2. The keywords for Table 2.2 are summarized in Table 2.3. . Additional information is presented in Table 2.4.

The questionnaire confirmed that most of the state DOT's uses American Association of State Highway and Transportation Officials (AASHTO) Standard (1996) specified GDF's. Some states uses the new AASHTO LRFD code specified GDF's.

Table 2.1. Questionnaire

Your name: _____
Affiliation: _____

Mailing Address: _____
_____
_____

Phone: _____
Fax: _____
E-mail: _____

In this questionnaire, reference is made to two documents: The AASHTO Standard Specifications for Highway Bridges, Sixteenth Edition (1996), and the AASHTO LRFD Bridge Design Specifications, Second Edition (1998).

1. In the **design** of steel girder bridges with two or more lanes present, which Girder Distribution Factor (GDF) formulas for moments do you use?

   ❑ S/7 (AASHTO Standard 1996, one traffic lane, US units)
   ❑ S/5.5 (AASHTO Standard 1996, two traffic lanes, US units)
   ❑ $0.06 + (S/14)^{0.4}(S/L)^{0.3}(K_g/12.0Lt_s^3)^{0.1}$ (AASHTO LRFD, one lane loaded, US units)
   ❑ $0.075 + (S/9.5)^{0.6}(S/L)^{0.2}(K_g/12.0Lt_s^3)^{0.1}$ (AASHTO LRFD, two or more lanes loaded, US units)
   ❑ Other (please indicate formula & units):

   _____

2. In the **design** of steel girder bridges with two or more lanes present, which method do you use to correct moment GDF's for skew?

   ❑ None
   ❑ $1 - c_1(\tan\theta)^{1.5}$ (AASHTO LRFD correction factor)
   ❑ Other (please indicate formula & units):

   _____

3. In the **operating rating evaluation** of steel girder bridges with two or more lanes present, which moment GDF formulas do you use?

   ❑ S/7 (AASHTO Standard 1996, one traffic lane, US units)
   ❑ S/5.5 (AASHTO Standard 1996, two traffic lanes, US units)
   ❑ $0.06 + (S/14)^{0.4}(S/L)^{0.3}(K_g/12.0Lt_s^3)^{0.1}$ (AASHTO LRFD, one lane loaded, US units)
   ❑ $0.075 + (S/9.5)^{0.6}(S/L)^{0.2}(K_g/12.0Lt_s^3)^{0.1}$ (AASHTO LRFD, two or more lanes loaded, US units)
   ❑ Other (please indicate formula & units):

   _____

4. In the **operating rating evaluation** of steel girder bridges with two or more lanes present, which method do you use to correct moment GDF's for skew?

- ❑ None
- ❑ $1 - c_1(\tan\theta)^{1.5}$ (AASHTO LRFD correction factor)
- ❑ Other (please indicate formula & units):

_____

5. Please mark what bridge design live load you use:

	Interstate routes	US routes	State routes
HS20 (AASHTO Standard 1996)	❑	❑	❑
HS25	❑	❑	❑
HL93 (AASHTO LRFD)	❑	❑	❑
Other (please describe):			

_____

6. Please mark what method of bridge analysis you have used to determine steel girder distribution factors (GDF) for moment (mark all that apply):

- ❑ GDF determined by formula, such as specified in the AASHTO Standard or LRFD
- ❑ Grillage Method
- ❑ Finite Element Method
- ❑ Other method (please describe):

_____

7. Would you like a copy of the survey results?

- ❑ Yes
- ❑ No

8. Comments? Please write below or attach additional forms.

_____

_____

_____

Please return by March 26, 1999 to:

Professor Andrzej S. Nowak
Dept. of Civil and Env. Engineering
University of Michigan
Ann Arbor, MI 48109-2125
Phone (734) 764-9299, fax (734) 764-4292
e-mail Nowak@umich.edu

Table 2.2. The Summary of responses

DOT Steel Girder Bridge Questionnaire Results

State DOT	(1) GDF, Design					(2) Skew, Design			(3) GDF, Operating Rating					(4) Skew, Op Rtg			(5) Live Load					(6) GDF Analysis		
41	S/7	S/5.5	LRFD1	LRFD2	OTHR	NONE	LRFD	OTHR	S/7	S/5.5	LRFD1	LRFD2	OTHR	NONE	LRFD	OTHR	HS20	HS25	HL93	OTHR		FORM	GRIL	FEM
Alabama		*				*				*				*			I,US,S					*		
Alaska		*			*	*	*		*					*				US, S	I,US,S			*		*
Arizona	*	*				*			*	*				*			I,US,S					*		
Arkansas		*			*	*	*		*					*			I,US,S		I,US,S			*		
California		*				*				*				*			I,US,S				"P-13"	*	*	*
Colorado		*				*		*		*				*		*		I,US,S				*		
Connecticut		*				*				*				*			I,US,S					*		
Delaware		*	*		*	*			*	*				*				I,US,S	I,US,S			*		
Flordia					*		*					*			*				I,US,S			*		*
Georgia		*				*				*				*			I,US,S					*		
Illinois	*	*				*			*	*				*			I,US,S					*		
Iowa		*				*				*				*			I,US,S					*		
Kansas		*				*				*				*			S	I,US				*		
Kentucky		*				*				*				*				I,US,S				*		
Maine		*			*		*			*				*				I,US,S				*		
Massachusetts		*				*				*				*			I,US,S					*		
Michigan		*				*			*					*				I,US,S				*		*
Minnesota		*			*	*	*			*				*				I,US,S	I,US,S			*	*	*
Mississippi		*				*				*				*			I,US,S					*		
Missouri		*			*	*	*			*				*			S	I,US	I,US,S			*		
Montana		*	*		*		*			*				*			I,US,S		I,US,S			*		
Nebraska		*	*		*		*		*	*				*				I,US,S	I,US,S			*		
New Jersey	*	*				*				*				*				I,US,S				*		
New Mexico	*	*				*			*	*				*			I,US,S	I,US,S				*		
New York		*				*				*				*				I,US,S				*	*	
North Carolina		*				*				*				*			I,US,S	I,US				*		
North Dakota		*				*			*					*				I,US,S				*		
Ohio		*				*				*				*			I,US,S					*		
Oklahoma			*	*			*			*				*					I,US,S			*		*
Oregon		*			*	*				*				*				I,US,S	I,US,S					
Pennsylvania	*	*	*	*			*	*	*	*	*	*			*	*		I,US,S	I,US,S				*	*	*
Rhode Island	*	*				*			*	*				*				I,US,S				*		
South Carolina		*				*				*				*				I,US,S				*		
South Dakota		*				*				*				*				I,US,S				*		
Tennessee		*	*		*	*	*			*				*	*		I,US,S		I,US,S			*		
Texas		*				*				*				*			I,US,S					*		
Vermont		*				*				*				*				I,US,S				*		
Virginia	*	*				*			*	*				*			I,US,S	I,US,S				*		
Washington		*			*	*				*			*	*				I,US,S				*		
Wisconsin		*				*				*				*				I,US,S				*		
Wyoming		*			*	*				*				*				I,US,S						*

Table 2.3. Summary of keywords used in Table 2.2.

Keywords

Questions:
1. In the design of steel girder bridges with two or more lanes present, which GDF formulas for moments do you use?
2. In the design of steel girder bridges with two or more lanes present, which method do you use to correct moment GDF's for skew?
3. In the operating rating evaluation of steel girder bridges with two or more lanes present, which moment GDF formulas do you use?
4. In the operating rating evaluation of steel girder bridges with two or more lanes present, which method do you use to correct moment GDF's for skew?
5. What bridge design live load do you use?
6. What methods of bridge analysis have you used to determine steel GDF's for moment?

LRFD1	LRFD, single lane loaded GDF formula
LRFD2	LRFD, two lanes loaded GDF formula
OTHR	Other
LRFD	LRFD Skew factor formula
I	Interstate Routes
US	US Routes
S	State Routes
FORM	GDF Formula as in AASHTO Code
GRIL	Grillage Analogy
FEM	Finite Element Method

Table 2.4. Additional Comments

	Comments
Alabama	Uses S/5.5 for interior girders. FEM used for rating if there is an overstress consideration for a special overload.
Alaska	Use Standard (WSD) and LRFD Methods. Load Ratings down per FHWA LFD. Use H25 for WSD and LFD, HL93 for LRFD.
Arizona	Does not use LRFD Code.
Arkansas	--
California	Uses P-13 Live Load
Colorado	For large skews, use grillage for evaluation of exterior girders. Use HS25 with LFD method. Will use LRFD for steel by 2000.
Connecticut	Some consultants are designing by LRFD. Planned transition to LRFD over next 2-3 years.
Delaware	--
Flordia	Uses a FEM program BRUFEM for analysis
Georgia	--
Illinois	Op. rating used for permit loading for 1 or 2 lanes.
Iowa	Will use LRFD in future.
Kansas	Use HS25 with State routes of high ADTT. Will use LRFD methods in Fall, 1999.
Kentucky	--
Maine	Would not usually use steel for 10-20m span range.
Massachusetts	--
Michigan	--
Minnesota	Designed using LRFD since 1 year. Uses Grillage or FEM for curved steel only. Ratings done by Standard Specs.
Mississippi	--
Missouri	Most bridges designed by Standard; some recently by LRFD.
Montana	--
Nebraska	Moving toward LRFD specs. Use no skew correction for Std. Specs.
New Jersey	
New Mexico	Use HS20 for spans <100' and HS25 for spans >100'
New York	Some bridges designed by LRFD GDF and load methods. For op rtg, sometimes use AASHTO "Guide Spec. for Dist. of Loads for Hwy Bridges."
North Carolina	--
North Dakota	--
Ohio	--
Oklahoma	--
Oregon	Moving toward LRFD specs. Currently about 1/2 Standard, 1/2 LRFD.
Pennsylvania	Both 1 and 2 lanes loaded for both Standard and LRFD are checked; highest governs. FEM is sometimes used for skew eval.
Rhode Island	--
South Carolina	--
South Dakota	--
Tennessee	Design old bridges by ASD. For all, compare S/5.5 to "Henry's Method;" take least value. Designed 3 bridges by LRFD, no LRFD for rating.
Texas	HS25 rarely used. Responses assume plate girders with max. spacing of 10' and max. skew 60 degrees
Vermont	--
Virginia	Uses HS25 for "major" structures using LFD
Washington	Checks exterior girders per AASHTO 3.23.2.3.1.2 or 3.23.2.3.1.5. Plans to soon use LRFD method for steel; currently LFD used.
Wisconsin	--
Wyoming	--

3. Selected Bridges

Bridges were selected for tests based of the following criteria:

- Structural type: steel girder bridges.
- Span length: phase I of the report covered short span bridges, with span length between 10 m and 18 m. This study covers the verification of distribution factors for medium spans between 18 m and 30 m.
- Number of lanes: only two lane bridges were considered.
- Skewness: Bridges with skew angle of more than 15 degrees were excluded.
- Accessibility: some structures could not be considered because of deep water or excessive height.
- Traffic volume: very busy bridges were not considered because of the expected difficulties traffic control. Therefore, only bridges with an average daily traffic of 10,000 were selected.

More than forty bridges were inspected to verify the feasibility of load test. Finally, six bridges were selected for this study as listed in Table 3.1.

MDOT ID Number	Location (County)	Tested Span(m)	Number of Girders	Girder Spacing (m)	Year of Construction	Skew Angle	Operating Rating(kN)	ADT
B02-46062	Lenawee	20.4	7	1.44	1933	0	952	9600
R01-78054	St.Joseph	18.8	6	1.9	1965	11	1148	3500
B04-77012	St.Clair	22.8	9	1.22	1928	0	1157	3500
S03-13074	Calhoun	29.8	5	2.82	1970	0,	694	800
B01-29041	Gratiot	21.3	11	1.37	1936	0	783	5600
B01-59041	Montcalm	26.4	10	1.37	1932	0	979	4200

Table 3.1. Selected Bridges.

Note:

Intentionally left blank

4. Load Testing Procedure

4.1 Instrumentation and Data Acquisition

The strain transducers were attached to the lower or upper surface of the bottom flange of the steel girders at midspan (Figure 4.1), depending on the accessibility. In addition, they were installed in selected girders at supports to measure the moment restraint provided by the supports and at intermediate span locations to measure variation in moment along the span. Linear Variable Differential Transformers (LVDT's) were used to measure deflections and to monitor the global response of the structure during proof load testing of Bridge S03-13074. Each LVDT was placed on a tripod and connected to the bottom of the girder by a wire. Figure 4.2 shows an example of a LVDT setup for the measurement of a girder deflection. For all tested bridges, the deflection of the girder that was anticipated to carry the heaviest load was measured using the PSM-R device manufactured by Noptel, Co. in Finland. This device can be used for long distance displacement measurement applications. It is based on a combined LED transmitter and opto-electronic receiver that measures the position of the reflector or prism attached to the target.

Strain transducers and LVDTs were connected to the SCXI data acquisition system from the National Instruments. The data acquisition mode is controlled from the external PC notebook computer, and acquired data are processed and directly saved in PC's hard drive (Figure 4.3).

The data acquisition system consists of a four slot SCXI-1000 chassis, one SCXI-1200 data acquisition module and two SCXI-1100 multiplexers. Each multiplexer can handle up to 32 channels of input data. The current system is capable of handling 64 channels of strain

or deflection inputs. Up to 32 additional channels can be added if required. A portable field computer is used to store, process and display the data on site. A typical data acquisition setup is shown in Figure 4.3. The data from all instruments is collected after placing the trucks in desired positions or while trucks are passing on the bridge. For the normal speed tests, a sampling rate of 200 per second was used for calculation of dynamic effects. This is equivalent to 7.6 samples per meter at a truck speed of 95 km/h. The real time responses of all transducers are displayed on the monitor during all stages of testing, assuring the safety of the bridge load test.

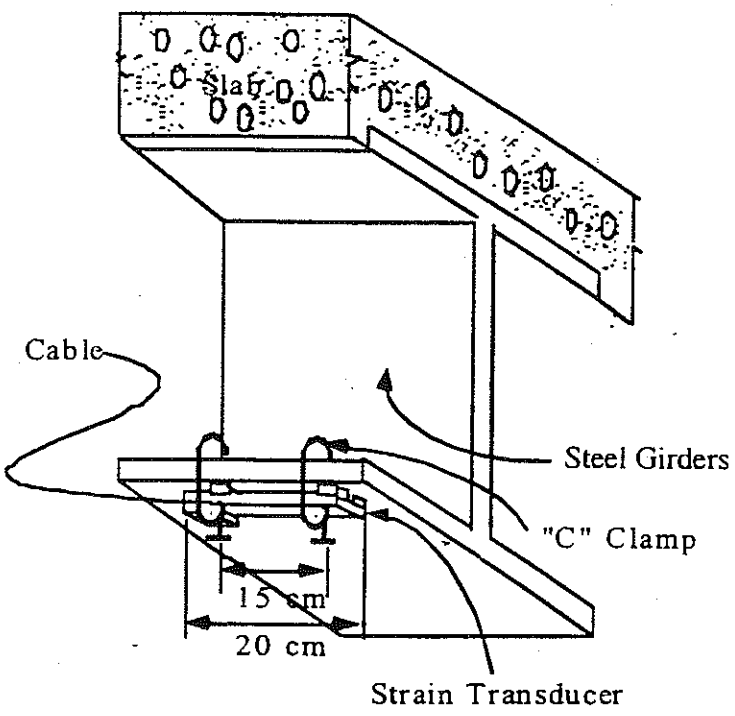

Figure 4.1 Removable Strain Transducer Mounted to the Lower Flange.

4.2 Test Loads for Load Distribution Tests

Strain data necessary to calculate girder distribution and dynamic load factors were taken from bottom-flanges of girders in the middle of a

span. Strain data were obtained under passes of two, three-unit 11-axle trucks with known weight and configuration for all bridges. The actual axle weights of the test trucks were measured at the weigh stations just prior to the tests for all bridges. Strain data obtained from side-by-side truck tests were used to calculate load distribution and dynamic load factors. Superposition of strain data from each truck provided the verification of the obtained data and the linear-elastic behavior of the bridge.

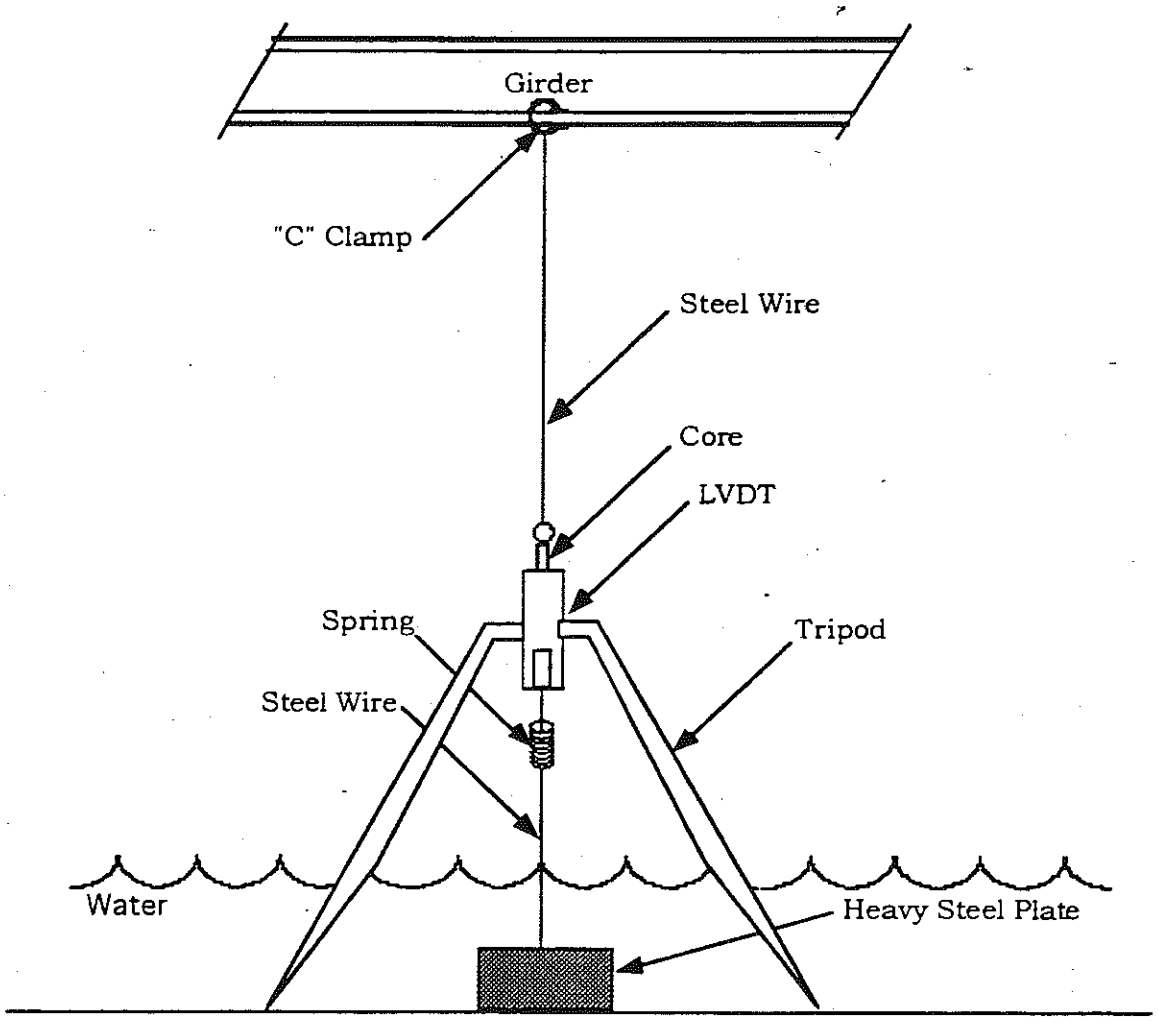

Figure 4.2 Typical LVDT setup.

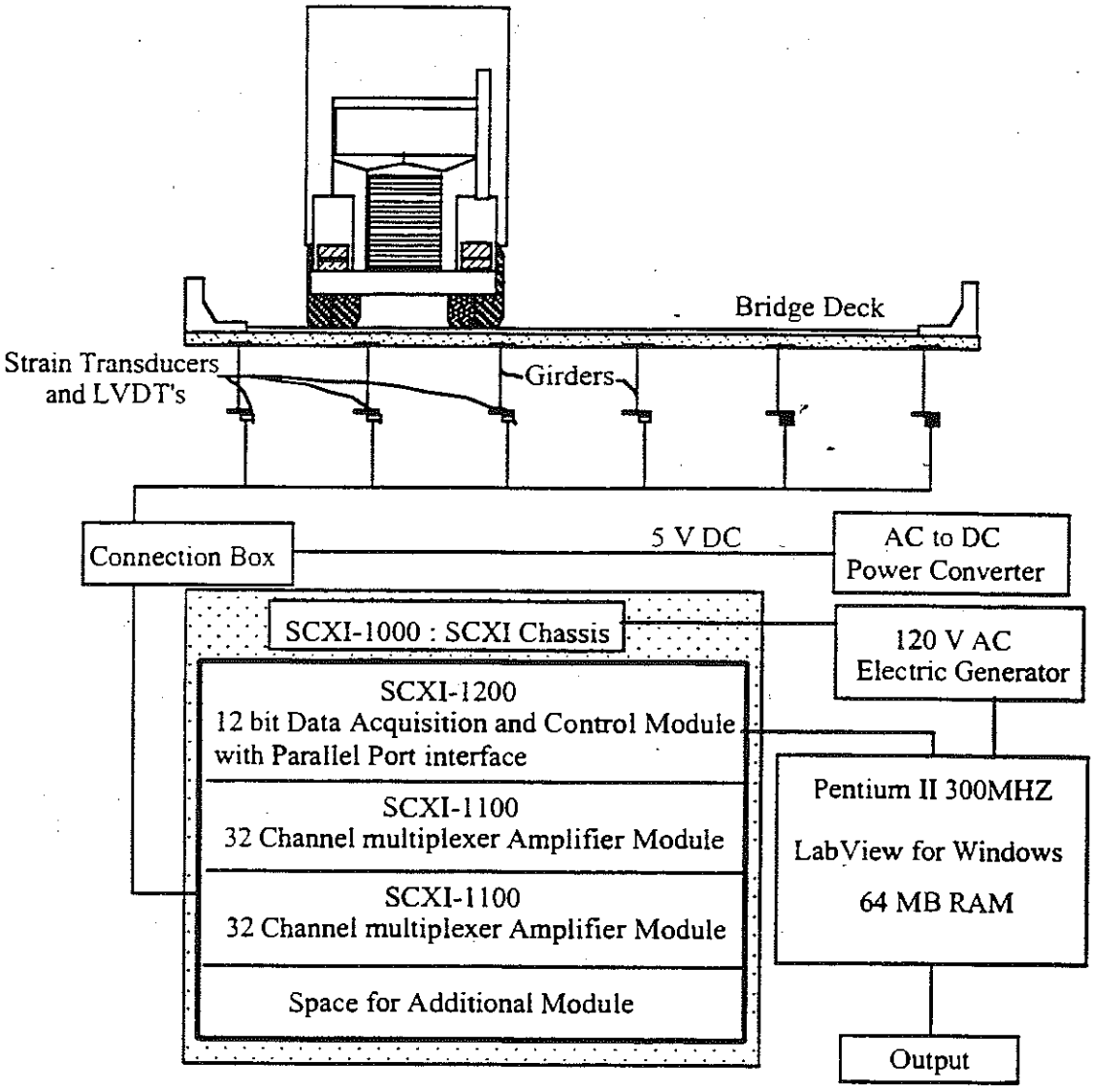

Figure 4.3. SCXI Data Acquisition System Setup.

Trucks were driven over the bridge at crawling speed to simulate static loads and at high speed to obtain dynamic effect on the bridge. In the previous bridge tests, trucks were placed at the analytical maximum bending position. However, the strains obtained from crawling speed tests were always greater than those from the analytical maximum bending position because of other factors not included in the analysis, such as the partial fixity of supports, the structural contribution of non-structural members, and so on.

Therefore, bridges were tested under crawling speed and the maximum speed obtained by a test truck at a bridge site (high speed).

In general, the following load cases were applied for bridges with two lanes. Lane 1 and lane 2 indicate east and west lane for bridge R01-78054 and B04-77012, respectively, and north and south lane for all other bridges. Table 4.1. shows typical sequence of test runs.

Run Number	Trucks	Lane	Position in Lane	Truck Speed
1	Truck A	1	Center	Crawling Speed
2	Truck A	1	Curb	Crawling Speed
3	Truck B	1	Center	Crawling Speed
4	Truck B	1	Curb	Crawling Speed
5	Truck B	1	Center	Normal Speed
6	Truck A	1	Center	Normal Speed
7	Truck A	2	Center	Crawling Speed
8	Truck A	2	Curb	Crawling Speed
9	Truck B	2	Center	Crawling Speed
10	Truck B	2	Curb	Crawling Speed
11	Truck B	2	Center	Normal Speed
12	Truck A	2	Center	Normal Speed
13	Truck A and B	1 and 2	Center	Crawling Speed
14	Truck B and A	1 and 2	Center	Crawling Speed
15	Truck A and B	1 and 2	Center	Normal Speed
16	Truck B and A	1 and 2	Center	Normal Speed

Table 4.1. Sequence of Typical Test Runs for All Bridges.

4.3 Test Loads for Proof Load Tests

4.3.1 Proof Load Level

Proof load tests are carried out to verify if the bridge can safely carry the maximum allowable legal load. For the considered bridges,

the maximum mid-span moment in medium span bridges is caused by 11-axle two-unit trucks with the wheel configuration shown in Figure 4.10. For an 11-axle truck, the gross vehicle weight (GVW) can be up to 730 kN, which is more than twice the HS 20 design load. Other states allow a maximum GVW of only 356 kN. The proof load testing was designed to verify the moment capacity of steel girders close to mid-span. Before the proof load tests, the target proof load has to be calculated. If the test load reaches the target proof load level without causing any distress to the bridge, then the operating rating factor for 11-axle two-unit truck is 1.0.

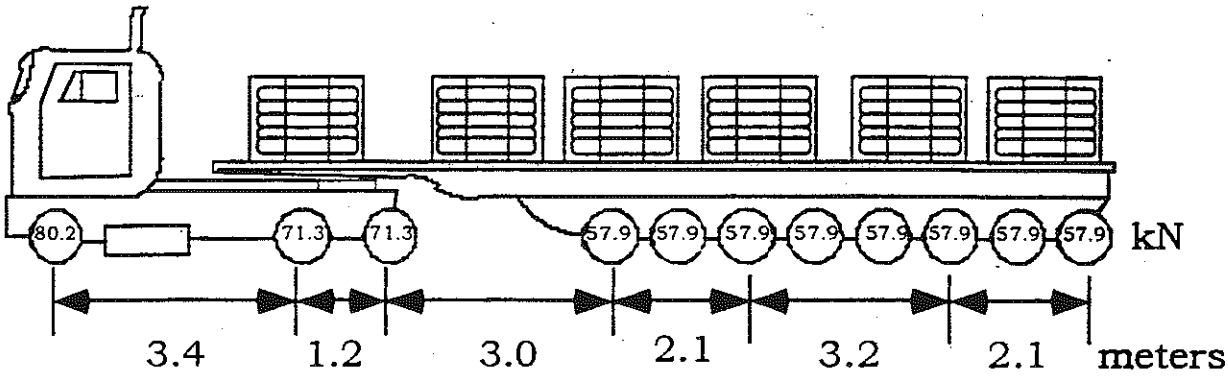

Figure 4.10. 11-Axle Two-Unit Truck.

The proof load level should be sufficiently higher than that from 11-axle truck, to ensure the desired safety level. The NCHRP Report 12-28(13)A titled "Manual for Bridge Rating Through Load Testing" by A.G. Lichtenstein (1998) provides guidelines for calculating the target proof load level. It suggests that the maximum allowable legal load should be multiplied by a factor Xp, which represents the live load factor needed to bring the bridge to an operating rating factor of 1.0. The guide recommends that Xp should be 1.4 before any adjustments are made. It also recommends the following adjustments to Xp, that should be considered in selecting a target live load magnitude.

- Increase X_p by 15 percent for one lane structures or for other spans in which the single lane loading augmented by an additional 15 percent would govern.
- Increase X_p by 10 percent for spans with fracture critical details.
- Increase X_p by 10 percent for structures without redundant load paths.
- Reduce X_p by 5 percent if the structure is ratable, that is, there are no hidden details, and if the calculated rating factor exceeds 1.0.
- Additional factors including traffic intensity and bridge condition may also be incorporated in the selection of the live load factor X_p.

Application of the recommended adjustment factors, leads to the target live load factor X_{pa}. The net percent increase in X_p, Σ, is found by summing the appropriate adjustments given above. Then

$$X_{pa} = X_p (1 + \Sigma/100) \tag{4-1}$$

The target proof load (L_t) is then:

$$L_t = X_{pa} (1 + DLF) L_r \tag{4-2}$$

$$1.3 \leq X_{pa} \leq 2.2 \tag{4-3}$$

where,

L_r = the comparable live load due to the rating vehicle for the loaded lanes.

DLF = dynamic load factor

X_{pa} = the target live load factor.

Based on the span length, the AASHTO Standard Specifications (1996) specifies the dynamic load factors of less than 0.3. However, previous studies by several researchers have indicated that the

dynamic load factor is much smaller for heavy loads (Hwang and Nowak 1991, Nassif and Nowak 1995, Nowak, Laman and Nassif 1994). Therefore, for this study, a dynamic load factor of 0.1 was selected in calculation of the proof load level for Bridge S03-13074. The load distribution test prior to the proof load test on this bridge also confirmed that for the most heavily loaded girder (Girder No.3), the dynamic load factor does not exceed 0.1 under two trucks side-by-side loading.

4.3.2 Proof Load Selection

The M-1 A1 military tanks plus two, 3-unit 11-axle trucks were selected as proof load. The tanks were provided by the Michigan National Guard. The trailers of 11-axle trucks were detached from the cabs and positioned separately to cause the maximum bending moment. Each M-1 tank used in the proof load test weighs 533 kN (obtained from tank weight information from the Michigan National Guard), and it is 30 kN heavier than M-60 tank used in the previous tests. The load is distributed over a track length of 4.6 m. The front and side views of a M-1 tank are shown in Figures 4.11 and 4.12. The detailed proof load positions are shown in chapter 9.

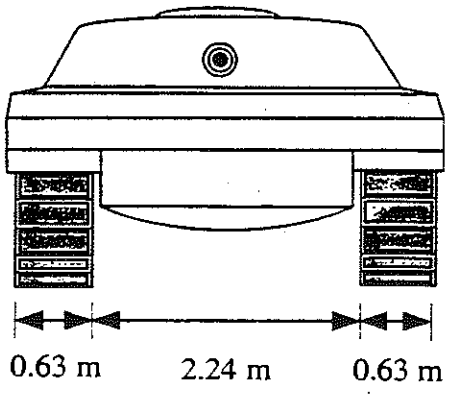

Figure 4.11 Front View of M-1 Tank.

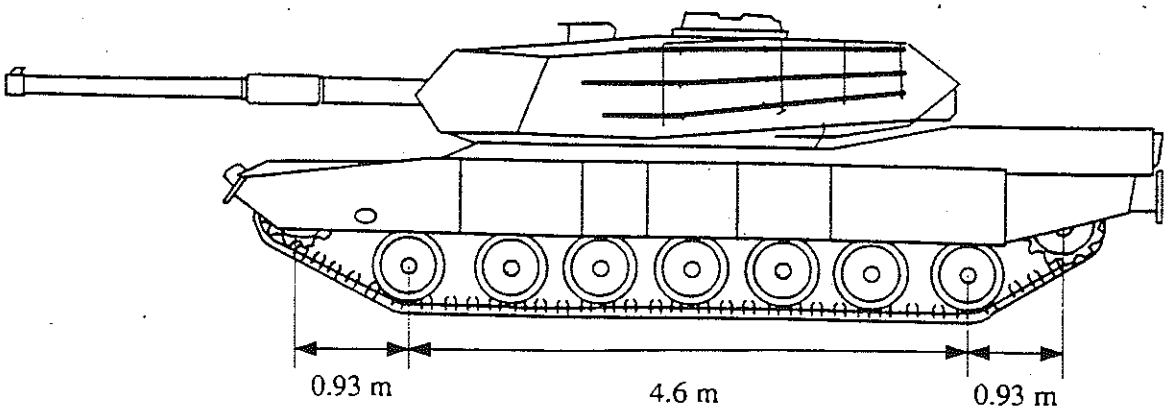

Figure 4.12 Side Elevation of M-1 Tank.

4.4. Load Distribution and Dynamic Load Factor Calculation from Test Results

Collected strain data from the tests were processed to identify dynamic load and girder distribution factors. Girder Distribution Factors (GDF) are calculated from the maximum static strain obtained from the static loading at each girder at the same section along the length of the bridge. Ghosn *et al.* (1986) assumed that GDF was equal to the ratio of the static strain at the girder to the sum of all the static strains. Stallings and Yoo (1993) used the weighted strains to account for different section moduli of the girders. Accordingly, GDF for the ith girder, GDF_i, can be derived as follows:

$$GDF_i = \frac{M_i}{\sum_{j=1}^{k} M_j} = \frac{ES_i\varepsilon_i}{\sum_{j=1}^{k} ES_j\varepsilon_j} = \frac{\frac{S_i}{S_t}\varepsilon_i}{\sum_{j=1}^{k}\frac{S_j}{S_t}\varepsilon_j} = \frac{\varepsilon_i w_i}{\sum_{j=1}^{k}\varepsilon_j w_j} \qquad (4\text{-}4)$$

where M_i = bending moment at the ith girder; E = modulus of elasticity; S_i = section modulus of the ith girder; S_t = typical interior section modulus; ε_i = maximum bottom-flange static strain at the ith girder; w_i = ratio of the section modulus of the ith girder to that of a

typical interior girder; and k = number of girders. When all girders have the same section modulus (that is, when weigh factors, w_i, are equal to one for all girders), Eq. (4-4) is equivalent to that of Ghosn *et al.* (1986). Because of edge stiffening effect due to curbs and barrier walls, the section modulus in exterior girders is slightly greater than in interior girders. In other words, the weigh factors, w_i, for exterior girders are greater than one. Therefore, from Eq. (4-4), the assumption of the weigh factors, w_i, equal to one will cause slightly overestimated girder distribution factors in interior girders and underestimated girder distribution factors in exterior girders. In this study, the weigh factors, w_i, are assumed to be one.

For two trucks side-by-side, the girder distribution factors calculated from Eq. (4.4) must be multiplied by two to be comparable with the bridge code because the AASHTO code specified girder distribution factors are based on the effect of one truck load.

Dynamic load factors (DLF's) are defined in several ways, as discussed in previous studies (Paultre *et al.* 1992; Bakht and Pinjarkar 1989). In this study, the dynamic load factor was taken as the ratio of the maximum dynamic strain and the maximum static strain (Figure 4.13):

$$DLF = \frac{\varepsilon_{dyn}}{\varepsilon_{stat}} \tag{4-5}$$

where ε_{dyn} = absolute maximum dynamic strain under the vehicle traveling at normal speed; and ε_{stat} = maximum static strain obtained by filtering the dynamic response. Collected data are filtered by applying some numerical procedures, such as averaging filtering technique, to increase the signal-to-noise ratio, and to reduce the effect of random, and non-periodic noise.

Dynamic load factor is calculated for all instrumented girders. However, for comparison with the code specified DLF, it is necessary to consider DLF corresponding to the largest static strains, because this is the governing case.

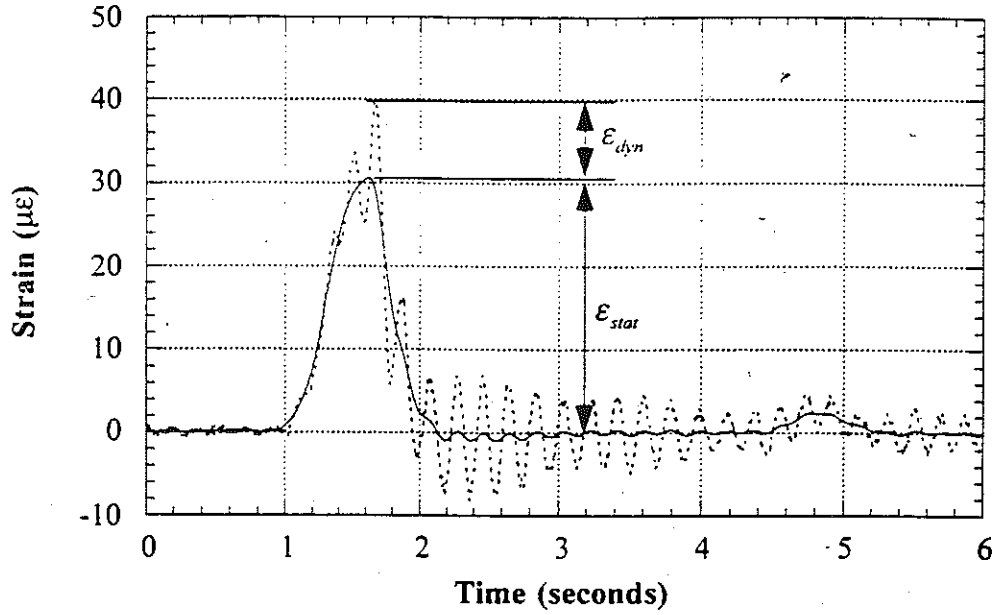

Figure 4.13 Dynamic and Static Strain under a Truck at Highway Speed.

4.5. Verification of Wireless Transmitters

One of the objectives of the project was verification of reliability and usability of wireless transmitters as a replacement for cables connecting the strain transducers and the main computer unit. The test was performed on bridge ID R01-78054 (M66/RR). This bridge was selected because the number of girders is 6, and therefore, we

could install two parallel strain transducer systems, one with cables and the other one with wireless transmitters.

The wireless transmitters were purchased in 1997, but lab test showed they were not working properly and they were fixed by the manufacturer several times. Prior to the field test on bridge ID R01-78054, the equipment was tested on the parking lot at the G.G. Brown Lab at the University of Michigan and on Huron Parkway Bridge in Ann Arbor.

The strains caused by test trucks were recorded by two parallel and independent data acquisition systems. The results are shown in Figures 4.14-16. In Figure 4.14 and Figure 4.15, the strains are plotted for a single truck passing in the west lane and then in the east lane. In Figure 4.16, the strains are shown for two trucks side-by-side. It turned out that the wireless transmitter in girder 1 was not working. Therefore, there are no strains were recorded there. The difference between the strains obtained using the system with cables and wireless system is small, within 5%.

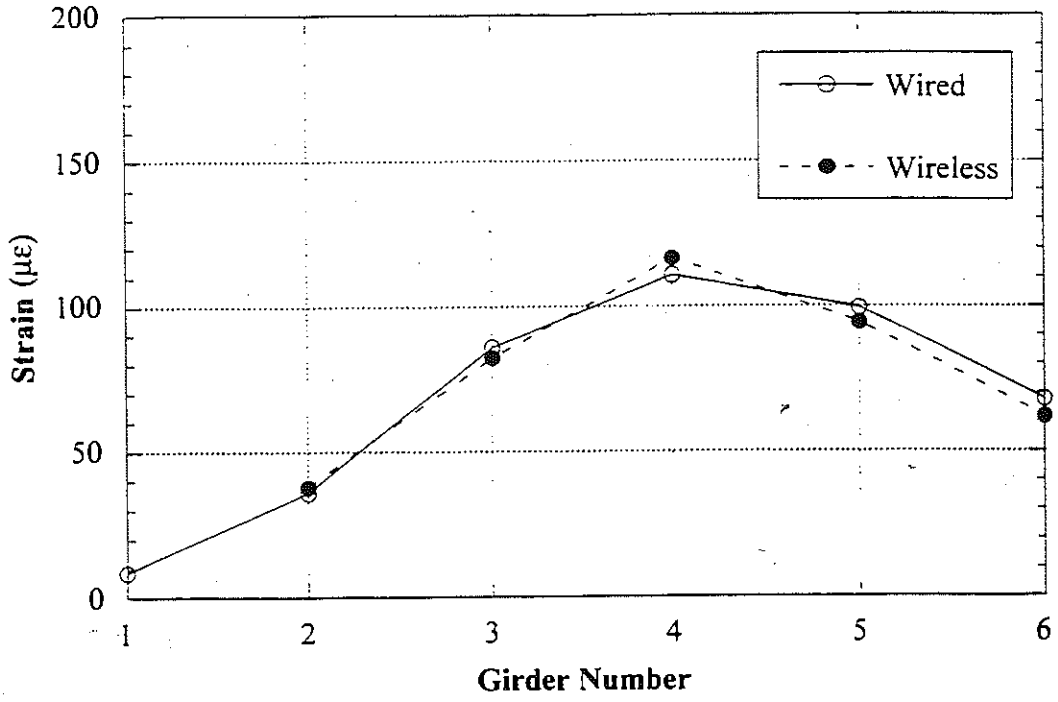

Figure 4.14. Strain Values from Wired and Wireless Equipment, West Lane Loading, Bridge M66/RR

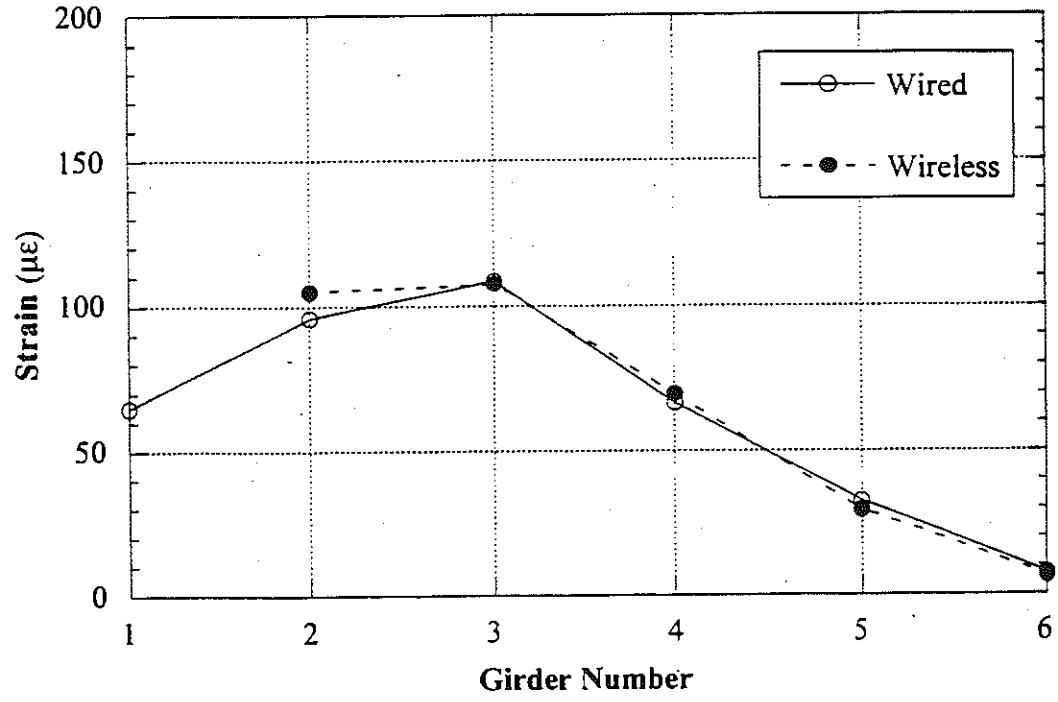

Figure 4.15. Strain Values from Wired and Wireless Equipment, East Lane Loading, Bridge M66/RR

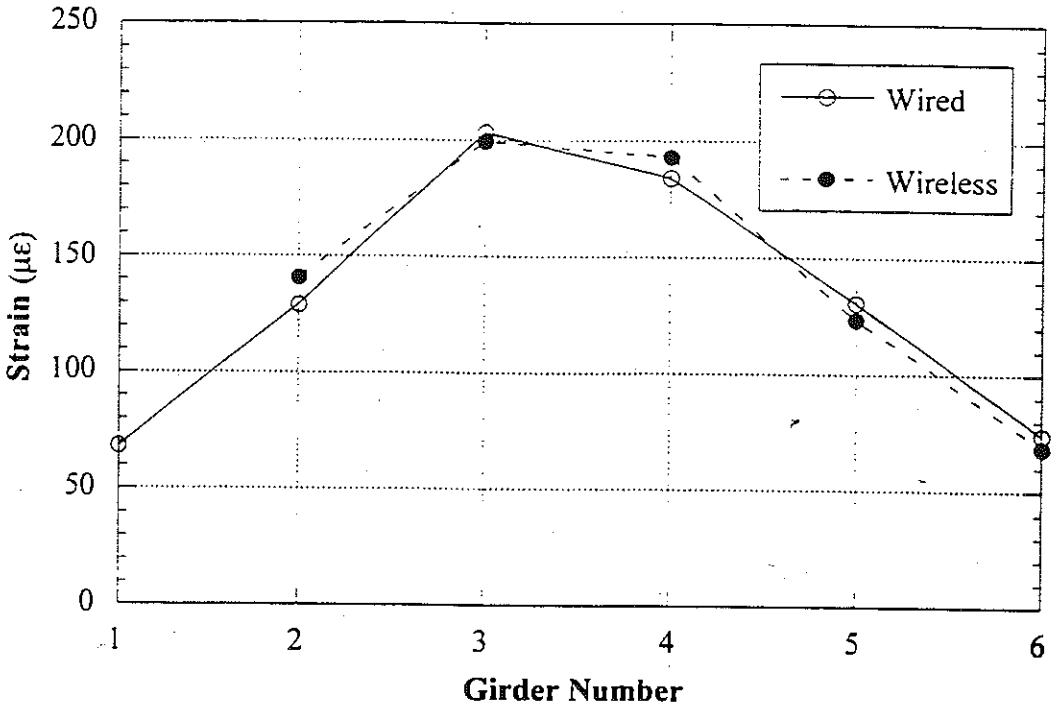

Figure 4.16. Strain Values from Wired and Wireless Equipment, Two Trucks Side-by-Side Loading, Bridge M66/RR.

5. Specified Load Distribution Factors and Dynamic Load Factors

Measured girder distribution factors (GDF) and dynamic load factors (DLF) are compared in tables and figures with the values calculated according to the current design codes. Throughout the report, distribution factors are expressed in terms of axle load for the full truck rather than a line of wheel loads for the half truck. For the bending moment in interior girders, the AASHTO Standard (1996) specifies GDF's as follows. For one lane steel girder and prestressed concrete girder bridges, GDF is:

$$GDF = \frac{S}{4.27} \tag{5-1}$$

and for multi lane steel and prestressed concrete girder bridges,

$$GDF = \frac{S}{3.36} \tag{5-2}$$

where S = girder spacing (m).

The AASHTO LRFD Code (1998) specifies GDF as a function of girder spacing, span length, stiffness parameters, and bridge skew. For the bending moment in interior girders with one lane loading, GDF is:

$$GDF = \left\{0.06 + \left(\frac{S}{4300}\right)^{0.4}\left(\frac{S}{L}\right)^{0.3}\left(\frac{K_g}{Lt_s^3}\right)^{0.1}\right\}\left\{1 - c_1(\tan\theta)^{1.5}\right\} \tag{5-3}$$

and for multi lane loading:

$$GDF = \left\{0.075 + \left(\frac{S}{2900}\right)^{0.6}\left(\frac{S}{L}\right)^{0.2}\left(\frac{K_g}{Lt_s^3}\right)^{0.1}\right\}\left\{1 - c_1(\tan\theta)^{1.5}\right\} \tag{5-4}$$

$$c_1 = 0.25\left(\frac{K_g}{Lt_s^3}\right)^{0.25}\left(\frac{S}{L}\right)^{0.5} \qquad \text{for } 30° < \theta < 60° \tag{5-5}$$

$$c_1 = 0 \qquad \text{for } \theta < 30° \tag{5-6}$$

where S = girder spacing (mm); L = span length (mm); $K_g = n(I + Ae_g^2)$; t_s = thickness of concrete slab (mm); n = modular ratio between girder and slab materials; I = moment of inertia of the girder (mm^4); A = area of the girder (mm^2); e_g = distance between the centers of gravity of the girder and the slab (mm); and θ = skew angle in degrees. Because the term $K_g/(Lt_s^3)$ implies more accuracy than exists for bridge evaluation, it is recommended that they be taken as 1.0. In this report, however, actual values of the term $K_g/(Lt_s^3)$ are used in calculation of girder distribution factors. The AASHTO LRFD (1998) formulas have been developed based on a NCHRP Project 12-26 (Zokaie *et al.* 1991). The method includes the longitudinal stiffness parameter, K_g, and the span length, L, in addition to the girder spacing, S. AASHTO Guide for Load Distribution (1994) specifies similar load factors to those of AASHTO LRFD (1998).

Most bridge design codes specify the dynamic load as an additional static live load. In the AASHTO Standard (1996), dynamic load factors are specified as a function of span length only:

$$\text{DLF} = \frac{50}{3.28L + 125} \qquad (5\text{-}7)$$

where DLF = dynamic load factor (maximum 30 percent); and L= span length (m). This empirical equation has been used since 1944. In the AASHTO LRFD (1994), live load is specified as a combination of HS20 truck (AASHTO 1996) and a uniformly distributed load of 9.3 kN/m. The dynamic load factor is equal to 0.33 of the truck effect, with no dynamic load applied to the uniform loading.

6. Bridge on US-223 over Raisin River, in Palmyra. (B02-46062, US223/RR)

6.1 Description

This bridge was built in 1933 and it is located on US-223 over Raisin River near Palmyra, in Lenawee County, Michigan. The bridge deck was replaced in 1967. There is one lane in each direction. The total span length is 37.6 m. The bridge has seven steel girders spaced at 1.44 m, as shown in Figure 6.1. The bridge carries an average daily traffic (ADT) of 9,600. As shown in Figure 6.2, it is a three span, simply supported composite structure. There is no rigid connection between the main span and side spans. However, small amount of moment transfer was noticed between the main span and side-spans during the test. The test was performed on the center span. The length of the main span is 20.5 m without skew. The deck slab of the bridge is in a relatively good condition, although some transverse cracks were noticed. The bridge has a load rating of 952 kN, according to the Michigan Structure Inventory.

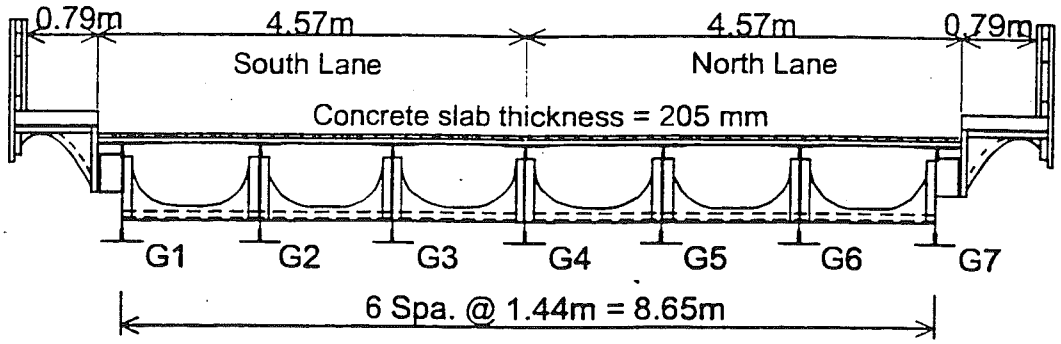

Figure 6.1. Cross Section of Bridge US223/RR (B02-46062), in Palmyra

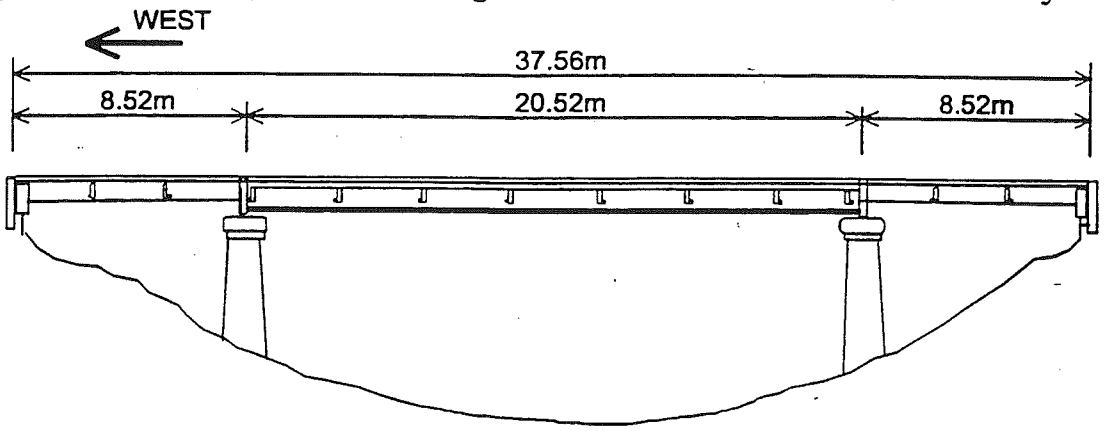

Figure 6.2. The Elevation of the Bridge US223/RR (B02-46062), in Palmyra.

6.2 Instrumentation

Strain transducers were installed on the bottom flanges of girders at midspan (Figure 6.3) of the main span on May 5, 1999. The reflector for the PSM-R device from Noptel was installed at the girder No. 4 for deflection measurement. The test equipment was installed on May 5, 1999. The bridge test was performed on May 6, 1999.

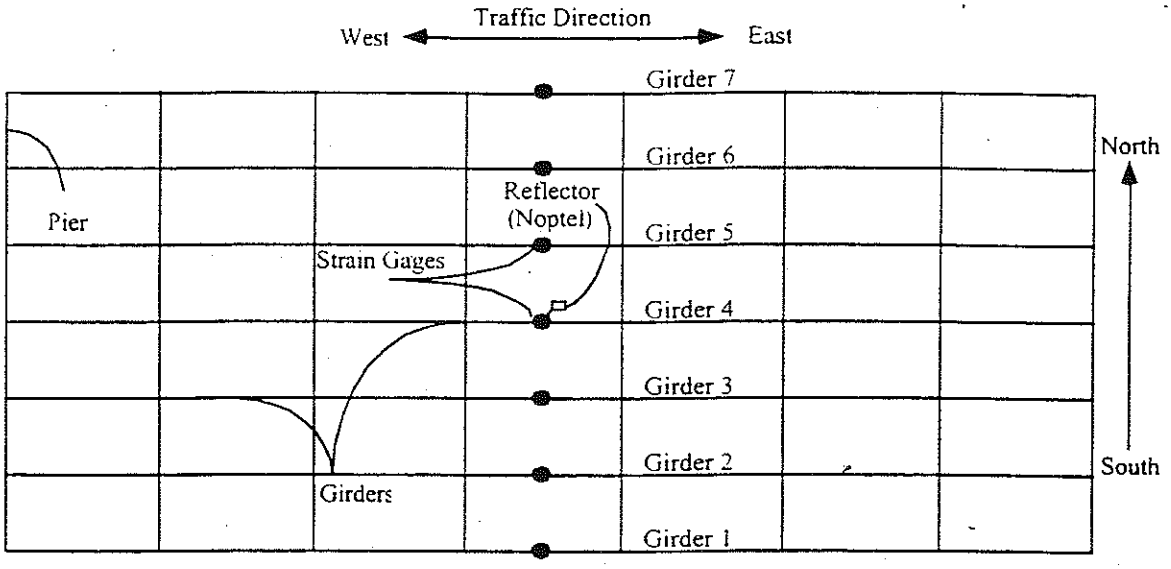

Figure 6.3. Strain Gage Locations in Bridge US223/RR (B02-46062), in Palmyra.

6.3 Truck Loads

The girder distribution factors (GDF) and dynamic load factors (DLF) were calculated using the strains measured at midspan. The bridge was loaded with two 11-axle trucks (three-unit vehicles). The gross vehicle weight and the truck axle configurations are shown in Figures 6.4 and 6.5.

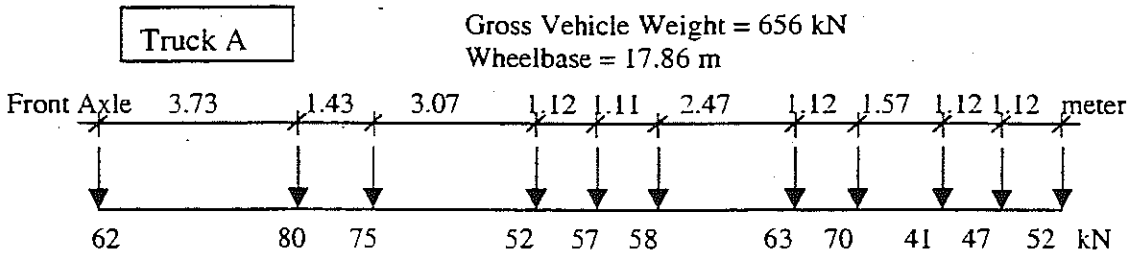

Figure 6.4. Truck A Configuration, US223/RR (B02-46062).

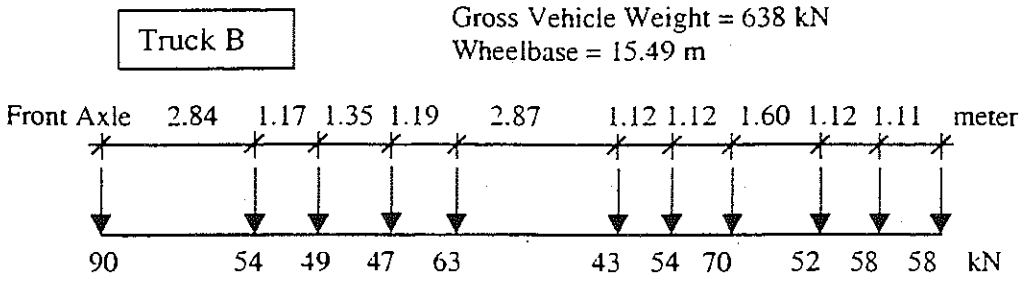

Figure 6.5. Truck B Configuration, US223/RR (B02-46062).

A total of 16 load cases were considered, as shown in Table 6.1. First each truck was driven by itself at the center of one lane, at crawling speed. Then, the same truck was driven close to the curb. The runs in the center of the lane were repeated at a normal highway speed (about 50 km/h for this location). The same was repeated for the other lane. Finally, two trucks were driven simultaneously, side-by-side, at crawling speed and normal highway speed. For side-by-side cases, the runs were repeated after the trucks switched lanes, i.e. first truck A was in North lane, and B in South lane, then truck A was in South lane, and B in North lane.

Table 6.1. Sequence of Test Runs, US223/RR (B02-46062).

Run#	Truck	Lane Side	Position in Lane	Truck Speed
1	Truck A	South	Center	Crawling
2	Truck A	South	Curb	Crawling
3	Truck B	South	Center	Crawling
4	Truck B	South	Curb	Crawling
5	Truck B	South	Center	50 km/h
6	Truck A	South	Center	50 km/h
7	Truck A	North	Center	Crawling
8	Truck A	North	Curb	Crawling
9	Truck B	North	Center	Crawling
10	Truck B	North	Curb	Crawling
11	Truck B	North	Center	50 km/h
12	Truck A	North	Center	50 km/h
13	Truck A and B	both	Center	Crawling
14	Truck B and A	both	Center	Crawling
15	Truck A and B	both	Center	50 km/h
16	Truck B and A	both	Center	50 km/h

6.4. Analysis Results

The three-dimensional finite element method (FEM) was applied to investigate the structural behavior of the bridge US223/RR (B02-46062). The concrete slab was modeled with isotrophic, eight node solid elements, with three degrees of freedoms at each node. The girder flanges and web were modeled using three-dimensional, quadrilateral, four node shell elements with six degrees of freedom at each node. The structural effects of the secondary members, such as the sidewalk and parapet, were also taken into account in the finite element analysis models.

Two cases of the boundary conditions were employed in the FEM models. In the first FEM model, it was assumed that the supports are represented by a hinge at one end and a roller with a hinge at the other end. In the other FEM model, it was assumed that both supports are hinged, with no movement in horizontal direction.

Figure 6.6 illustrates the mesh of the FEM model, and Figure 6.7 shows the deformed shape of the bridge when it is loaded with two trucks side-by-side.

Figure 6.8 shows the results of the finite element analysis for two trucks side-by-side (Run 13). It includes the experimental results and analytical results for the two considered models. The FEM results show that the maximum strain at the most heavily loaded girder is about 185 με, while the maximum strain recorded from the test is about 160 με. In addition, the experimental response lies between the two considered analytical models. This indicates that a partial fixity exists at the supports of the bridge.

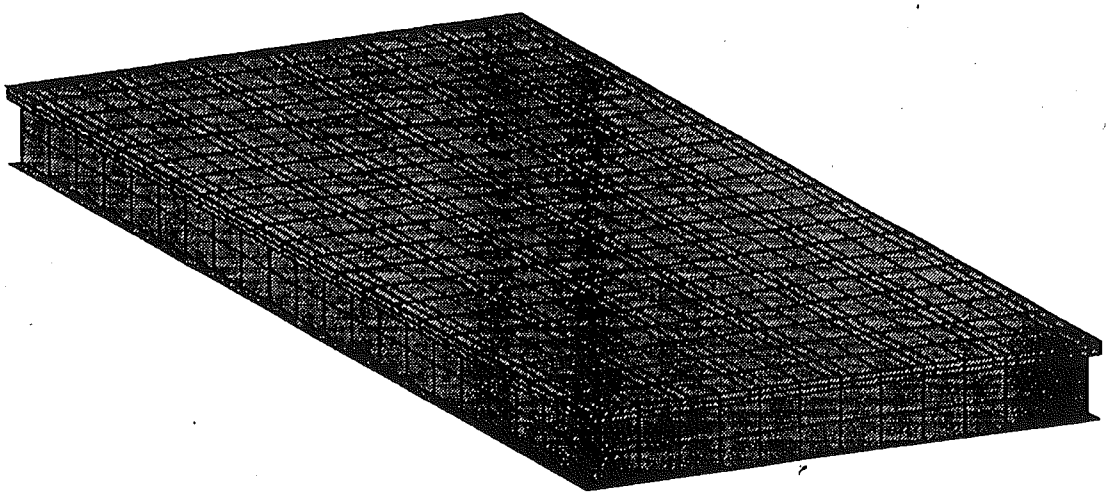

Figure 6.6. The Mesh of the Finite Element Model.
US223/RR (B02-46062).

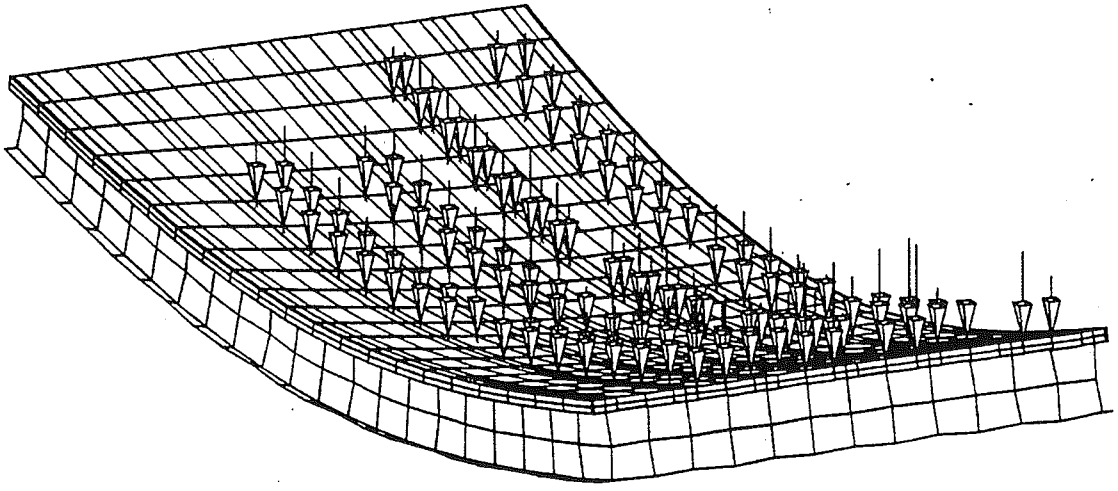

Figure 6.7. The Deformed Shape of the Bridge under Two Lane Loading.
US223/RR (B02-46062).

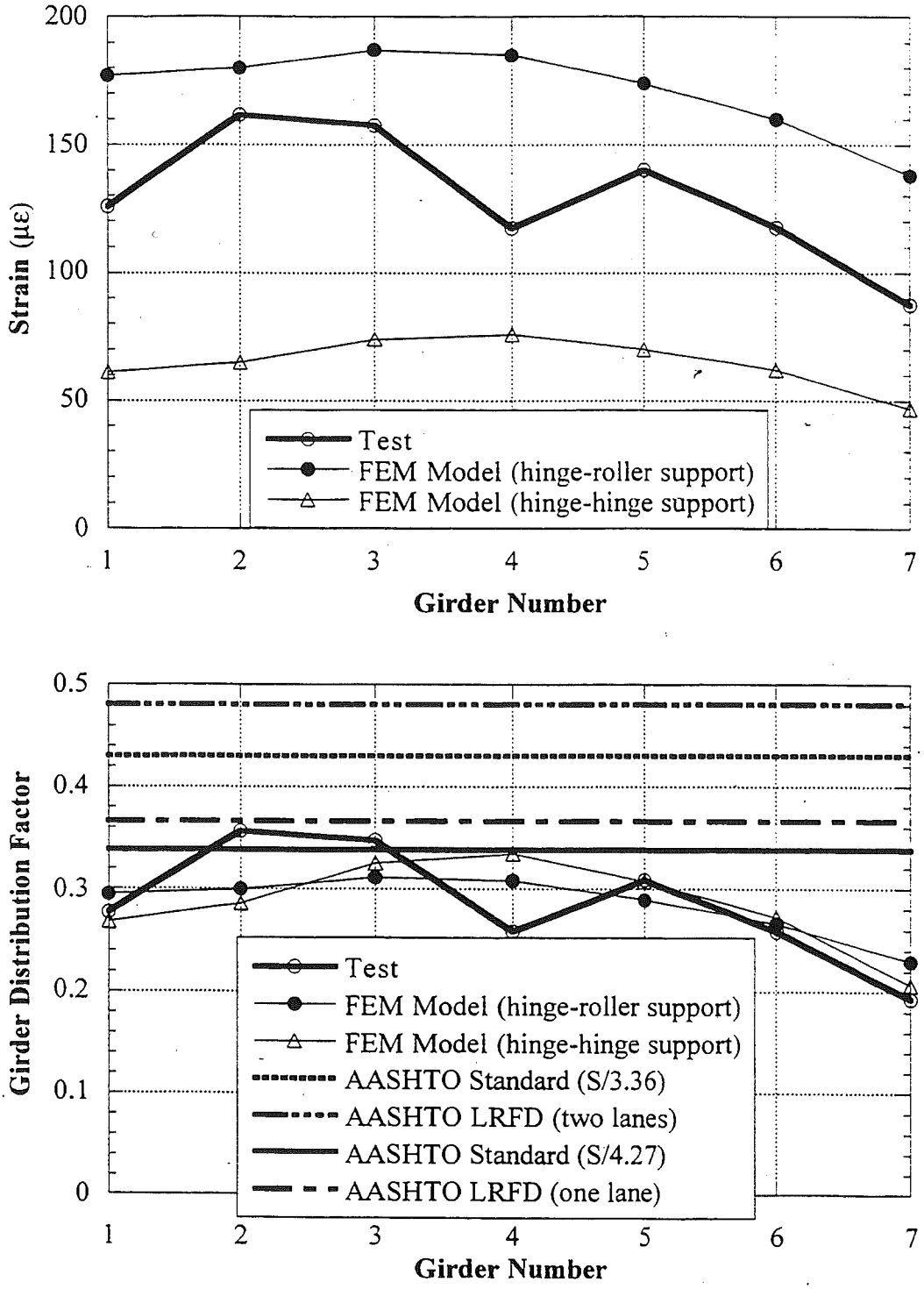

Figure 6.8. Results of the Finite Element Analysis for Two Lane Loading (truck A-south lane, truck B-north lane), US223/RR (B02-46062).

6.5. Test Results

The resulting strains and GDF's are shown in Figures 6.9 through 6.13. Figures 6.9 to 6.11 present the results of all crawling-speed (static) tests. Figures 6.9 to 6.10 present static strains and GDF's for one truck on the bridge. The maximum strain due to a single truck was observed in the exterior girders, about 175 με, when a truck is loaded close to curb. This corresponds to about 35 MPa. Some uplift was also observed in the exterior girder (for the truck at close to the curb position).

Figure 6.11 shows static strains and GDF's from side-by-side static load tests. For two vehicles side-by-side the maximum strain is less than 170 με (which corresponds to 34 MPa). The superposition of strains due to a single truck in South and North lanes produces almost the same results as strain due to two trucks side-by-side.

For two trucks side-by-side, the girder distribution factor for girder i is determined using Eq. 4.4. For comparison, GDF are also calculated according to AASHTO Standard (1996) and AASHTO LRFD Code (1998). Two cases were considered, a single lane loaded, and two lanes loaded. The resulting GDF's are shown in Figures 6.9 through 6.13.

The results indicate that code-specified GDF's are conservative. A single lane GDF specified in AASHTO LRFD (1998) is also sufficient for two lane load cases for this bridge. However, a single lane GDF specified in AASHTO Standard (1996) is not enough for two lane load cases for this bridge.

Figures 6.12 and 6.13 shows the resulting strain and distribution factors from normal speed tests. There is practically no difference between the crawling speed and normal speed results.

In Figure 6.14, dynamic load factors (DLF's) are calculated using Eq. 4-5, and plotted for all load cases involving normal speed (no dynamic load was measured for crawling speed runs). Dynamic load factors for exterior girders are high because the static strains in these girders are very low. In other words, large values of DLF in exterior girders correspond to load cases with a single truck in the opposite lane (resulting in very low static strain).

The relationship between DLF and static and dynamic strains is shown in Figure 6.15. The open circles correspond to static strain, ε_{stat}, and black solid squares correspond to dynamic strain, ε_{dyn}. For each static strain value (open circle), the corresponding dynamic strain is denoted by solid square (the numbers of circles and squares are same). Figure 6.15 shows that the dynamic load factor decreases with increasing static load effect. Also, it is clear from the Figure 6.15 that dynamic strains are less than 10 με (2 MPa) for all the cases while the static strain can exceed 150 με in normal speed test. Dynamic strains remain nearly constant, while static strains increase as truck loading increases. This results in large dynamic load factors for low static strains. DLF corresponding to the maximum strain caused by two trucks side-by-side, is less than 0.10 for the most heavily loaded girder.

Girder No. 4 was instrumented with remote deflection measurement device manufactured by Noptel. The reflector was installed at midspan. The result is shown in Table 6.2. The maximum deflection recorded during the test is 6.23 mm for girder number 4.

Table 6.2. Maximum deflections measured at the center of Girder No.4.

Run #	Horizontal (mm)	Vertical (mm)
1	-0.40	3.10
2	-0.71	2.75
3	-0.48	2.93
4	-0.66	2.74
5	-0.38	3.03
6	-0.31	3.23
7	0.51	3.14
8	0.93	2.47
9	NA	NA
10	NA	NA
11	0.56	3.02
12	0.46	3.14
13	0.11	6.20
14	0.30	6.16
15	0.23	6.23
16	0.11	6.13

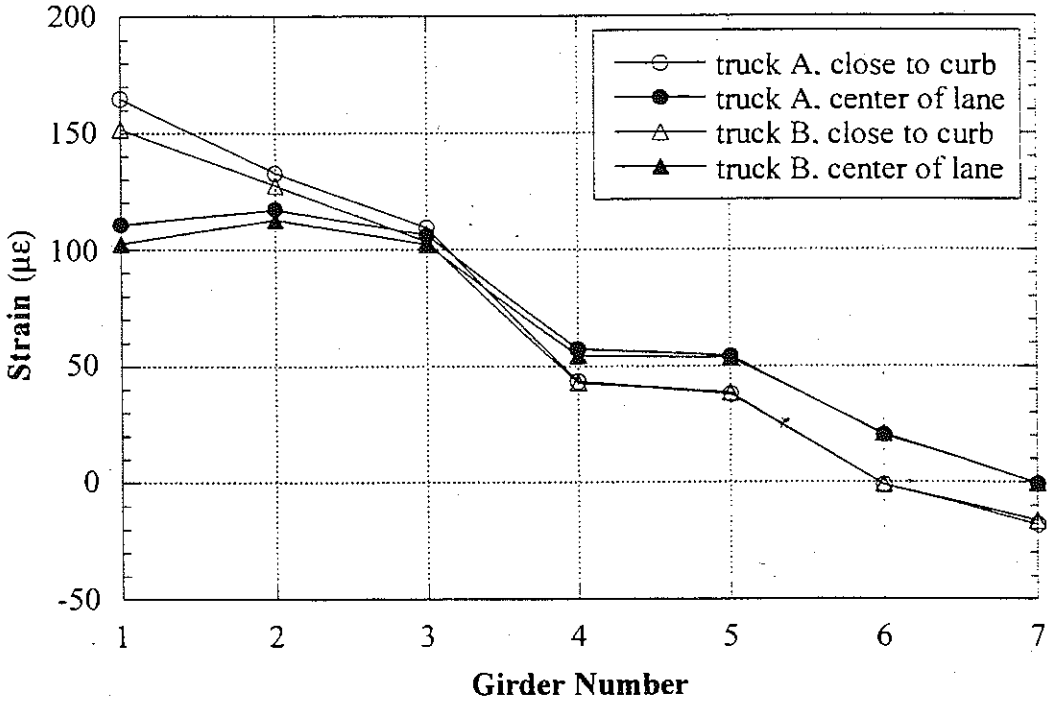

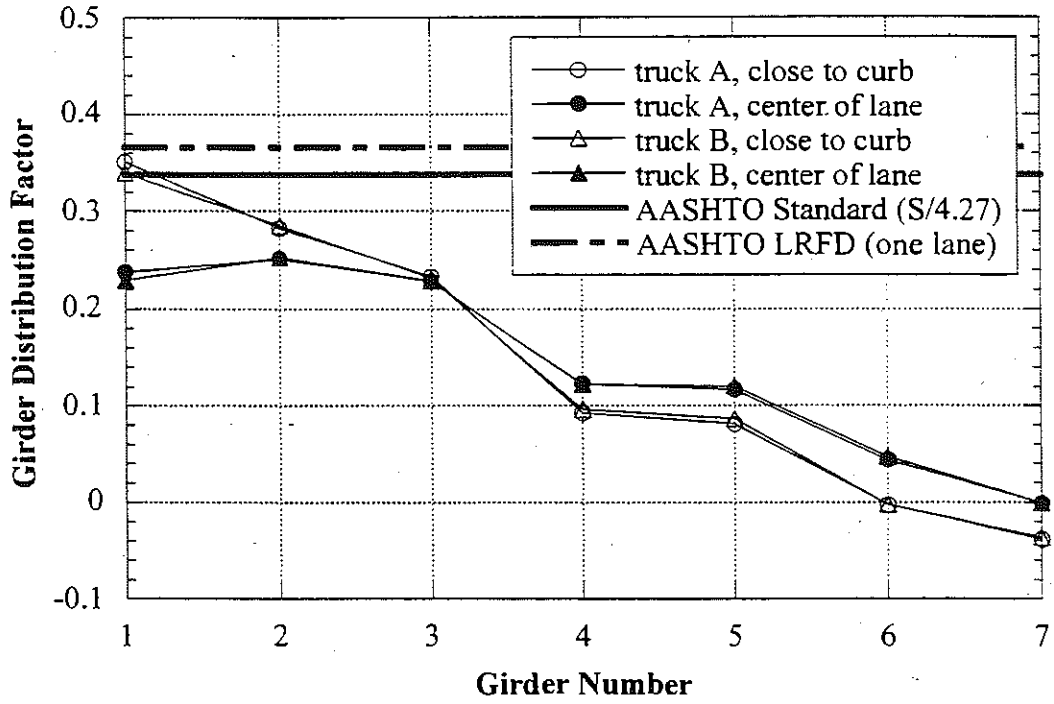

Figure 6.9. South Lane, Crawling Speed, US223/RR (B02-46062)

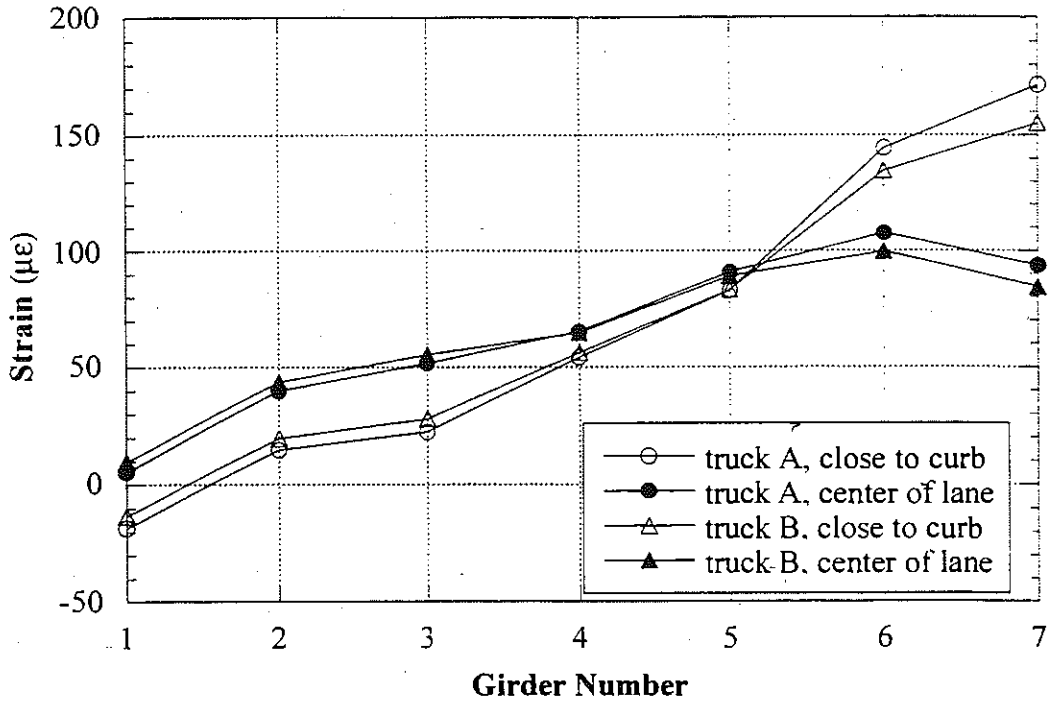

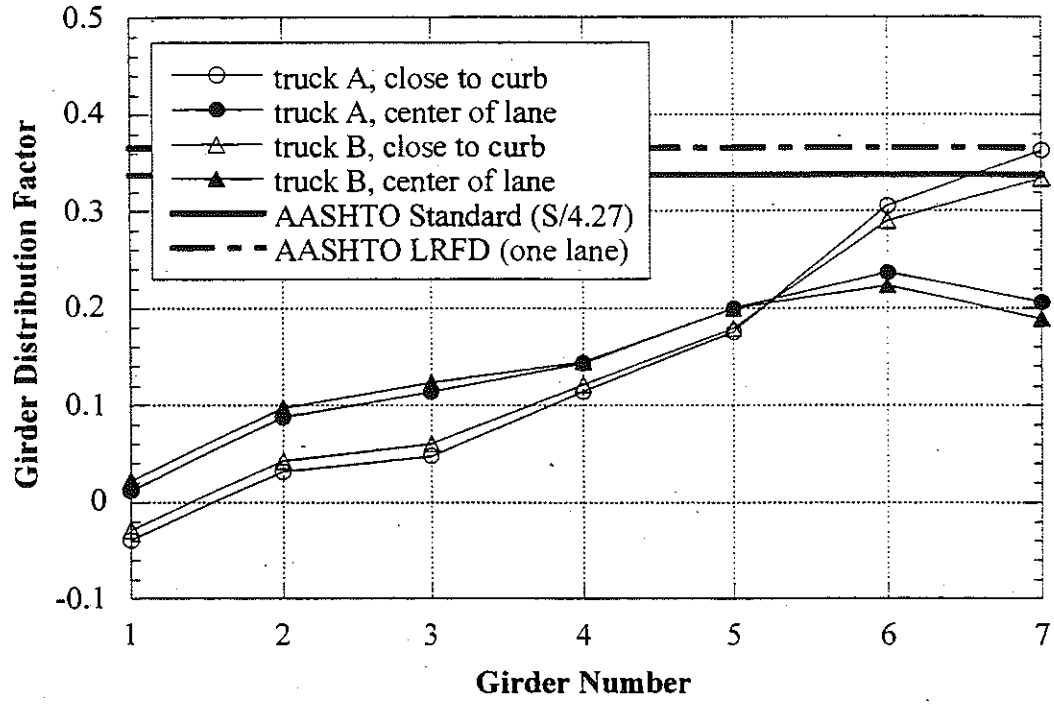

Figure 6.10. North Lane, Crawling Speed, US223/RR (B02-46062).

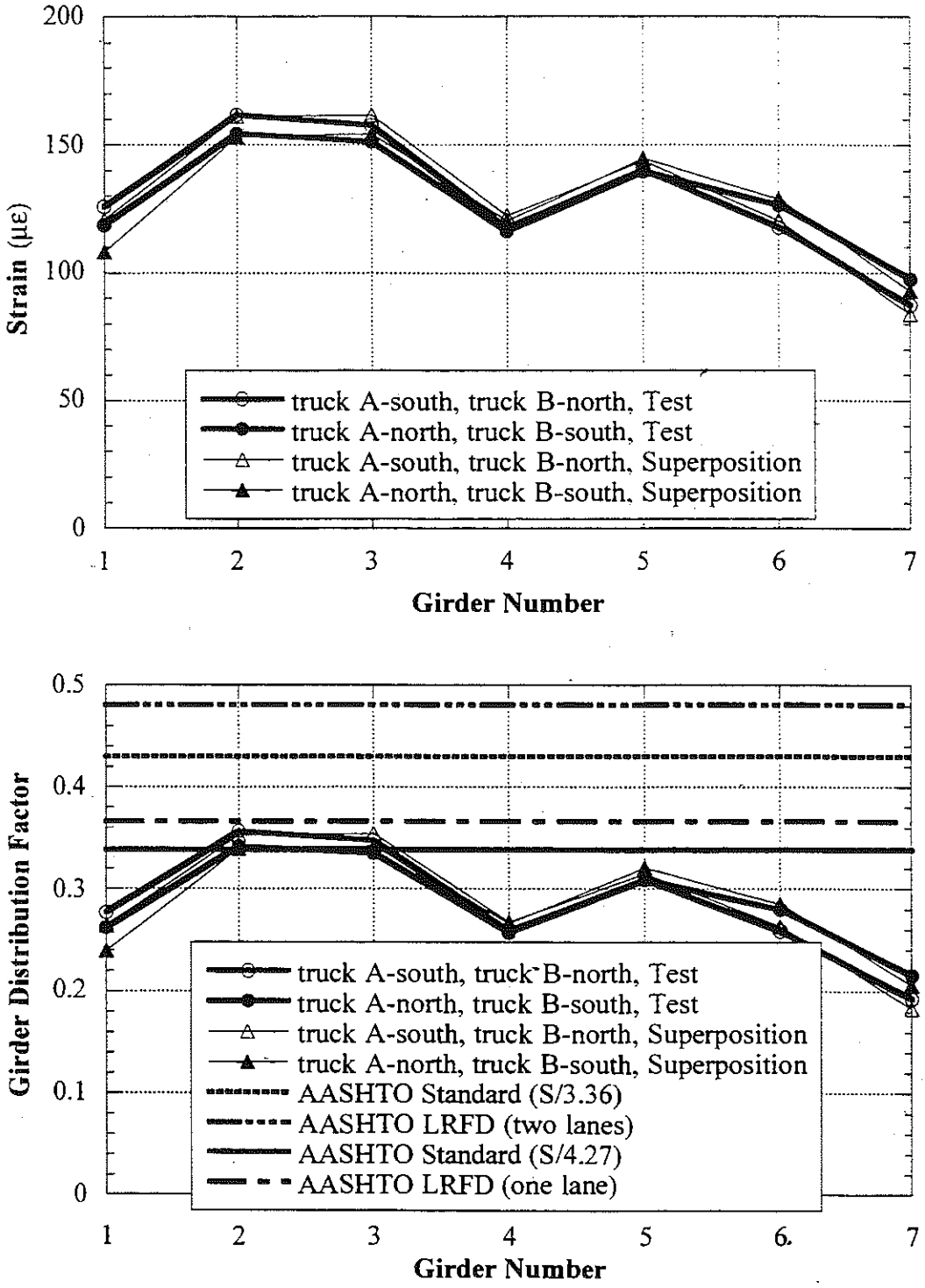

Figure 6.11. Side-by-Side Loading, Center of Lane, Crawling Speed, US223/RR (B02-46062).

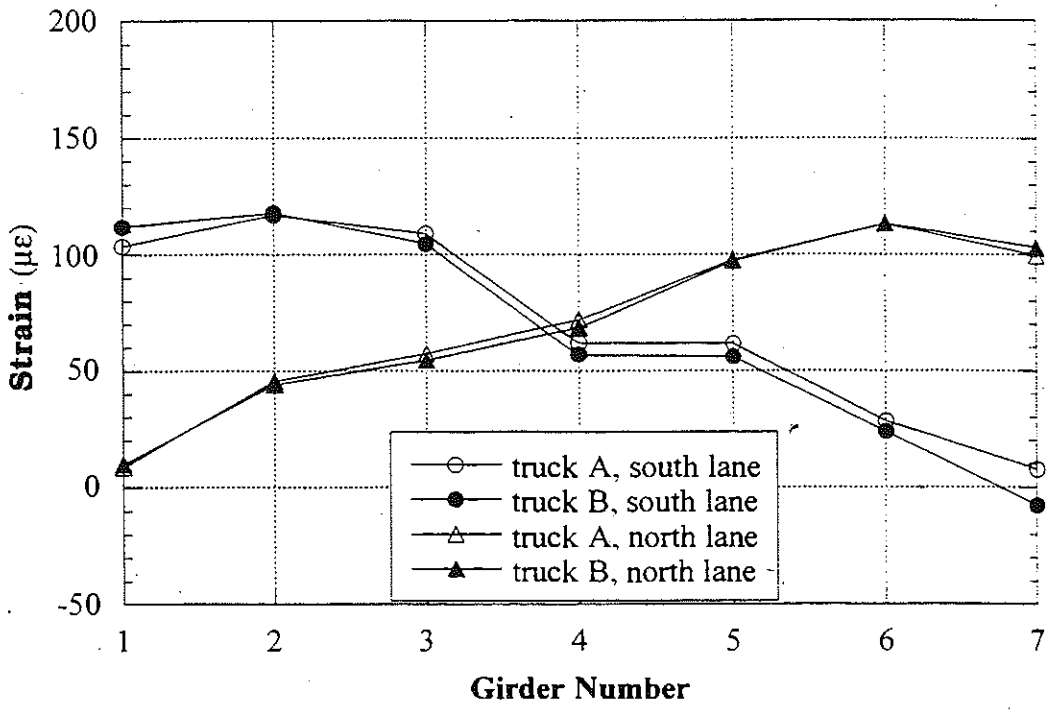

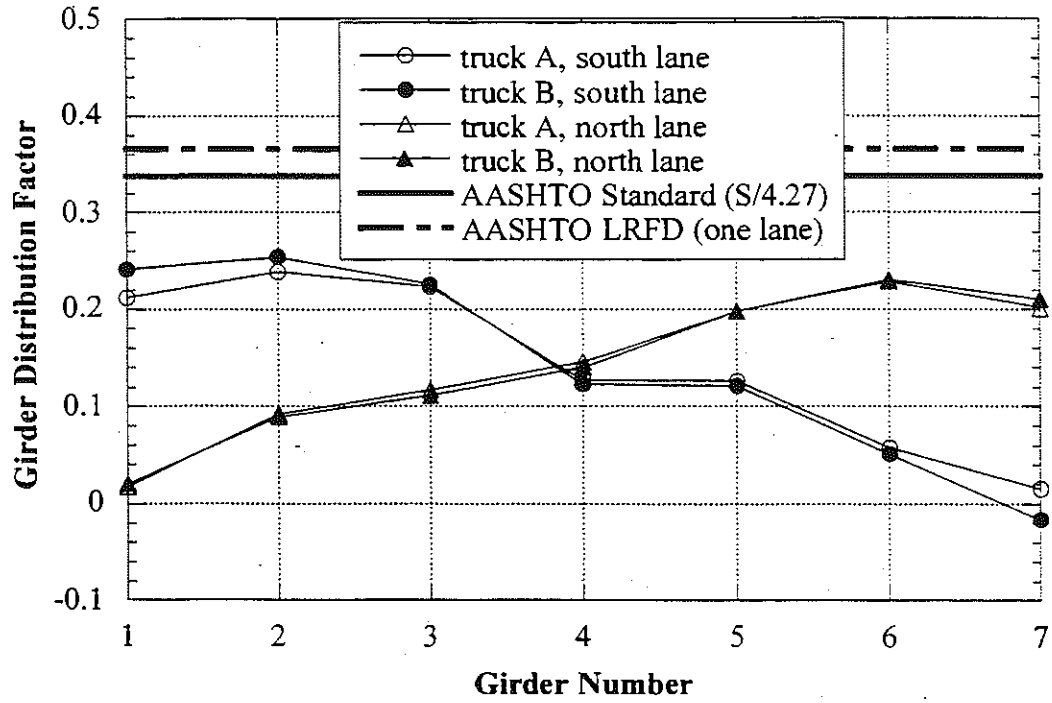

Figure 6.12. Strain and GDF under One Truck Loading at Regular Speed, US223/RR (B02-46062).

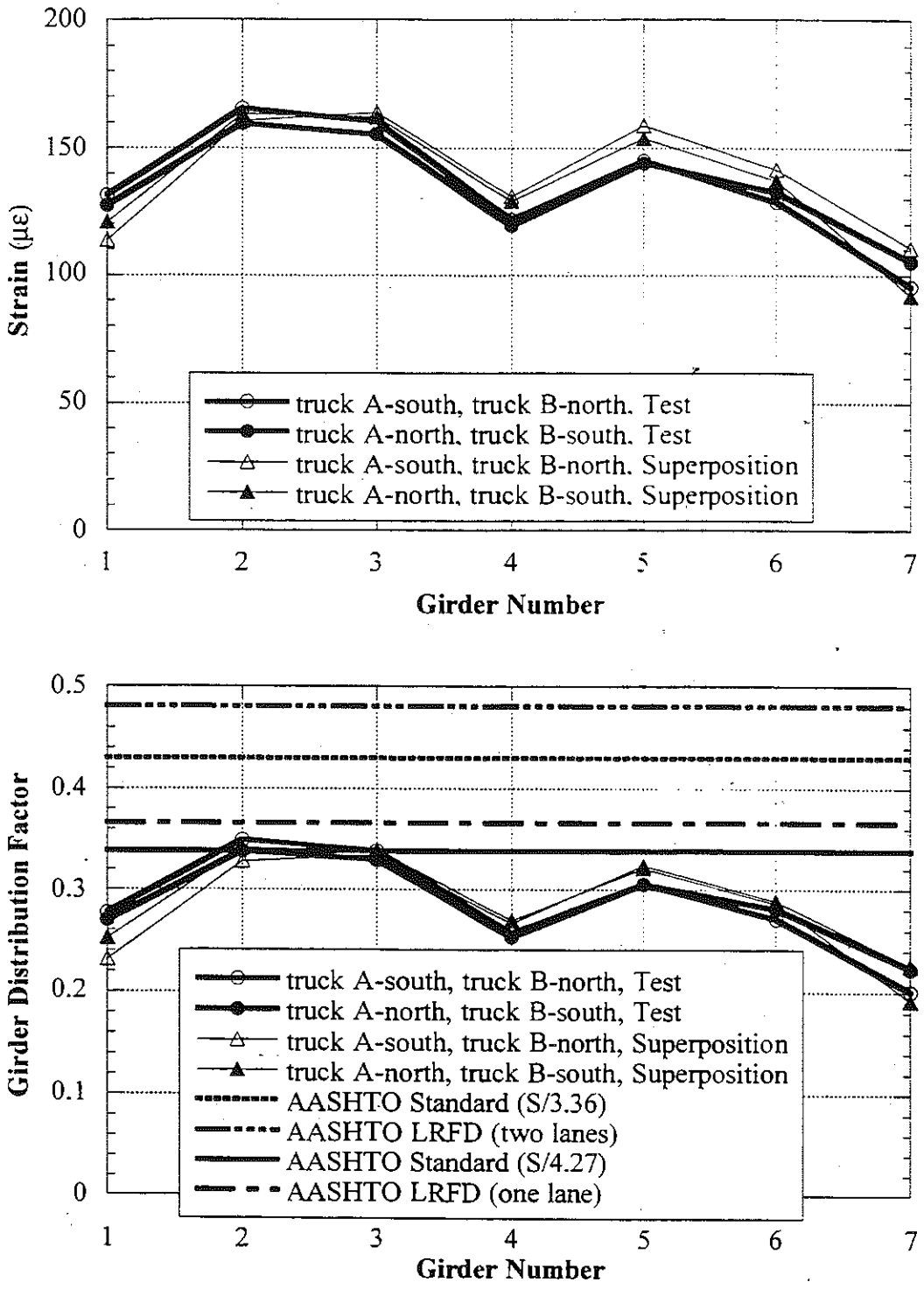

Figure 6.13. Strain and GDF under Side-by-Side Loading at Regular Speed, US223/RR (B02-46062).

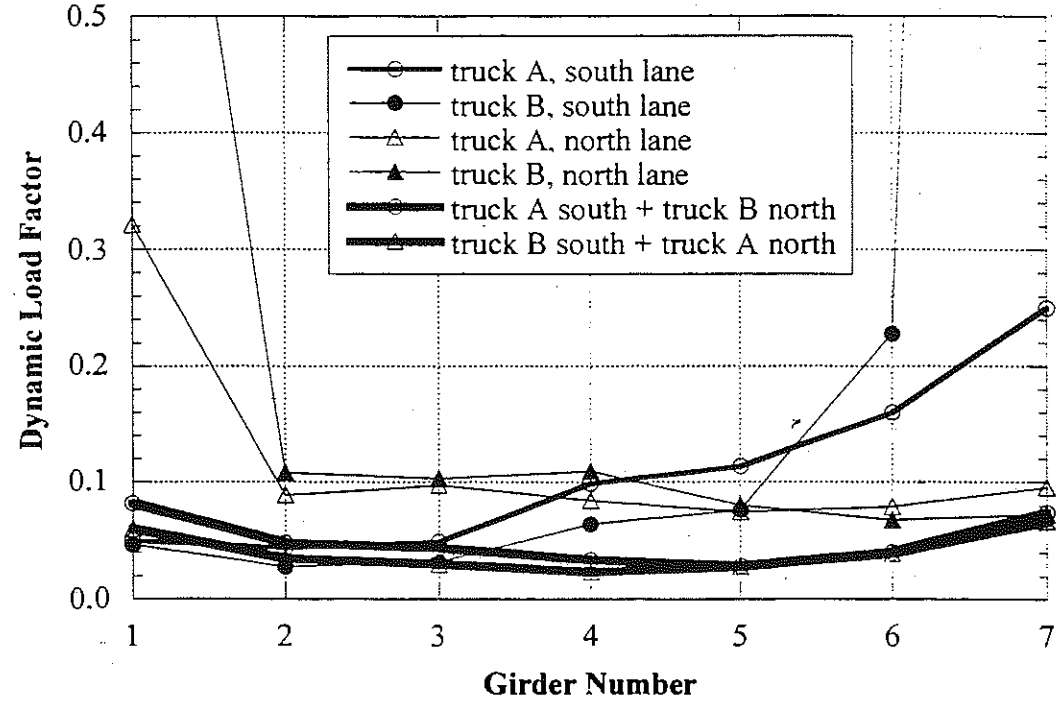

Figure 6.14. Dynamic Load Factors, US223/RR (B02-46062).

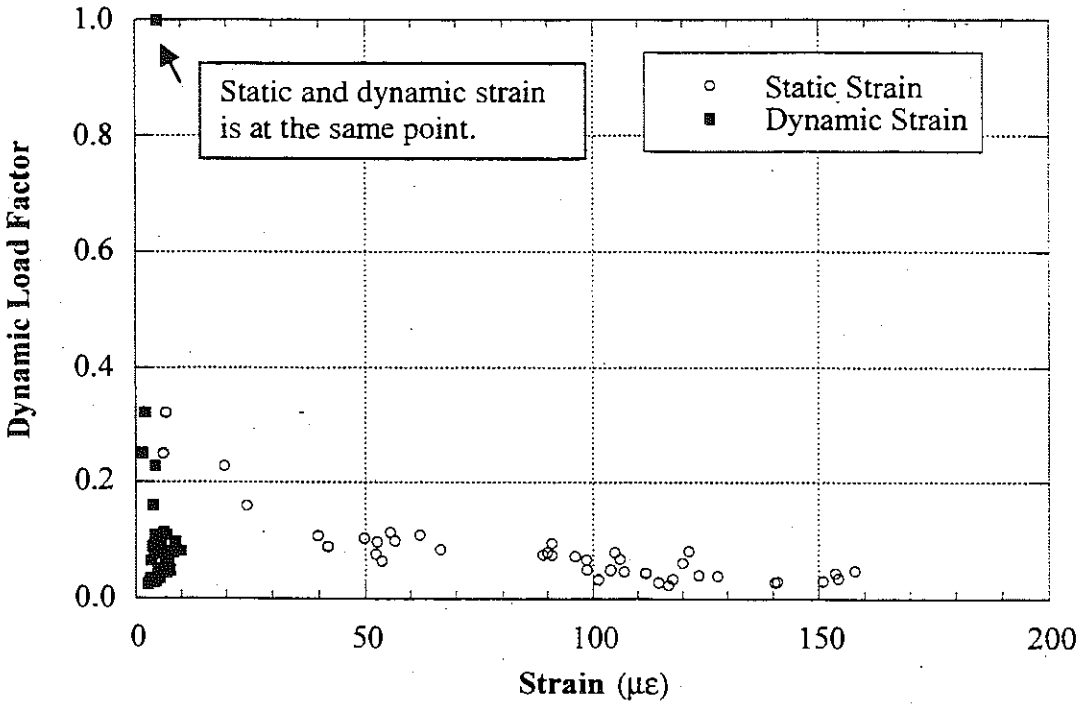

Figure 6.15. Strain vs. Dynamic Load Factors, US223/RR (B02-46062).

Note:

Intentionally left blank

7. Bridge on M-66 over Abandoned NYC Railroad, near Colon. (R01-78054, M66/RR)

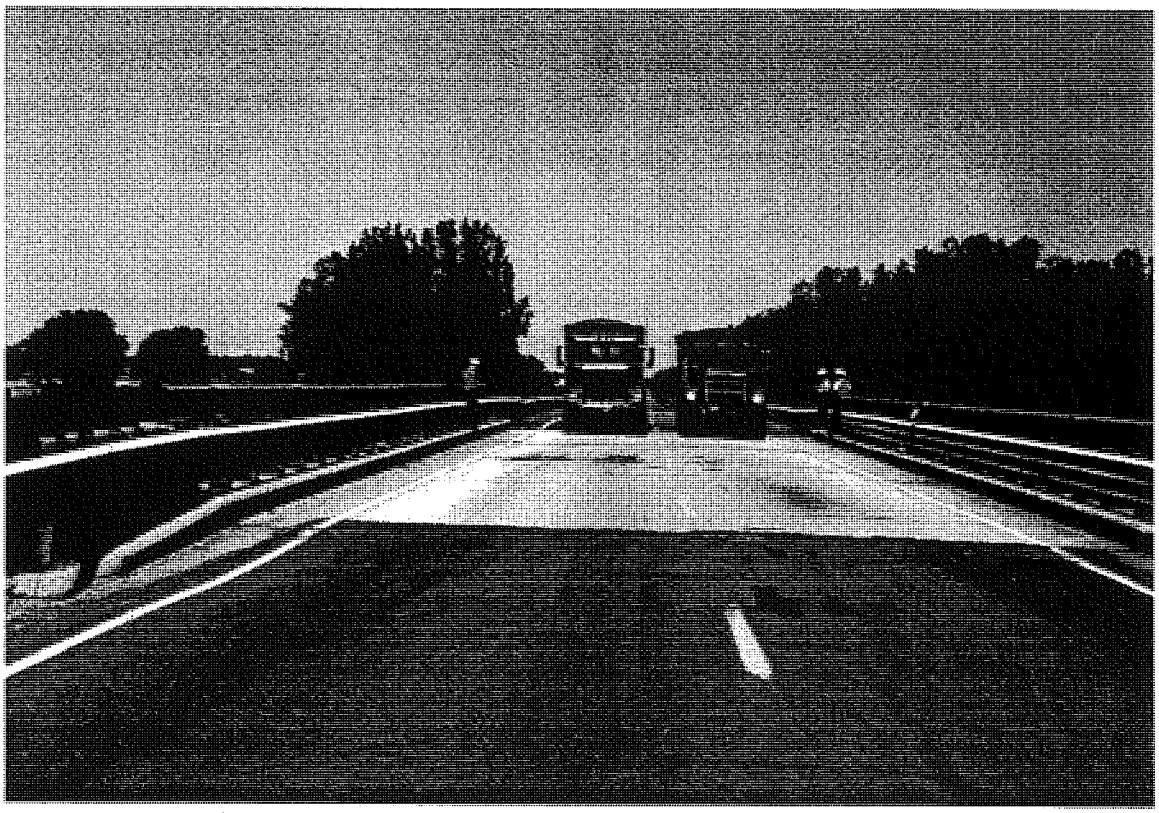

7.1 Description

This bridge was built in 1965 and it is located on M-66 over abandoned NYC railroad near Colon in St. Joseph County, Michigan. It is a three span, simply supported composite structure with six steel girders spaced at 1.9 m. The total bridge length is 49.2 m. The total length of the main span is 21.9 m with a cantilever overhang. The clear span length is 18.8 m with skew of 11 degrees. The bridge carries an average daily traffic (ADT) of 3,500. The bridge has a load rating of 1,148 kN. according to the Michigan Structure Inventory. The test was performed on the center span.

7.2 Instrumentation

Strain transducers were installed on the bottom flanges of girders at midspan (Figure 7.3) of the main span. In addition, wireless transmitters were installed at the same locations so that the accuracy of

wireless transmitters could be verified. The results comparing two different strain transducer systems, one with cables and the other with wireless transmitters are shown in Section 4.5. The reflector for the PSM-R device from Noptel was installed at the girder No. 3 to measure deflection. The bridge test was performed on May 27, 1999.

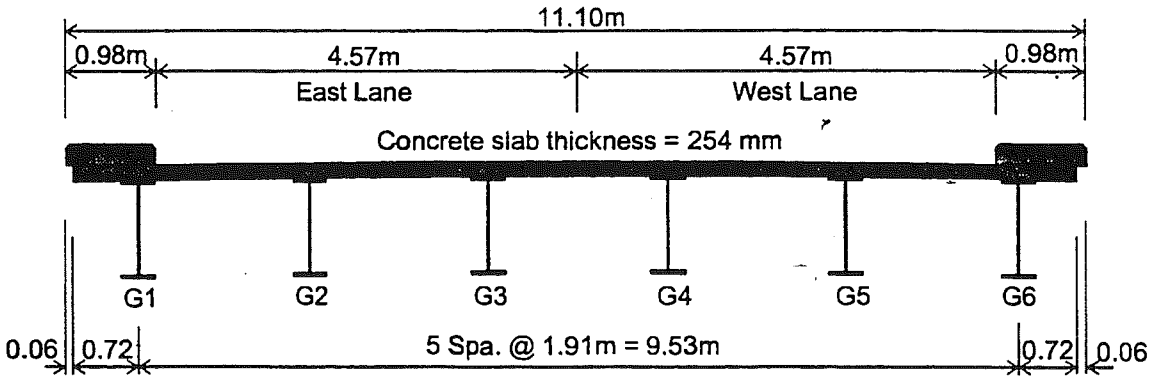

Figure 7.1. Cross-Section of the Bridge M66/RR (R01-78054), St. Joseph County.

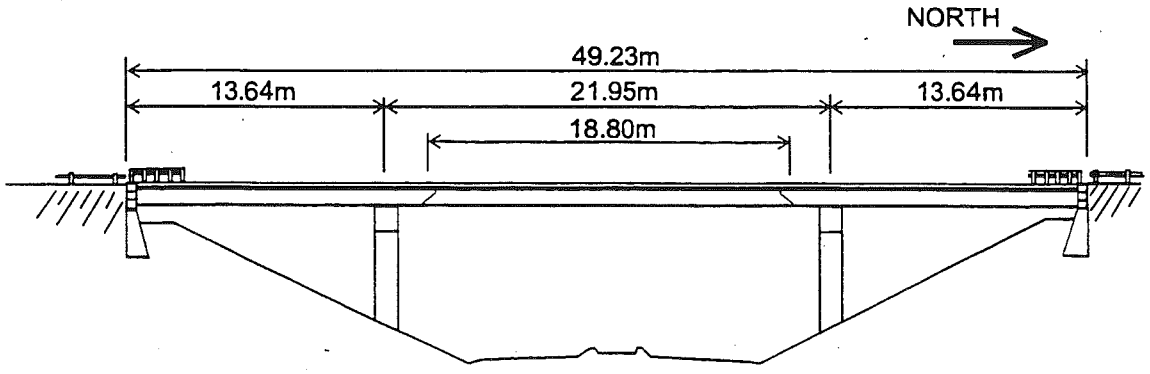

Figure 7.2. Elevation of the Bridge M66/RR (R01-78054), St. Joseph County.

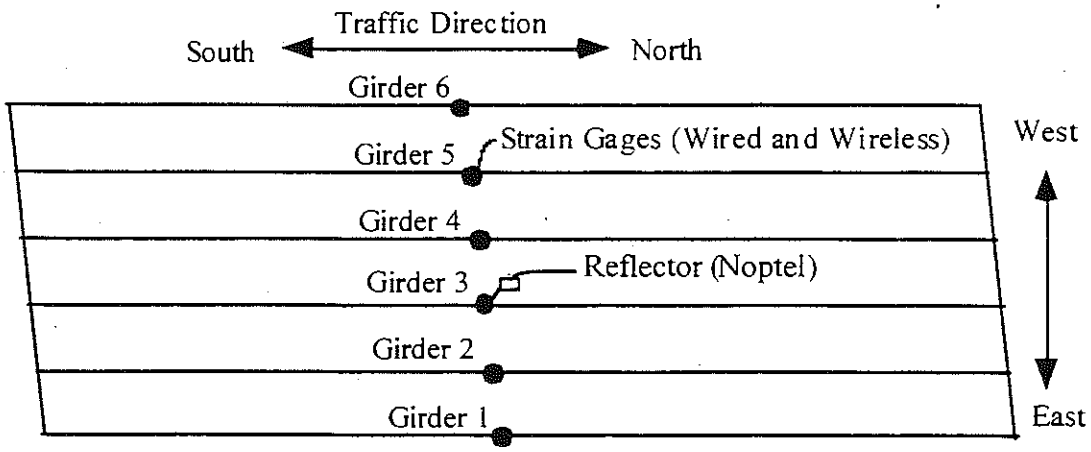

Figure 7.3. Strain Gage Locations in Bridge M66/RR (R01-78054).

7.3 Truck Loads

The girder distribution factors (GDF) and dynamic load factors (DLF) were calculated using the strains measured at midspan. The bridge was loaded with two 11-axle trucks (three-unit vehicles). The gross vehicle weight and the truck axle configurations are shown in Figures 7.4 and 7.5.

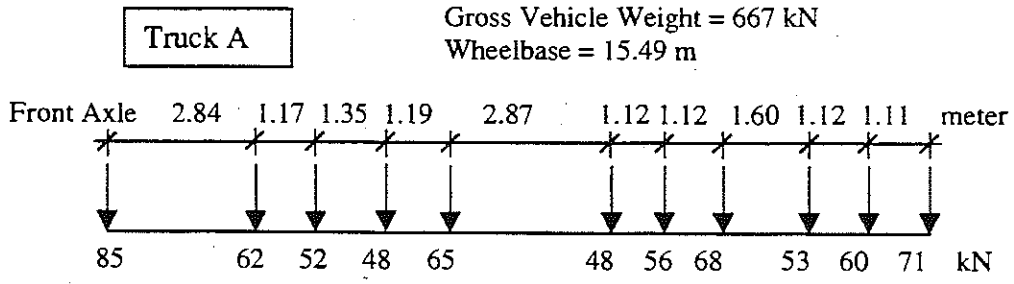

Figure 7.4. Truck A Configuration, Bridge M66/RR (R01-78054).

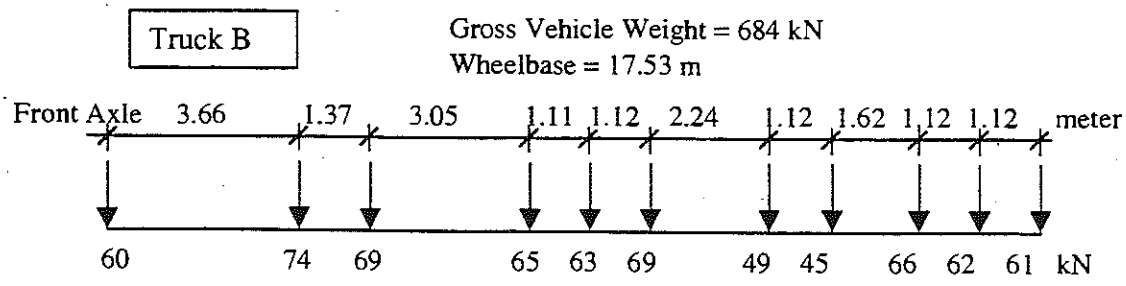

Figure 7.5. Truck B Configuration, Bridge M66/RR (R01-78054).

A total of 16 load cases were considered, as shown in Table 7.1. First each truck was driven by itself at the center of one lane, at crawling speed. Then, the same truck was driven close to the curb. The runs in the center of the lane were repeated at a normal highway speed (about 40km/h for this location). The same was repeated for the other lane. Finally, two trucks were driven simultaneously, side-by-side, at crawling speed and normal highway speed. For side-by-side cases, the runs were repeated after the trucks switched the lanes, i.e. first truck A was in East lane, and B in West lane, then truck A was in West lane, and B in East lane.

Table 7.1. Sequence of Test Runs, Bridge M66/RR (R01-78054).

Run#	Truck	Lane Side	Position in Lane	Truck Speed
1	Truck A	West	Center	Crawling
2	Truck A	West	Curb	Crawling
3	Truck B	West	Center	Crawling
4	Truck B	West	Curb	Crawling
5	Truck B	West	Center	40 km/h
6	Truck A	West	Center	40 km/h
7	Truck A	East	Center	Crawling
8	Truck A	East	Curb	Crawling
9	Truck B	East	Center	Crawling
10	Truck B	East	Curb	Crawling
11	Truck B	East	Center	40 km/h
12	Truck A	East	Center	40 km/h
13	Truck A and B	both	Center	Crawling
14	Truck B and A	both	Center	Crawling
15	Truck A and B	both	Center	40 km/h
16	Truck B and A	both	Center	35 km/h

7.4. Analysis Results

The three-dimensional finite element method (FEM) was applied to investigate the structural behavior of the bridge M66/RR (R01-78054). The concrete slab was modeled with isotrophic, eight node solid elements, with three degrees of freedoms at each node. The girder flanges and web were modeled using three-dimensional, quadrilateral, four node shell elements with six degrees of freedom at each node. The structural effects of the secondary members, such as the sidewalk and parapet, were also taken into account in the finite element analysis models.

Two cases of the boundary conditions were employed in the FEM models. In the first FEM model, it was assumed that the supports can be represented by a hinge at one end, and a roller with a hinge at the other end. In the other FEM model, it was assumed that both supports are hinged, with no movement in horizontal direction.

Figure 7.6 illustrates the mesh of the FEM model, and Figure 7.7 shows the deformed shape of the bridge when it is loaded with two trucks side-by-side.

Figure 7.8 shows the results of the finite element analysis for two trucks side-by-side (Run 13). It includes the experimental results and analytical results for the two considered models. The FEM results show that the maximum strain at the most heavily loaded girder is about 230 με, while the maximum strain recorded from the test is about 200 με. In addition, the experimental response lies between the two considered analytical models. This indicates that a partial fixity exists at the supports of the bridge.

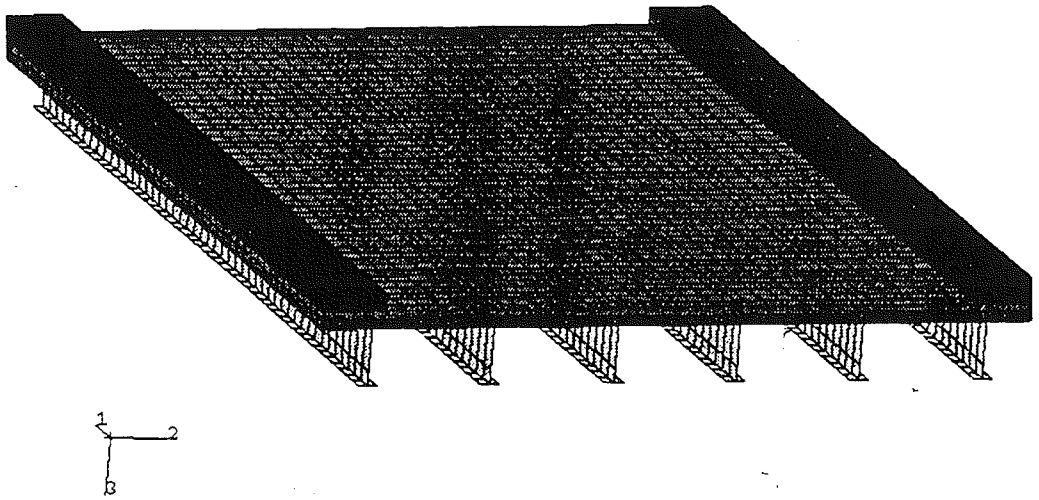

Figure 7.6. The Mesh of the Finite Element Model.
M66/RR (R01-78054).

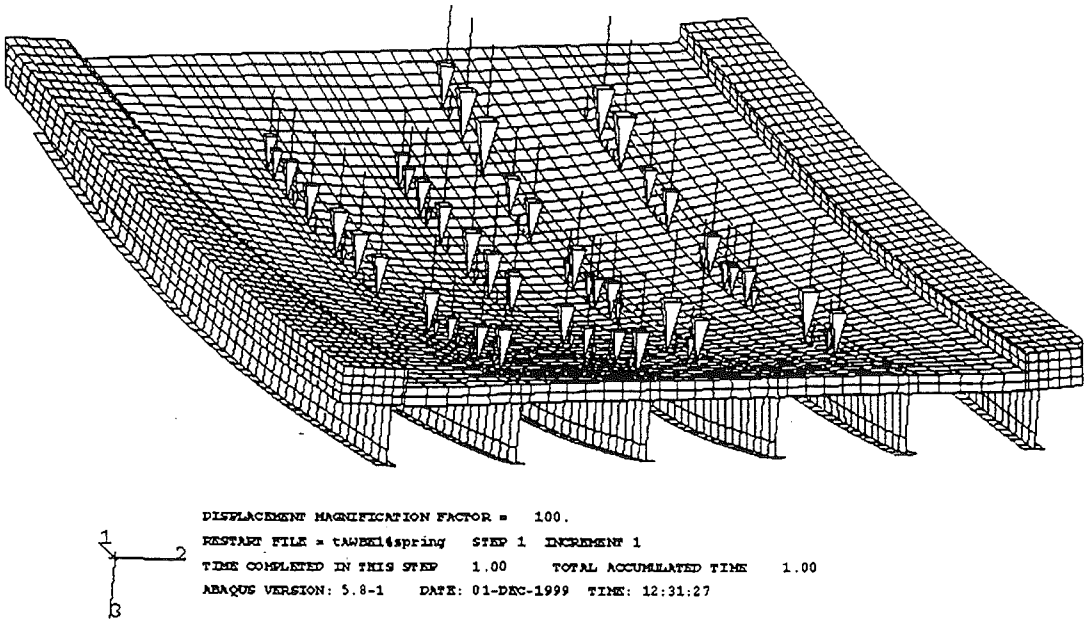

Figure 7.7. The Deformed Shape of the Bridge under Two Lane Loading.
M66/RR (R01-78054).

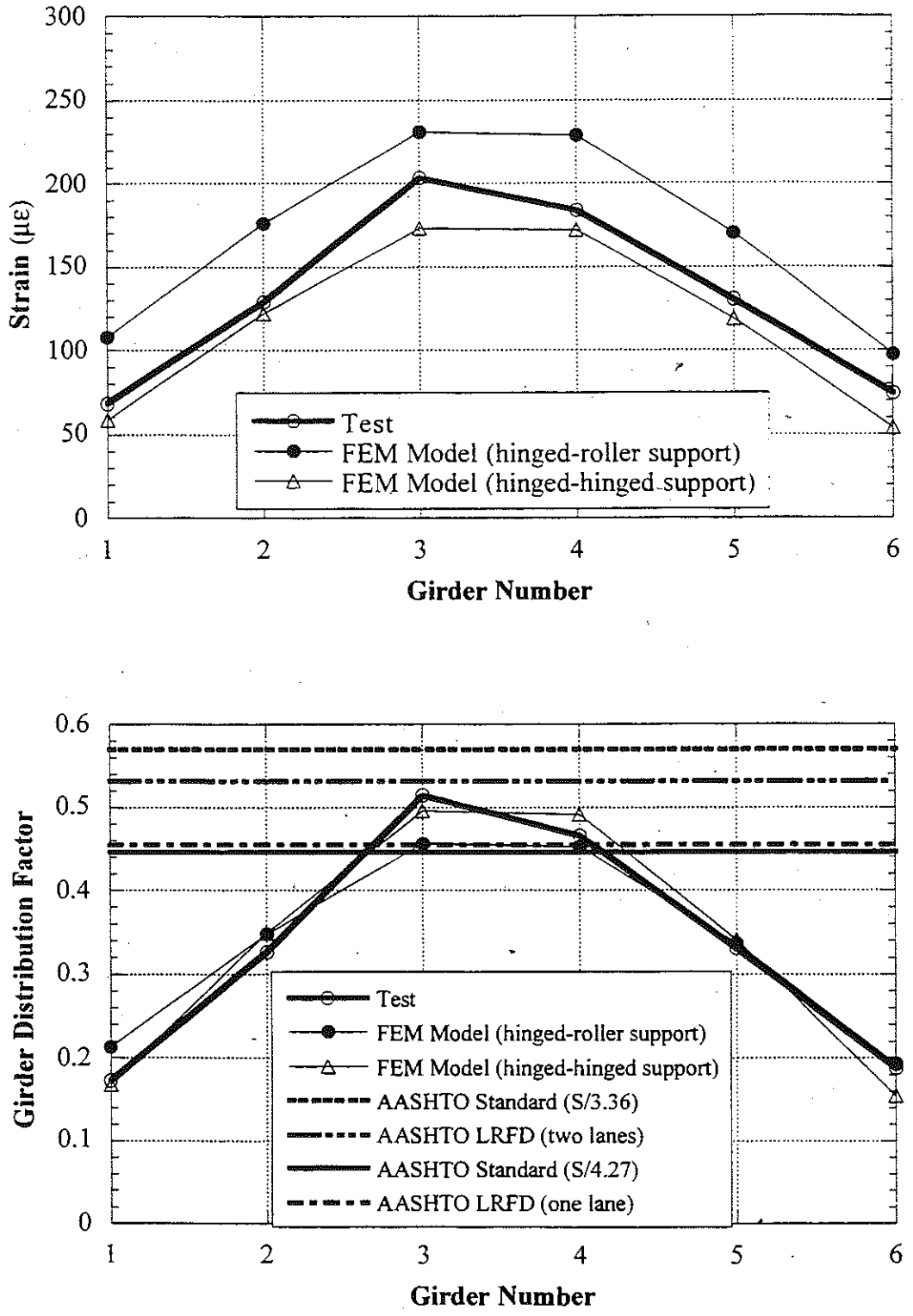

Figure 7.8. Results of the Finite Element Analysis for Two Lane Loading (truck A-east lane, truck B-west lane), M66/RR (R01-78054).

7.5. Test Results.

The resulting strains and GDF's are shown in Figure 7.9 through 7.13. Figures 7.9 to 7.11 present the results of all crawling-speed (static) tests. Figures 7.9 to 7.10 present static strains and GDF's for one truck on the bridge. The maximum strain due to a single truck was observed in the middle girders, about 120 με. This corresponds to about 24 MPa.

Figure 7.11 shows static strains and GDF's from side-by-side static load tests. For two vehicles side-by-side the maximum static strain is about 200 με (which corresponds to 40 MPa). The superposition of strains due to a single truck in West and East lanes produces almost the same results as strain due to two trucks side-by-side.

For comparison, GDF are also calculated according to AASHTO Standard (1996) and AASHTO LRFD Code (1998). Two cases were considered, a single lane loaded, and two lanes loaded. The resulting GDF's are shown in Figures 7.9 through 7.13.

The results indicate that code-specified GDF's are conservative. GDF's specified for a single lane are not sufficient for two lane load cases. However, the absolute values of the values of the strains are less than 200 με for the heaviest load case (two fully-loaded trucks side-by-side). Therefore, the total load effect per girder estimated using GDF specified for single lane is also conservative, considering that the stresses found from the test were lower than the FEM results, as shown in the Figure 7.8.

Figures 7.12 and 7.13 shows the resulting strain and distribution factors from normal speed tests. There is practically no difference between the crawling speed and normal speed results.

Dynamic load factor (DLF) is defined in Section 4.4. In Figure 7.14, DLF's are plotted for all load cases involving normal speed (no dynamic load was measured for crawling speed runs). Dynamic load factors for exterior girders are high because the static strains in these girders are very low. In other words, large values of DLF in exterior girders correspond to load cases with a single truck in the opposite lane (resulting in very low static strain).

The relationship between DLF and static and dynamic strains is shown in Figure 7.15. The open circles correspond to static strain, ε_{stat}, and black solid squares correspond to dynamic strain, ε_{dyn}. For each static strain value (open circle), the corresponding dynamic strain is denoted by solid square (the numbers of circles and squares are same). It is clear from the Figure 7.15 that dynamic strains are less than 20 με for all the cases while the static strain can exceed 200 με in normal speed test. The dynamic load factor corresponding to the maximum strain caused by two trucks side-by-side, is less than 0.10 for the most heavily loaded girder (Girder No. 3). Dynamic strains remain nearly constant, while static strains increase as truck loading increases. This results in large dynamic load factors for low static strains.

Girder No. 3 was instrumented with remote deflection measurement device manufactured by Noptel. The reflector was installed at midspan. The result is shown in Table 7.2. The maximum deflection recorded during the test is 8.91 mm for girder number 3.

Two separate strain data acquisitions systems were used in the load test as parallel systems, one with cables and the other one with wireless transmitters, to verify the accuracy of the wireless system. The results are shown in Figures 4.14-16. In Figure 4.14 and Figure 4.15, the strains are plotted for a single truck passing in the west lane and then in the east lane. In Figure 4.16, the strains are shown for two

trucks side-by-side. It turned out that the wireless transmitter in girder 1 was not working. Therefore, there are no strains were recorded there. The difference between the strains obtained using the system with cables and wireless system is small, within 5%.

Table 7.2.. Maximum deflections measured at the center of Girder No.3, Bridge M66/RR (R01-78054)

Run #	Horizontal (mm)	Vertical (mm)
1	NA	NA
2	NA	NA
3	-0.70	3.60
4	-0.59	2.57
5	-0.67	3.89
6	-0.67	3.42
7	0.09	4.96
8	0.32	3.80
9	0	5.43
10	0.30	3.82
11	0	5.18
12	-0.09	5.04
13	-0.76	8.91
14	-0.67	8.91
15	-0.73	8.47
16	-0.76	8.65

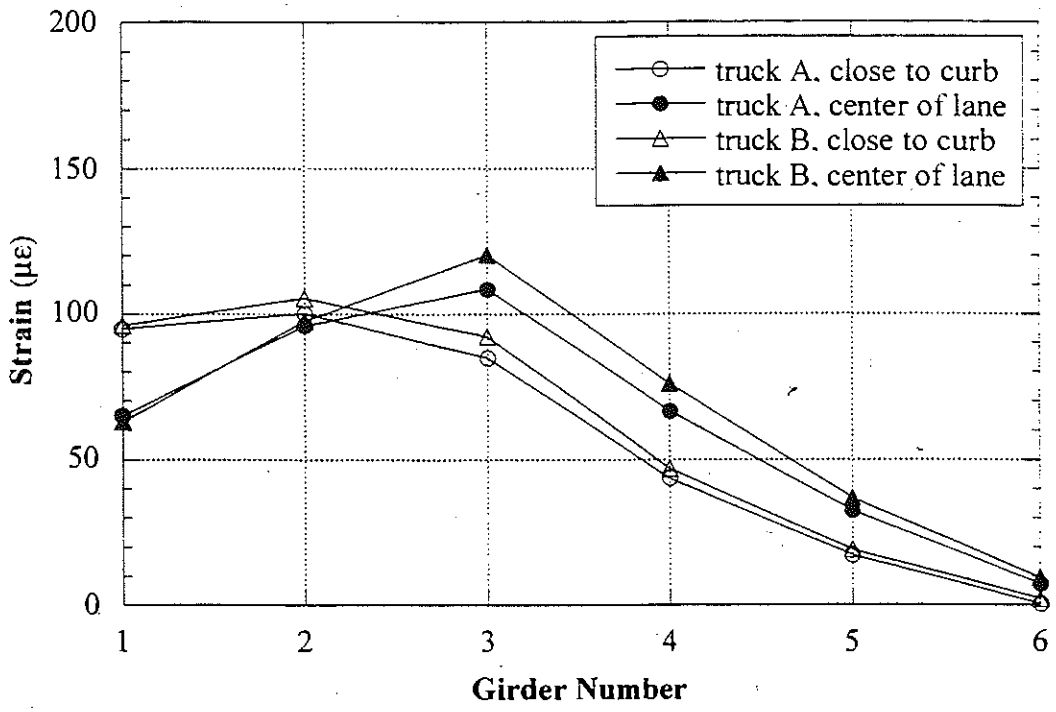

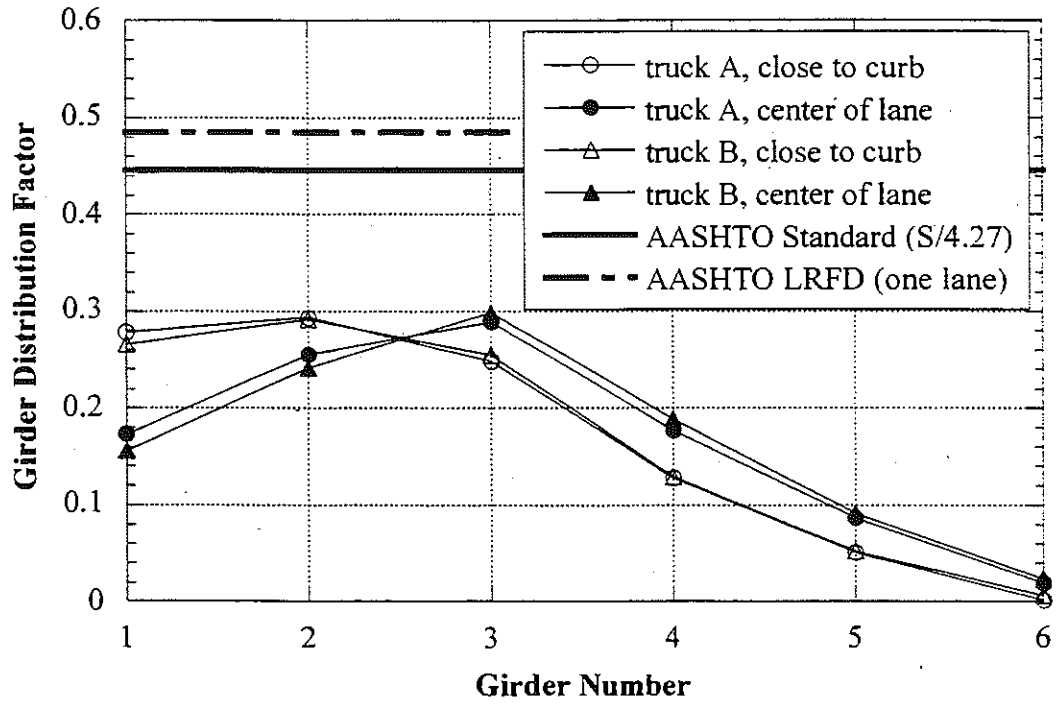

Figure 7.9. East Lane, Crawling Speed, M66/RR (R01-78054).

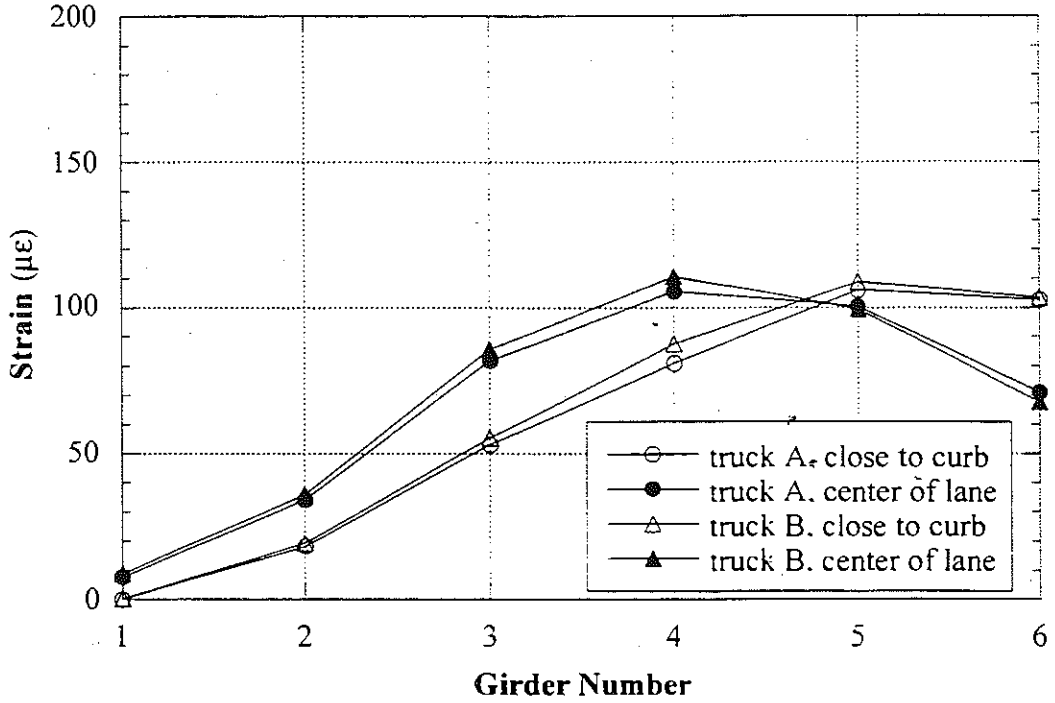

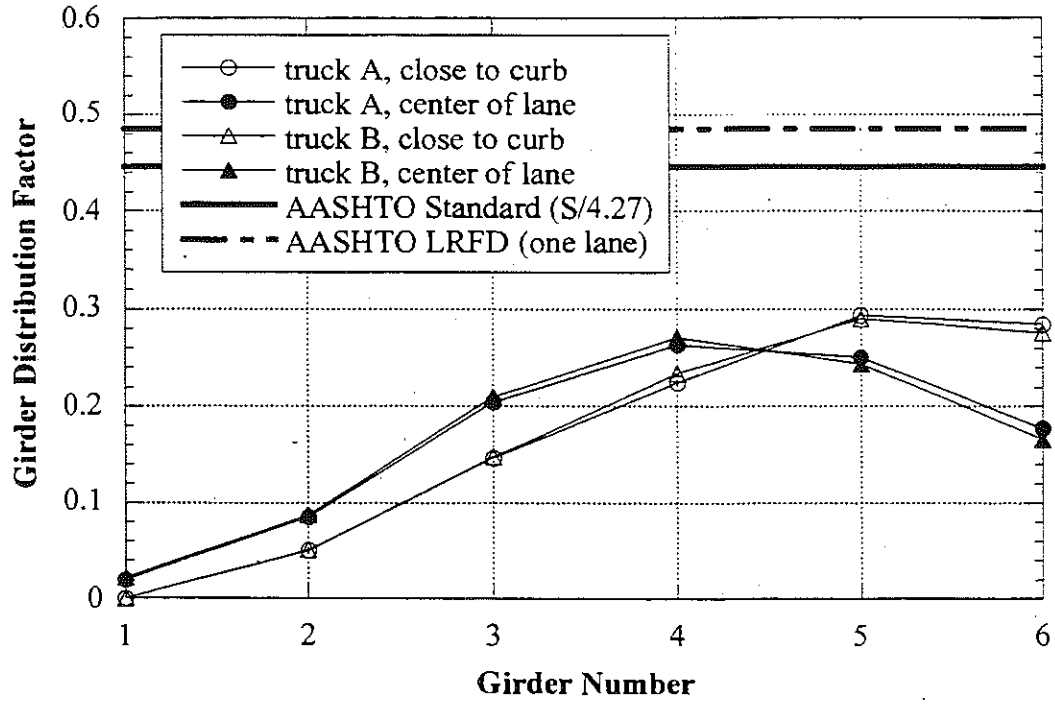

Figure 7.10. West Lane, Crawling Speed, M66/RR (R01-78054).

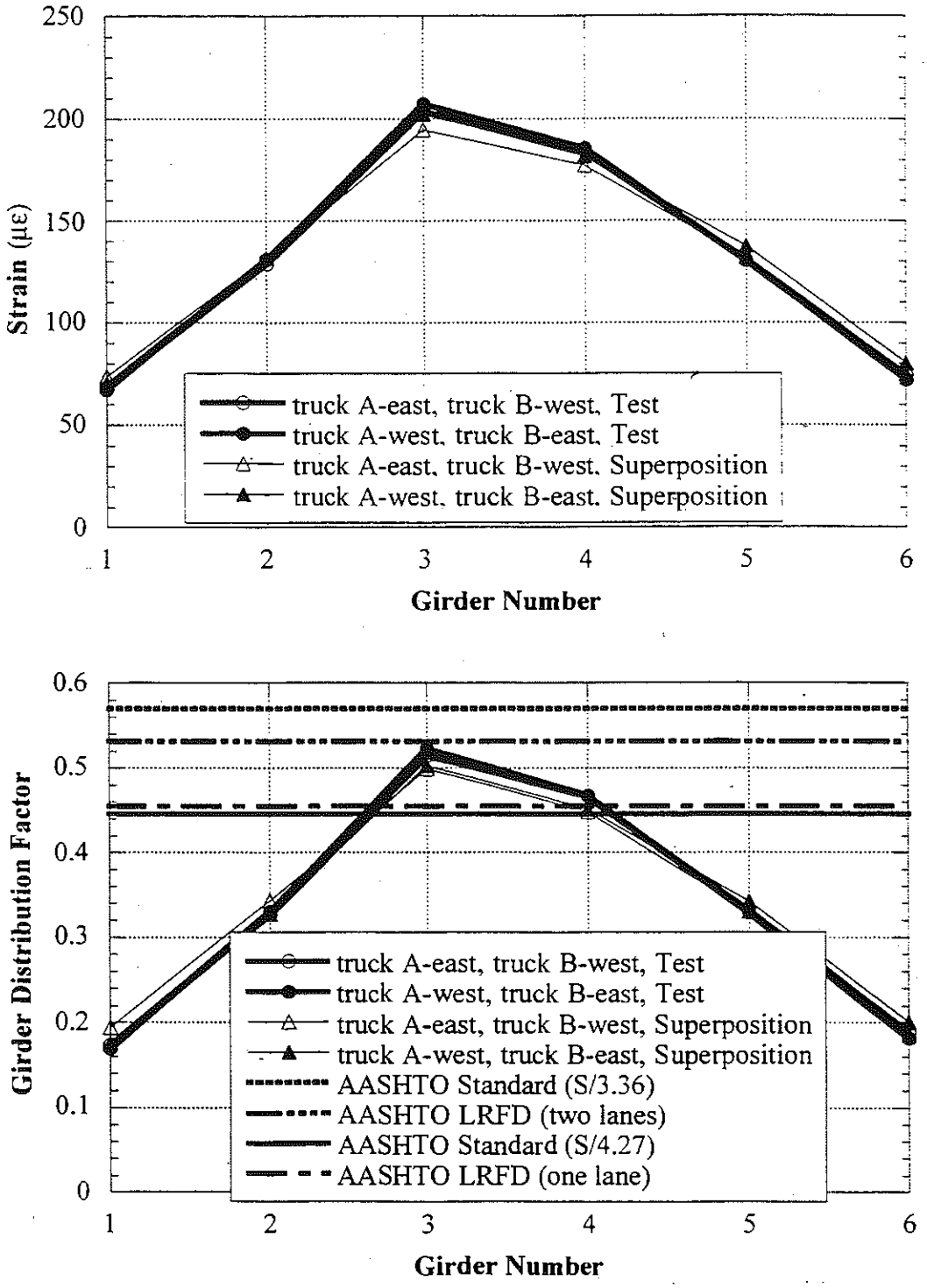

Figure 7.11. Side-by-Side Loading, Center of Lane, Crawling Speed, M66/RR (R01-78054).

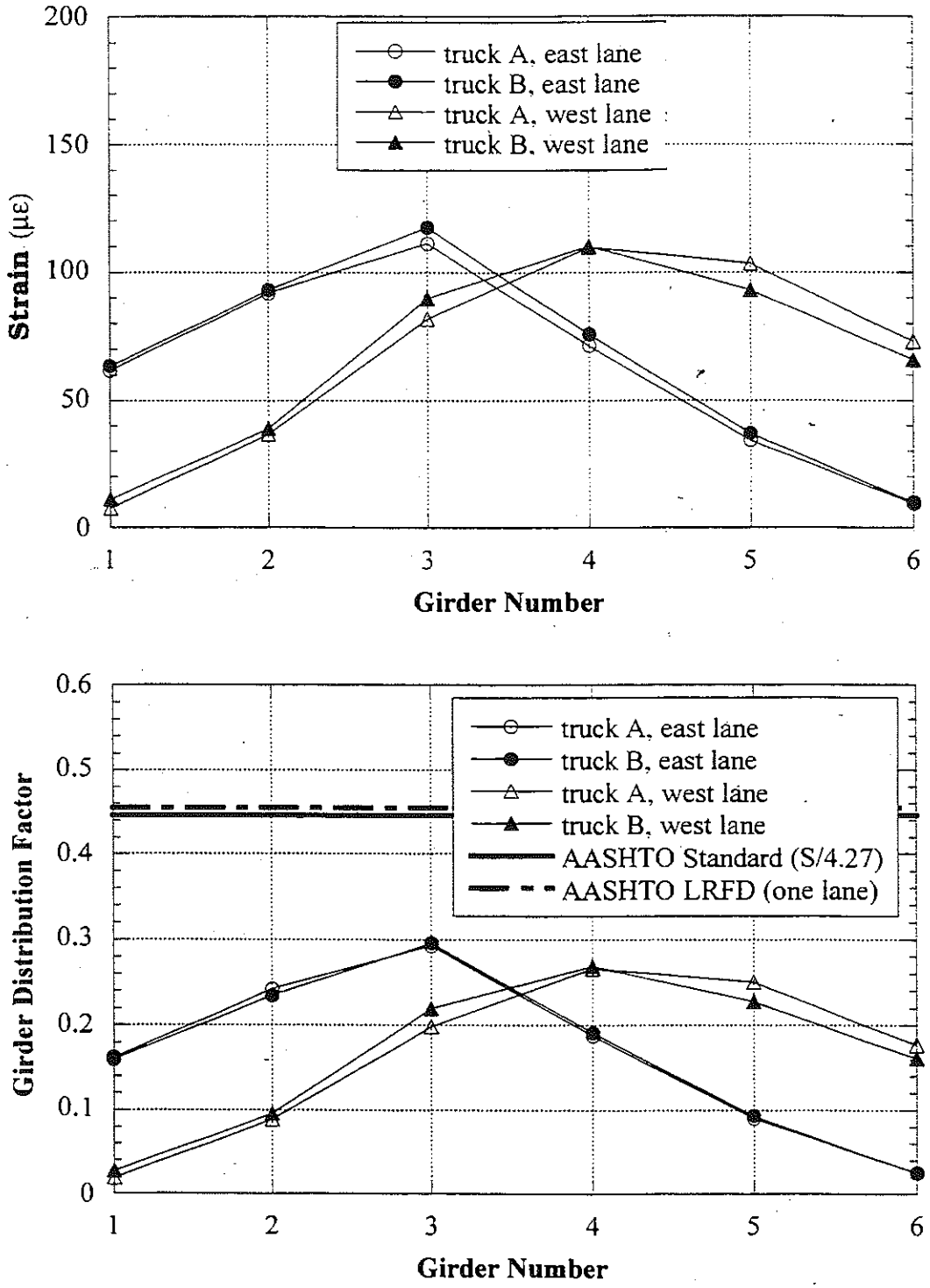

Figure 7.12. Strain and GDF under One Truck Loading at Regular Speed, M66/RR (R01-78054).

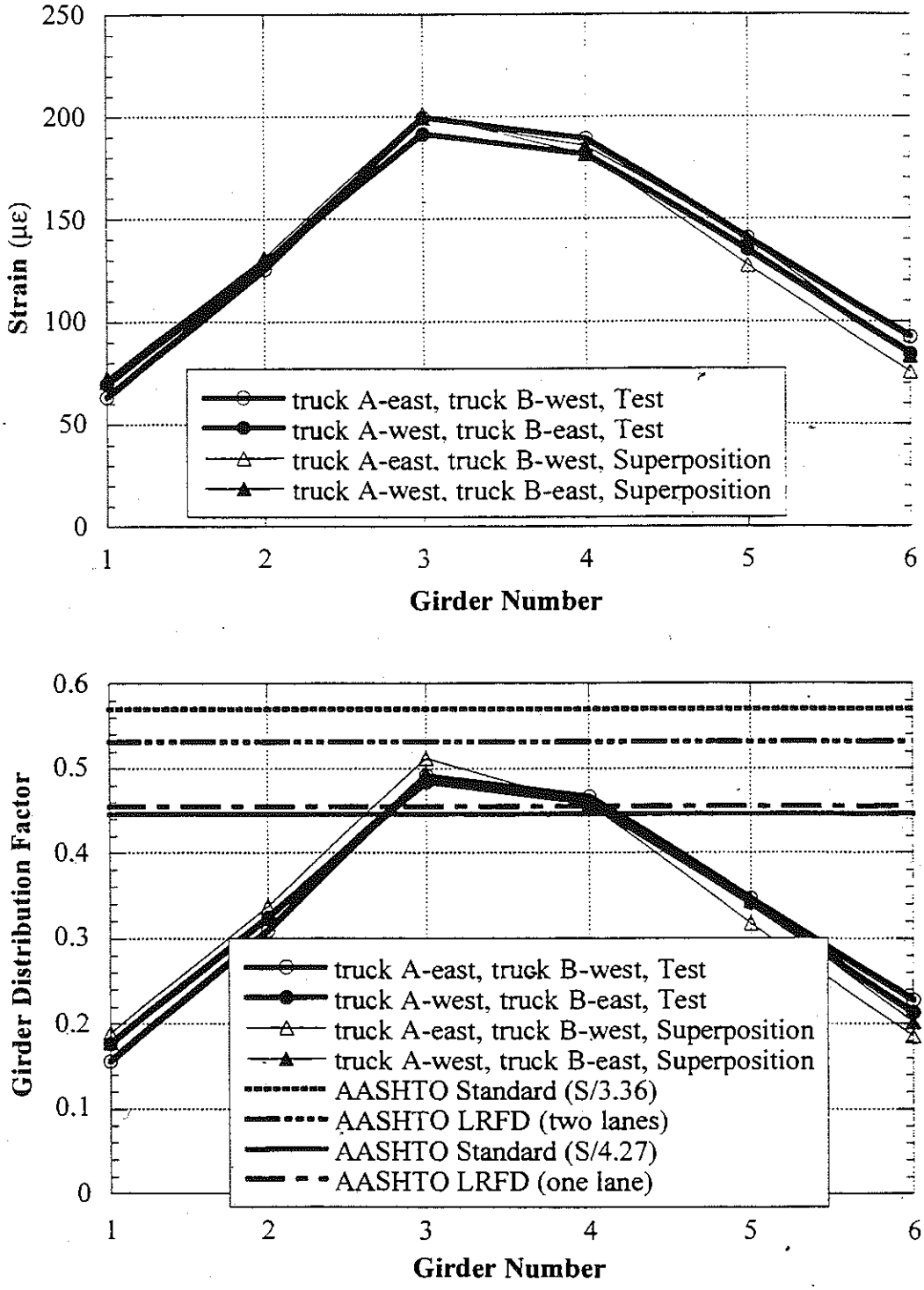

Figure 7.13. Strain and GDF under Side-by-Side Loading at Regular Speed, M66/RR (R01-78054).

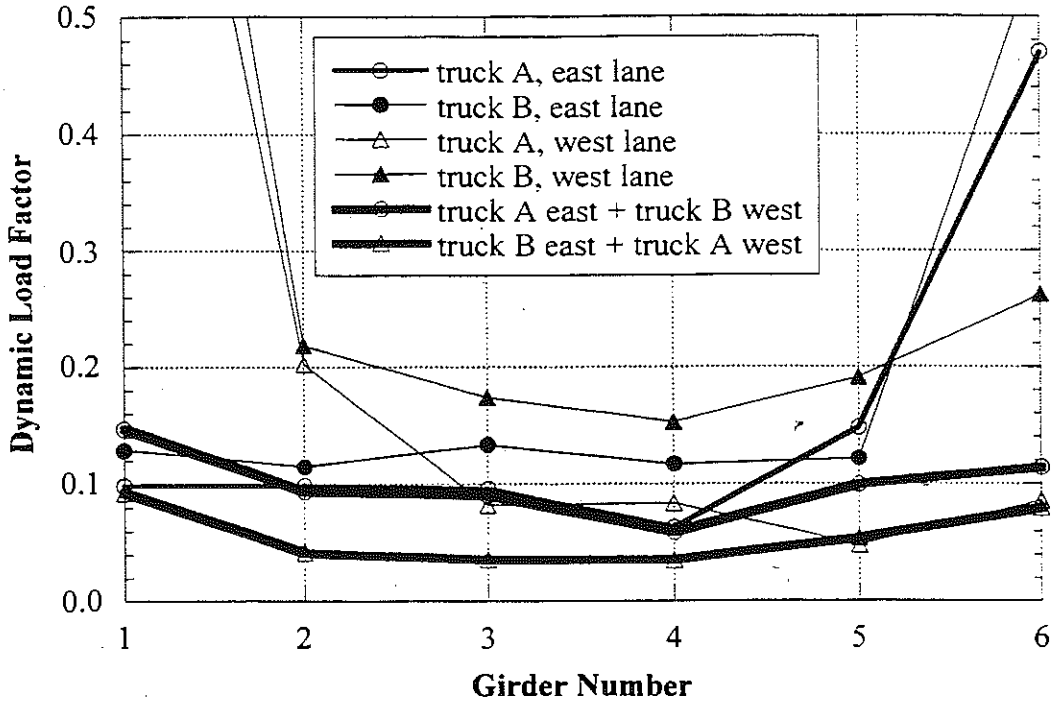

Figure 7.14. Dynamic Load Factors, M66/RR (R01-78054).

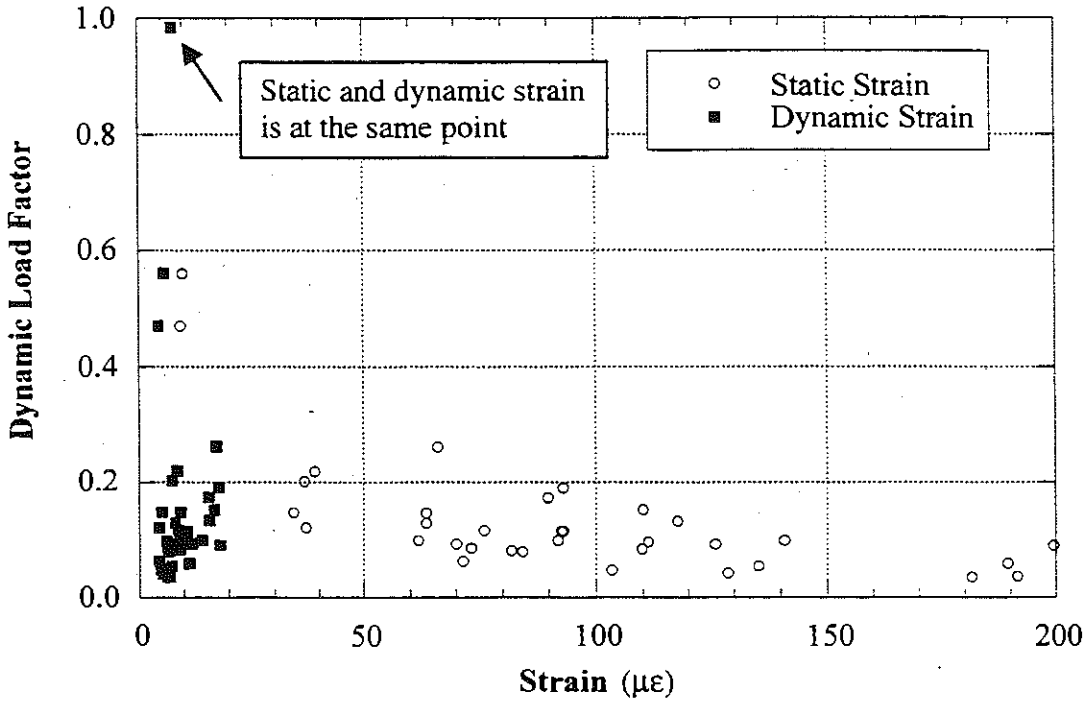

Figure 7.15. Strain vs. Dynamic Load Factors, M66/RR (R01-78054).

8. Bridge on M-19 over Mill Creek, in St. Clair County (B04-77012, M19/MC)

8.1 Description

This bridge was built in 1928 and it is located on M-19 over Mill Creek in St. Clair County, Michigan. The concrete deck was replaced in 1971. It is a single span, simply supported composite structure with nine steel girders spaced at 1.22 m. The total span length is 22.9 m, without any skew. The bridge has one lane in each direction and it carries an average daily traffic (ADT) of 3,500. The load rating is1,157 kN, according to the Michigan Structure Inventory.

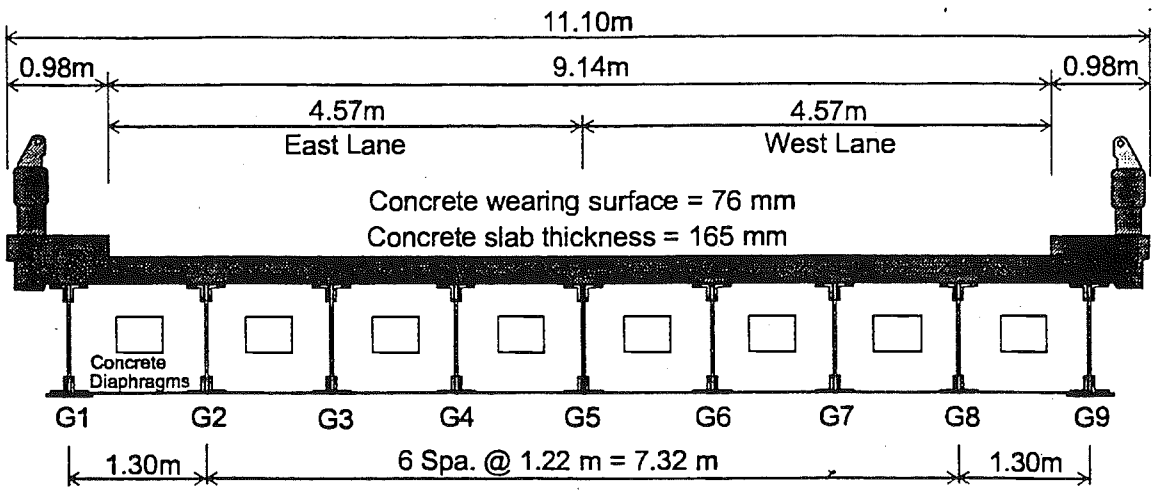

Figure 8.1. Cross-Section of the Bridge M19/MC (B04-77012).

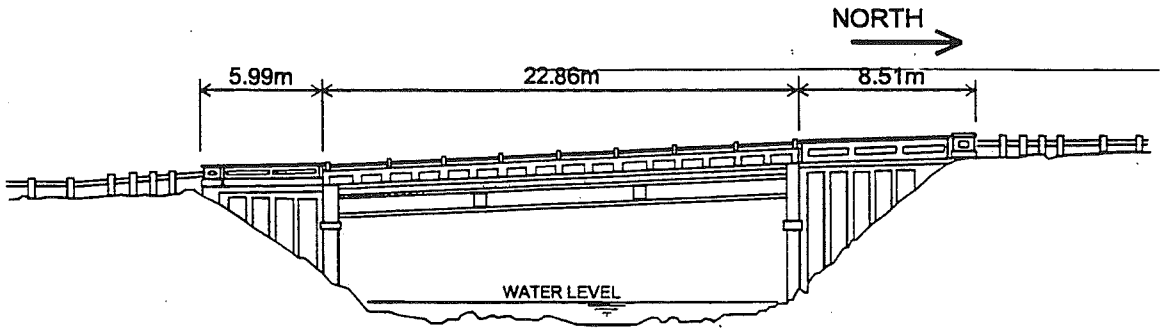

Figure 8.2. Elevation of the Bridge M19/MC (B04-77012).

8.2 Instrumentation

Strain transducers were installed on the bottom flanges of girders at midspan and at selected support locations (Figure 8.3). The reflector for the PSM-R device from Noptel was installed at the girder No. 5 to measure deflection. The test equipment was installed on June 23, 1999. The bridge test was performed on June 24, 1999.

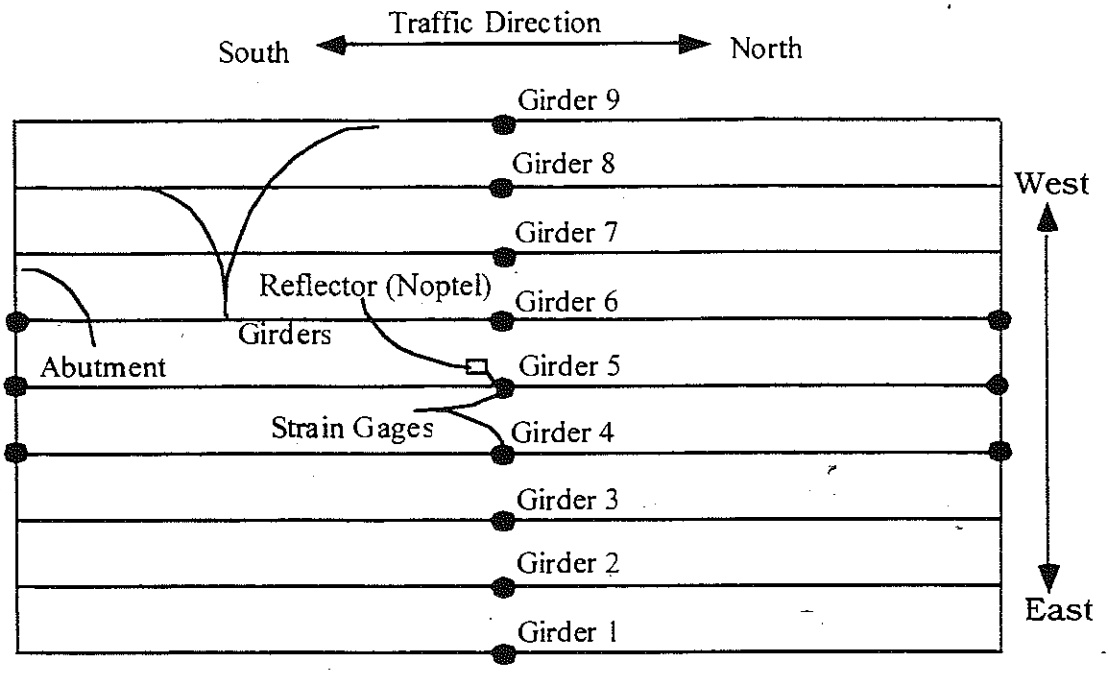

Figure 8.3. Strain Gage Locations in Bridge M19/MC (B04-77012).

8.3 Load Cases

The girder distribution factors (GDF) and dynamic load factors (DLF) were calculated using the strains measured at midspan. The bridge was loaded with two 11-axle trucks (three-unit vehicles). The gross vehicle weight and the truck axle configurations are shown in Figures 8.4 and 8.5.

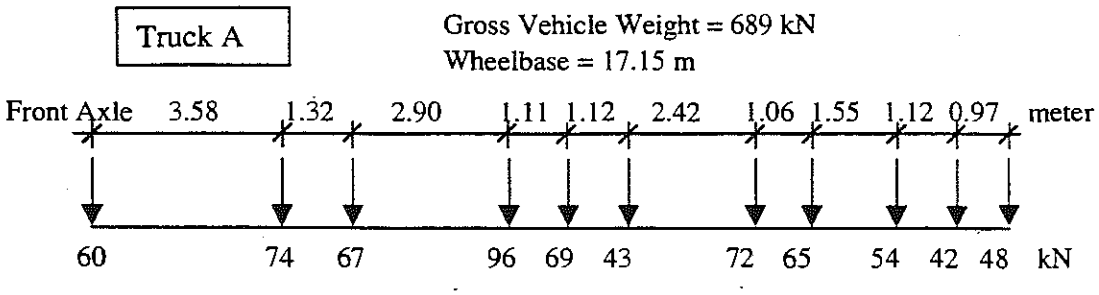

Figure 8.4. Truck A Configuration, Bridge M19/MC (B04-77012).

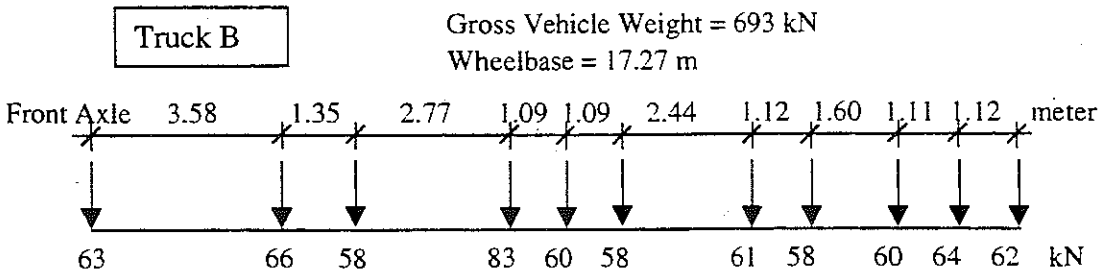

Figure 8.5. Truck B Configuration, Bridge, M19/MC (B04-77012).

A total of 16 load cases were considered, as shown in Table 8.1. First each truck was driven by itself at the center of one lane, at crawling speed. Then, the same truck was driven close to the curb. The runs in the center of the lane were repeated at a normal highway speed (about 50 km/h for this location). The same was repeated for the other lane. Finally, two trucks were driven simultaneously, side-by-side, at crawling speed and normal highway speed. For side-by-side cases, the runs were repeated after the trucks switched lanes, i.e. first truck A was in East lane, and B in West lane, then truck A was in West lane, and B in East lane.

Table 8.1. Sequence of Test Runs, Bridge M19/MC (B04-77012).

Run#	Truck	Lane Side	Position in Lane	Truck Speed
1	Truck A	East	Center	Crawling
2	Truck A	East	Curb	Crawling
3	Truck B	East	Center	Crawling
4	Truck B	East	Curb	Crawling
5	Truck B	East	Center	40 km/h
6	Truck A	East	Center	50 km/h
7	Truck A	West	Center	Crawling
8	Truck A	West	Curb	Crawling
9	Truck B	West	Center	Crawling
10	Truck B	West	Curb	Crawling
11	Truck B	West	Center	40 km/h
12	Truck A	West	Center	40 km/h
13	Truck A and B	both	Center	Crawling
14	Truck B and A	both	Center	Crawling
15	Truck A and B	both	Center	40 km/h
16	Truck B and A	both	Center	55 km/h

8.4. Analysis Results

The three-dimensional finite element method (FEM) was applied to investigate the structural behavior of the bridge M19/MC (B04-77012). The concrete slab was modeled with isotrophic, eight node solid elements, with three degrees of freedoms at each node. The girder flanges and web were modeled using three-dimensional, quadrilateral, four node shell elements with six degrees of freedom at each node. The structural effects of the secondary members, such as the sidewalk and parapet, were also taken into account in the finite element analysis models.

Two cases of the boundary conditions were employed in the FEM models. In the first FEM model, it was assumed that the supports could be represented by a hinge at one end and a roller with a hinge at the other end. In the other FEM model, it was assumed that both supports were hinged, with no movement in horizontal direction.

Figure 8.6 illustrates the mesh of the FEM model, and Figure 8.7 shows the deformed shape of the bridge when it is loaded with two trucks side-by-side.

Figure 8.8 shows the results of the finite element analysis for two trucks side-by-side (Run 13). It includes the experimental results and analytical results for the two considered models. The FEM results show that the maximum strain at the most heavily loaded girder is about 150 με, while the maximum strain recorded from the test is about 100 με. In addition, the experimental response lies between the two considered analytical models. This indicates that a partial fixity exists at the supports of the bridge.

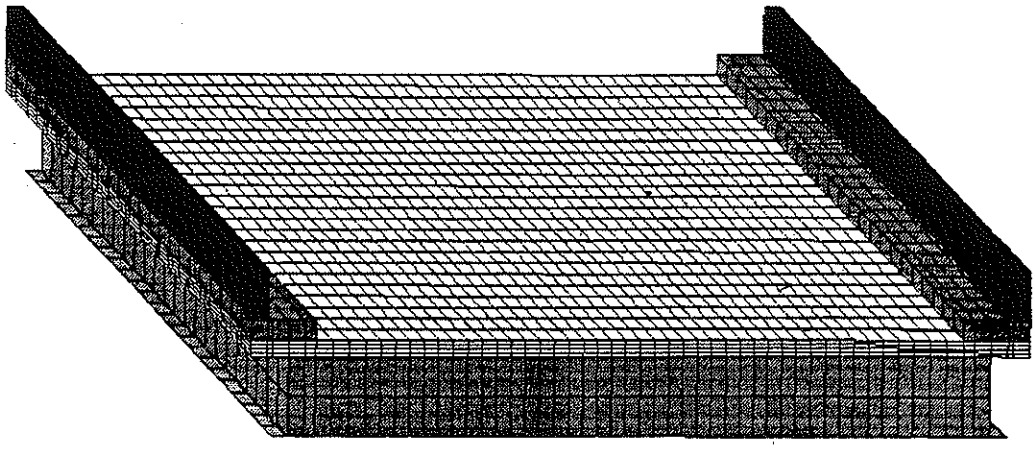

Figure 8.6. The Mesh of the Finite Element Model.
M19/MC (B04-77012).

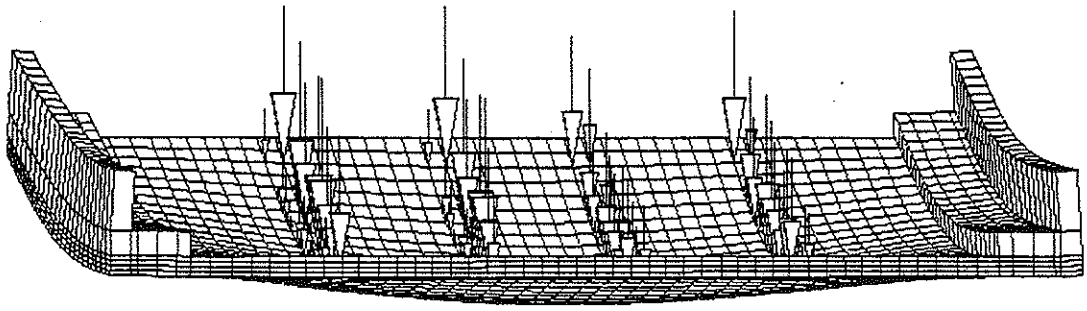

Figure 8.7. The Deformed Shape of the Bridge under Two Lane Loading.
M19/MC (B04-77012).

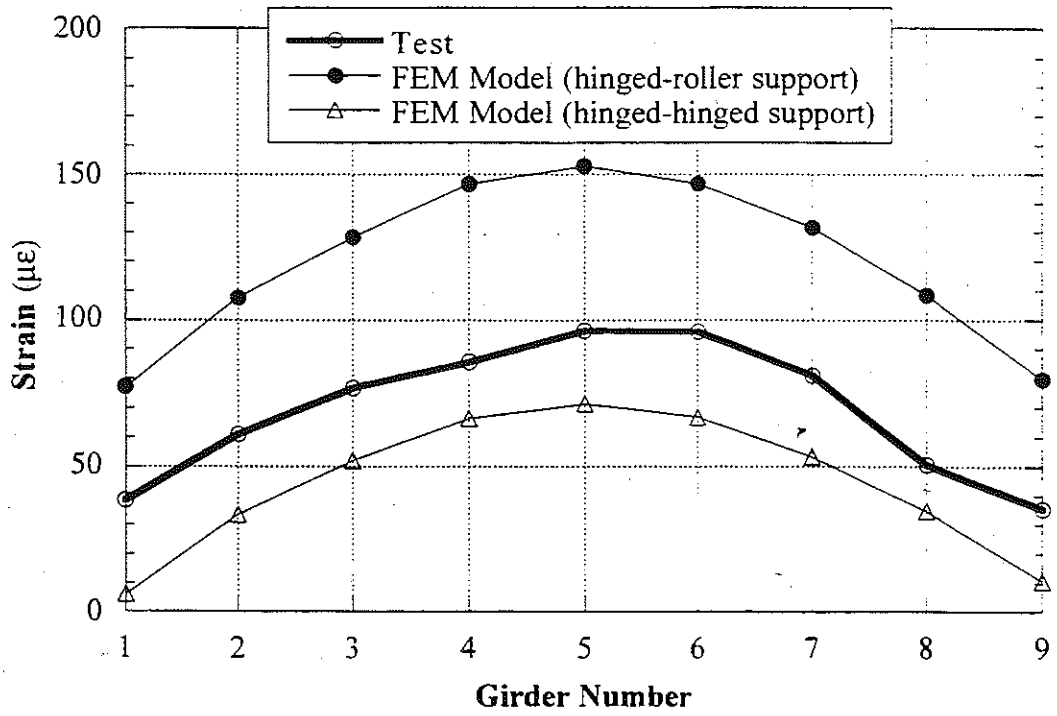

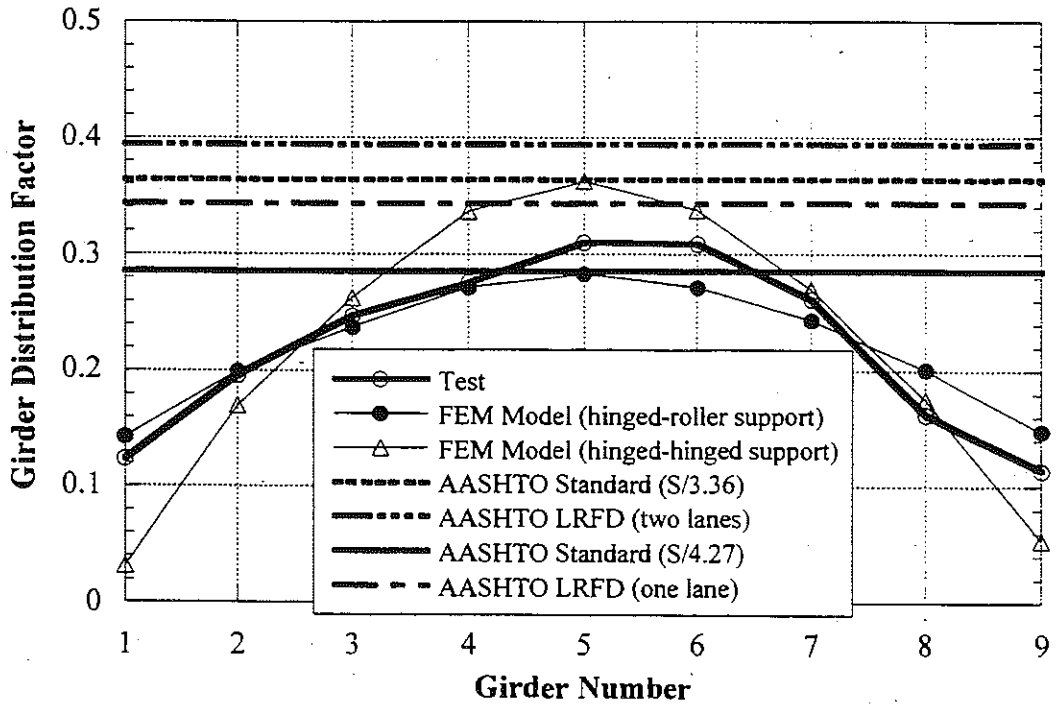

Figure 8.8. Results of the Finite Element Analysis, for truck A-east truck B-west loading, M19/MC (B04-77012).

8.5. Test Results.

The resulting strains and GDF's are shown in Figures 8.9 through 8.13. Figures 8.9 to 8.11 present the results of all crawling-speed (static) tests. Figures 8.9 to 8.10 present static strains and GDF's for one truck on the bridge. The maximum strain due to a single truck is about 60 με. This corresponds to about 12 MPa.

Figure 8.11 shows static strains and GDF's from side-by-side static load tests. For two vehicles side-by-side the maximum strain is about 100 με (which corresponds to 20 MPa). The superposition of strains due to a single truck in West and East lanes produces almost the same results as strain due to two trucks side-by-side.

For two trucks side-by-side, the girder distribution factor for girder i is determined using Eq. 4.4. For comparison, GDF are also calculated according to AASHTO Standard (1996) and AASHTO LRFD Code (1998). Two cases were considered, a single lane loaded, and two lanes loaded. The resulting GDF's are shown in Figures 8.9 through 8.13.

The results indicate that code-specified GDF's are conservative. A single lane GDF specified in AASHTO LRFD (1998) is also sufficient for two lane load cases for this bridge. However, a single lane GDF specified in AASHTO Standard (1996) is not enough for two lane load cases for this bridge. However, the absolute values of the strains are less than 100 με for the heaviest load case (two fully-loaded trucks side-by-side). Therefore, the total load effect per girder estimated using GDF specified for single lane in AASHTO Standard (1996) is also conservative (less than design value).

Figure 8.12 and 8.13 shows the resulting strain and distribution factors from normal speed tests. There is practically no difference between the crawling speed and normal speed results.

Dynamic load factor is defined in section 4.4. In Figure 8.14, DLF's are plotted for all load cases involving normal speed (no dynamic load was measured for crawling speed runs). Dynamic load factors for exterior girders are high because the static strains in these girders are very low. In other words, large values of DLF in exterior girders correspond to load cases with a single truck in the opposite lane (resulting in very low static strain).

The relationship between DLF and static and dynamic strains is shown in Figure 8.15. The open circles correspond to static strain, ε_{stat}, and black solid squares correspond to dynamic strain, ε_{dyn}. For each static strain value (open circle), the corresponding dynamic strain is denoted by solid square (the numbers of circles and squares are same). Dynamic strains remain nearly constant, while static strains increase as truck loading increases. This results in large dynamic load factors for low static strains. It is clear from the Figure 8.15 that dynamic strains does not exceed 10 $\mu\varepsilon$ for all the cases while the static strain can exceed 100 $\mu\varepsilon$ in normal speed test. DLF corresponding to the maximum strain caused by two trucks side-by-side, is less than 0.10 at girder No. 5, the most heavily loaded girder (Girder No. 5).

The strains were also measured close to the support. The results are shown in Figures 8.16 through 8.21. Negative strain values indicate the strains recorded at the bottom flanges near supports were in compression, due to the partial fixity of support. The strain values near the support were measured when the loads caused the maximum strain at the midspan. As shown in the Figures, the levels of support fixity are highly unpredictable. Even in a bridge, each girder has different support

behavior. There are differences in the sign of strain between the girders. This requires some further investigation, and it is necessary to collect more test data.

Girder No. 5 was instrumented with remote deflection measurement device manufactured by Noptel. The reflector was installed at midspan. The result is shown in Table 8.2. The maximum deflection recorded during the test is 5.3 mm for girder number 5.

Table 8.2. Maximum deflections measured at the center of the Girder 5, Bridge M19/MC (B04-77012).

Run #	Horizontal (mm)	Vertical (mm)
1	-0.4	2.13
2	-0.3	1.17
3	-0.36	1.92
4	-0.40	1.31
5	-0.30	2.02
6	-0.38	2.00
7	0.21	3.07
8	0.37	2.85
9	0.18	3.17
10	NA	NA
11	0.12	3.00
12	0.16	3.08
13	-0.31	5.30
14	-0.33	5.24
15	-0.20	3.60
16	NA	NA

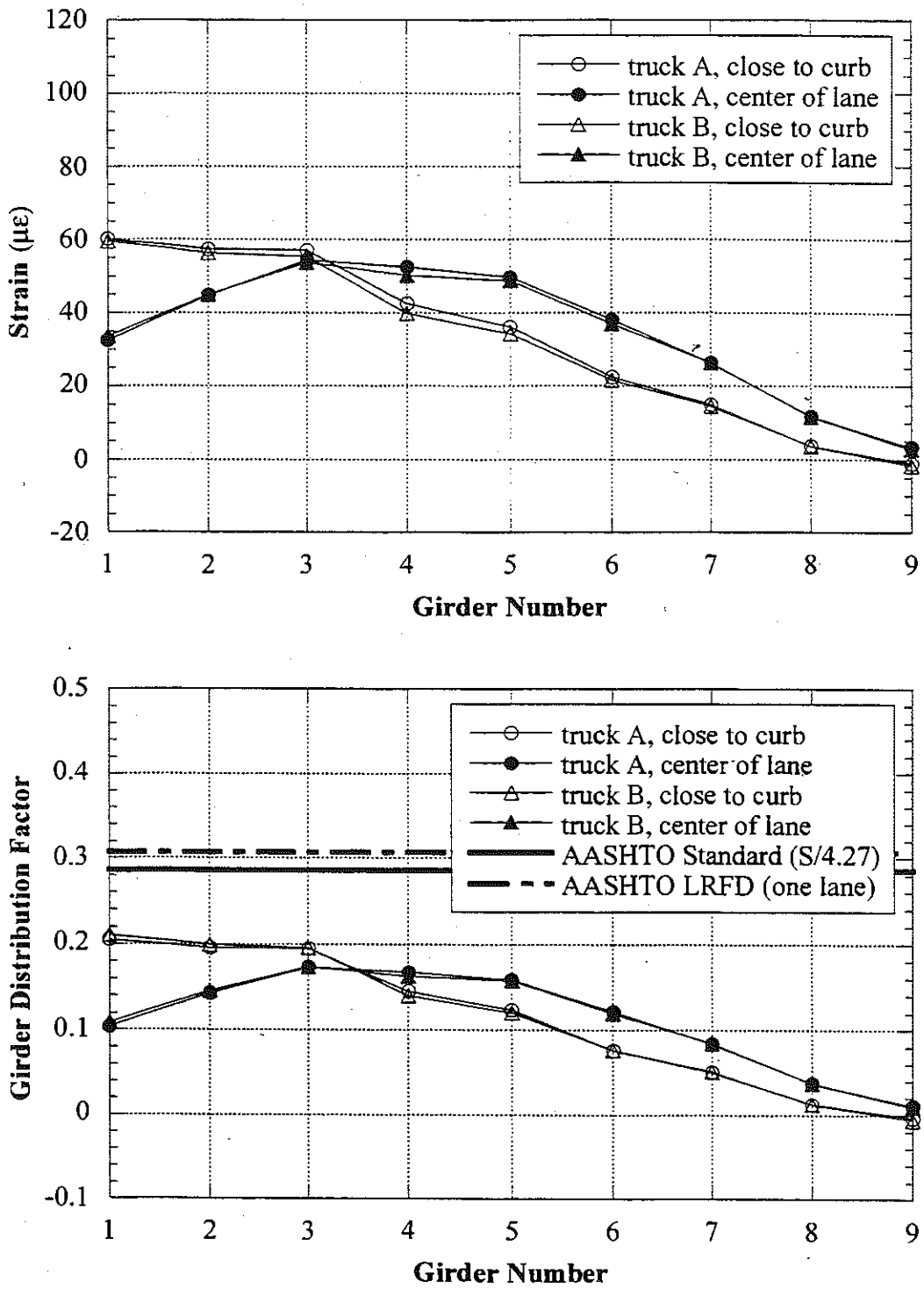

Figure 8.9. East Lane, Crawling Speed, M19/MC (B04-77012).

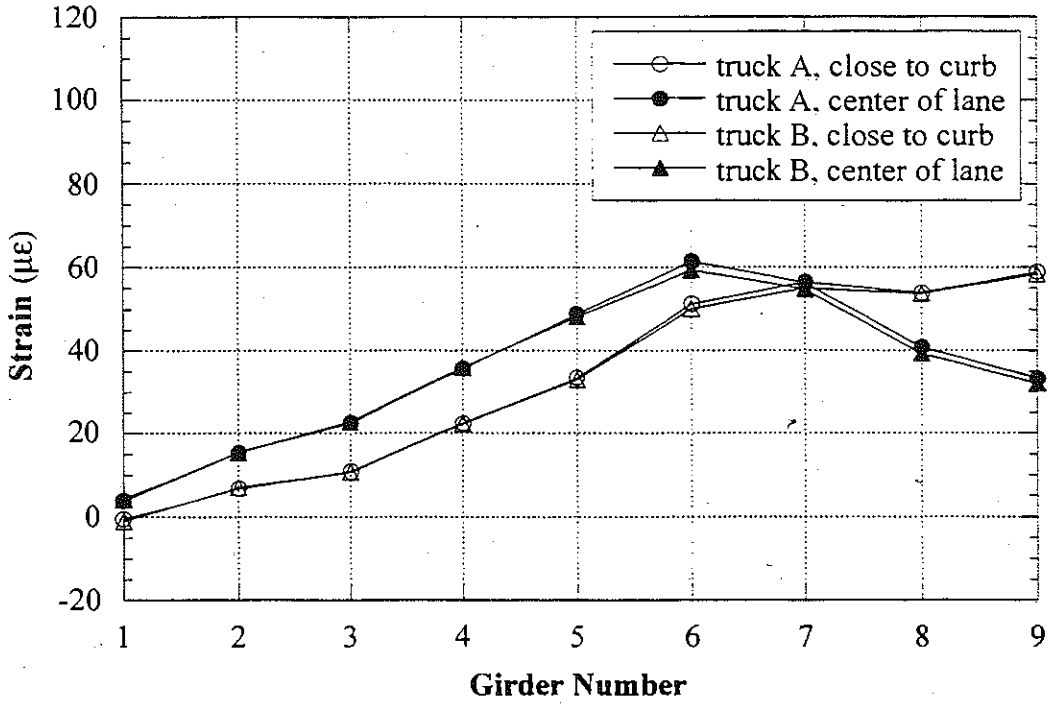

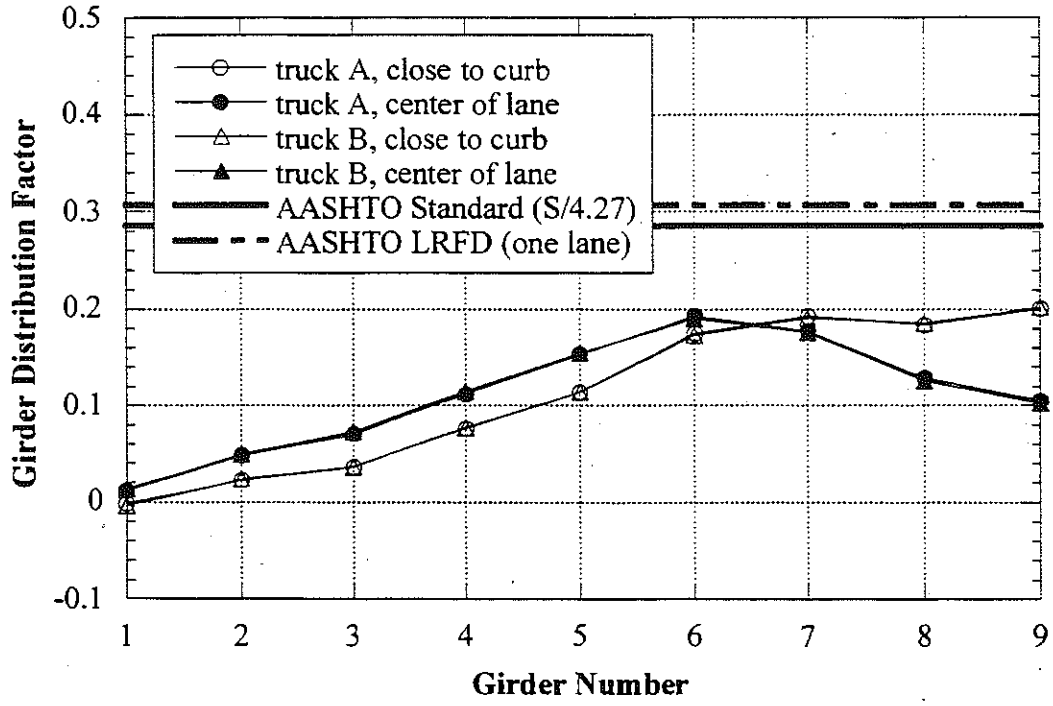

Figure 8.10. West Lane, Crawling Speed, M19/MC (B04-77012).

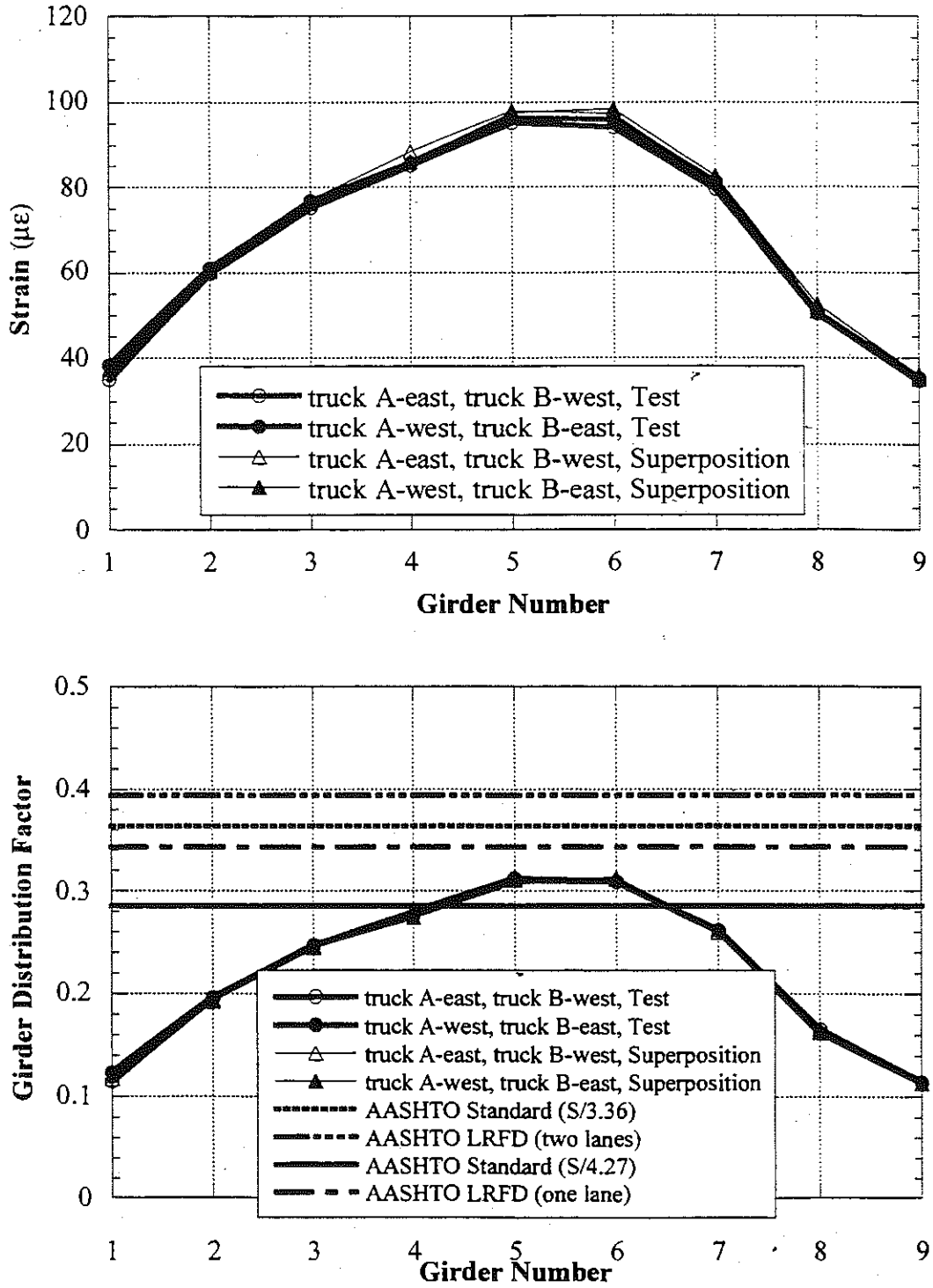

Figure 8.11. Side-by-Side Loading, Center of Lane, Crawling Speed, M19/MC (B04-77012).

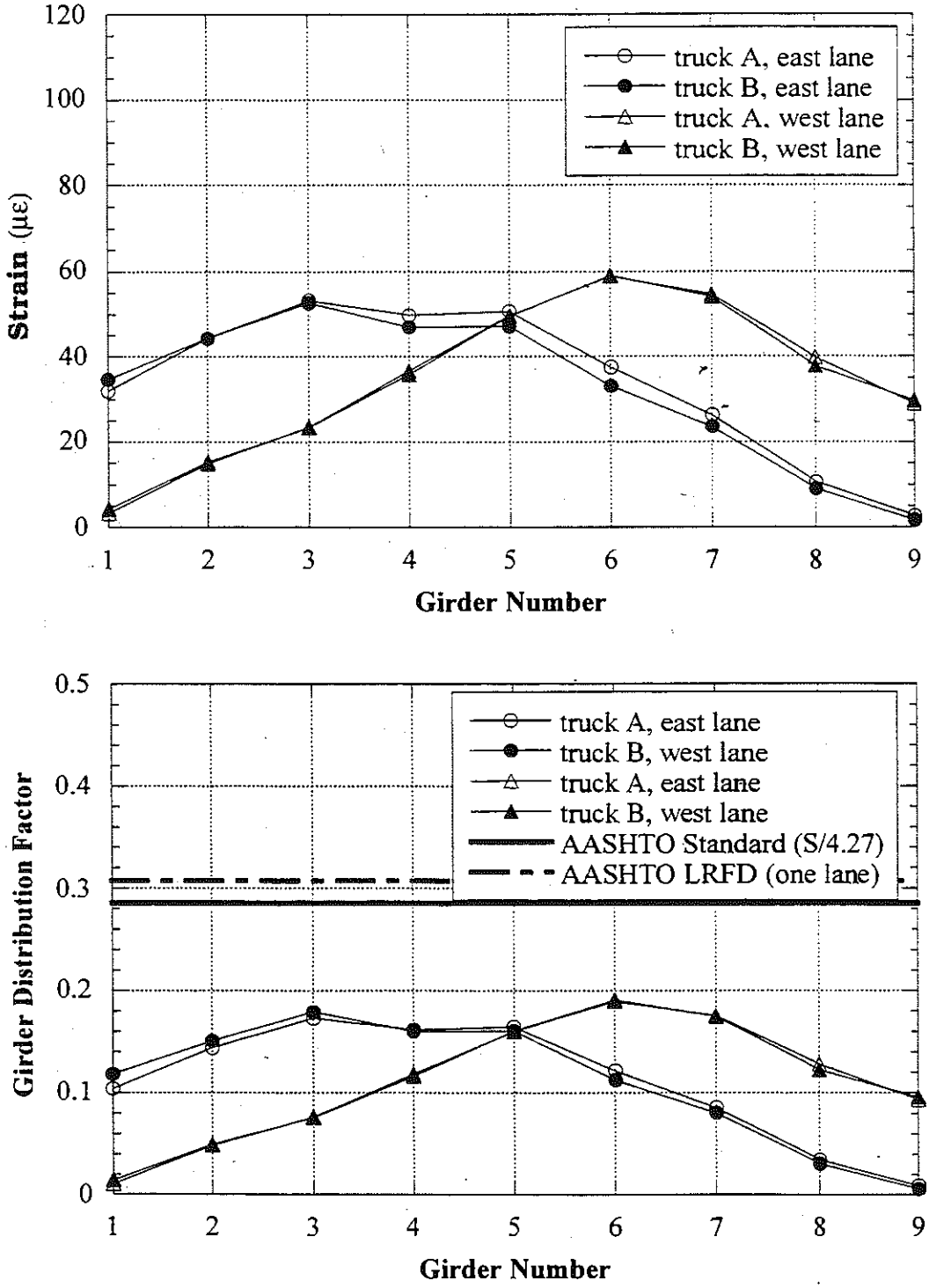

Figure 8.12. Strain and GDF under One Truck Loading at Regular Speed, M19/MC (B04-77012).

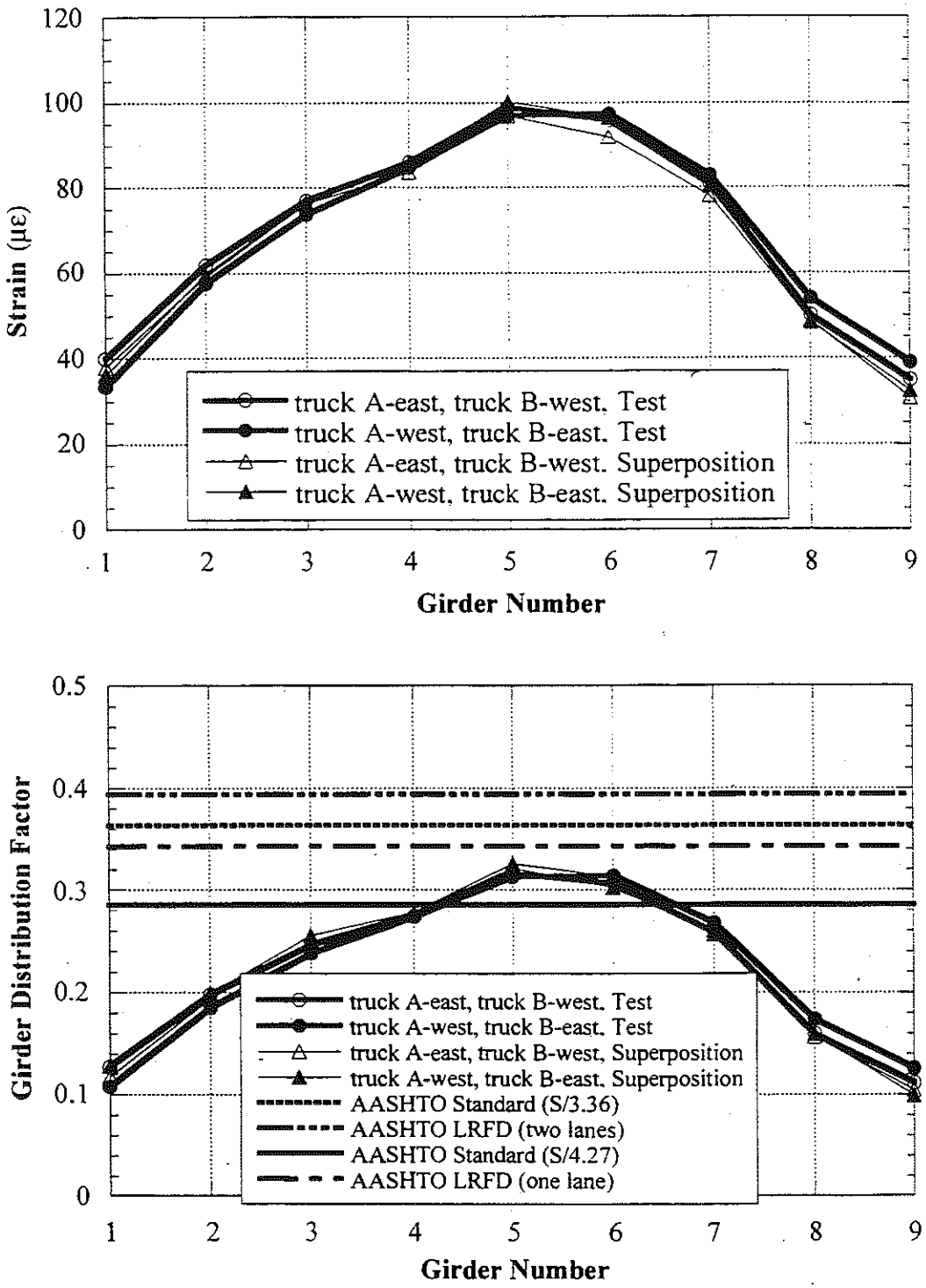

Figure 8.13. Strain and GDF under Side-by-Side Loading at Regular Speed, M19/MC (B04-77012).

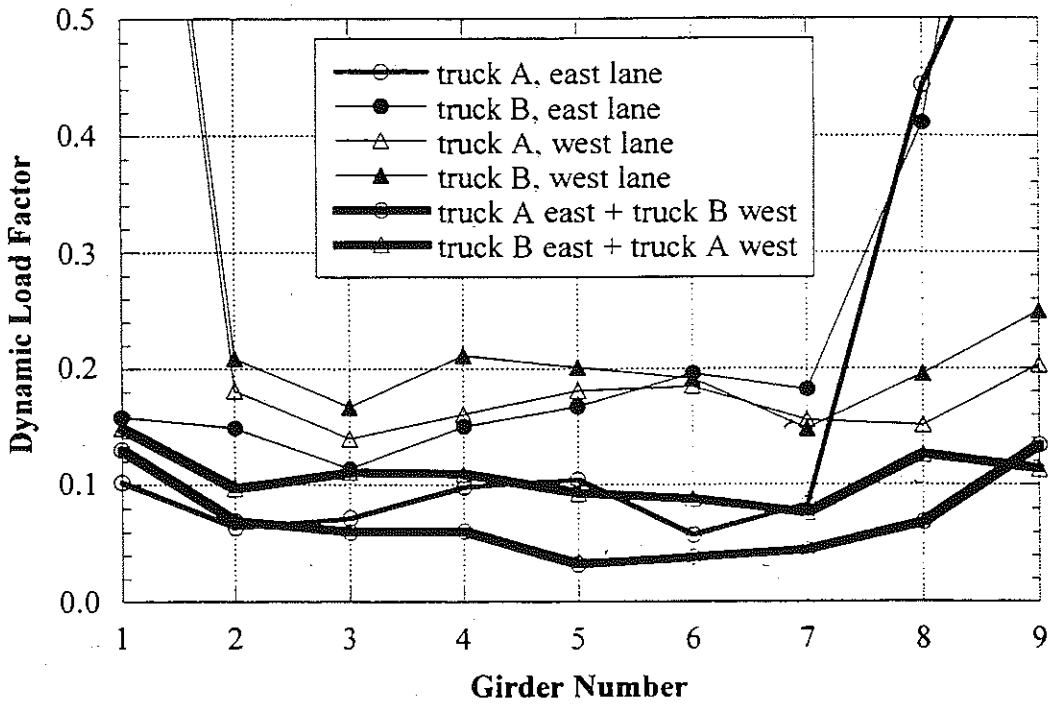

Figure 8.14. Dynamic Load Factors, M19/MC (B04-77012).

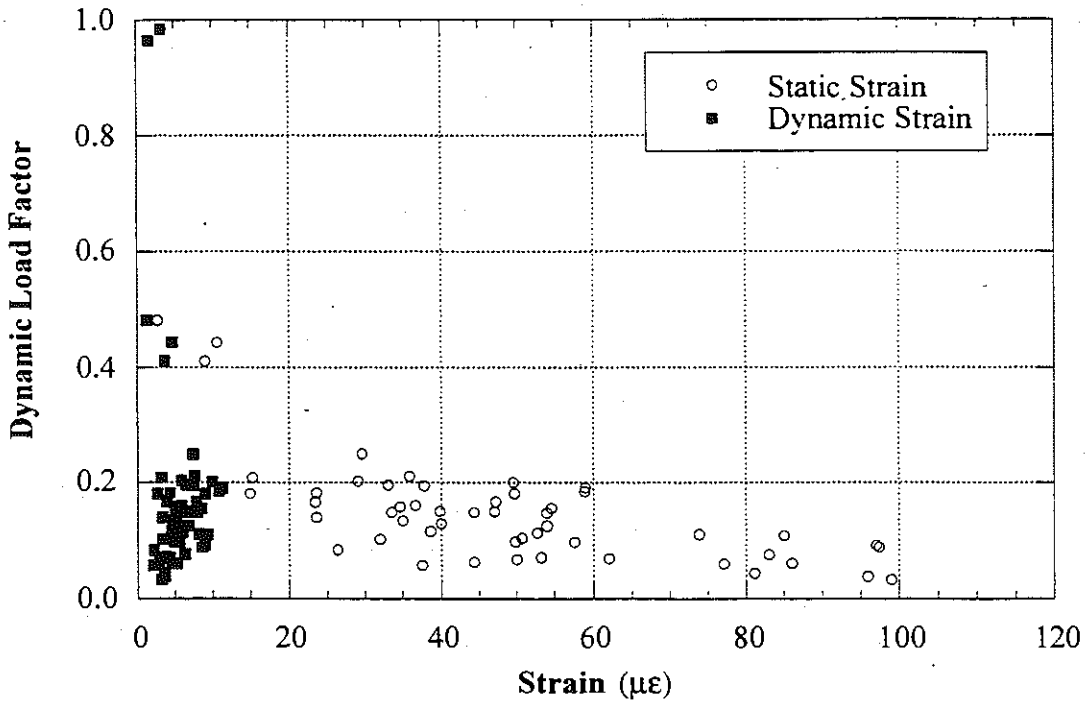

Figure 8.15. Strain vs. Dynamic Load Factors, M19/MC (B04-77012).

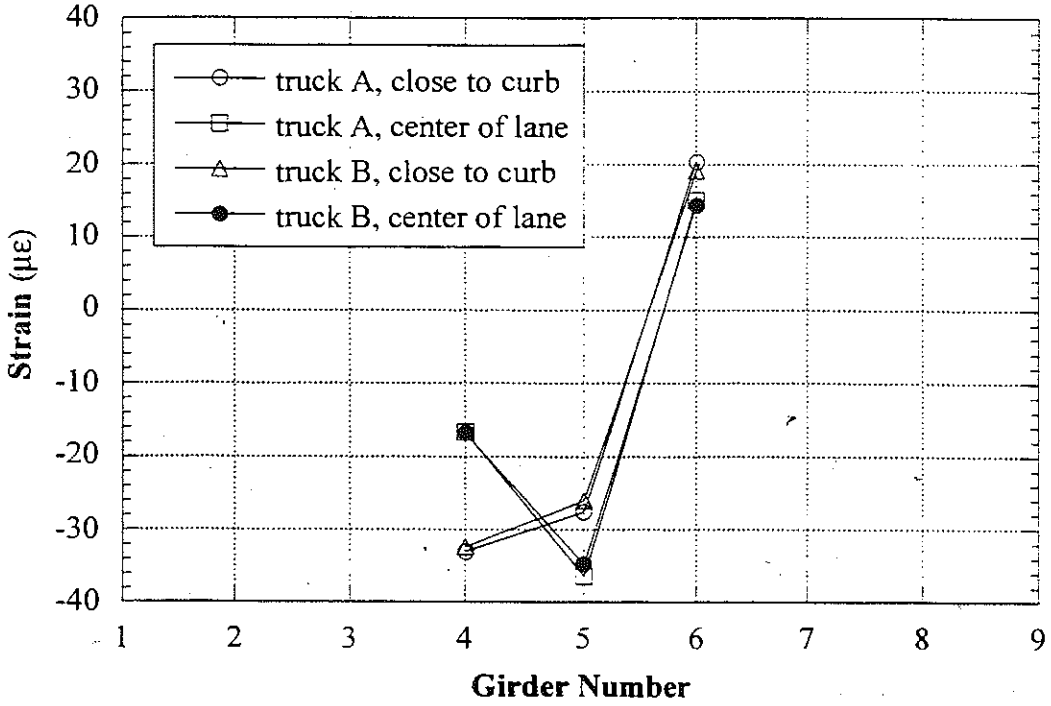

Figure 8.16. Strains at North End, East Lane Loading, Crawling Speed, M19/MC (B04-77012).

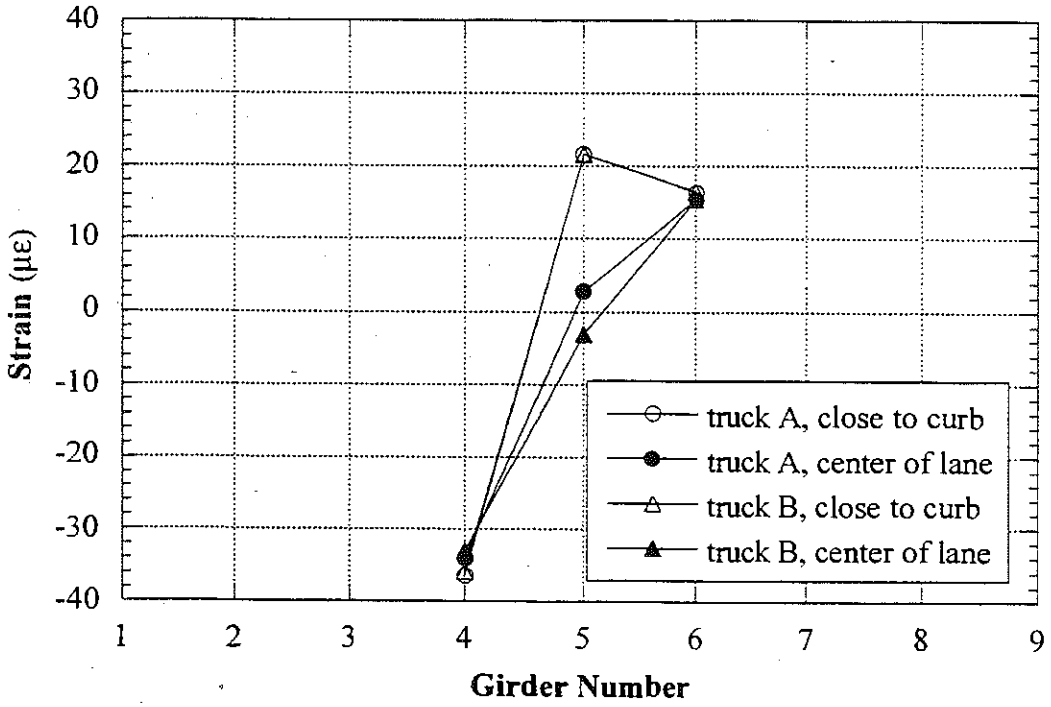

Figure 8.17. Strains at South End, East Lane Loading, Crawling Speed, M19/MC (B04-77012).

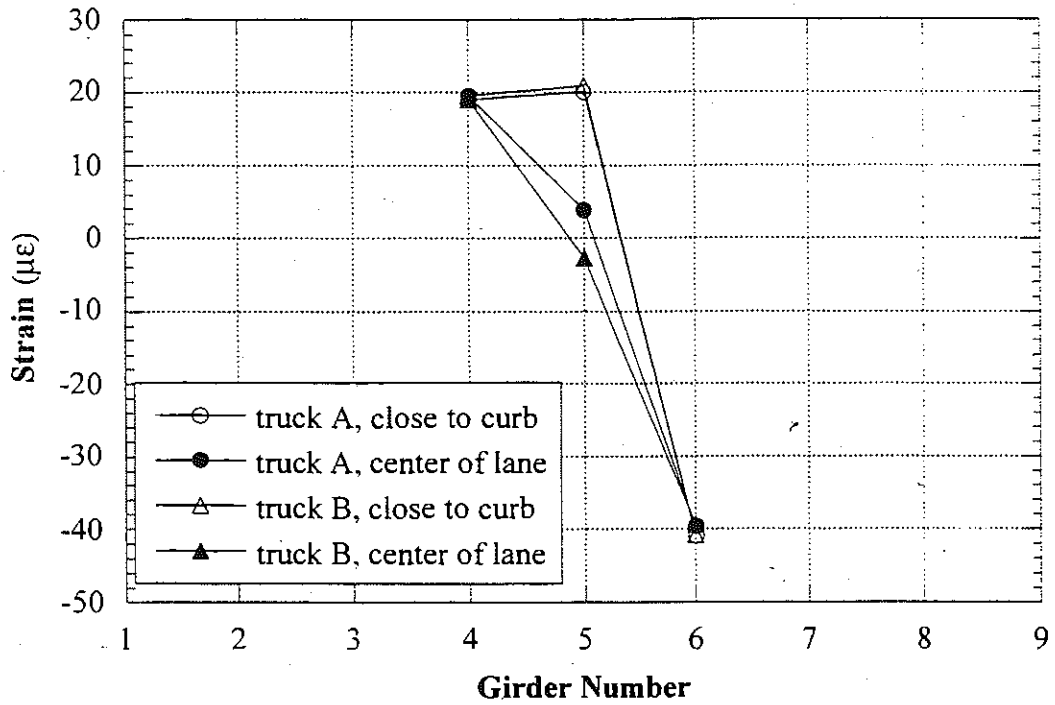

Figure 8.18. Strains at North End, West Lane Loading, Crawling Speed, M19/MC (B04-77012).

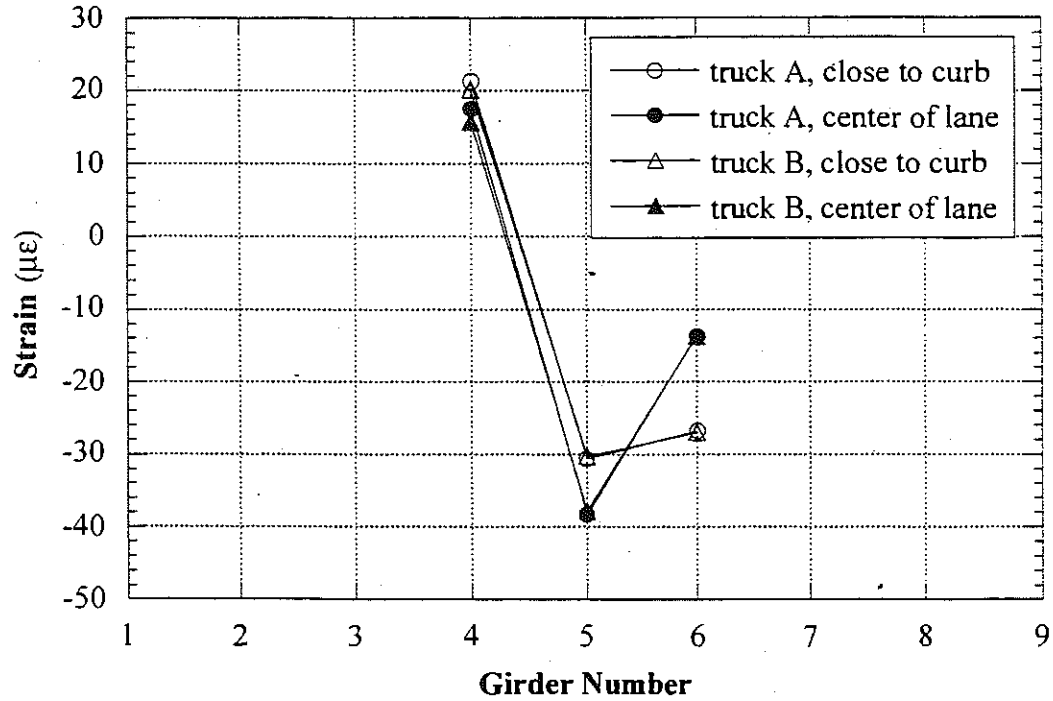

Figure 8.19. Strains at South End, West Lane Loading, Crawling Speed, M19/MC (B04-77012).

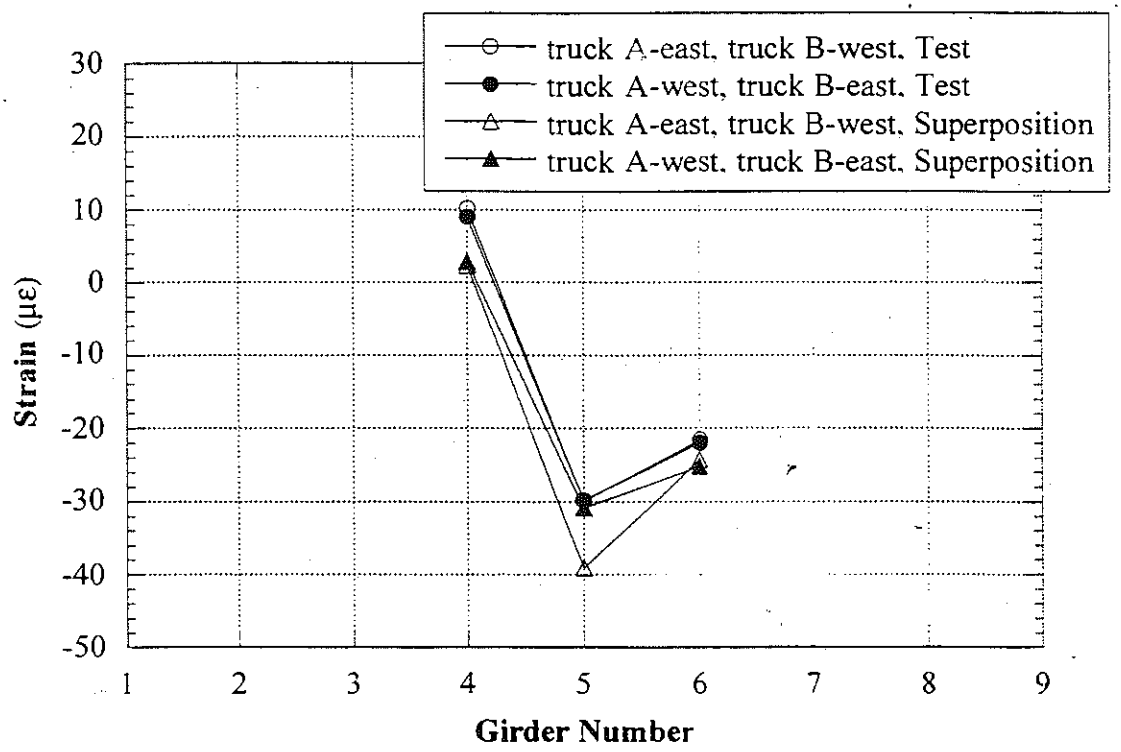

Figure 8.20. Strains at North End, Side-by-Side Loading, Crawling Speed, M19/MC (B04-77012).

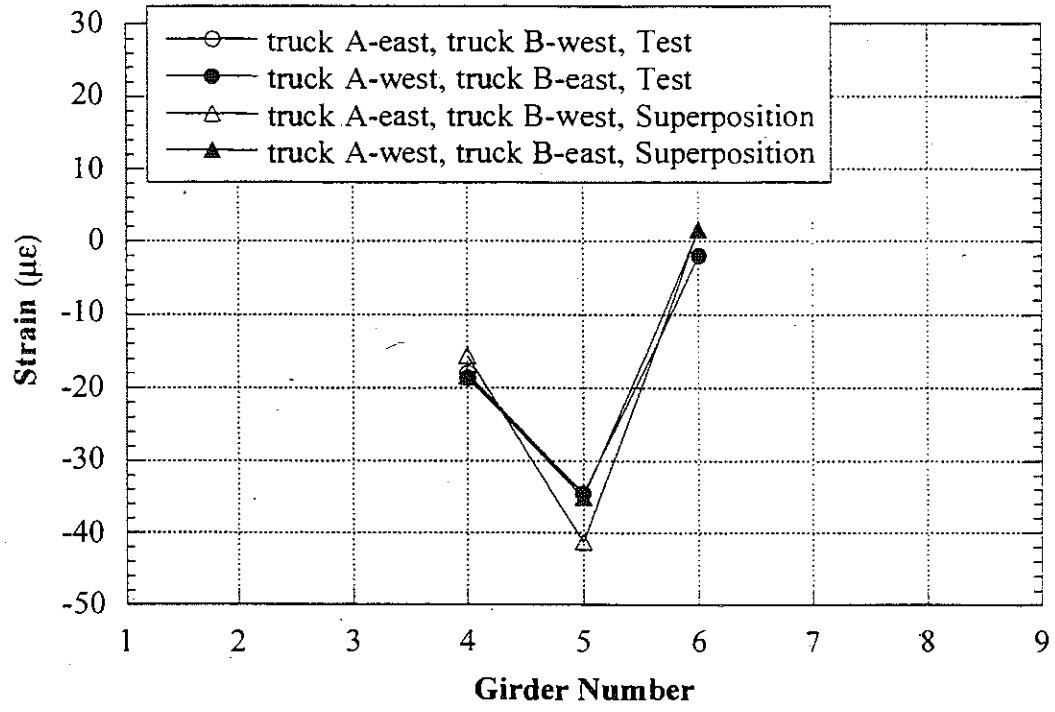

Figure 8.21. Strains at South End, Side-by-Side Loading, Crawling Speed, M19/MC (B04-77012).

9. Bridge on N Drive North over I-69, Calhoun County (S03-13074, NDN/I69)

9.1 Description

This bridge was built in 1970 and is located on N Drive North over I-69 in Calhoun County, Michigan. As shown in Figure 9.1, there is one lane in each direction. It has five steel girders spaced at 2.82 m. It is a five span, simply supported, composite structure, as shown in Figure 9.2. The total span length is 110.9 m. The centerspan of this bridge is over the median of the interstate highway. The test was performed on the center span. The length of the center span is 29.8 m. There is no skew. It carries average daily traffic (ADT) of 800. The bridge has a load rating of 694 kN, according to the Michigan Structure Inventory.

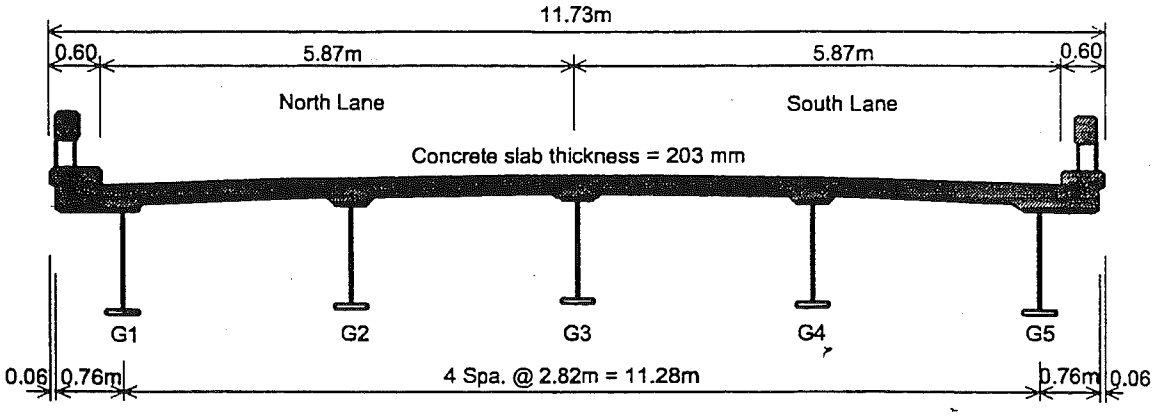

Figure 9.1. Cross-Section of Bridge NDN/I69 (S03-13074).

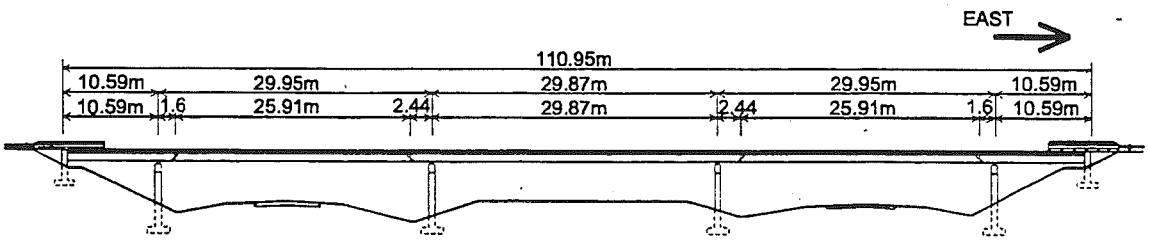

Figure 9.2. The Elevation of Bridg NDN/I69 (S03-13074).

9.2 Instrumentation

Strain transducers were installed on the bottom flanges of girders at midspan, selected supports, and between the transverse diaphragms (Figure 9.3) at the centerspan. LVDT's were installed at midspan of the center span. The reflector for the PSM-R deflection measurement device from Noptel was installed at the girder No. 3 so that the results could be compared with the those from LVDT. The test equipment was installed on July 21, 1999. The bridge test was performed on July 22, 1999.

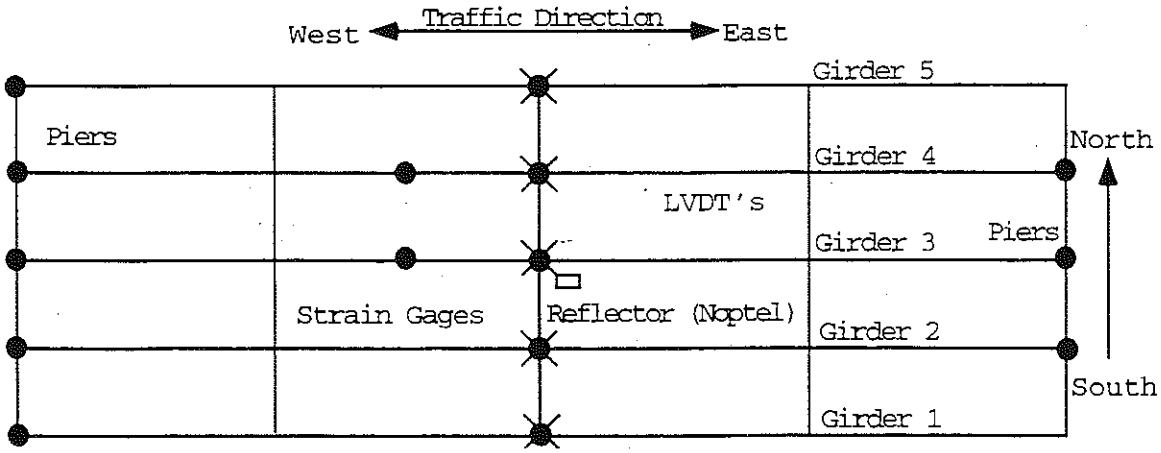

Figure 9.3. Strain Gage Locations in Bridge NDN/I69 (S03-13074).

9.3 Truck Loads

Both load distribution and proof load tests were performed on this bridge. For the load distribution test, two, three-unit 11-axle trucks were used. For the proof load test, two M-1 tanks and two, three-unit 11-axle trucks were used as proof load. The trucks were the same as for the load distribution test

Strain data necessary to calculate girder distribution and impact factors were taken from midspan transducers. The gross vehicle weight and the truck axle configurations are shown in Figures 9.4 and 9.5.

A total of 16 load cases were considered, as shown in Table 9.1. First each truck was driven by itself at the center of one lane, at crawling speed. Then, the same truck was driven close to the curb. The runs in the center of the lane were repeated at a normal highway speed (about 40 km/h for this location). The same was repeated for the other lane. Finally, two trucks were driven simultaneously, side-by-side, at crawling speed and normal highway speed. For side-by-side cases, the runs were repeated after the trucks switched lanes, i.e. first truck A was in North lane, and B in South lane, then truck A was in South lane, and B in North lane.

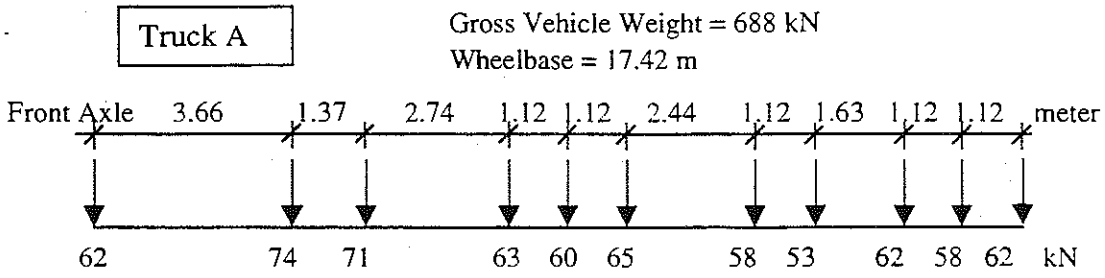

Figure 9.4. Truck A Configuration, Bridge NDN/I69 (S03-13074).

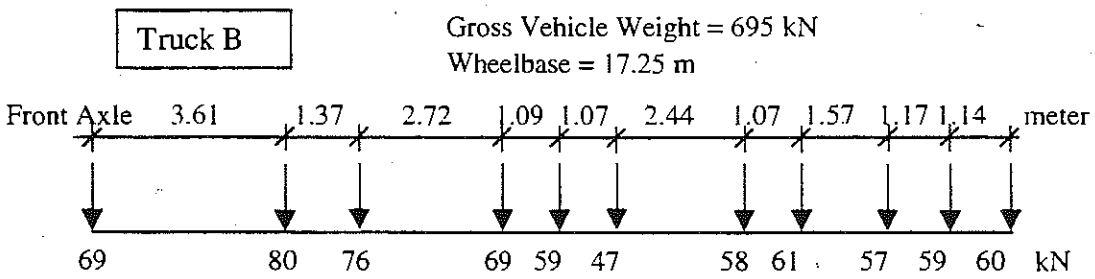

Figure 9.5. Truck B Configuration, Bridge NDN/I69 (S03-13074).

9.4. Loads for Proof Load Test

Two M-1 tanks and two, 3-unit 11-axle trucks were used for the proof load test. The trailers of the 11-axle trucks were detached and positioned at different locations to cause maximum load effect. The tanks and the trucks were placed adjacent to each other in three different longitudinal and different transverse positions. Traffic was allowed over a partial width of the bridge during the test, except during critical stages of the test. The maximum lane moment on the 29.8 m span due to the legal load is 3766 kN-m. The target proof load lane moment was obtained from Section 4.3.1. The bridge is ratable and has no hidden details. Therefore, the target proof load was reduced by 5 percent. No other adjustments were applicable to this bridge. The required proof load level was determined as follows:

$X_P = 1.4$ basic target load factor

$\Sigma = -5$ % because the bridge is ratable and has no hidden details

$X_{Pa} = 1.4(1+(\Sigma/100) = 1.33$ from Eq. (4-1)

Above X_{Pa} satisfies Eq. (4-3).

The target proof load (L_t) is, from Eq. (4-2),

$L_t = 1.33 \times 1.10\ L_r = 1.46\ L_r$, using DLF = 0.10

$L_r = 3766$ kN-m

$L_t = 1.46 \times 3766 = 5510$ kN-m

Table 9.1. Sequence of Test Runs, Bridge NDN/I69 (S03-13074).

Run#	Truck	Lane Side	Position in Lane	Truck Speed
1	Truck A	North	Center	Crawling
2	Truck A	North	Curb	Crawling
3	Truck B	North	Center	Crawling
4	Truck B	North	Curb	Crawling
5	Truck B	North	Center	40 km/h
6	Truck A	North	Center	40 km/h
7	Truck A	South	Center	Crawling
8	Truck A	South	Curb	Crawling
9	Truck B	South	Center	Crawling
10	Truck B	South	Curb	Crawling
11	Truck B	South	Center	40 km/h
12	Truck A	South	Center	40 km/h
13	Truck A and B	both	Center	Crawling
14	Truck B and A	both	Center	Crawling
15	Truck A and B	both	Center	35 km/h
16	Truck B and A	both	Center	35 km/h

Table 9.2 shows the maximum lane moments caused by the trucks and tanks. The loads were gradually increased to ensure the safety of the proof load test. Pretest analysis was performed to calculate the expected maximum strain and the deflection values based on the planned loading. The results are shown in Table 9.3. Detailed proof load positions are shown in Figures 9.6 to 9.21. Figure 9.22 is a view of the test while the Run 13 is in progress.

Table 9.2. Lane Moment due to Trucks and Tanks for 29.8 m span (S03-13074).

Load Type	Maximum Lane Moment
Test Truck A	3568 kN-m
Test truck B	3588 kN-m
One Tank only	3679 kN-m
One Tank + One 11-axle Truck (Truck Detached and Positioned to create maximum moment)	5903 kN-m

Table 9.3. Results of Pretest Analysis, Proof Load Test (S03-13074).

AASHTO GDF used in calculation	Maximum Strain	Maximum Deflection
Standard (S/4.27)	776 με	76 mm
Standard (S/3.36)	988 με	97 mm
LRFD (one lane)	633 με	62 mm
LRFD (two lanes)	797 με	78 mm

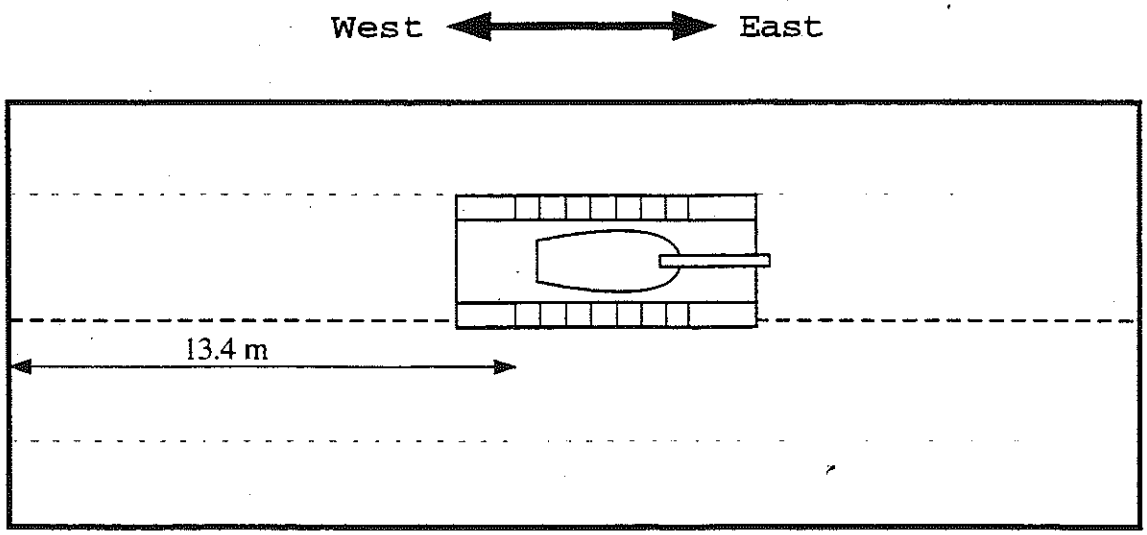

Figure 9.6. Location of Tanks and Trucks in Run 1.

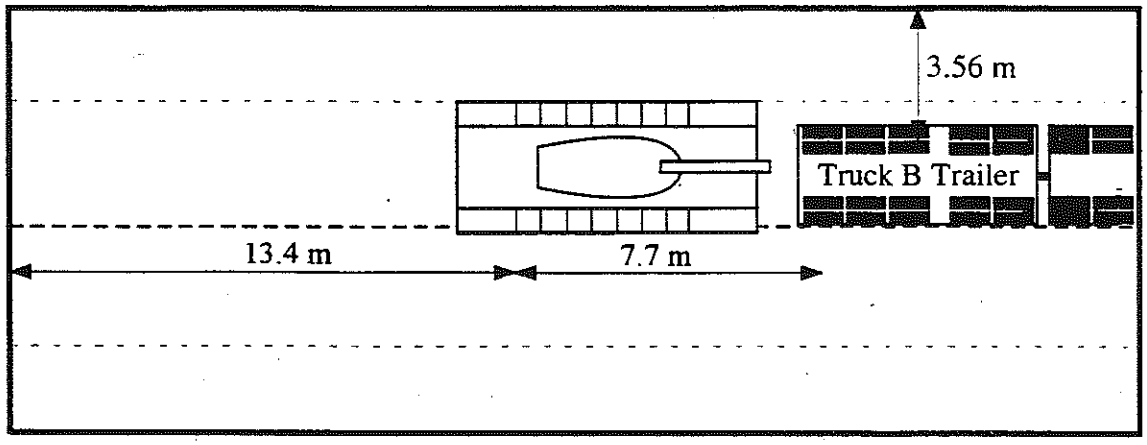

Figure 9.7. Location of Tanks and Trucks in Run 2.

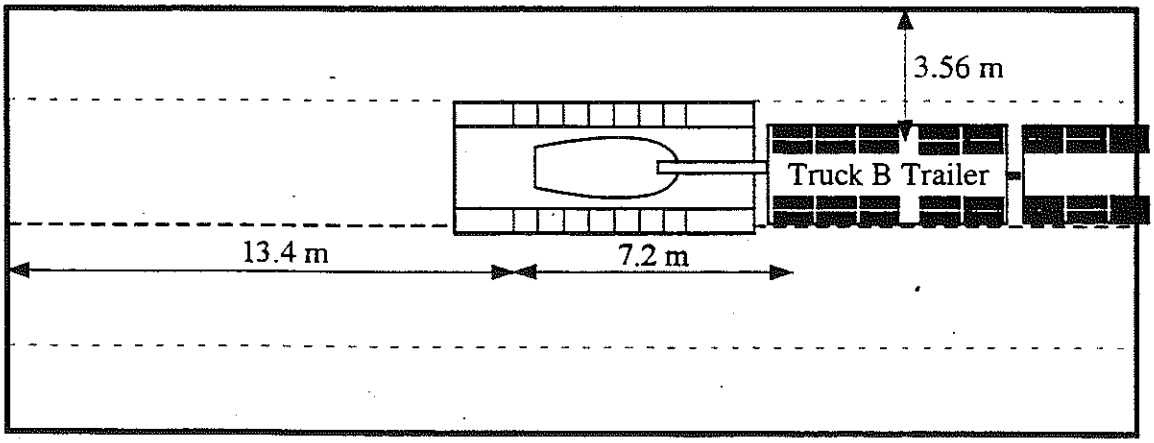

Figure 9.8. Location of Tanks and Trucks in Run 3.

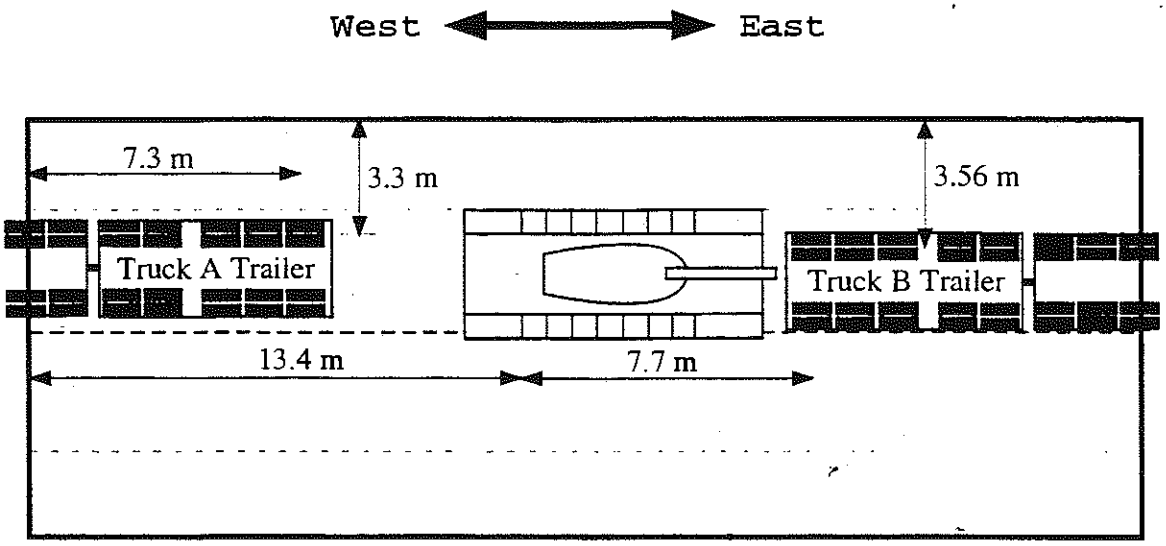

Figure 9.9. Location of Tanks and Trucks in Run 4.

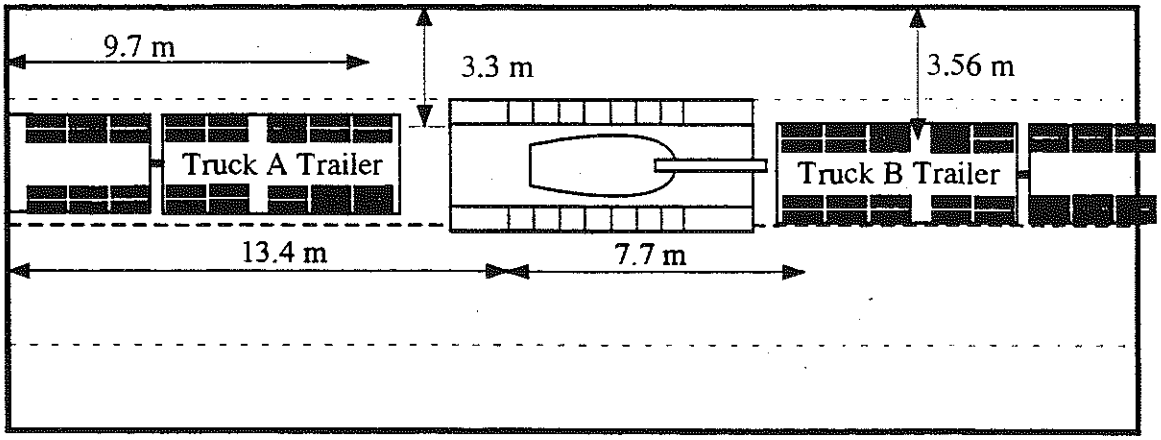

Figure 9.10. Location of Tanks and Trucks in Run 5.

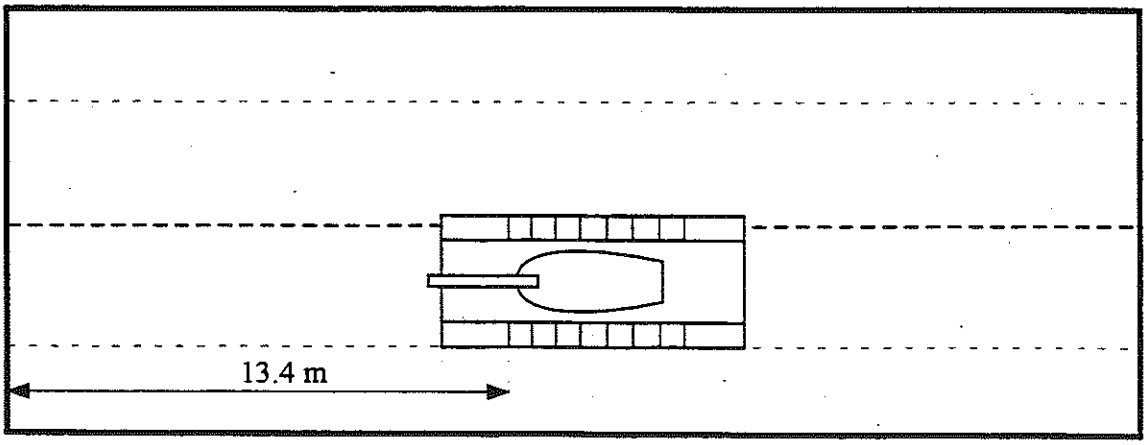

Figure 9.11. Location of Tanks and Trucks in Run 6.

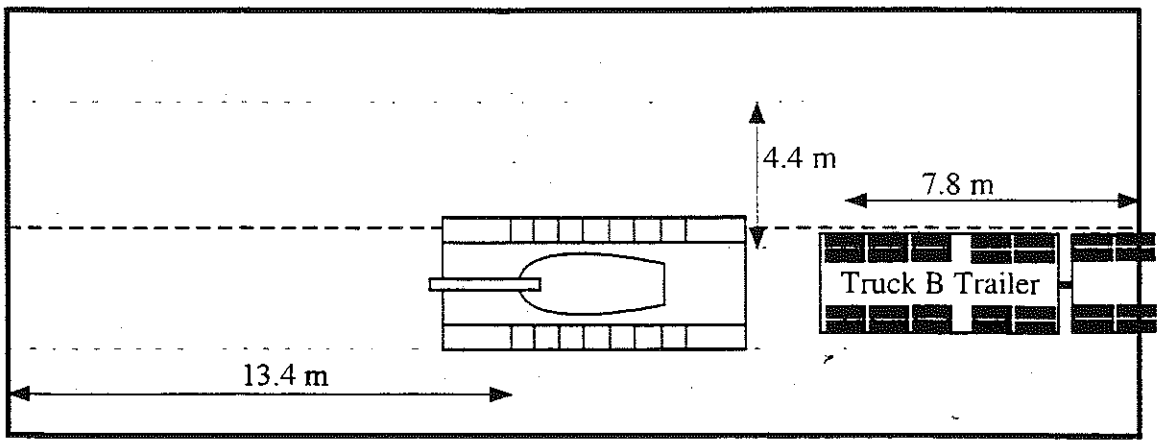

Figure 9.12. Location of Tanks and Trucks in Run 7.

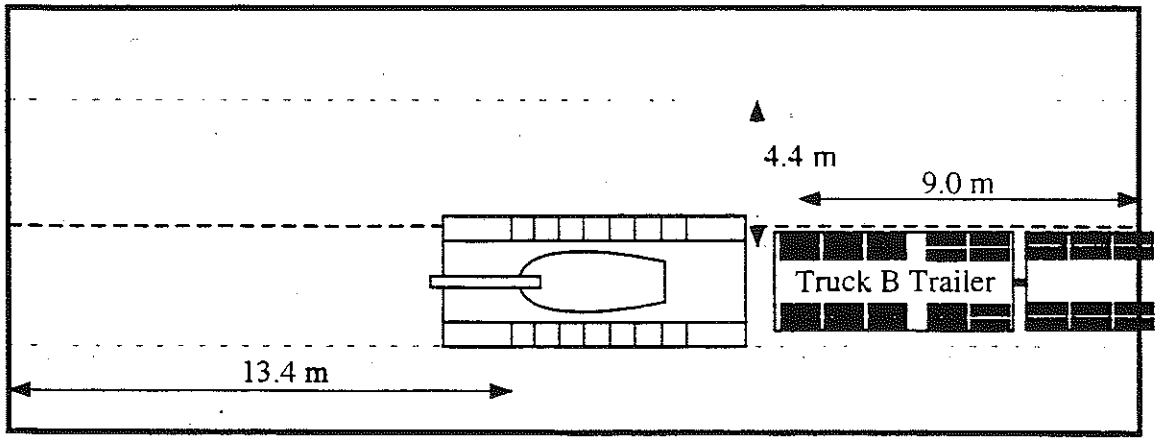

Figure 9.13. Location of Tanks and Trucks in Run 8.

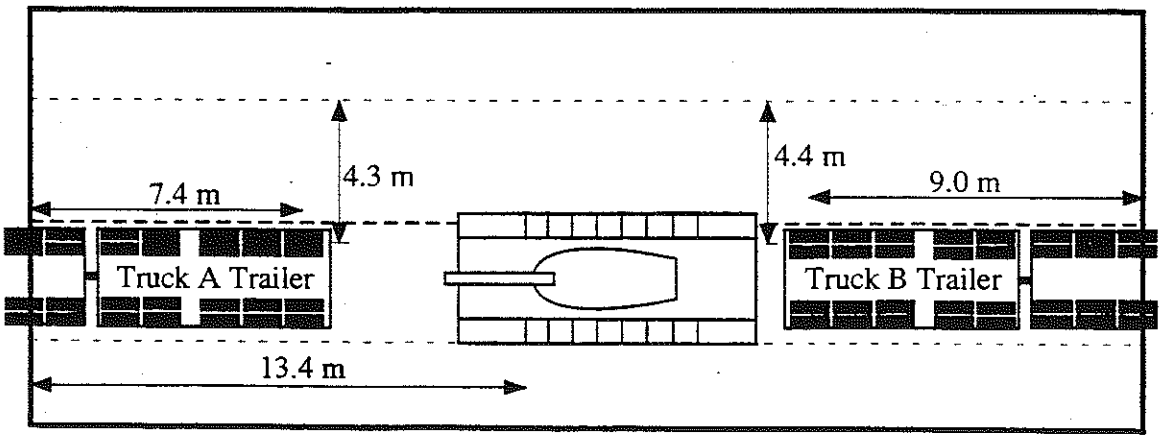

Figure 9.14. Location of Tanks and Trucks in Run 9.

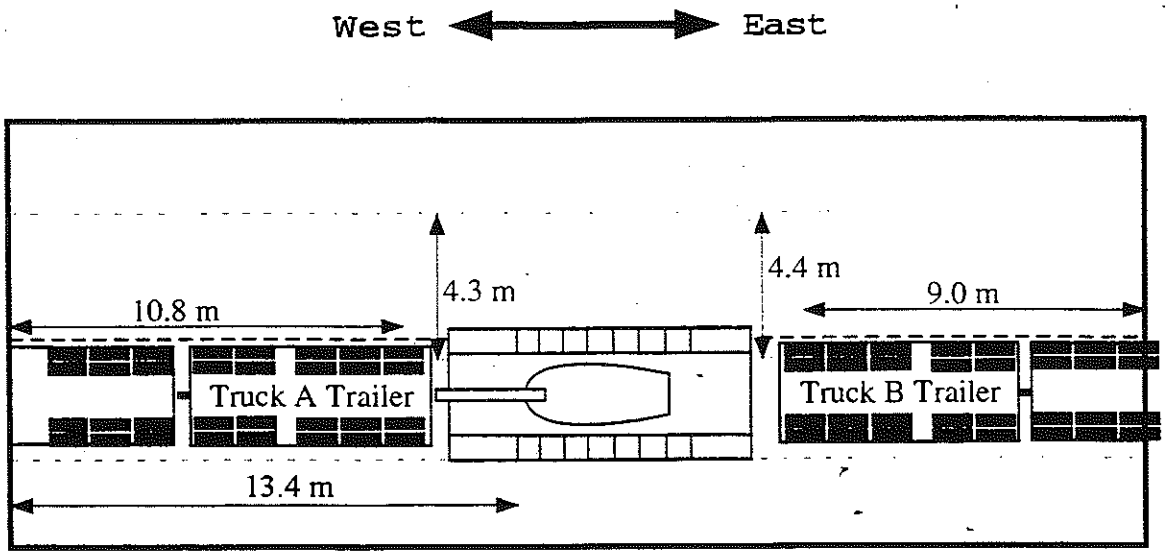

Figure 9.15. Location of Tanks and Trucks in Run 10.

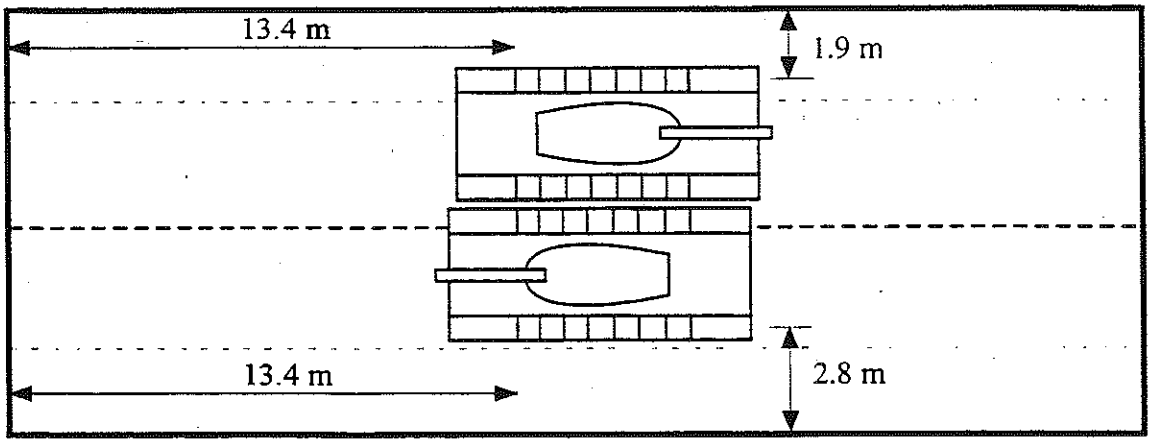

Figure 9.16. Location of Tanks and Trucks inRun 11.

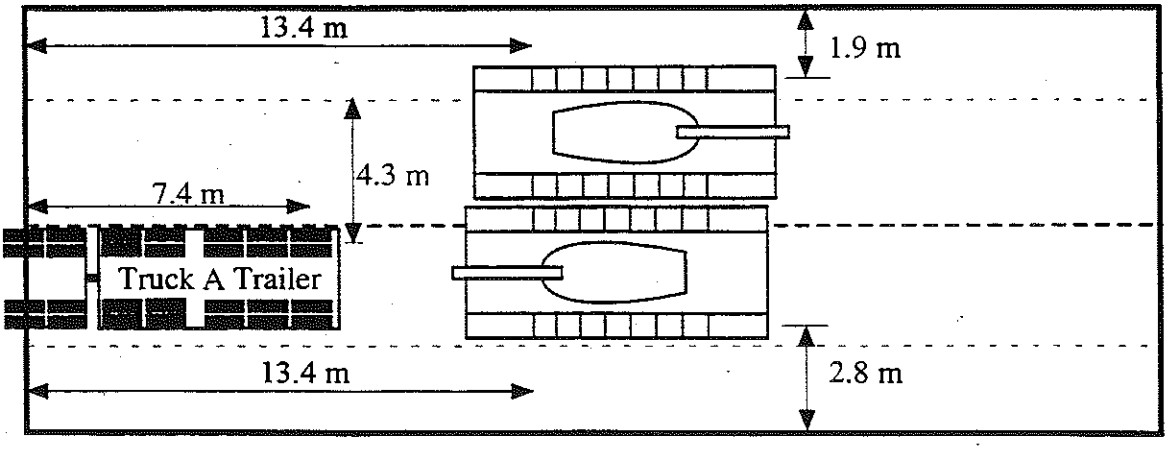

Figure 9.17. Location of Tanks and Trucks in Run 12.

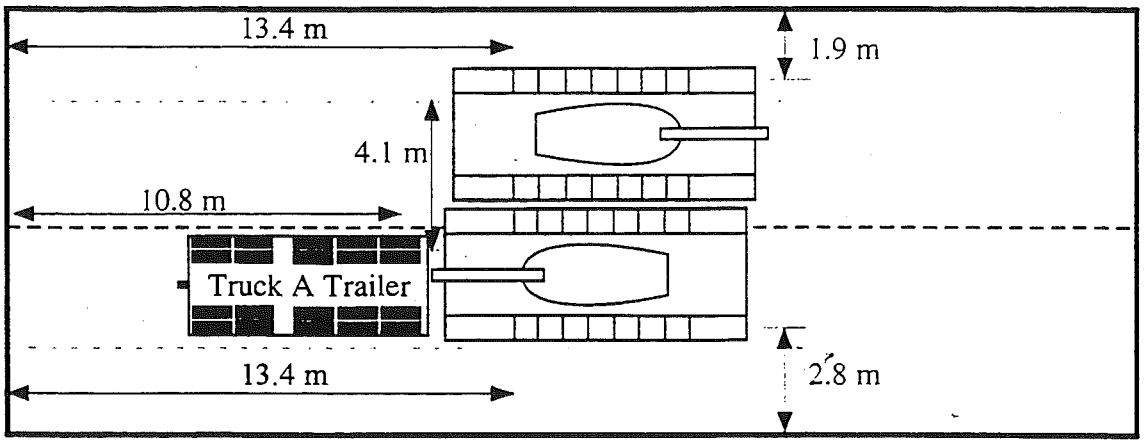

Figure 9.18. Location of Tanks and Trucks in Run 13.

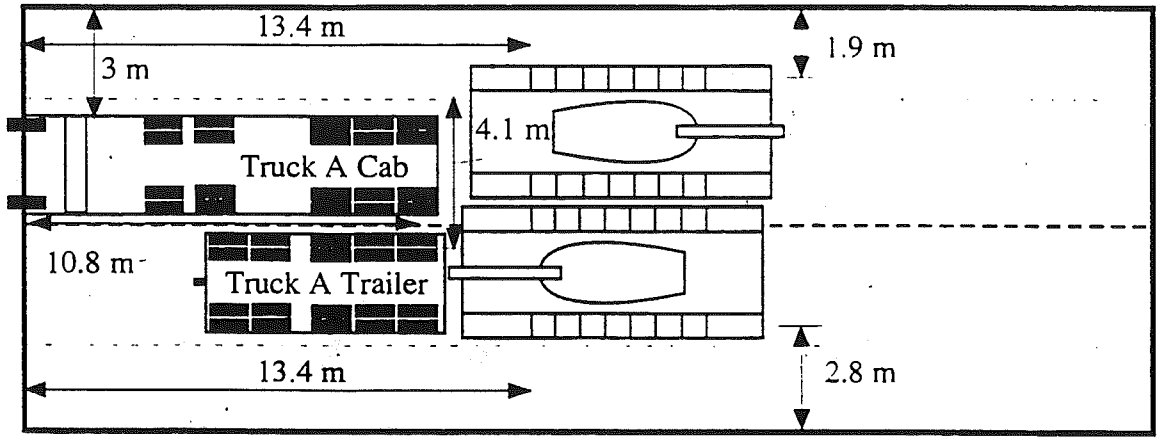

Figure 9.19. Location of Tanks and Trucks in Run 14.

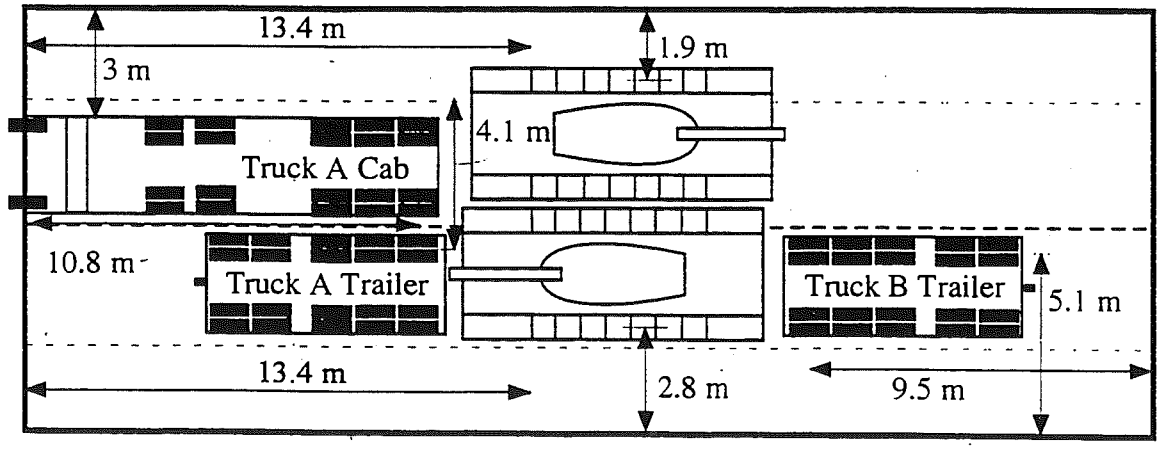

Figure 9.20. Location of Tanks and Trucks in Run 15.

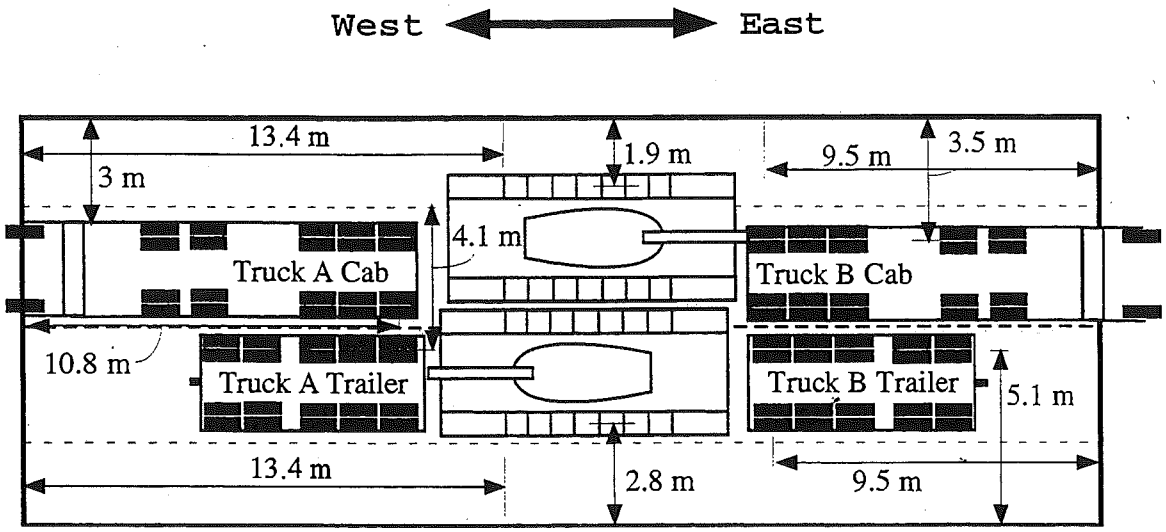

Figure 9.21. Location of Tanks and Trucks in Run 16.

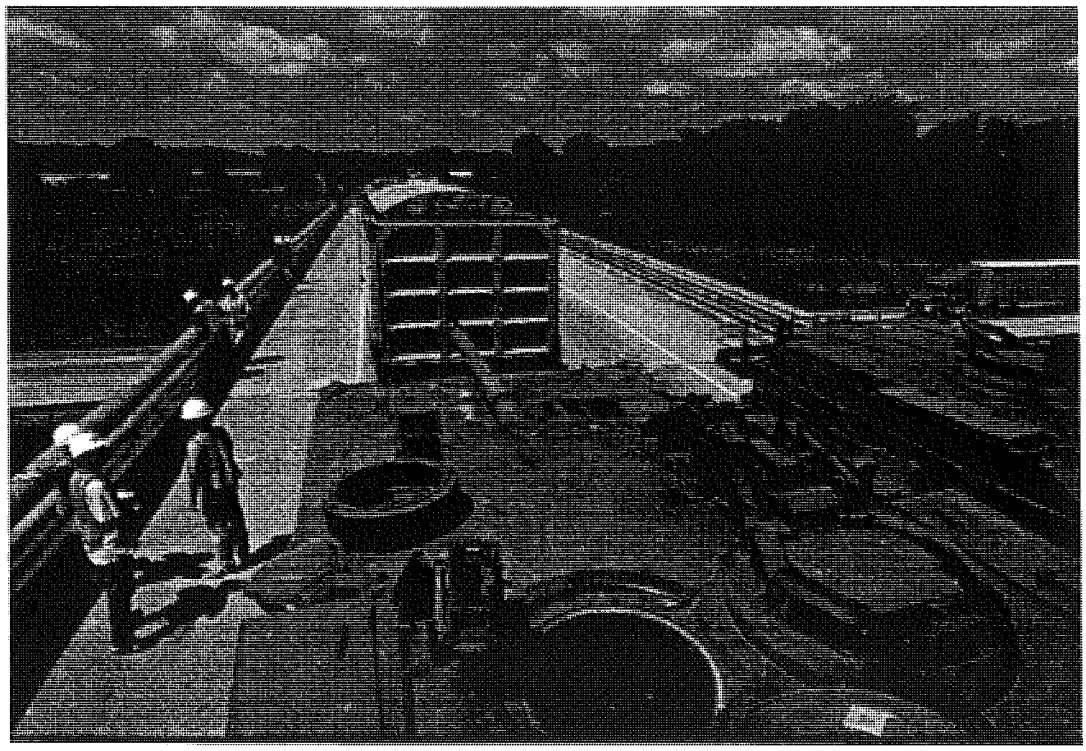

Figure 9.22. Proof Load Test in Progress.

9.5. Analysis Results

The three-dimensional finite element method (FEM) was applied to investigate the structural behavior of the bridge NDN/I69 (S03-13074). The concrete slab was modeled with isotrophic, eight node solid elements, with three degrees of freedoms at each node. The girder flanges and web were modeled using three-dimensional, quadrilateral, four node shell elements with six degrees of freedom at each node. The structural effects of the secondary members, such as the sidewalk and parapet, were also taken into account in the finite element analysis models.

Two cases of the boundary conditions were employed in the FEM models. In the first FEM model, it was assumed that the supports could be represented by a hinge at one end and a roller with a hinge at the other end. In the other FEM model, it was assumed that both supports were hinged, with no movement in horizontal direction.

Figure 9.23 illustrates the mesh of the FEM model, and Figure 9.24 shows the deformed shape of the bridge when it is loaded with two trucks side-by-side.

Figure 9.25 shows the results of the finite element analysis for two trucks side-by-side (Run 13). It includes the experimental results and analytical results for the two different models. In this bridge, the maximum strain from FEM is less than the measured value. FEM results show that the maximum strain at the most heavily loaded girder is about 290 με, while the maximum measured strain is about 340με. However, if the sum of strains for all girders is compared, test result is still lower than the FEM result. This indicates that the load distribution is less uniform than what is analytically obtained using FEM analysis.

Table 9.4 shows the results of the finite element analysis for the proof load test, compared with the test results. Only the most heavily loaded girder (Girder 3) was compared with test results for run 1 to 16. Figure 9.26 compares the strain values obtained by the finite element analysis with those from the test for run 16, which is the heaviest run in the proof load test. The result indicates that the maximum measured strain is still lower than expected from the finite element analysis. Also, the experimental response lies between the two different analytical models. This indicates that the partial fixity exists at the supports of the bridge. Deflection results of the FEM Models are summarized in Table 9.5 together with the test results.

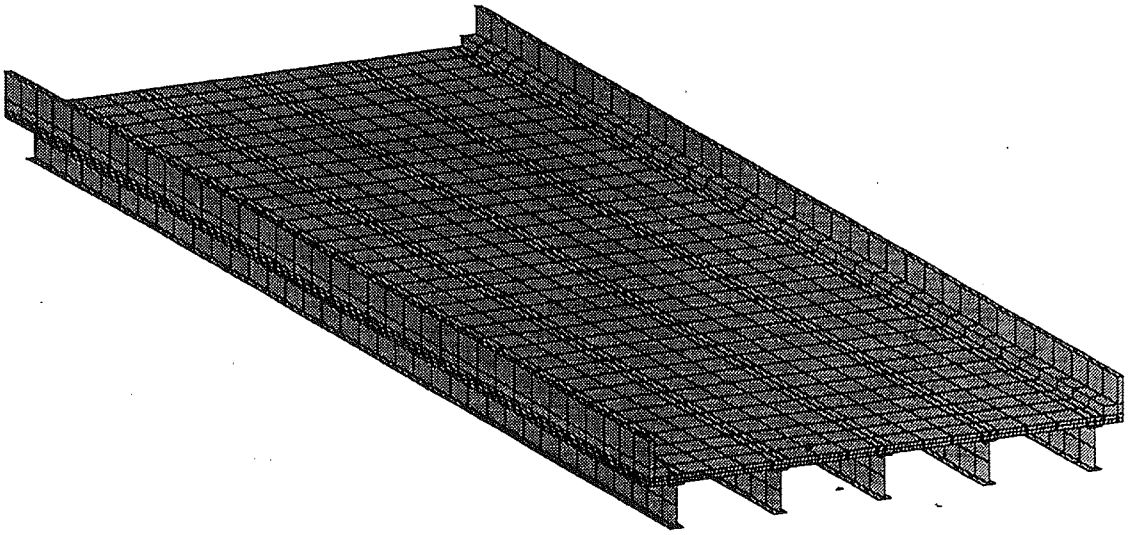

Figure 9.23. The Mesh of the Finite Element Model.
NDN/I69 (S03-13074).

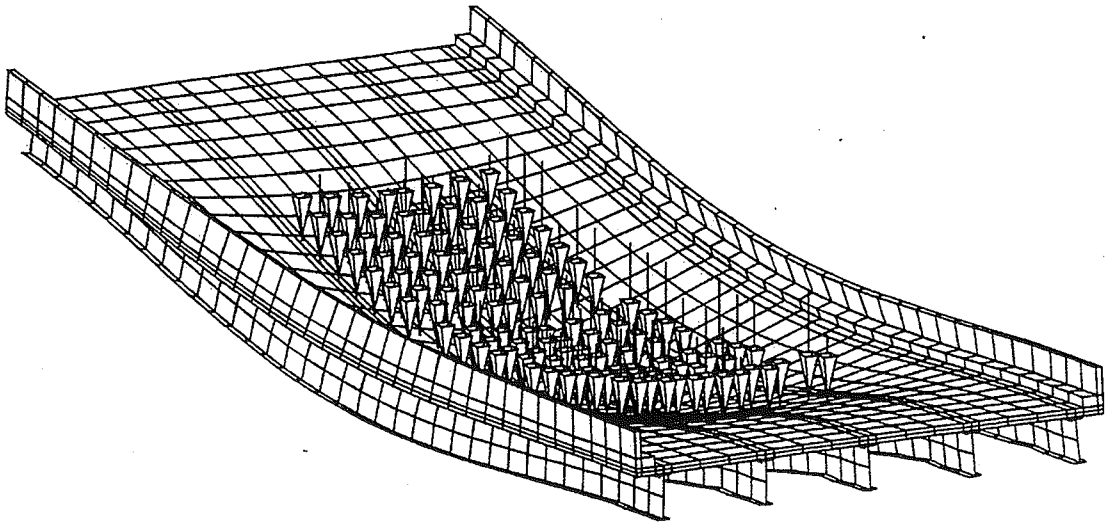

Figure 9.24. Deformed Shape of the Bridge NDN/I69 (S03-13074)
under Two Lane Loading.

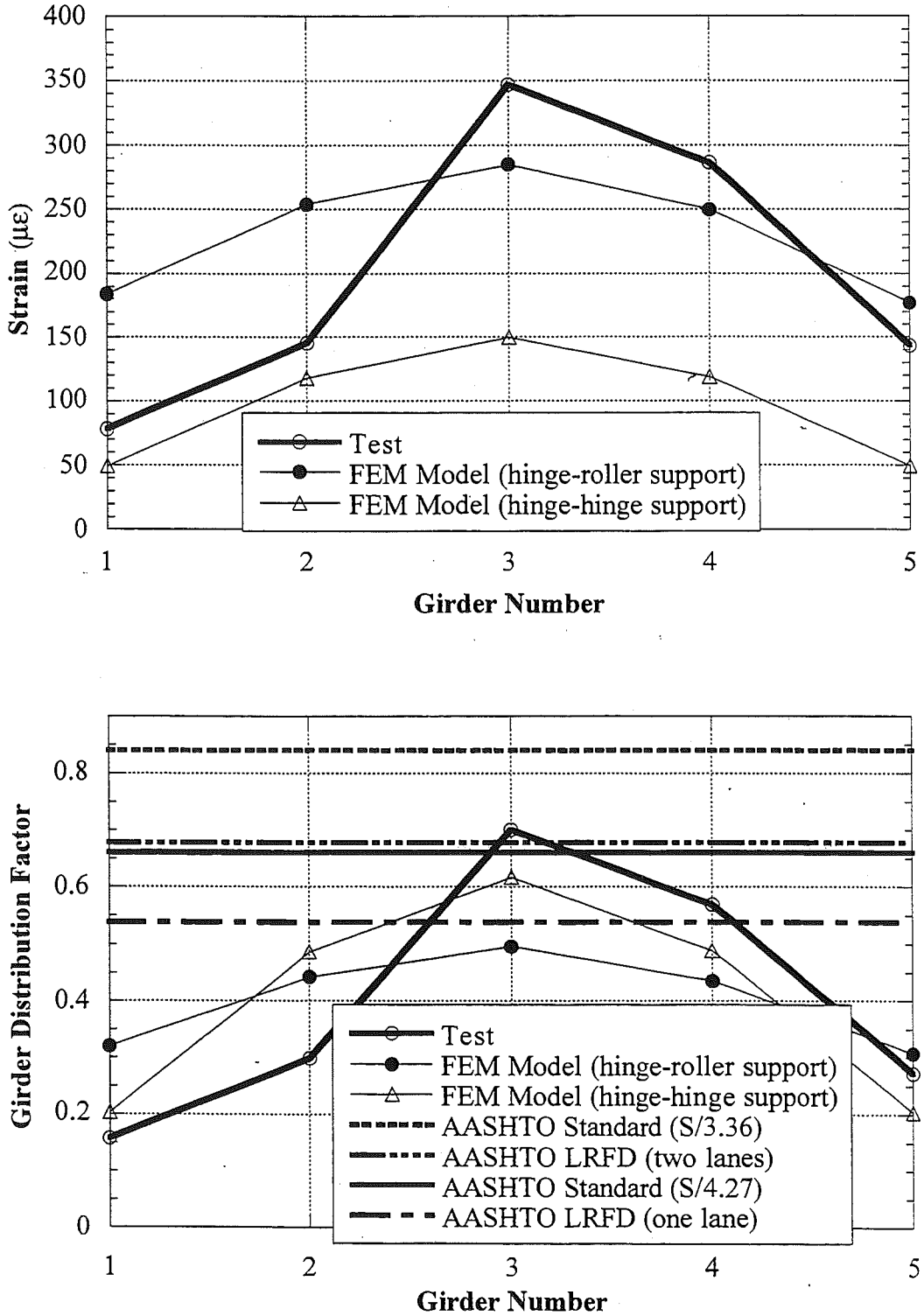

Figure 9.25. Results of the Finite Element Analysis, NDN/I69 (S03-13074).

Table 9.4. Comparison of the maximum strain from the test and FEM results for the poof load test.

Run #	Maximum Measured Strain (10^{-6})	Strain from Finite Element Analysis (10^{-6})	
		Hinge-Roller Support	Hinge-Hinge Support
1	153	145	93
2	167	173	101
3	175	177	103
4	186	190	109
5	203	211	119
6	182	145	93
7	218	166	99
8	225	175	102
9	243	189	109
10	275	219	124
11	289	274	171
12	298	288	178
13	330	318	192
14	351	365	213
15	380	397	224
16	402	428	233

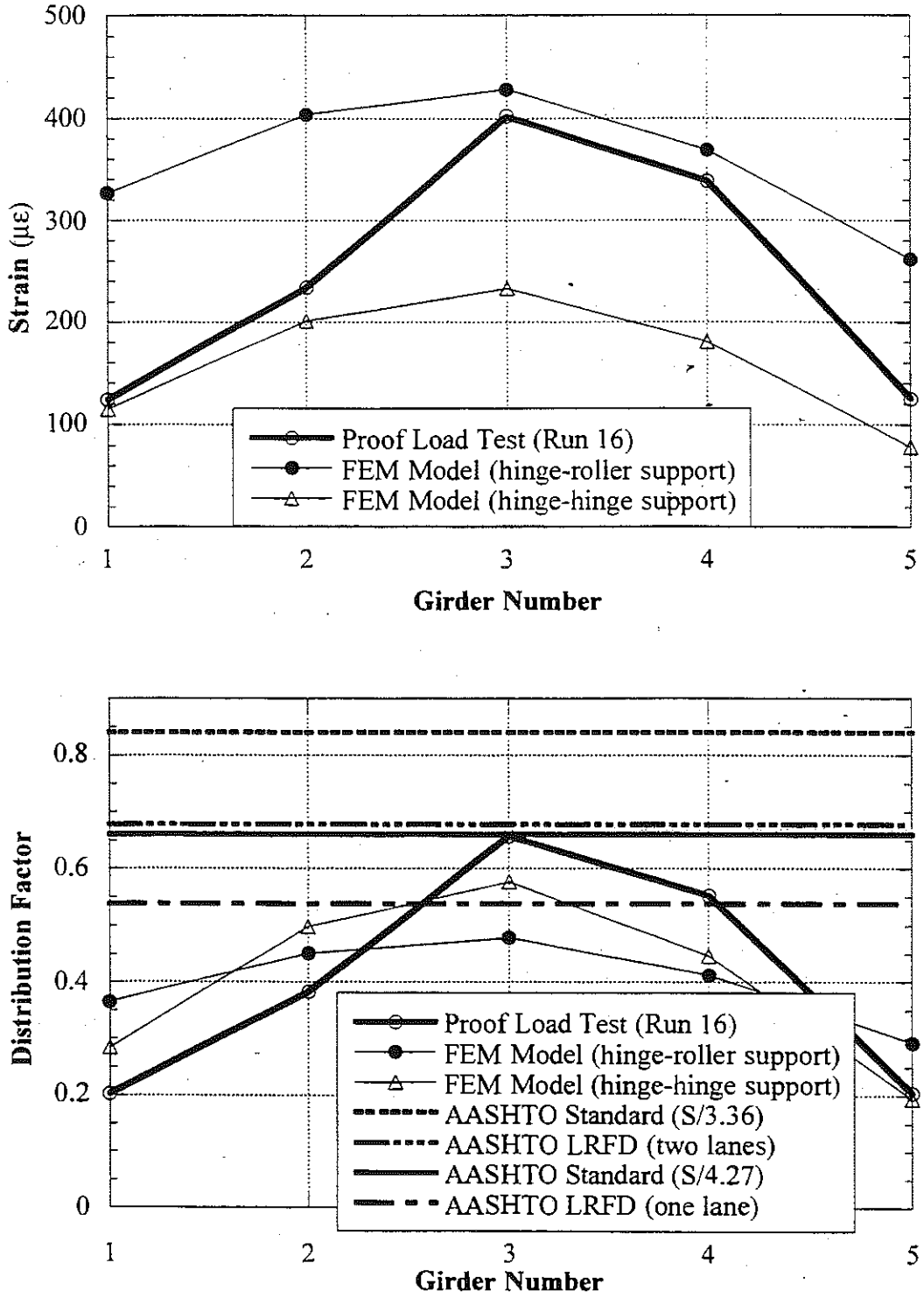

Figure 9.26. Finite Element Analysis Result for Proof Load Test Run 16. Bridge NDN/I69 (S03-13074)

9.6. Load Distribution Test Results

The resulting strains and GDF's are shown in Fig. 9.27 through 9.31. Figures 9.27 to 9.29 present the results of all crawling-speed (static) tests. Figures 9.27 to 9.28 present static strains and GDF's for one truck on the bridge. The maximum strain due to a single truck is about 230 με. This corresponds to about 45 Mpa.

Figure 9.29 shows static strains and GDF's from side-by-side static load tests. For two vehicles side-by-side the maximum strain is about 370 με (which corresponds to 75 MPa). The superposition of strains due to a single truck in North and South lanes produces almost the same results as strain due to two trucks side-by-side.

For two trucks side-by-side, the girder distribution factor for girder i is determined using Eq. 4.4. For comparison, GDF are also calculated according to AASHTO Standard (1996) and AASHTO LRFD Code (1998). Two cases were considered, a single lane loaded, and two lanes loaded. The resulting GDF's are shown in Fig. 9.27 through 9.31.

The results indicate that GDF values specified in AASHTO LRFD almost exactly predicted the actual behavior of this bridge. However, AASHTO Standard code-specified GDF's are conservative. GDF's specified for a single lane are not sufficient for two lane load cases.

Figure 9.30 and 9.31 shows the resulting strain and distribution factors from normal speed tests. There is practically no difference between the crawling speed and normal speed results.

Figures 9.32 through 9.34 show deflections of girders and corresponding girder distribution factors when truck load is applied at crawling speed. Figure 9.32 and 9.33 shows the strains and GDF's from north lane loading and south lane loading, respectively. The maximum

deflection caused by one lane loading was less than 17 mm. The girder distribution factors calculated from the deflection show better distribution than those from the strain values.

Figure 9.34 presents the deflections due to two truck side-by-side loadings. The range of the LVDT's installed for this bridge is 25.4 mm. Furthermore, it is not possible to use all the range of the LVDT's because the reference position of the LVDT's should be somewhere inside the usable range. As a result, the deflections at girder 3 and girder 4 were out of range during the test. Therefore, superposed values of one truck loadings are shown for the girder 3 and the girder 4 in Figure 9.34. For girder 1, 2, and 5, the deflections were still in the range of the LVDT's and actual values from the test are shown in Figure 9.34.

Dynamic load factor (DLF) is defined in section 4.4. In Figure 9.35, DLF's are plotted for all load cases involving normal speed (no dynamic load was measured for crawling speed runs). Large values of DLF in exterior girders correspond to load cases with a single truck in the opposite lane (resulting in very low static strain).

The relationship between DLF and static and dynamic strains is shown in Fig. 9.36. The open circles correspond to static strain, ε_{stat}, and black solid squares correspond to dynamic strain, ε_{dyn}. For each static strain value (open circle), the corresponding dynamic strain is denoted by solid square (the numbers of circles and squares are same). It is clear from the Figure 9.36 that dynamic strains does not exceed 25 $\mu\varepsilon$ for all the cases while the static strain can exceed 340 $\mu\varepsilon$ in normal speed test. It is concluded that DLF corresponding to the maximum strain caused by two trucks side-by-side, is less than 0.10 for the most heavily loaded girder. It also justifies the use of 0.10 as a dynamic load factor in the calculation of proof load.

Girder No. 3 was instrumented with remote deflection measurement device manufactured by Noptel. The reflector was installed

at midspan. The result is shown in Table 9.5. The maximum deflection recorded during the test is 26.6 mm for girder number 3. For two trucks side-by-side truck loading, LVDT's were out of range. Therefore, comparison could not be made for those runs. For other runs, results from LVDT and Noptel equipment are compared and the differences are tabulated in Table 9.5.

Table 9.5. Maximum deflections measured at the center of Girder No. 3 due to truckloads, Bridge NDN/169 (S03-13074).

Run #	Finite Element Analysis		Vertical Optic (mm)	Vertical LVDT (mm)	Difference Optic & LVDT (Vertical, %)
	Roller Support	Fixed Support			
1	12.54	7.24	NA	12.20	-
2	16.76	9.29	NA	7.40	-
3	17.25	9.53	NA	12.30	-
4	19.11	10.7	7.77	7.30	6.4
5	21.33	11.81	12.73	12.10	5.2
6	12.64	7.33	12.73	12.05	5.6
7	15.81	8.87	12.36	12.36	0
8	16.97	9.41	7.38	7.85	-6.0
9	18.91	10.61	12.42	12.36	0.5
10	22.11	12.23	7.00	7.56	-7.4
11	24.33	13.79	12.21	12.21	0
12	26.27	14.99	12.57	12.68	-0.9
13	29.39	16.46	25.18	OUT	-
14	34.71	19.19	26.61	OUT	-
15	39.19	21.40	24.74	OUT	-
16	43.67	23.60	24.74	OUT	-

9.7. Proof Load Test Results

The proof load test was successfully completed without any sign of distress to the structure. Figure 9.37 and 9.38 shows strains and girder distribution factors when proof load is applied on the north lane and south lane, respectively. The corresponding load positions for Figure 9.37 and 9.38 are shown in Figures 9.6 through 9.15. The maximum strain value caused by one lane loading is about 280 με. This corresponds to about 55 Mpa. Figure 9.39 shows strains and GDF's for side-by-side tanks and trucks. The load positions for Figure 9.39 are shown in Figure 9.16 through 9.21. The maximum strain due to the side-by-side loadings is about 400 με. This corresponds to about 80 Mpa, much lower than expected value from the pretest analysis, shown in Table 9.3.

Figures 9.40 and 9.42 show deflections of girders when proof load is applied on the north and south lane, respectively. The maximum deflection caused by one lane loading was about 20 mm. Figure 9.41 and 9.43 shows GDF's calculated from deflection caused by one lane loadings. The girder distribution factors calculated from the deflection show better distribution than those from the strain values. Figure 9.44 presents the deflections due to side-by-side loadings. The range of the LVDT's installed for this bridge is 25.4 mm. For runs 13 through 16, the deflection values at some girders exceed the limit of the LVDT's. Therefore, only runs 11 and 12 are shown in the figures. Figure 9.45 shows GDF's calculated from the deflections occurred due to side-by-side loadings.

The strains were also measured close to the support. Figures 9.46 and 9.47 present the strains recorded at the east and west support, respectively. Negative strain values indicate the strains recorded at the bottom flanges near supports were in compression, due to the partial fixity of support. The strain values near the support were measured

when the loads caused the maximum strain at the midspan. The levels of support fixity are highly unpredictable. Even in a bridge, each girder has different support behavior. There are differences in the sign of strain between the girders. This requires some further investigation.

Figures 9.48 to 9.52 plot applied moment per girder versus measured strain, for girder 1 to 5. The applied moment per girder was obtained by multiplying, for each load case, the total applied moment due to the load by the GDF from the strain values measured for that load case. All girders showed reasonably linear behavior.

Figure 9.53 to 9.57 present the applied moment per girder versus measured deflection, for girders 1 to 5. For runs 13 to 16, the LVDT's were out of range. Therefore, the deflection values obtained only from runs 1 through 12 are shown in the Figures. Again, all girders showed reasonably linear behavior.

As for the load distribution test, girder No. 3 was instrumented with remote deflection measurement device manufactured by Noptel, and deflections were measured. The result is shown in Table 9.6. The maximum deflection recorded during the test is 38.6 mm for girder number 3. For runs 13 through 16, LVDT's were out of range. Therefore, comparison could not be made for those runs. For other runs, results from LVDT and Noptel equipment are compared and the differences are tabulated in Table 9.6.

As it is seen in Table 9.4, the test results are in general between the analytical results of two different finite element models. This indicates that the supports of the bridge have partial fixity in horizontal direction. Moreover, the test GDF is not as uniform as those from the FEM analysis, as shown in Figure 9.26. This indicates that the level of partial fixity is not easily predictable.

Table 9.6. Maximum deflections measured at the center of the third girder due to proof loading, Bridge NDN/I69 (S03-13074).

Run #	Horizontal (mm)	Vertical (mm)	Vertical LVDT (mm)	Difference Optic & Vertical (%)
1	1.99	11.17	11.17	0
2	2.45	14.46	13.62	6.1
3	2.36	14.56	14.49	0.5
4	2.52	16.74	16.38	2.2
5	2.66	18.69	18.37	1.7
6	1.39	10.40	11.42	-9.0
7	1.65	13.01	13.97	-6.8
8	1.63	13.80	14.51	-4.9
9	1.46	15.84	16.35	-3.1
10	1.41	18.25	18.65	-2.1
11	2.30	21.02	21.09	-0.4
12	1.85	24.82	23.13	7.3
13	1.88	24.75	OUT	-
14	2.00	31.11	OUT	-
15	1.81	34.10	OUT	-
16	2.24	38.61	OUT	-

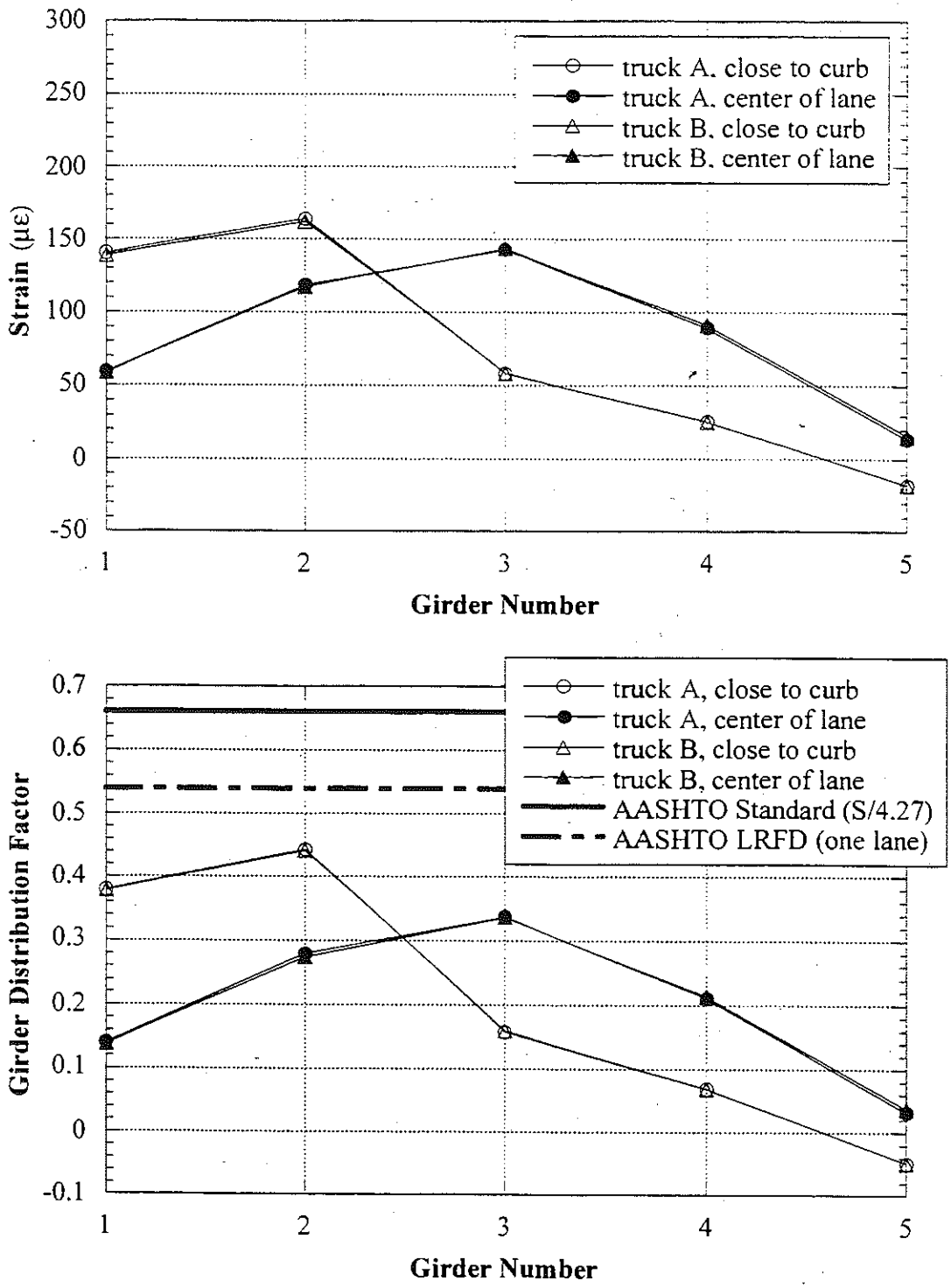

Figure 9.27. North Lane, Crawling Speed, NDN/I69 (S03-13074).

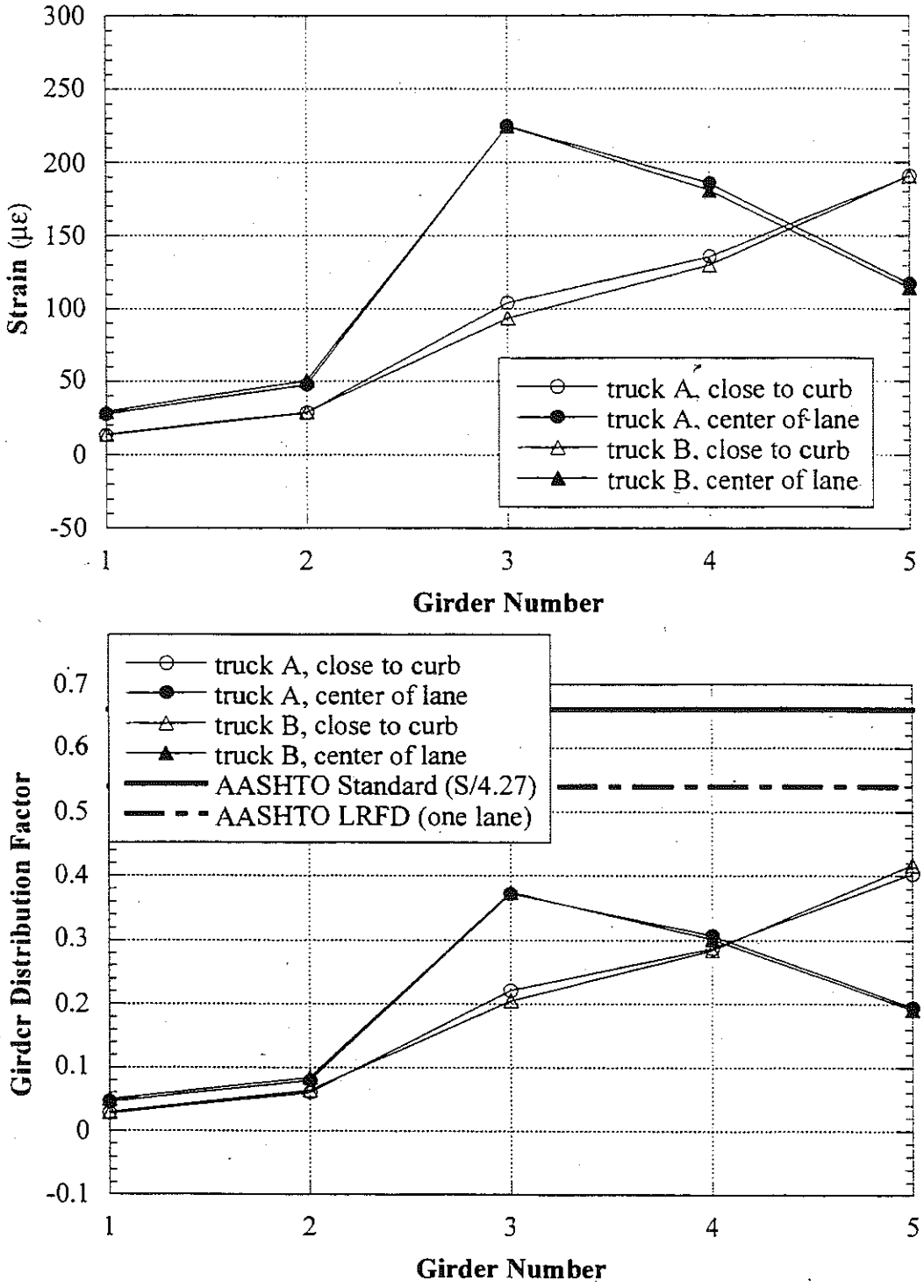

Figure 9.28. South Lane, Crawling Speed, NDN/I69 (S03-13074).

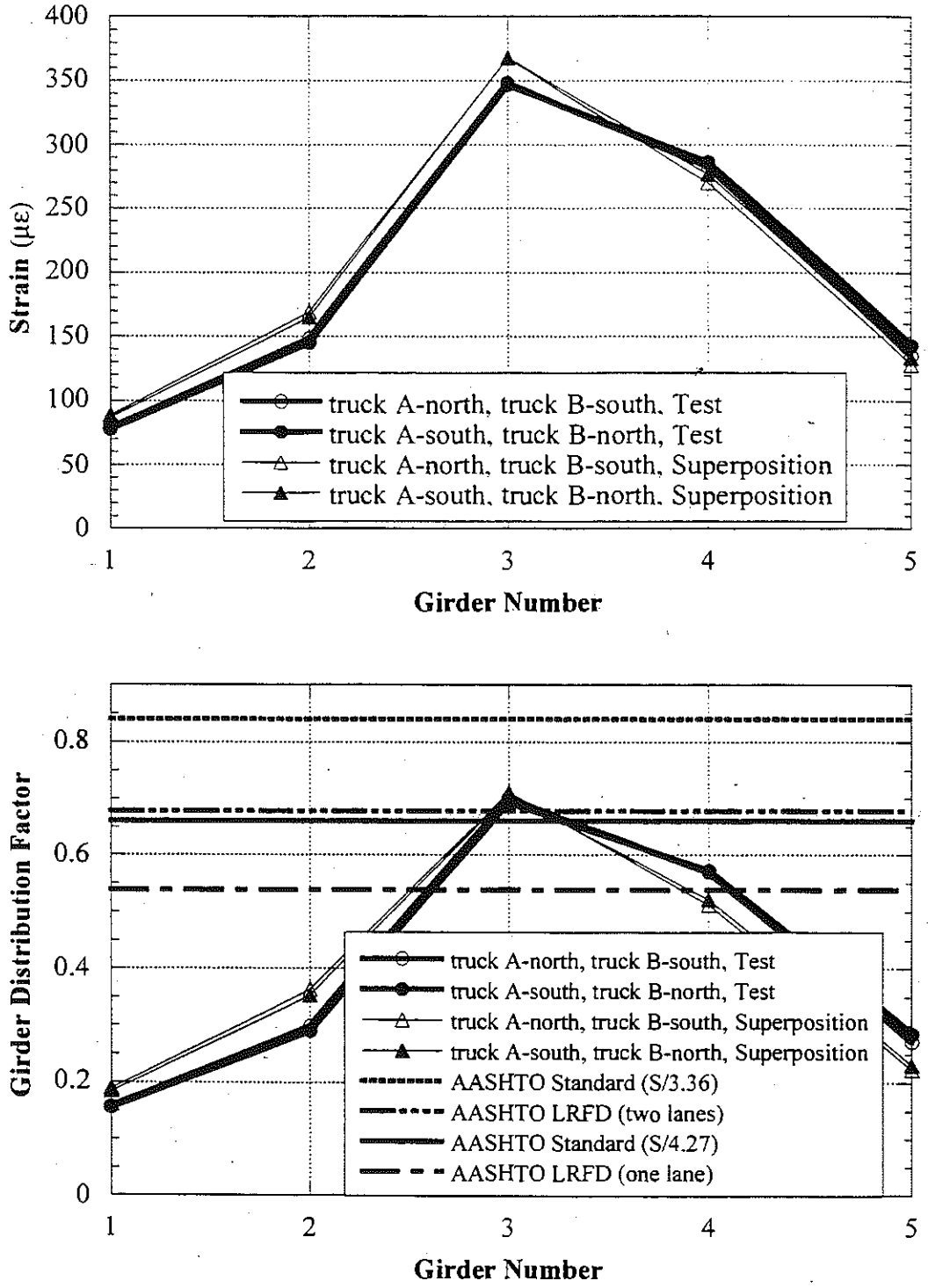

Figure 9.29. Side-by-Side Loading, Center of Lane, Crawling Speed, NDN/I69 (S03-13074).

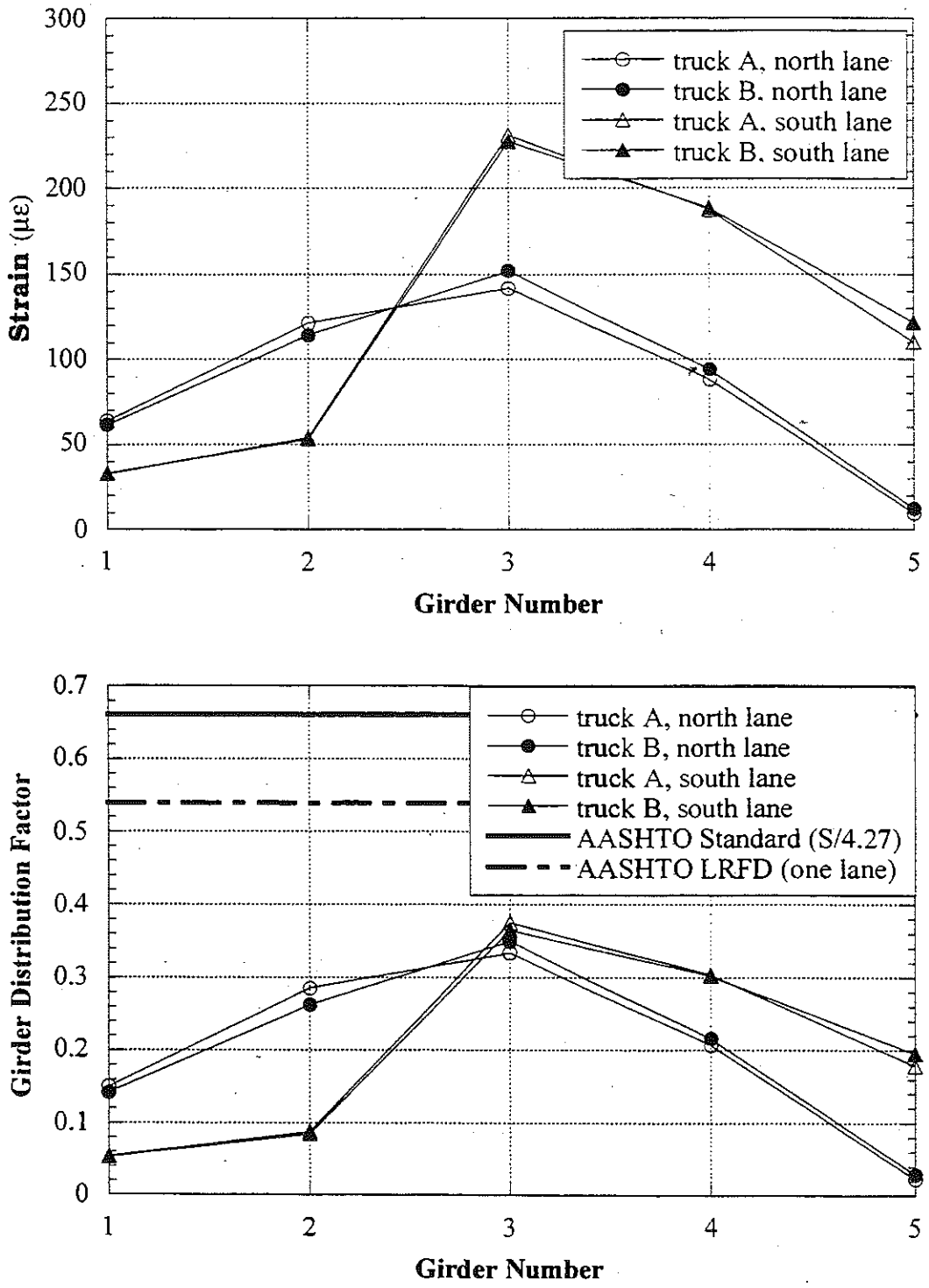

Figure 9.30. Strain and GDF under One Truck Loading at Regular Speed, NDN/169 (S03-13074).

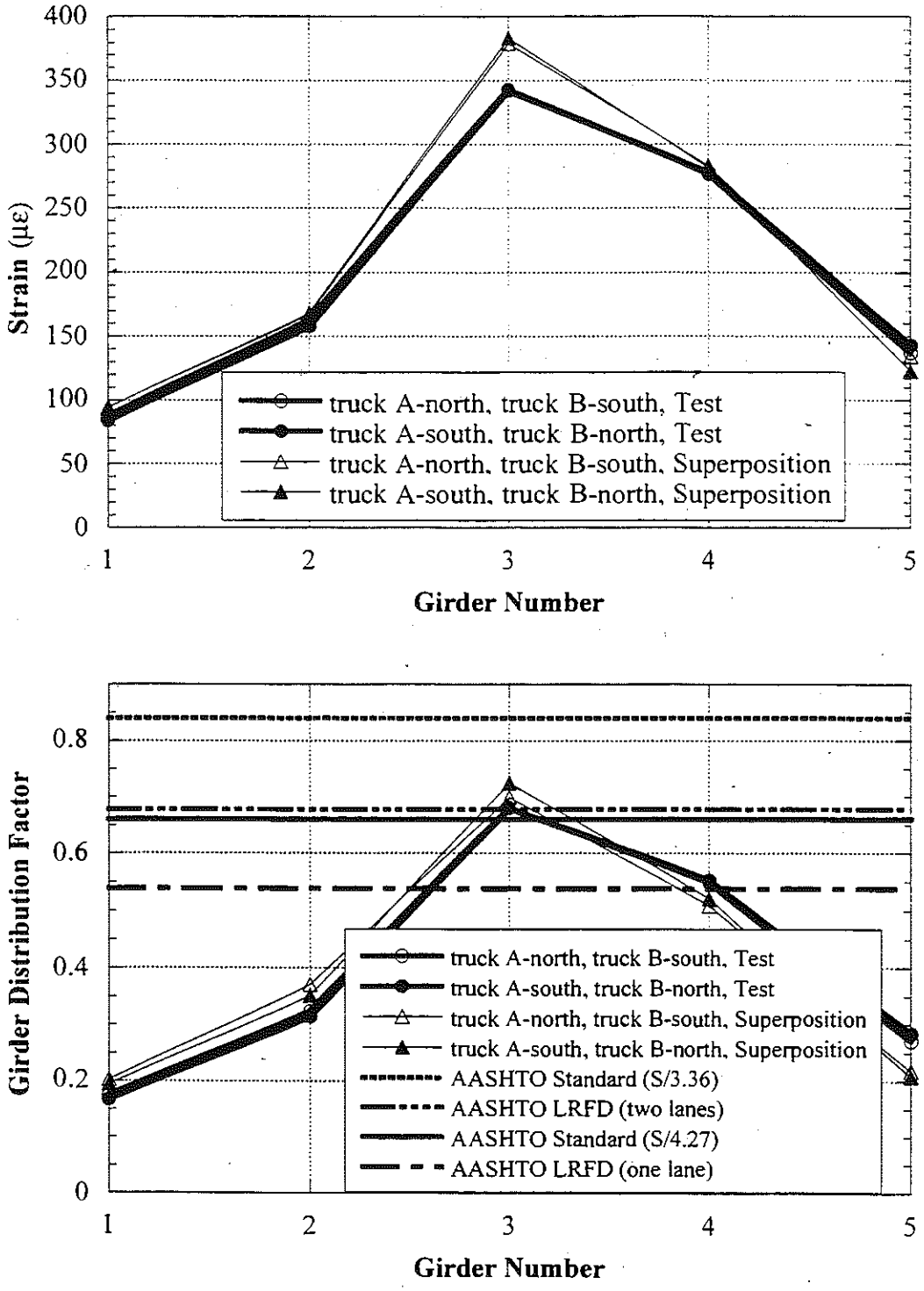

Figure 9.31. Strain and GDF under Side-by-Side Loading at Regular Speed, NDN/I69 (S03-13074).

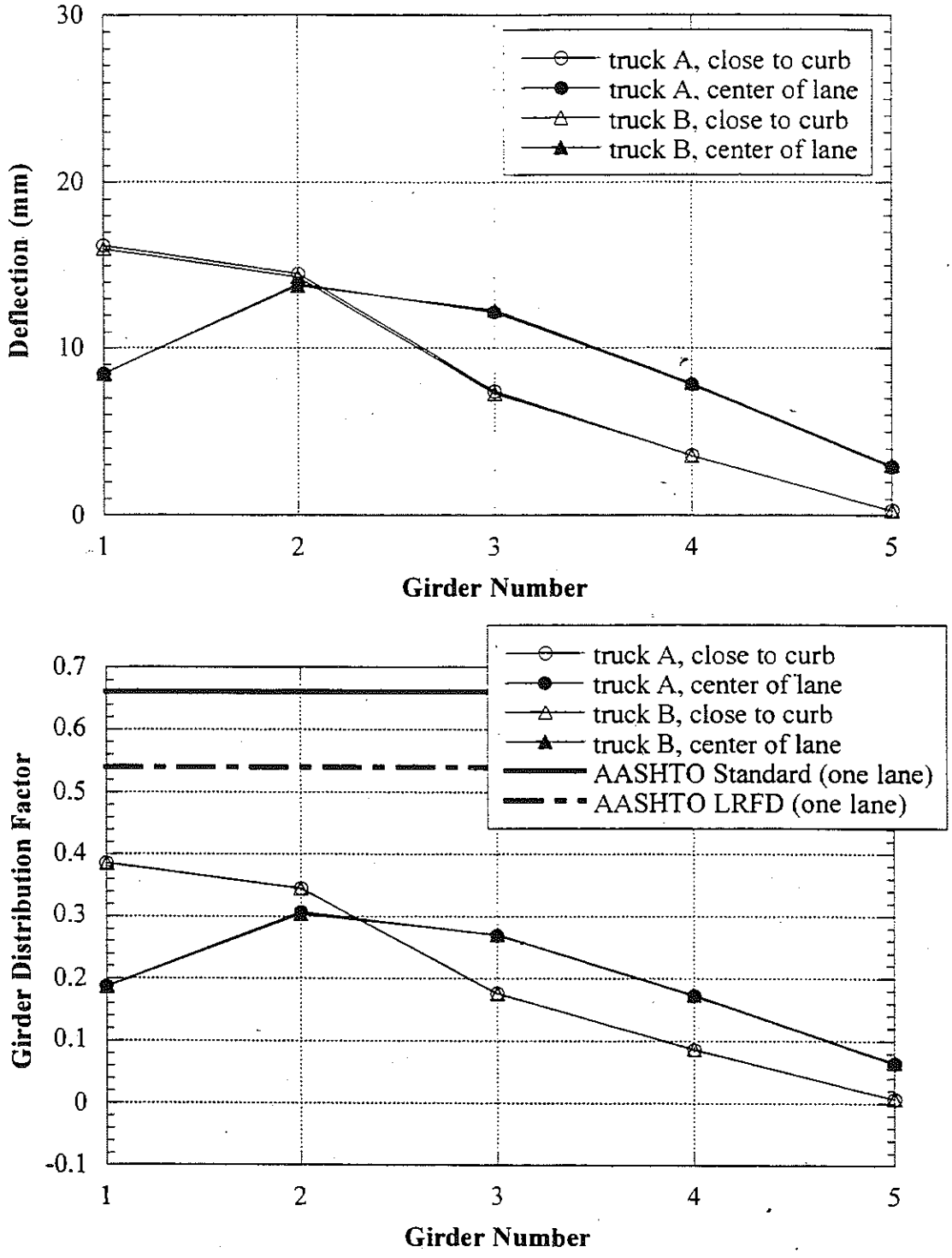

Figure 9.32. Deflection and GDF calculated from Deflections, North Lane Loading, Crawling Speed, NDN/I69 (S03-13074).

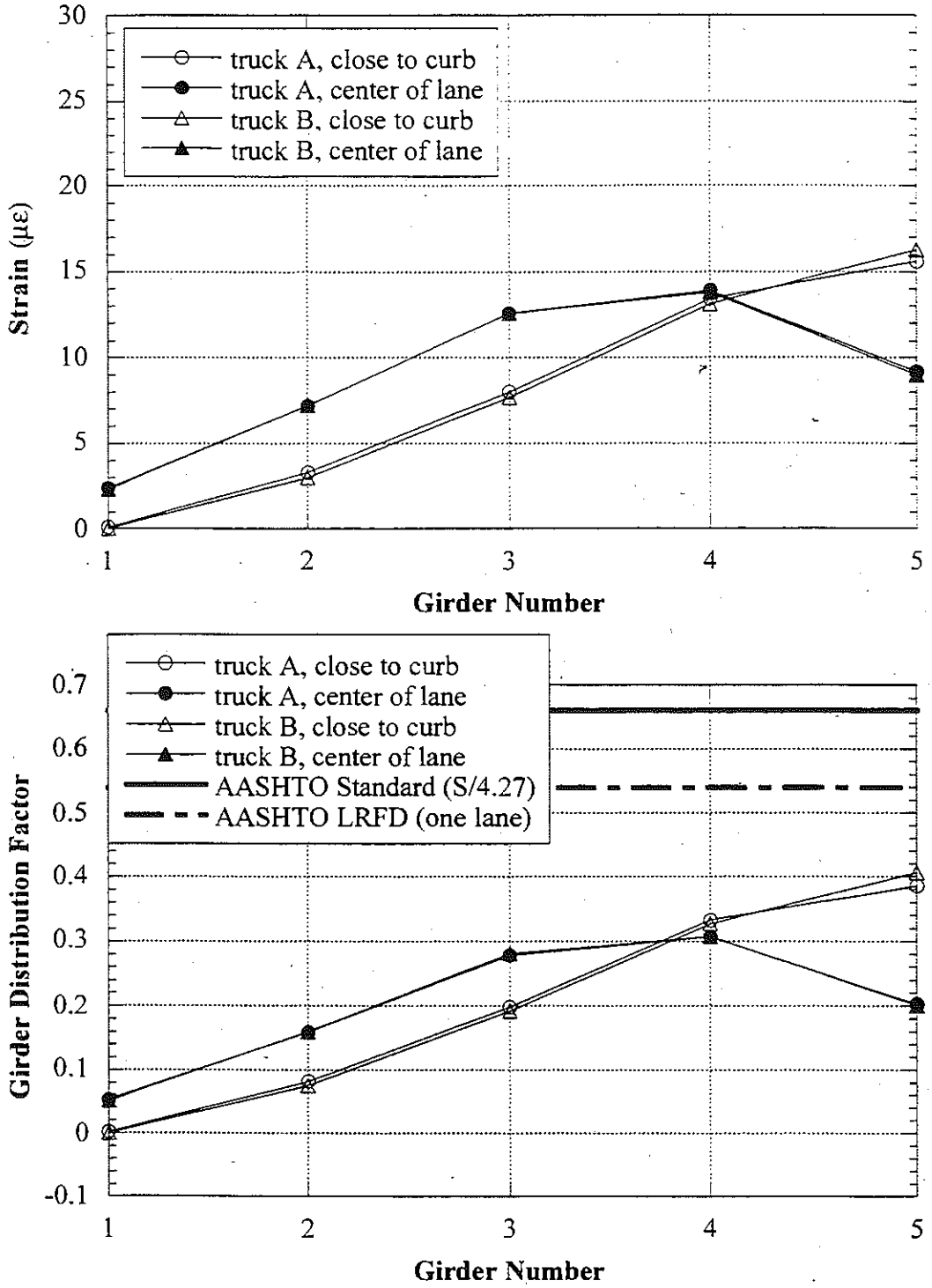

Figure 9.33. Deflection and GDF calculated from Deflections, South Lane Loading, Crawling Speed, NDN/I69 (S03-13074).

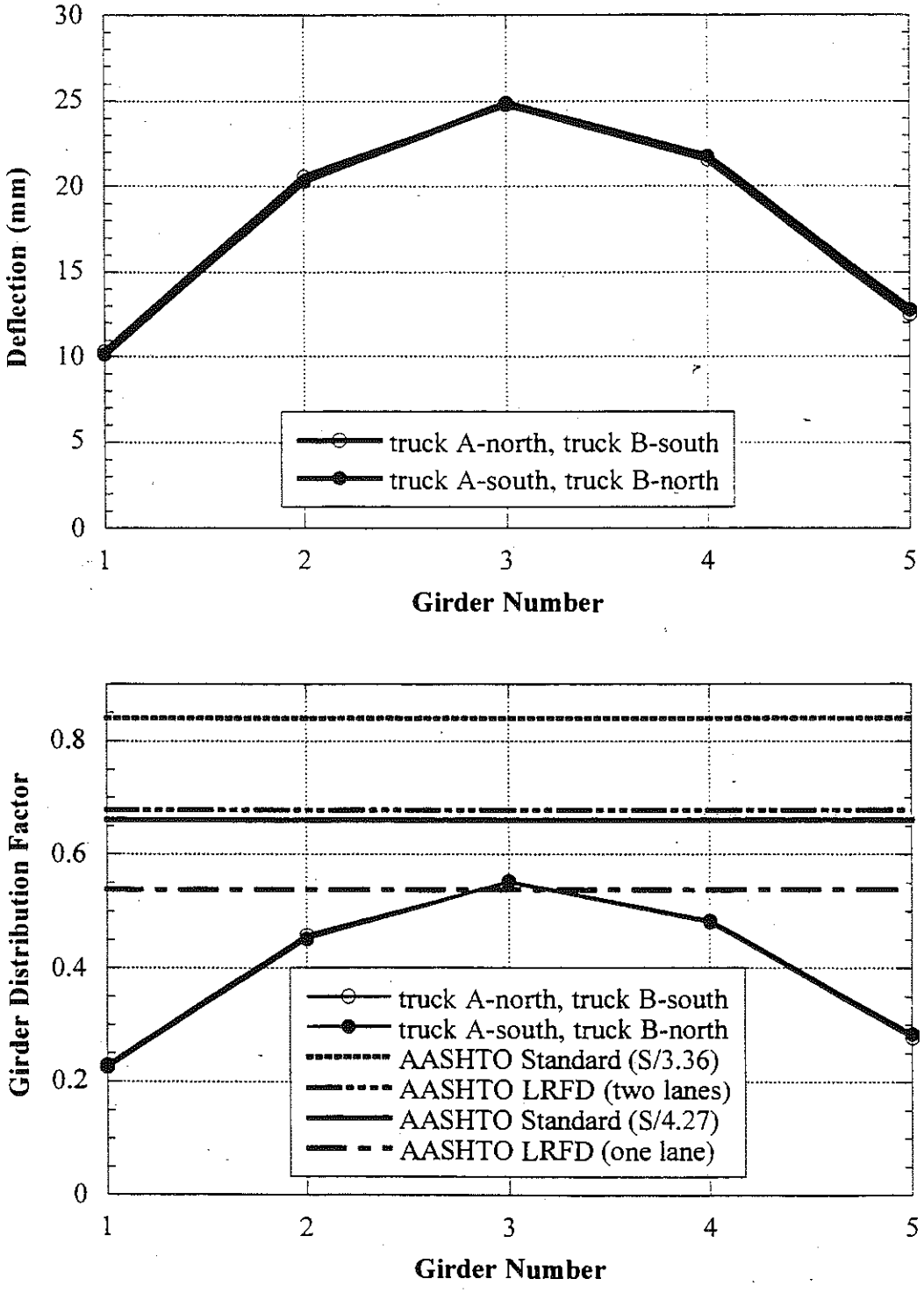

Figure 9.34. Deflection and GDF calculated from Deflections, Side-by-Side Loading, Crawling Speed, NDN/169 (S03-13074).

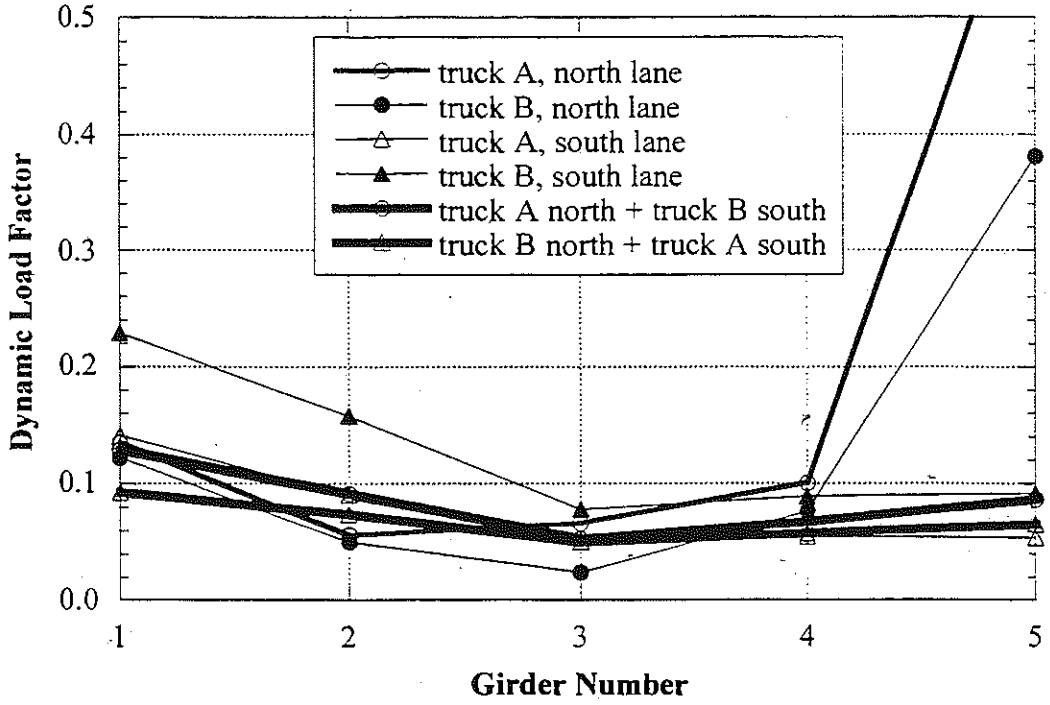

Figure 9.35. Dynamic Load Factor, NDN/I69 (S03-13074).

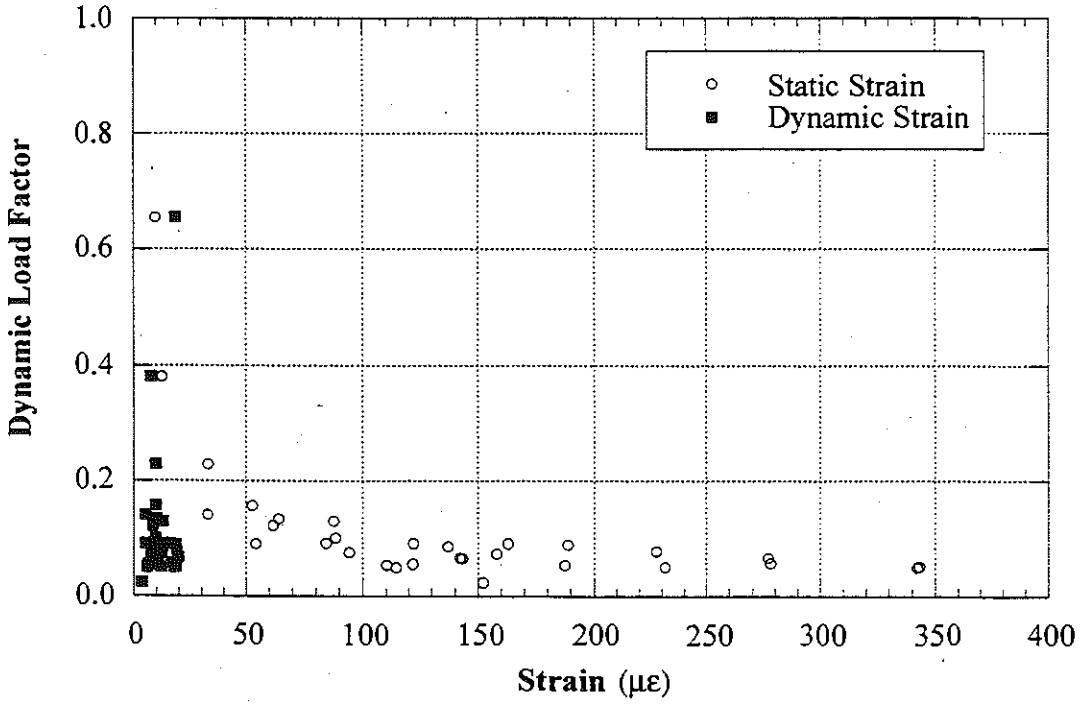

Figure 9.36. Strain vs. Dynamic Load Factor, NDN/I69 (S03-13074).

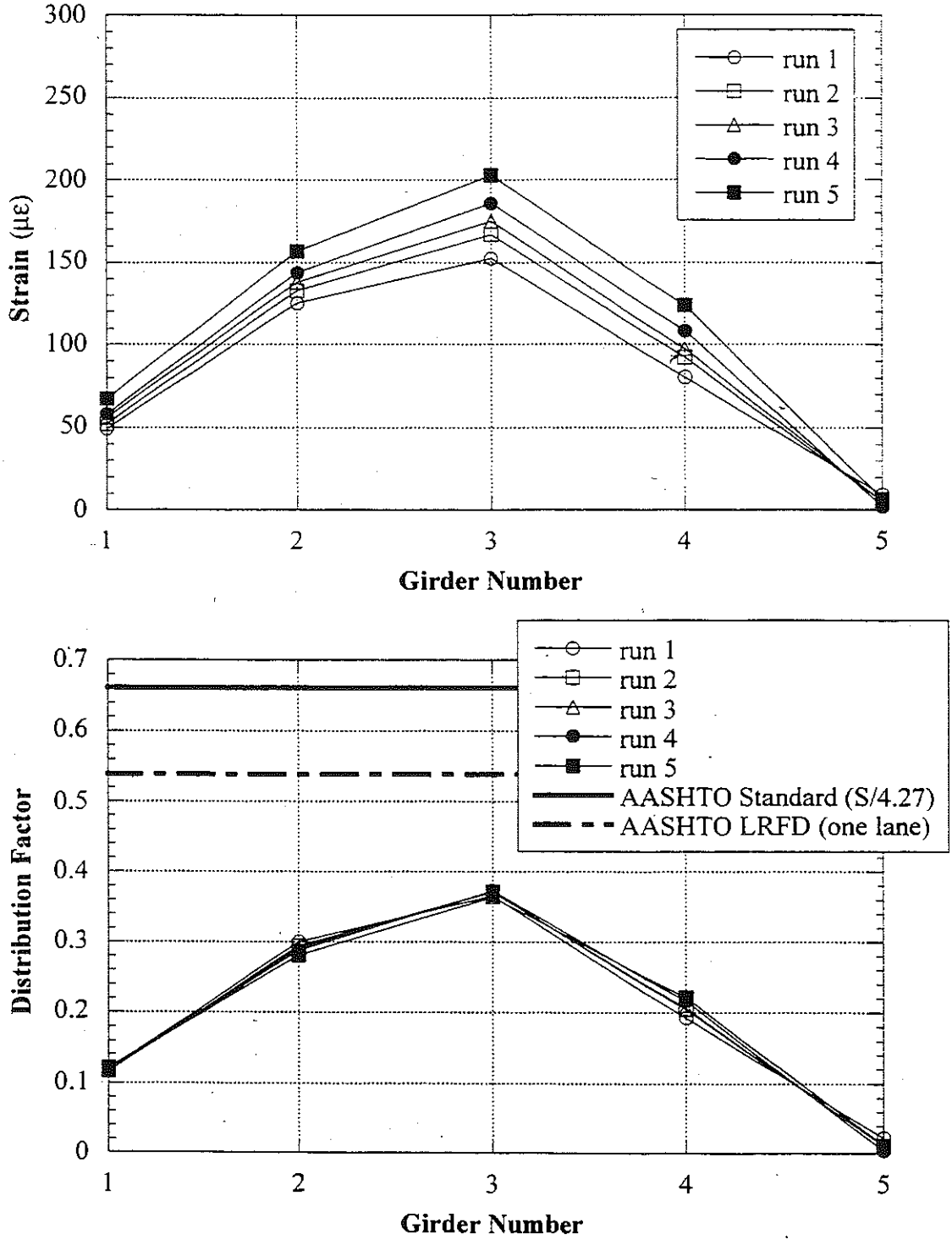

Figure 9.37. Proof Load, North Lane Loading, NDN/I69 (S03-13074).

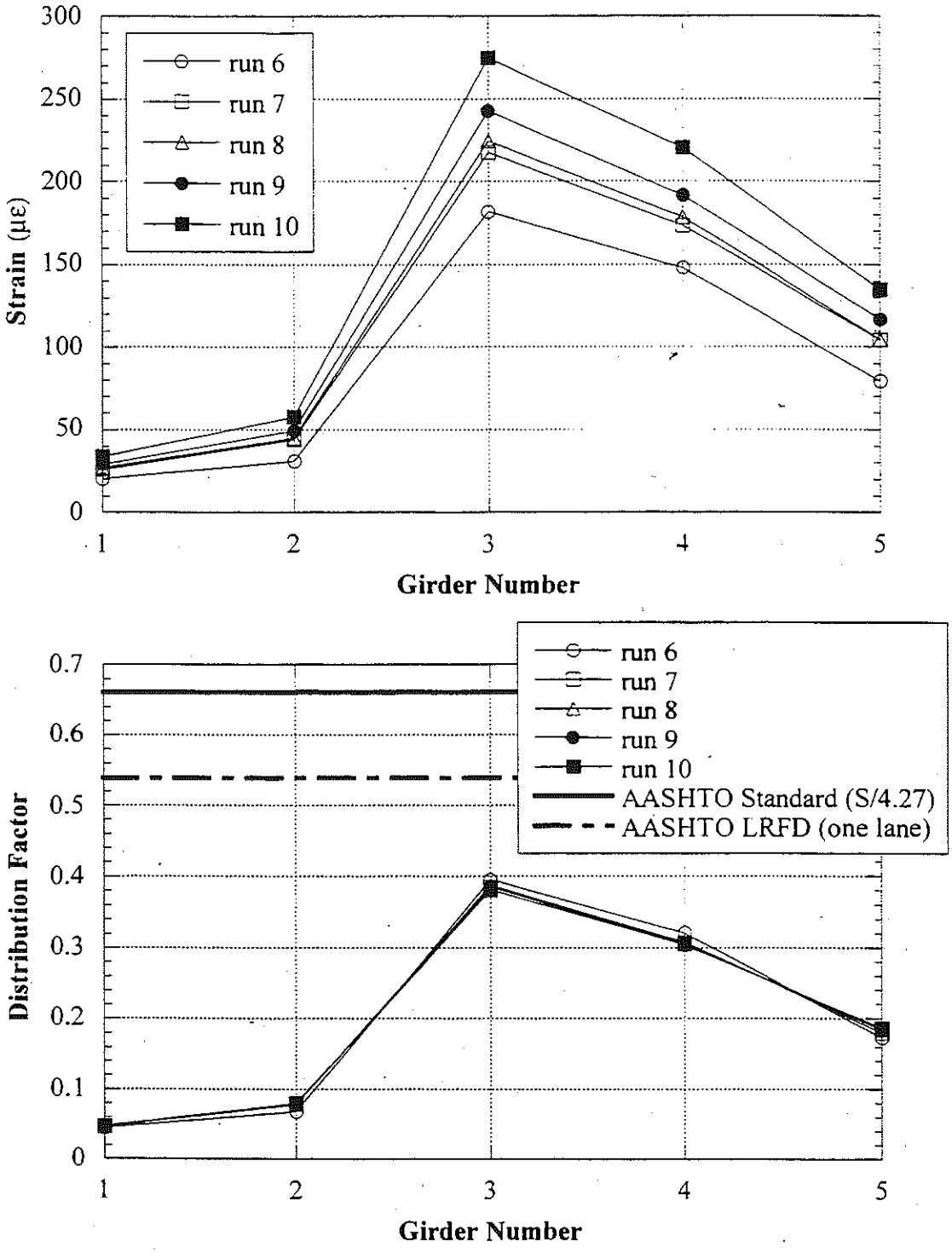

Figure 9.38. Proof Load, South Lane Loading, NDN/I69 (S03-13074).

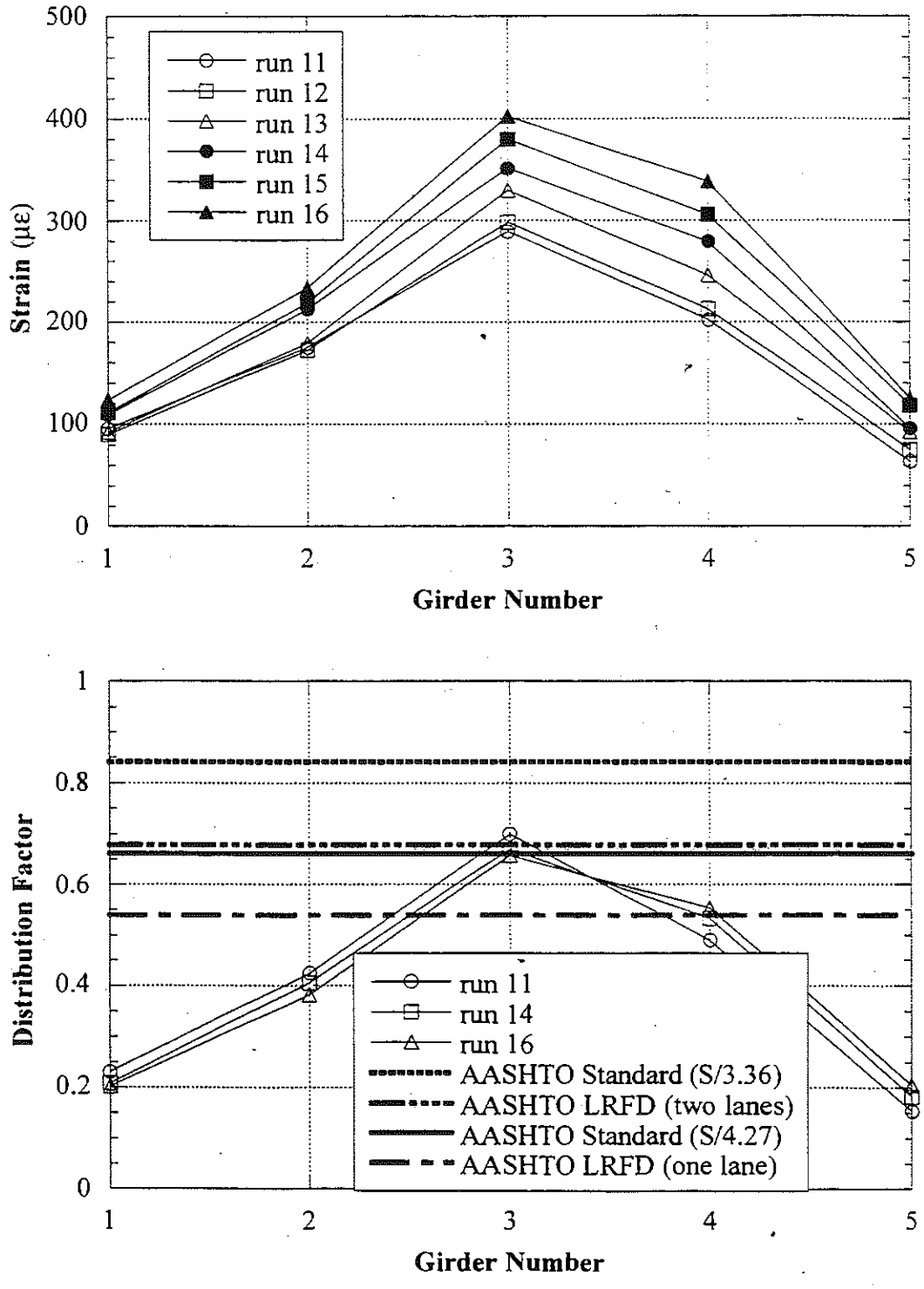

Figure 9.39. Proof Load, Side-by-Side Loading, NDN/I69 (S03-13074).

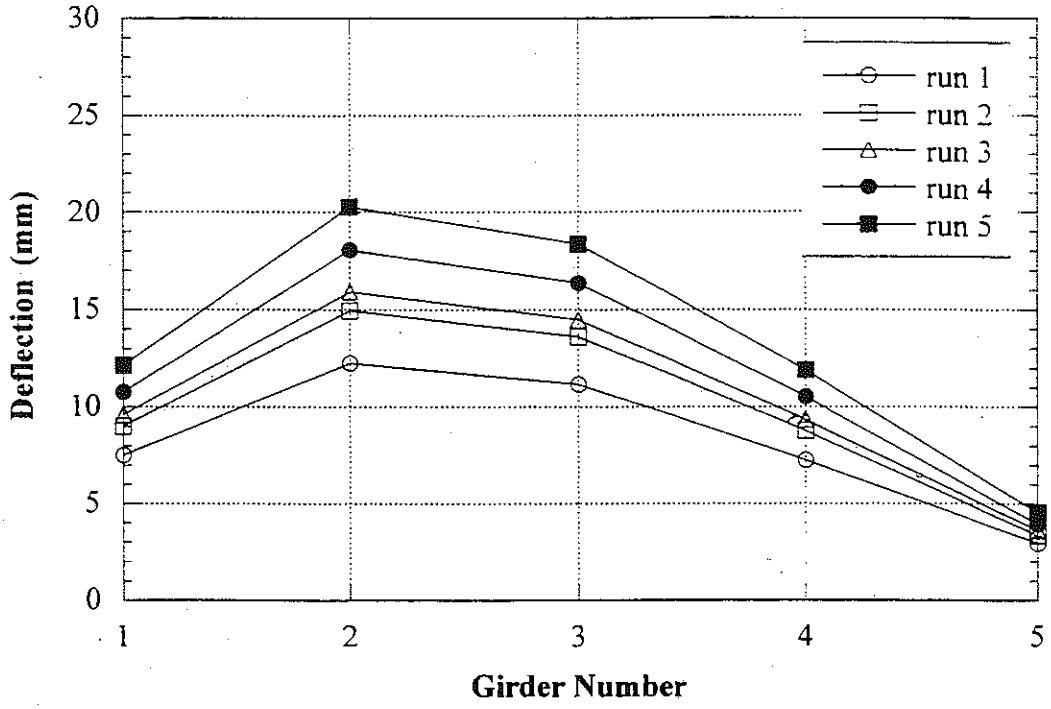

Figure 9.40. Deflections due to Proof Load, North Lane Loading, NDN/I69 (S03-13074).

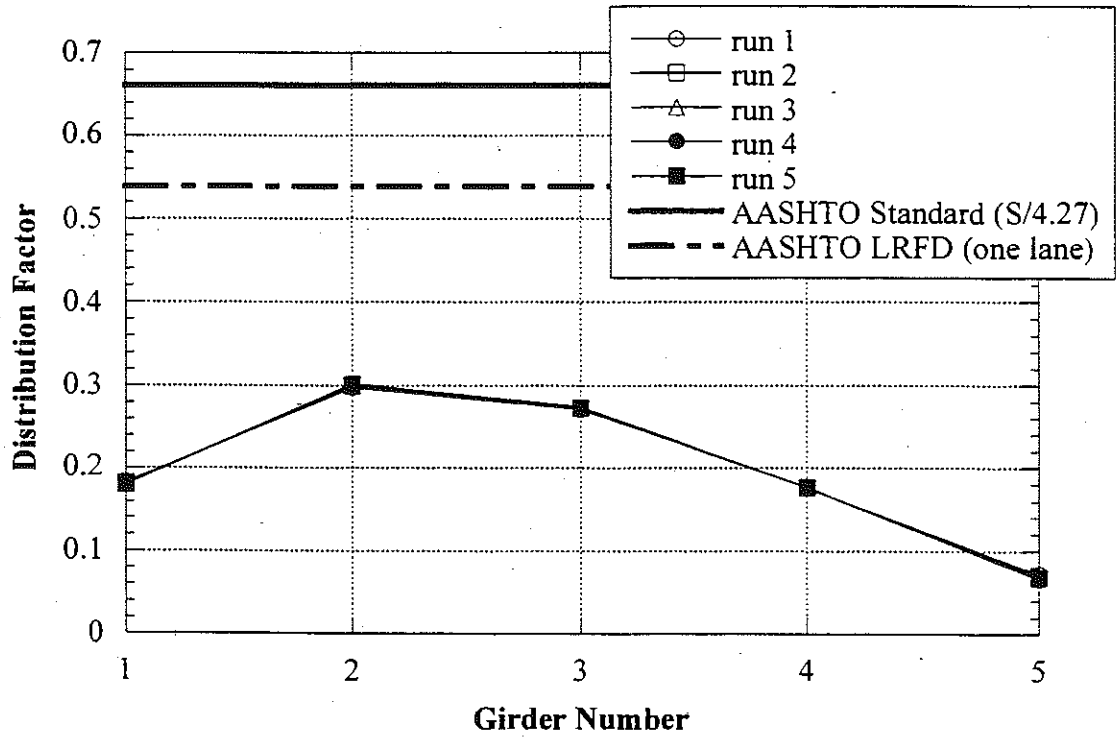

Figure 9.41. Girder Distribution Factor Calculated from the Deflections, North Lane Loading, NDN/I69 (S03-13074).

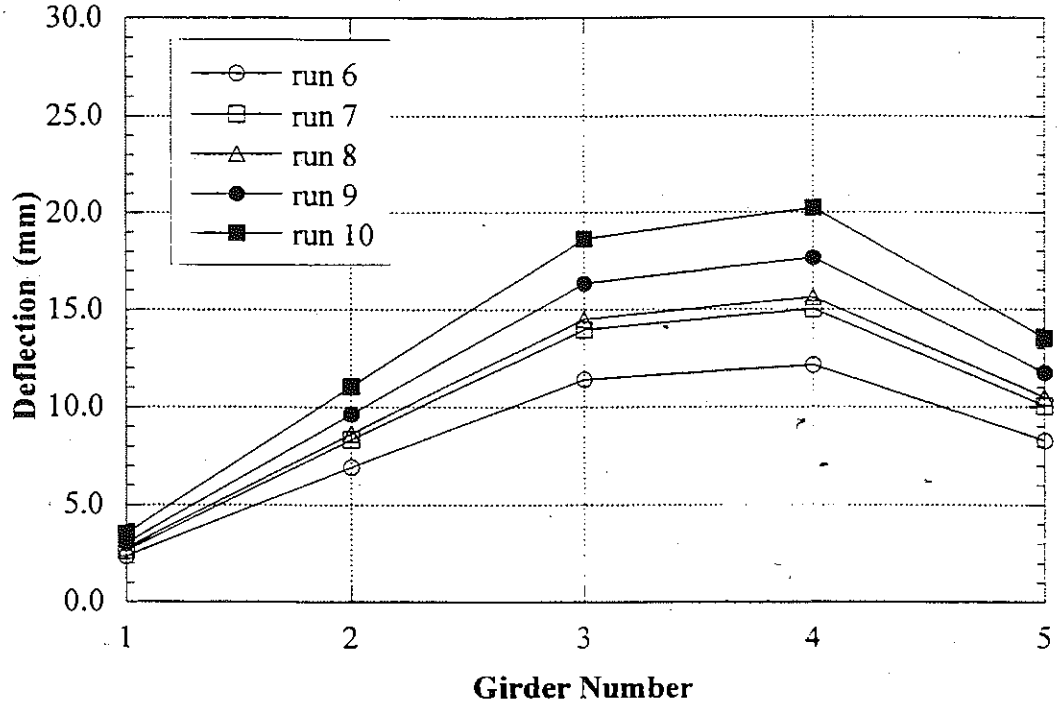

Figure 9.42. Deflections due to Proof Load, South Lane Loading, NDN/I69 (S03-13074).

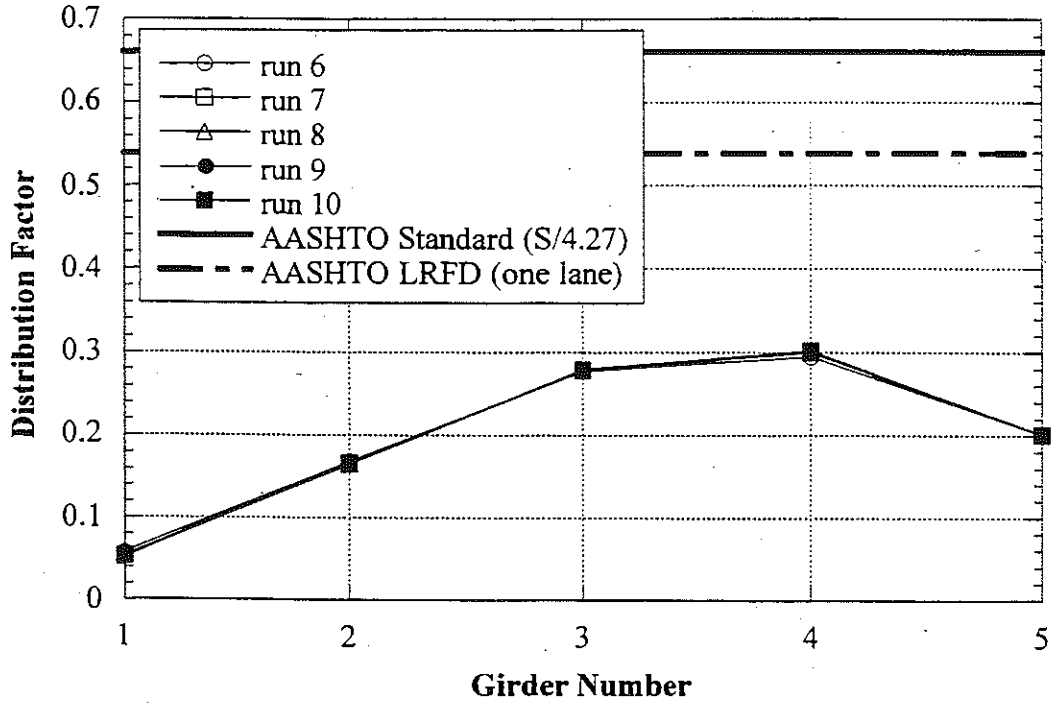

Figure 9.43. Girder Distribution Factor Calculated from the Deflections, South Lane Loading, NDN/I69 (S03-13074).

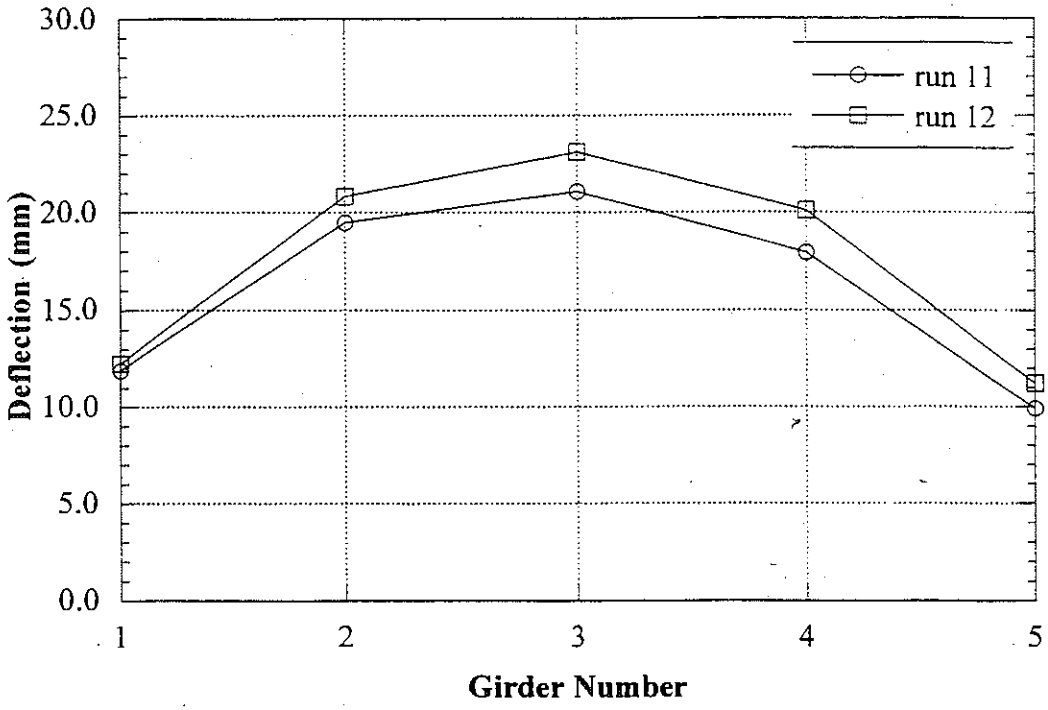

Figure 9.44. Deflections due to Proof Load, Side-by-Side Loading, NDN/I69 (S03-13074).

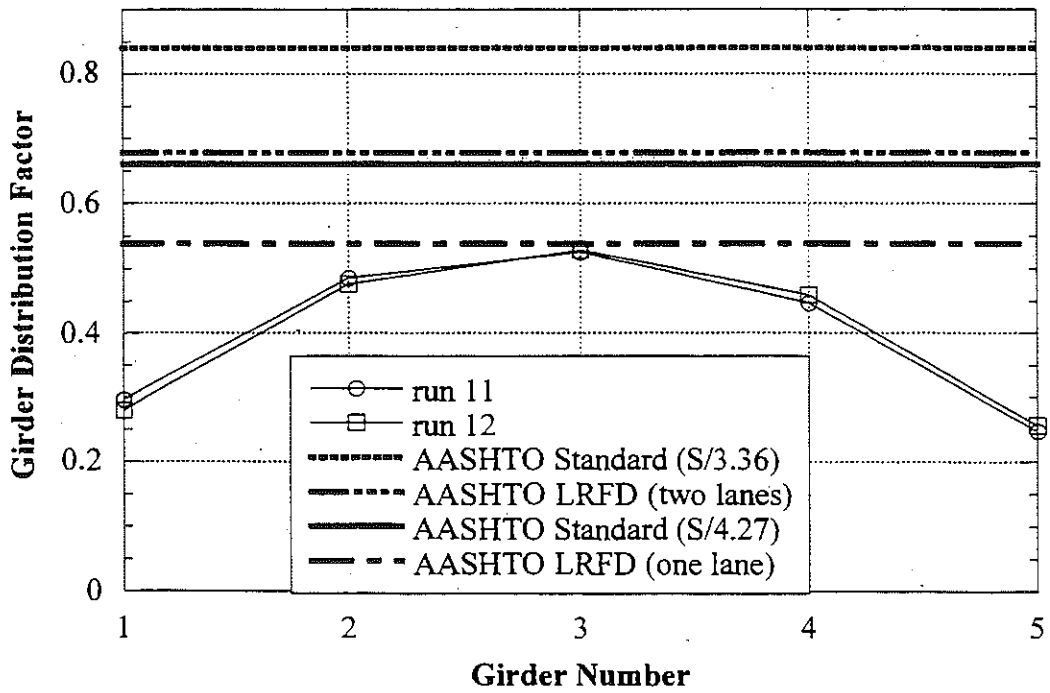

Figure 9.45. Girder Distribution Factor Calculated from the Deflections, Side-by-Side Loading, NDN/I69 (S03-13074).

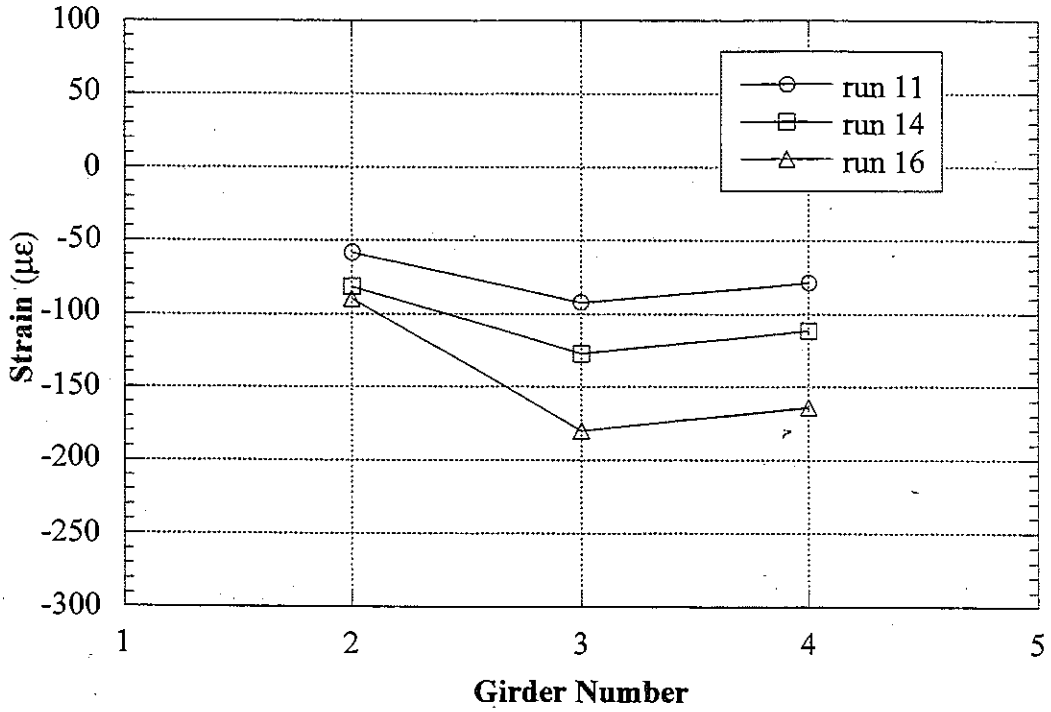

Figure 9.46. Strains at East End, Side-by-Side Loading, NDN/I69 (S03-13074).

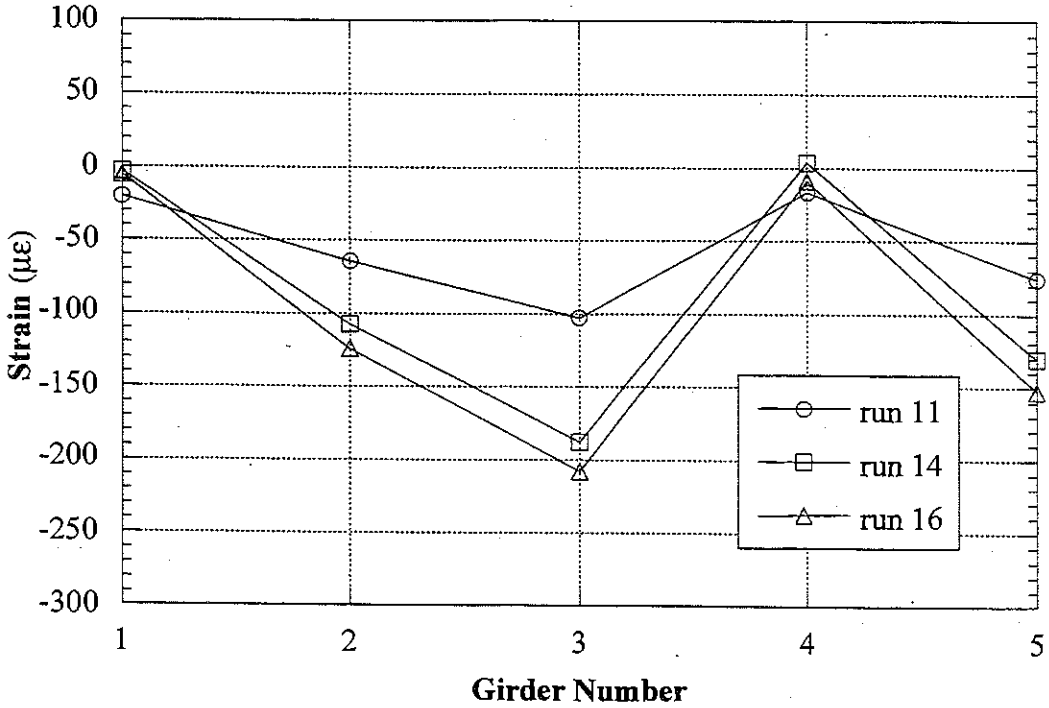

Figure 9.47. Strains at West End, Side-by-Side Loading, NDN/I69 (S03-13074).

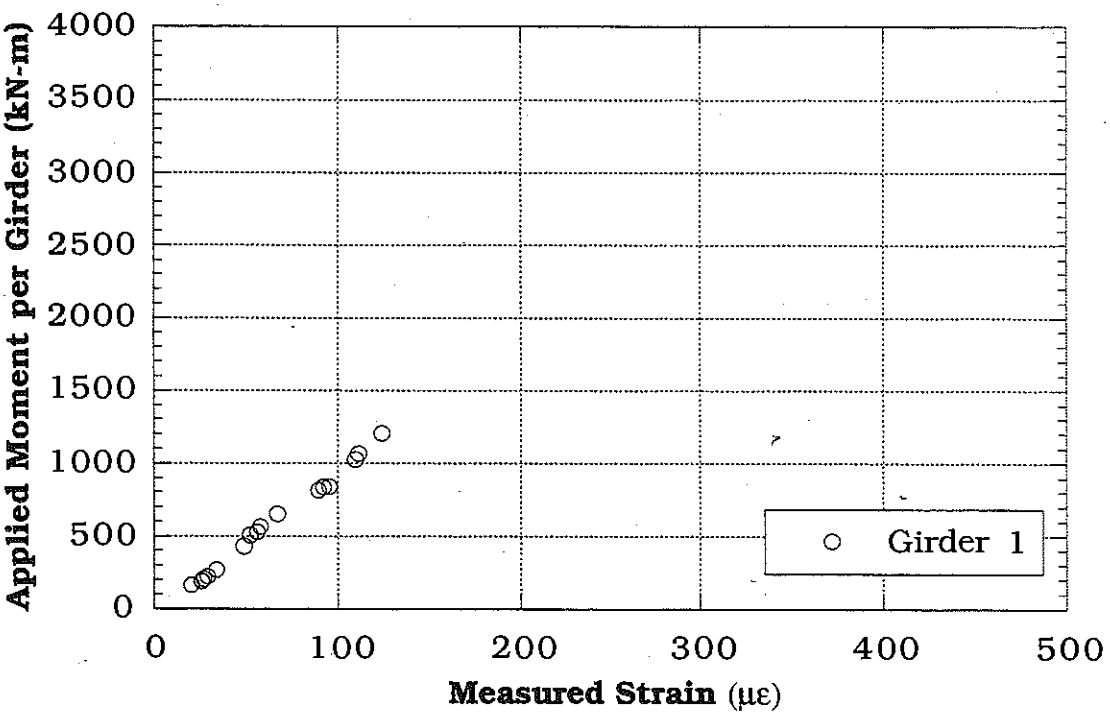

Figure 9.48. Moment per Girder vs. Measured Strain, Girder 1.

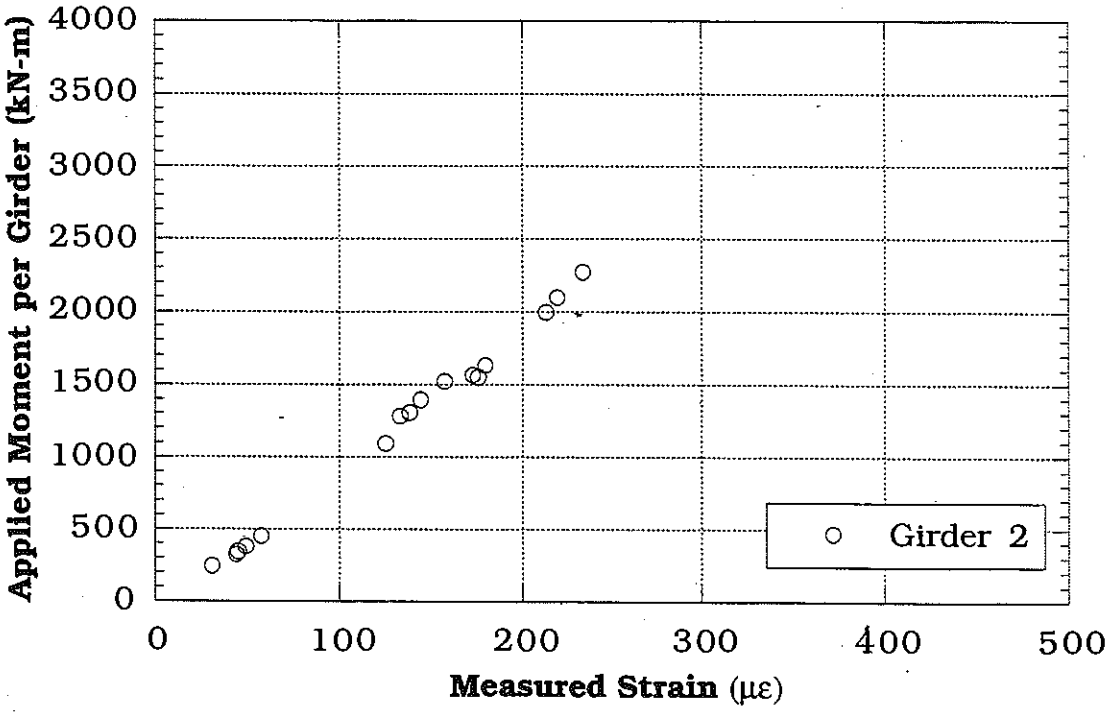

Figure 9.49. Moment per Girder vs. Measured Strain, Girder 2.

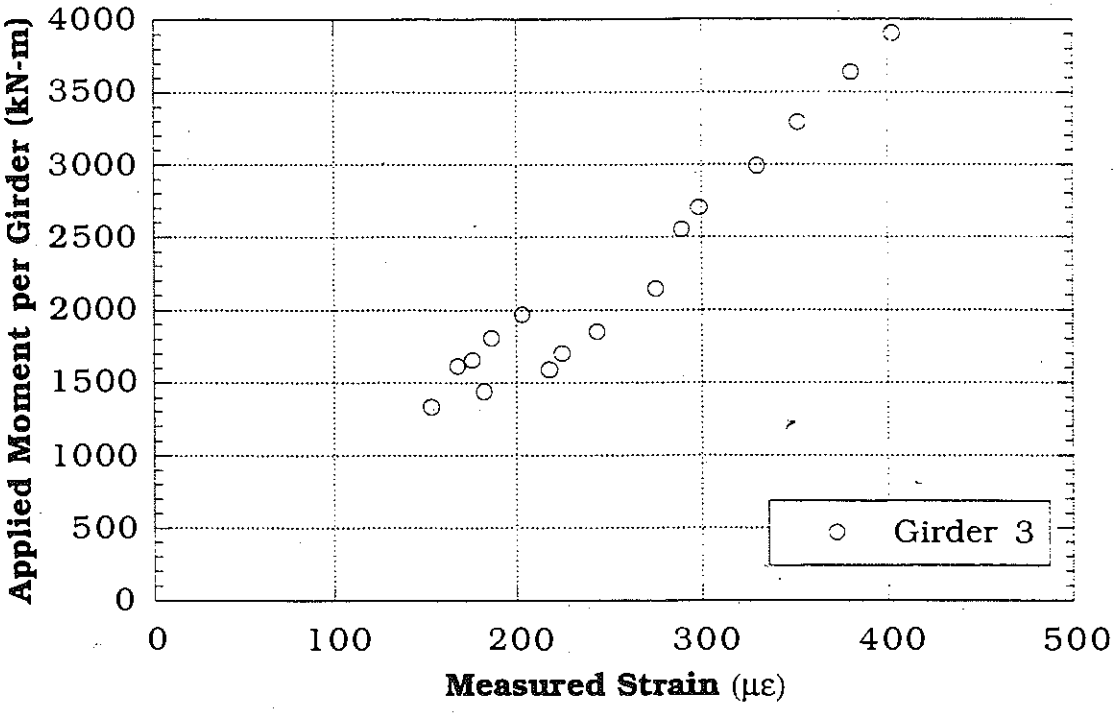

Figure 9.50. Moment per Girder vs. Measured Strain, Girder 3.

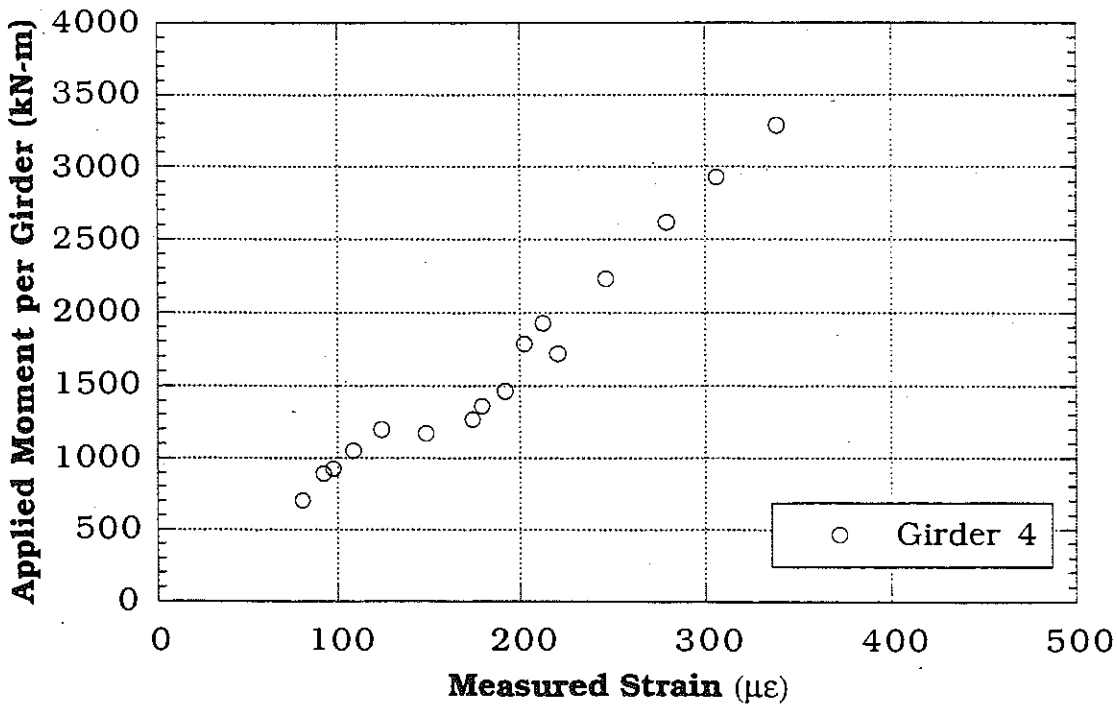

Figure 9.51. Moment per Girder vs. Measured Strain, Girder 4.

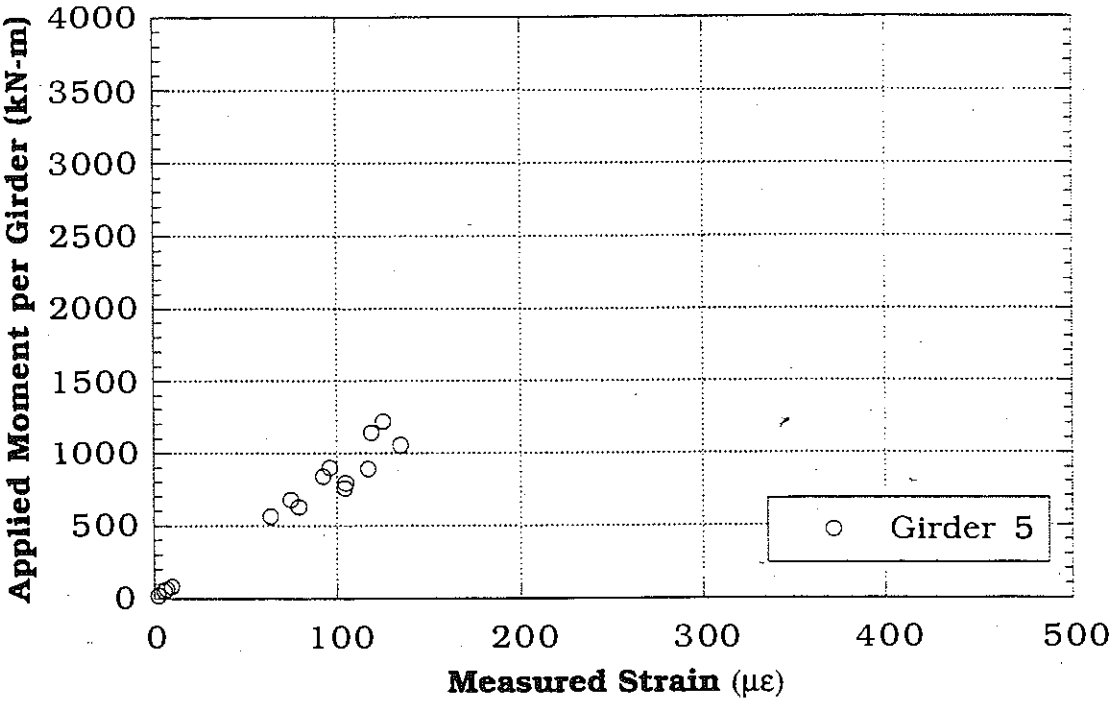

Figure 9.52. Moment per Girder vs. Measured Strain, Girder 5.

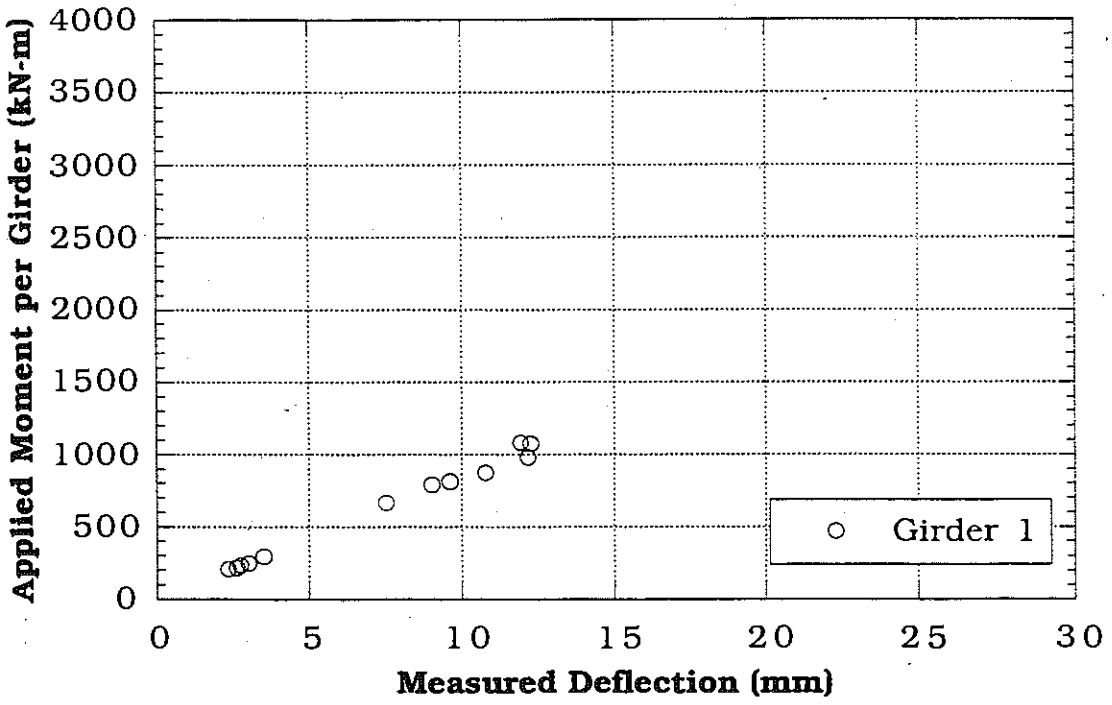

Figure 9.53. Moment per Girder vs. Measured Deflection, Girder 1.

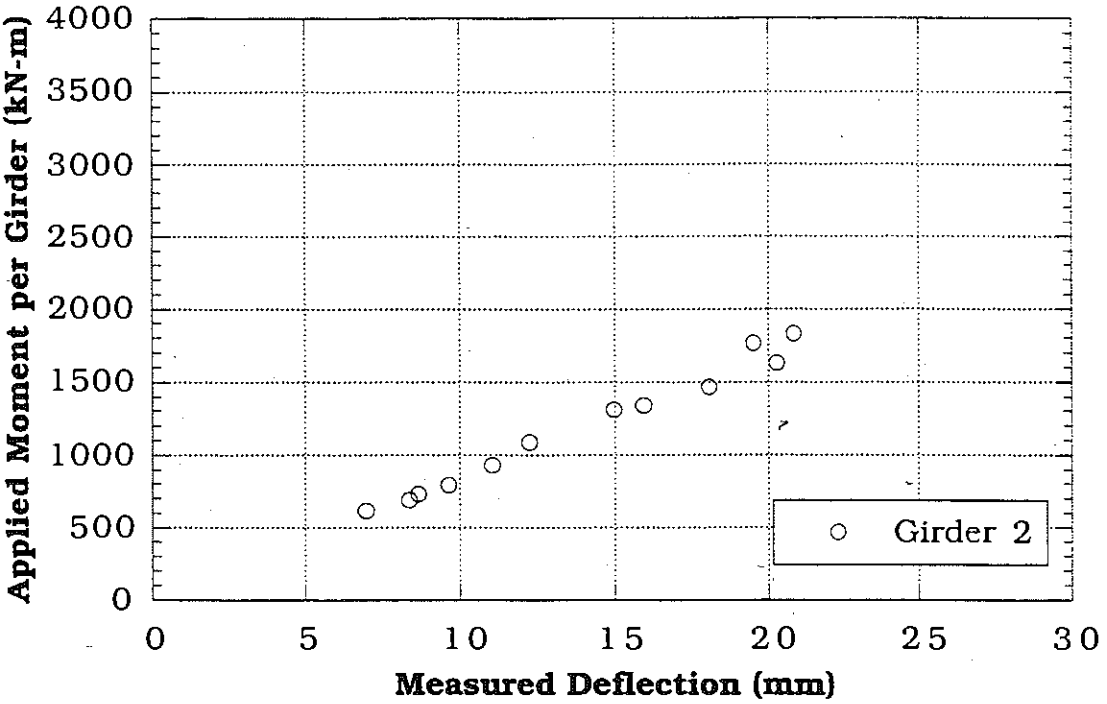

Figure 9.54. Moment per Girder vs. Measured Deflection, Girder 2.

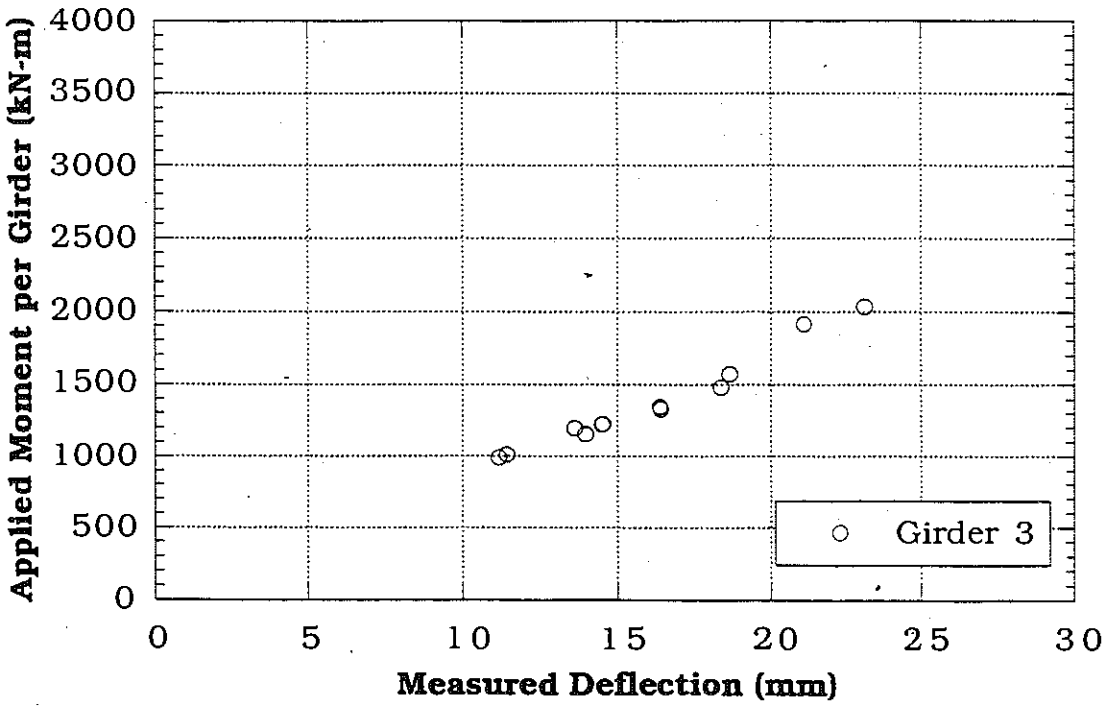

Figure 9.55. Moment per Girder vs. Measured Deflection, Girder 3.

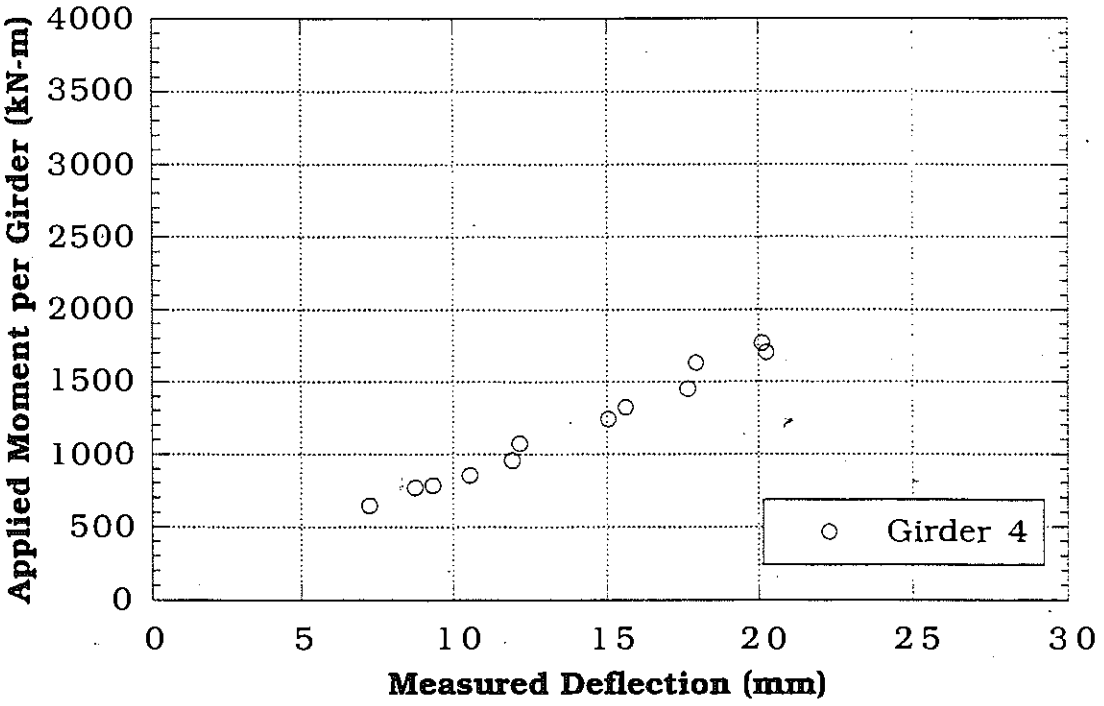

Figure 9.56. Moment per Girder vs. Measured Deflection, Girder 4.

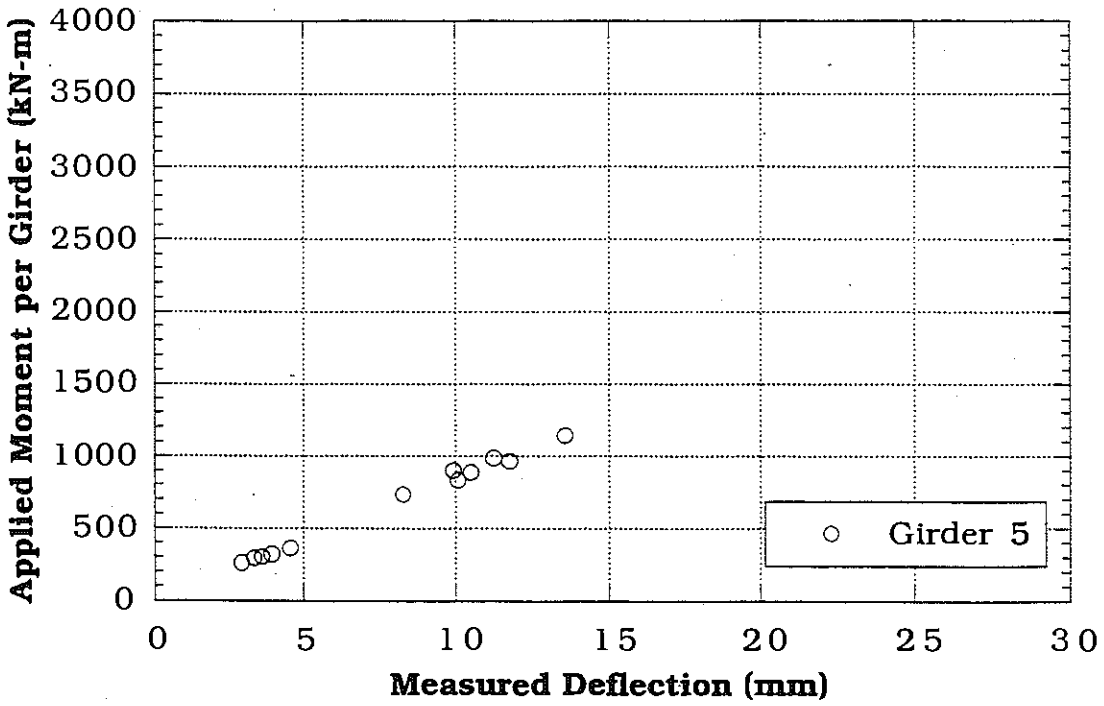

Figure 9.57. Moment per Girder vs. Measured Deflection, Girder 5.

Note:

Intentionally left blank

10. Bridge on M-46 over Pine River, in Gratiot County (B01-29041, M46/PR)

10.1 Description

This bridge was built in 1936 and is located on M-46 over Pine River in Gratiot County, Michigan. The deck was replaced and widened in 1994. As shown in Figure 10.1, there is one lane in each direction. It has eleven steel girders spaced at 1.37 m. The total span length is 21.3 m without skew. It carries average daily traffic (ADT) of 5,600, according to Michigan Structure Inventory. It is a single span, simply supported composite structure, as shown in Figure 10.2. The bridge has a load rating of 783 kN, according to the Michigan Structure Inventory.

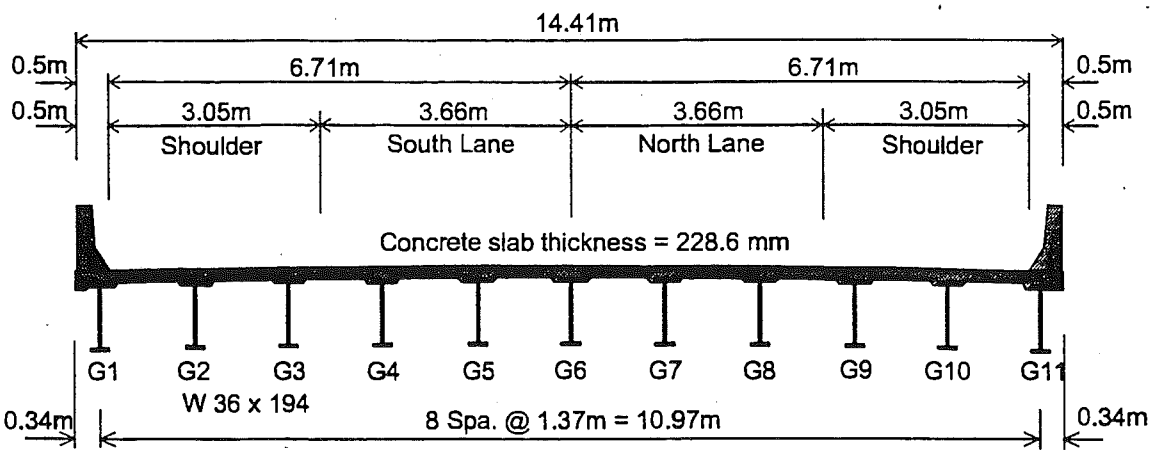

Figure 10.1. Cross-Section of Bridge M46/PR (B01-29041)

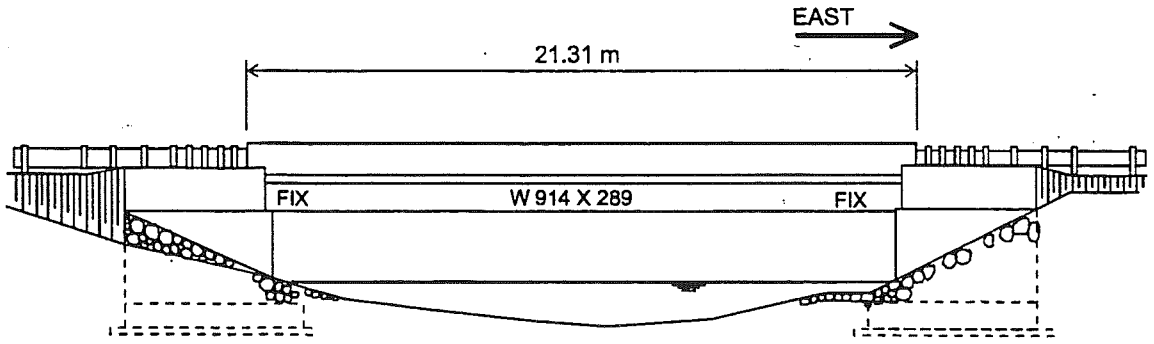

Figure 10.2. Elevation of Bridge M46/PR (B01-29041).

10.2 Instrumentation

Strain transducers were installed on the bottom flanges of girders at midspan and selected support locations (Figure 10.3). Two separate strain data acquisitions systems were used. For the girders 1 to girder 8, The wireless data transfer systems were installed at the center of the girders, and conventional wire based data transfer systems were installed for girders 9-11. The accuracy of the wireless system was verified in the test of bridge M66/RR (R01-78054), and explained in Section 4.5.

The reflector for the PSM-R device from Noptel was installed at the girder No. 6 to measure deflection. The installation of equipment was carried out on August 17, 1999. The bridge test was performed on August 18, 1999.

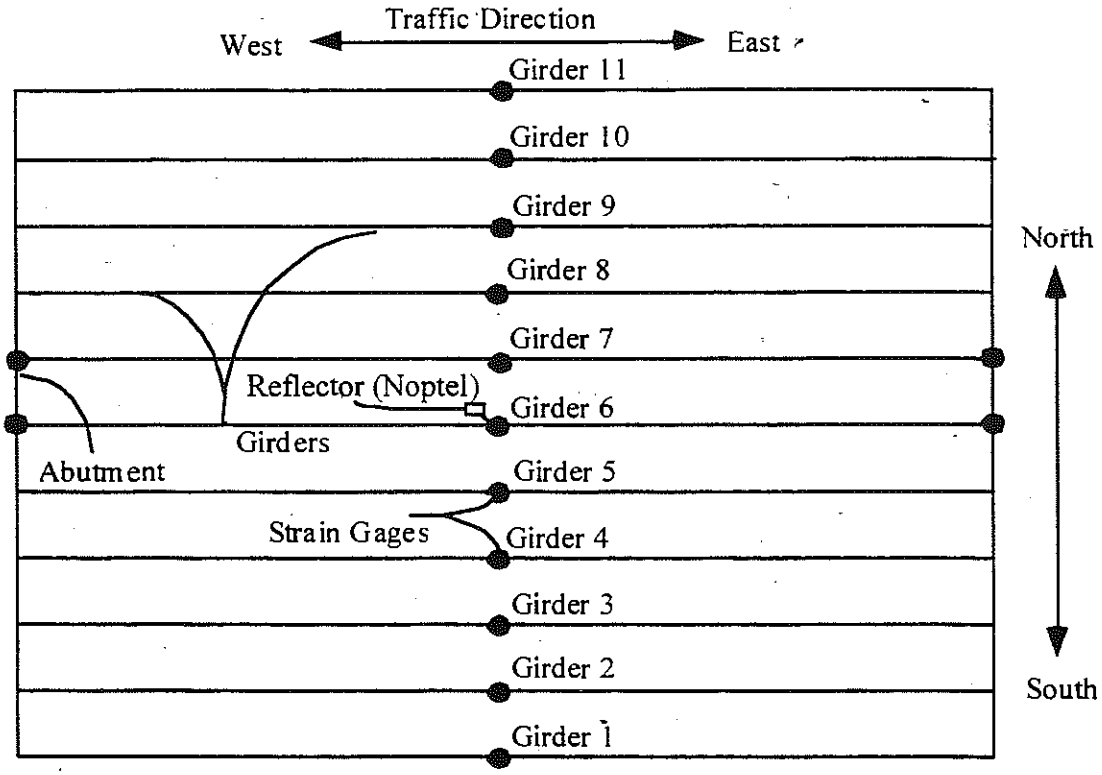

Figure 10.3. Strain Gage Locations in Bridge M46/PR (B01-29041).

10.3 Truck Loads

Strain data necessary to calculate girder distribution and impact factors were taken from midspan transducers. The bridge was loaded with two 11-axle trucks (three-unit vehicles). The gross vehicle weight and the truck axle configurations are shown in Figures 10.4 and 10.5.

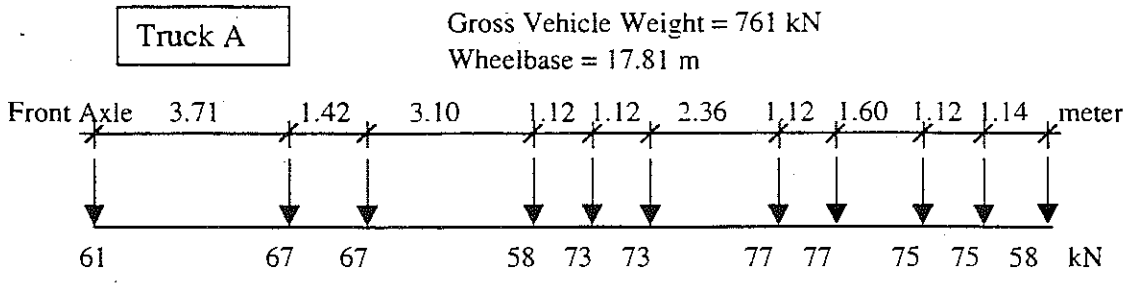

Figure 10.4. Truck A Configuration, Bridge M46/PR (B01-29041).

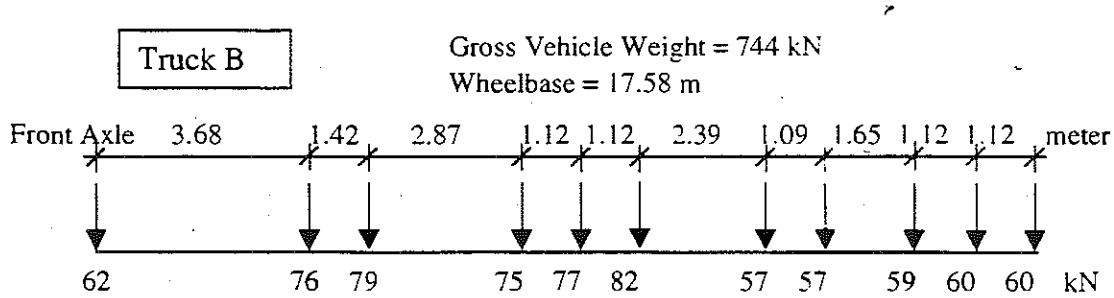

Figure 10.5. Truck B Configuration, Bridge M46/PR (B01-29041).

A total of 16 load cases were considered, as shown in Table 10.1. First each truck was driven by itself at the center of one lane, at crawling speed. Then, the same truck was driven close to the curb. The runs in the center of the lane were repeated at a normal highway speed. The same was repeated for the other lane. Finally, two trucks were driven simultaneously, side-by-side, at crawling speed and normal highway speed (about 60 km/h). For side-by-side cases, the runs were repeated after the trucks switched lanes, i.e. first truck A was in North lane, and B in South lane, then truck A was in South lane, and B in North lane.

Table 10.1. Sequence of Test Runs, Bridge M46/PR (B01-29041).

Run#	Truck	Lane Side	Position in Lane	Truck Speed
1	Truck A	North	Center	Crawling
2	Truck A	North	Curb	Crawling
3	Truck B	North	Center	Crawling
4	Truck B	North	Curb	Crawling
5	Truck B	North	Center	65 km/h
6	Truck A	North	Center	65 km/h
7	Truck A	South	Center	Crawling
8	Truck A	South	Curb	Crawling
9	Truck B	South	Center	Crawling
10	Truck B	South	Curb	Crawling
11	Truck B	South	Center	65 km/h
12	Truck A	South	Center	55 km/h
13	Truck A and B	both	Center	Crawling
14	Truck B and A	both	Center	Crawling
15	Truck A and B	both	Center	65 km/h
16	Truck B and A	both	Center	65 km/h

10.4. Analysis Results

The three-dimensional finite element method (FEM) was applied to investigate the structural behavior of the bridge M46/PR (B01-29041). The concrete slab was modeled with isotrophic, eight node solid elements, with three degrees of freedoms at each node. The girder flanges and web were modeled using three-dimensional, quadrilateral, four node shell elements with six degrees of freedom at each node. The structural effects of the secondary members, such as the sidewalk and parapet, were also taken into account in the finite element analysis models.

Two cases of the boundary conditions were employed in the FEM models. In the first FEM model, it was assumed that the supports could be represented by a hinge at one end and a roller at the other end. In the other FEM model, it was assumed that both supports were hinged, with no movement in horizontal direction.

Figure 10.6 illustrates the mesh of the FEM model, and Figure 10.7 shows the deformed shape of the bridge when it is loaded with two trucks side-by-side.

Figure 10.8 shows the results of the finite element analysis for two trucks side-by-side (Run 13). It includes the experimental results and analytical results for the two considered models. The FEM results show that the maximum strain at the most heavily loaded girder is about 160 με, while the maximum strain recorded from the test is about 120 με. In addition, the experimental response lies between the two considered analytical models. This indicates that a partial fixity exists at the supports of the bridge.

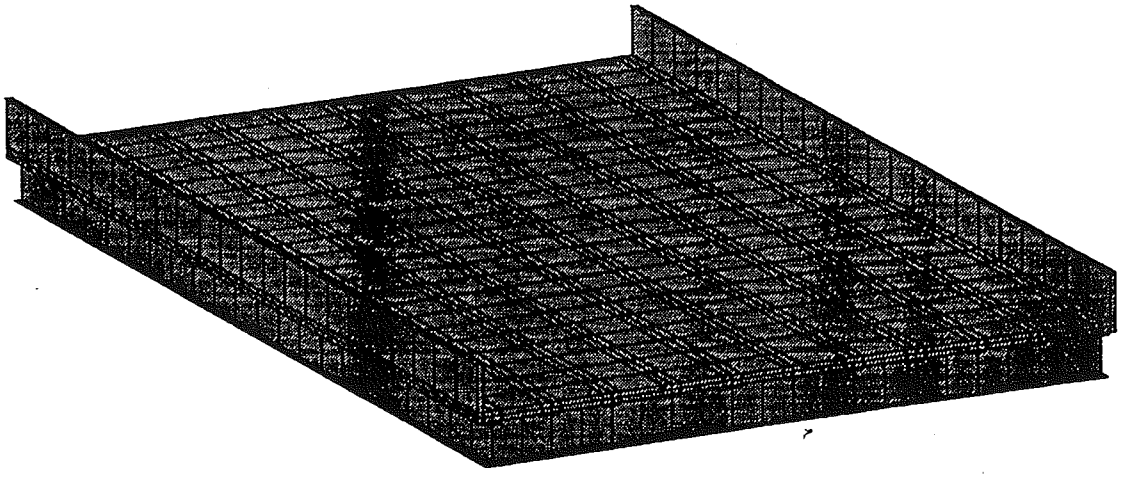

Figure 10.6. The Mesh of the Finite Element Model.
M46/PR (B01-29041).

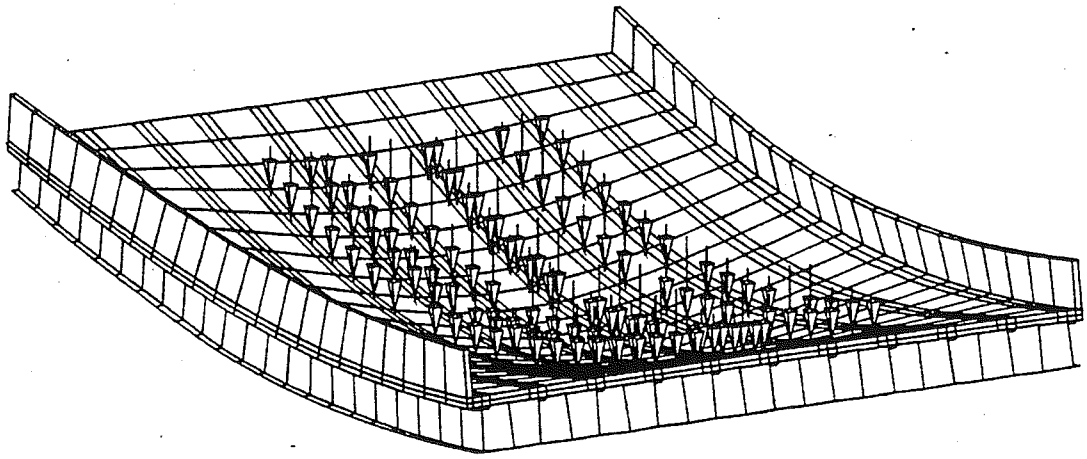

Figure 10.7. Deformed Shape of the Bridge M46/PR (B01-29041)
under Two Lane Loading.

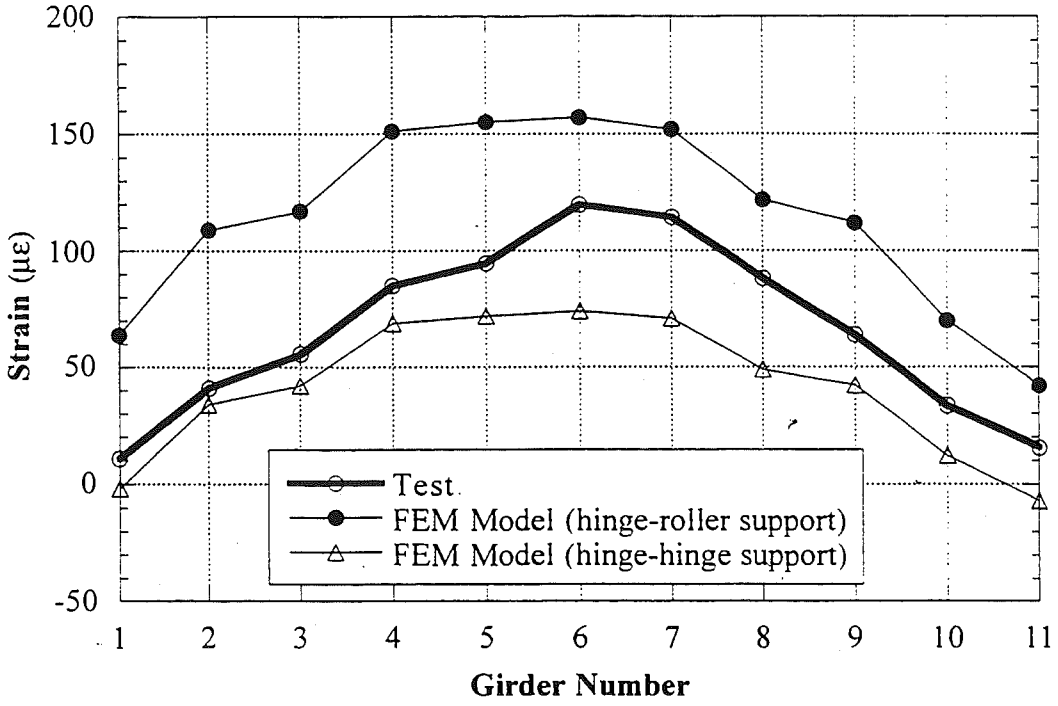

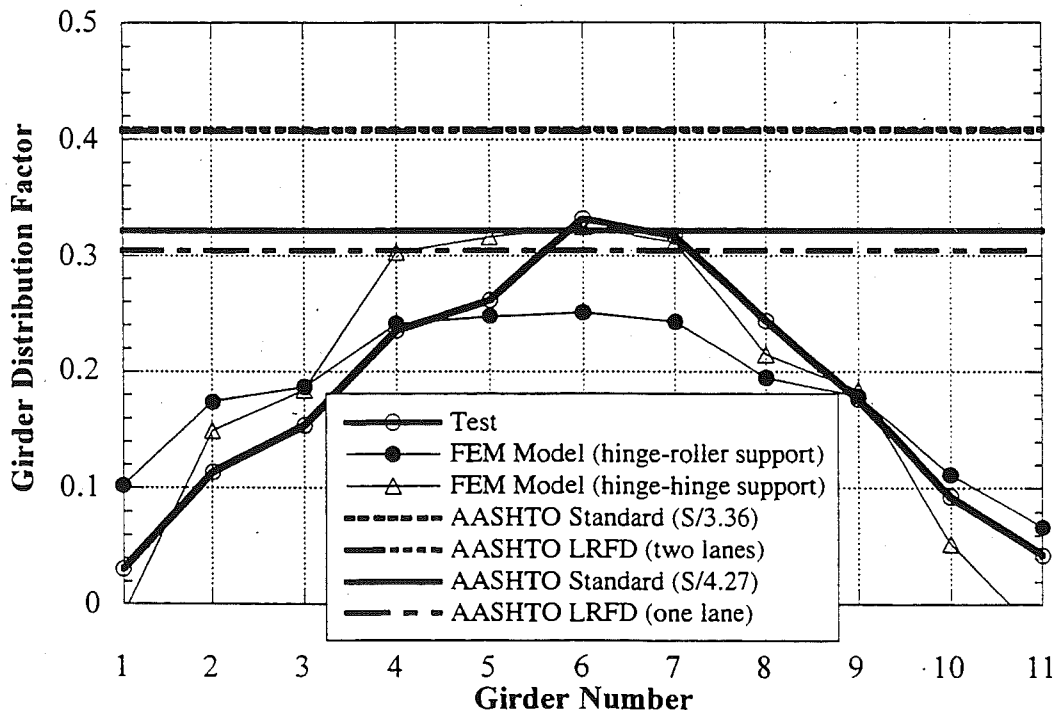

Figure 10.8. Results of the Finite Element Analysis, Truck A-north Truck B-south loading, M46/PR (B01-29041).

10.5. Load Test Results

The resulting strains and GDF's are shown in Fig. 10.9 through 10.13. Figures 10.9 to 10.11 present the results of all crawling-speed (static) tests. Figures 10.9 to 10.10 present static strains and GDF's for one truck on the bridge. The maximum strain due to a single truck is about 75 με. This corresponds to about 15 MPa.

Figure 10.11 shows static strains and GDF's from side-by-side static load tests. For two vehicles side-by-side the maximum strain is about 120 με (which corresponds to 24 MPa). The superposition of strains due to a single truck in south and north lanes produces almost the same results as strain due to two trucks side-by-side.

For two trucks side-by-side, the girder distribution factor for girder i is determined using Eq. 4.4. For comparison, GDF are also calculated according to AASHTO Standard Specifications (1996) and AASHTO LRFD Code (1998). Two cases were considered, a single lane loaded, and two lanes loaded. The resulting GDF's are shown in Fig. 10.9 through 10.13.

The results indicate that code-specified GDF's are conservative. GDF's specified for a single lane are close to the result from two lane loading.

Figure 10.12 and 10.13 shows the resulting strain and distribution factors from normal speed tests. There is practically no difference between the crawling speed and normal speed results.

Dynamic load factor (DLF) is defined in section 4.4. In Fig. 10.14, DLF's are plotted for all load cases involving normal speed (no dynamic load was measured for crawling speed runs). Large values of DLF in exterior girders correspond to load cases with a single truck in the opposite lane (resulting in very low static strain).

The relationship between DLF and static and dynamic strains is shown in Fig. 10.15. The open circles correspond to static strain, ε_{stat}, and black solid squares correspond to dynamic strain, ε_{dyn}. For each static strain value (open circle), the corresponding dynamic strain is denoted by solid square (the numbers of circles and squares are same). Dynamic strains remain nearly constant, while static strains increase as truck loading increases. This results in large dynamic load factors for low static strains. It is clear from the Figure 10.15 that dynamic strain does not exceed 15 με in normal speed test. As shown in Figure 10.15, it is concluded that DLF corresponding to the maximum strain caused by two trucks side-by-side, is about 0.10 for the most heavily loaded girder (Girder 6).

Girder Number 6 was instrumented with remote deflection measurement device manufactured by Noptel. The reflector was installed at midspan. The result is shown in Table 10.2. The maximum deflection recorded during the test is 6.06 mm for girder number 6.

Table 10.2. Maximum deflections measured at the center of the Girder 6, M46/PR (B01-29041).

Run #	Horizontal (mm)	Vertical (mm)
1	0.17	3.18
2	0.18	1.27
3	0.21	3.15
4	0.20	1.32
5	0.26	2.99
6	0.17	3.01
7	-0.50	2.95
8	-0.34	1.14
9	-0.56	3.03
10	-0.33	1.31
11	-0.45	2.86
12	-0.48	2.82
13	-0.34	6.06
14	-0.38	5.77
15	-0.31	5.69
16	-0.35	5.59

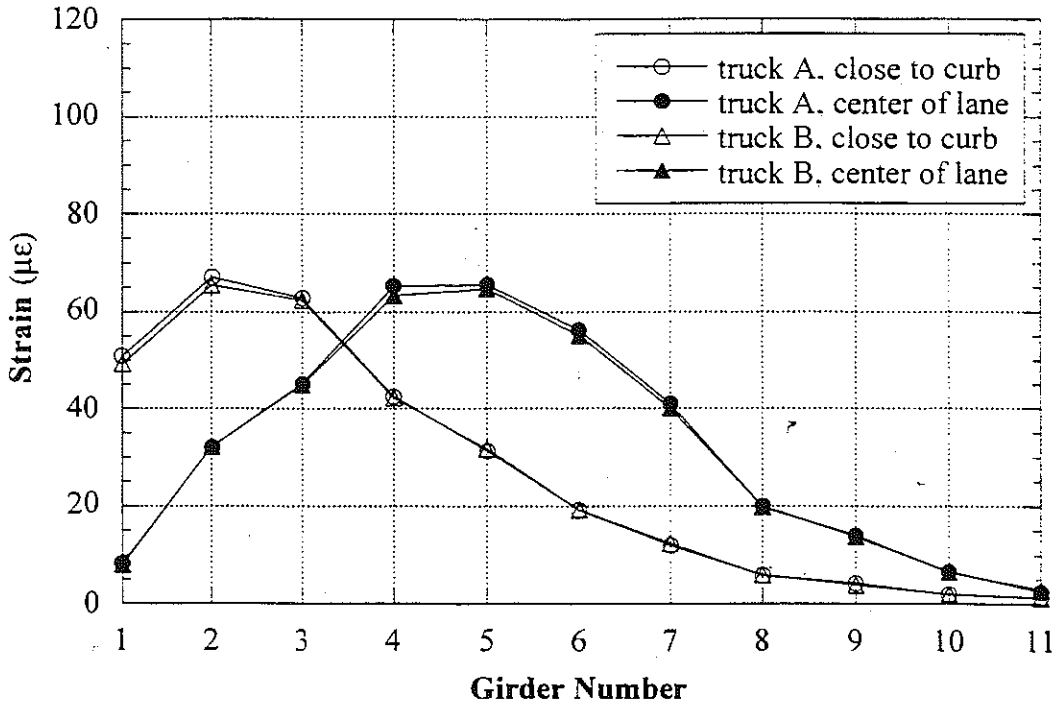

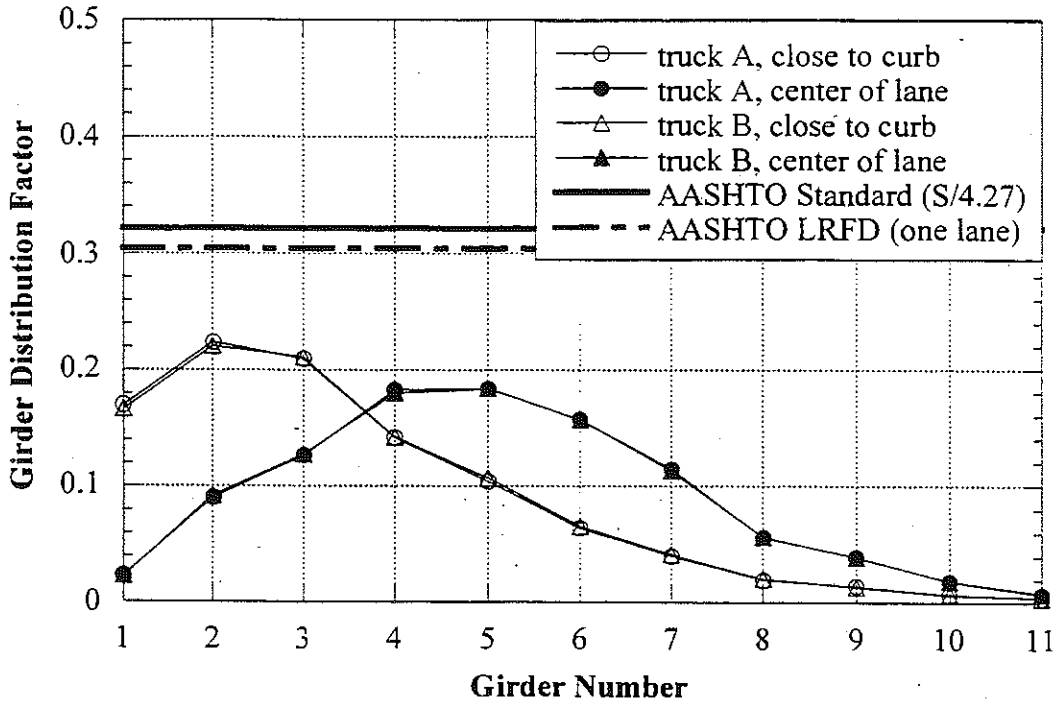

Figure 10.9. South Lane, Crawling Speed, M46/PR (B01-29041).

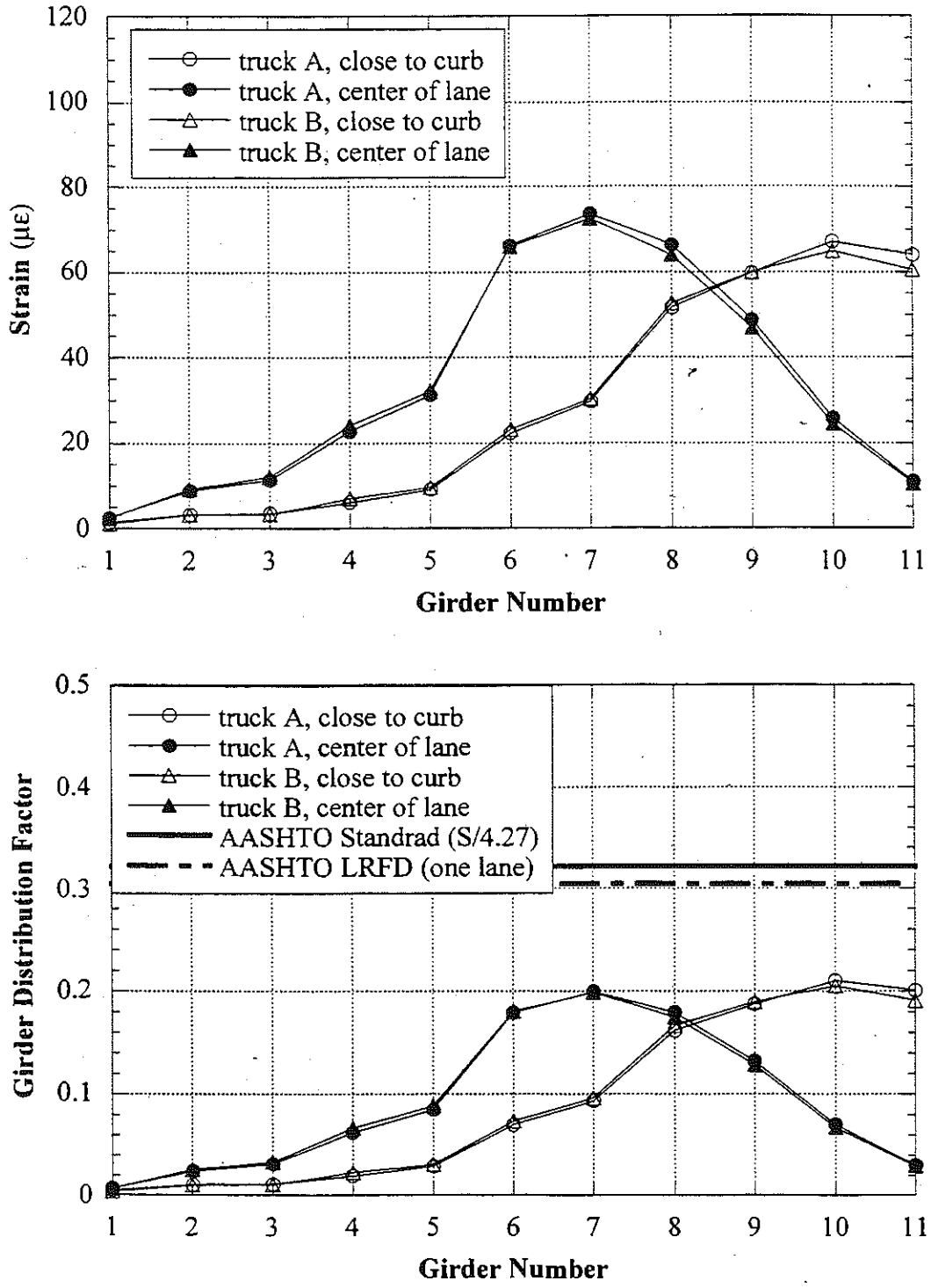

Figure 10.10. North Lane, Crawling Speed, M46/PR (B01-29041).

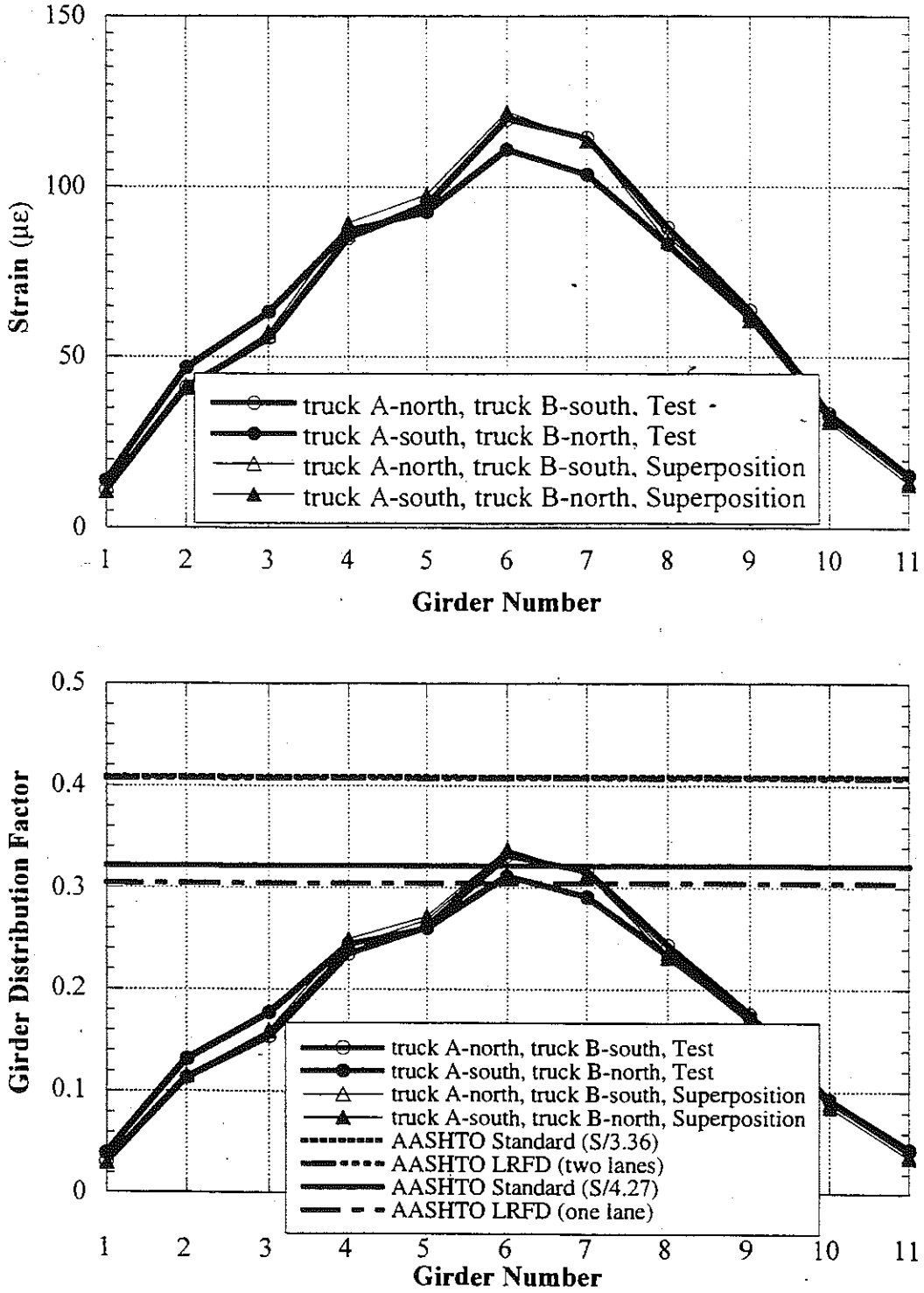

Figure 10.11. Side-by-Side Loading, Center of Lane, Crawling Speed, M46/PR (B01-29041).

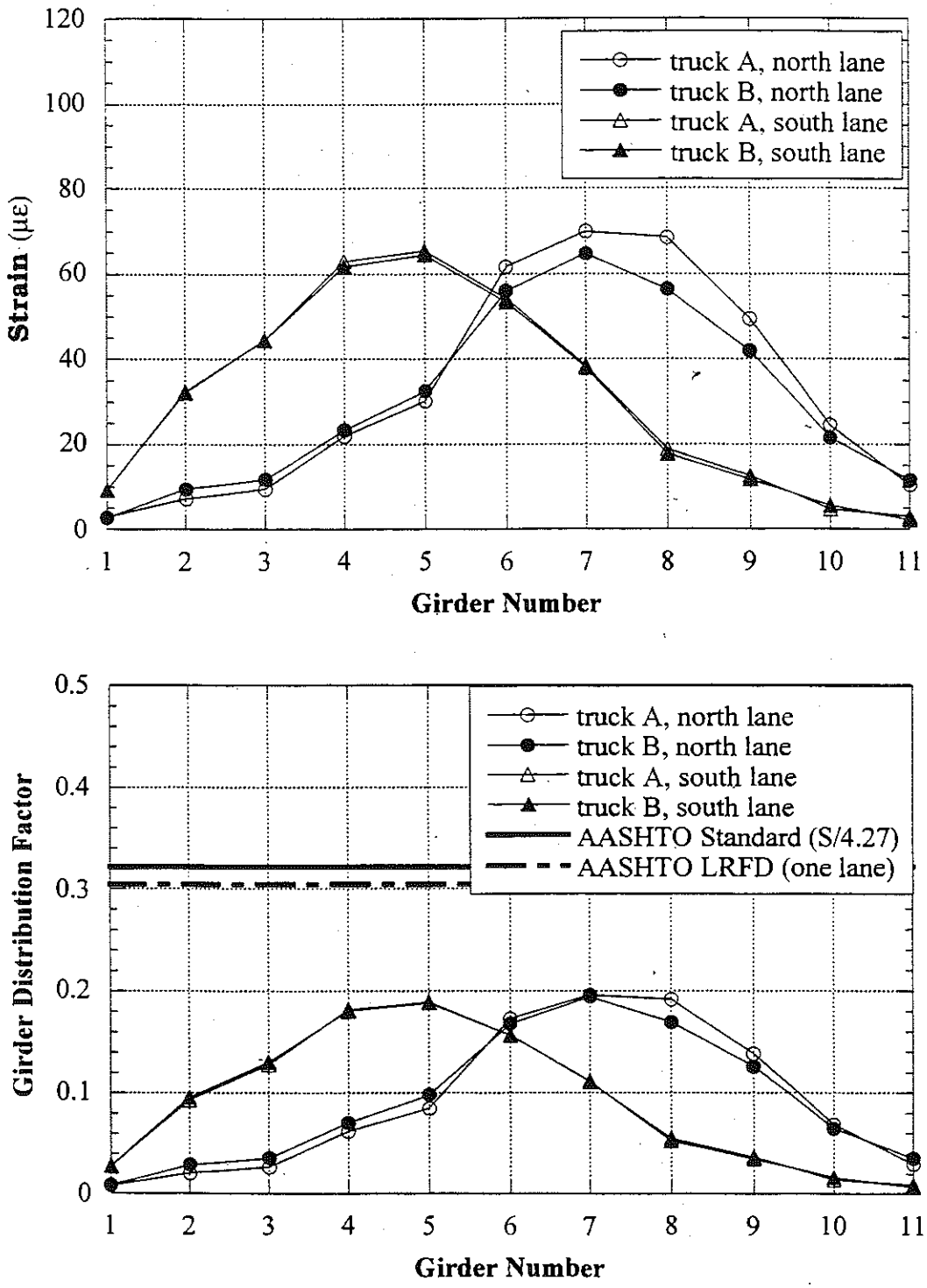

Figure 10.12. Strain and GDF under One Truck Loading at Regular Speed, M46/PR (B01-29041).

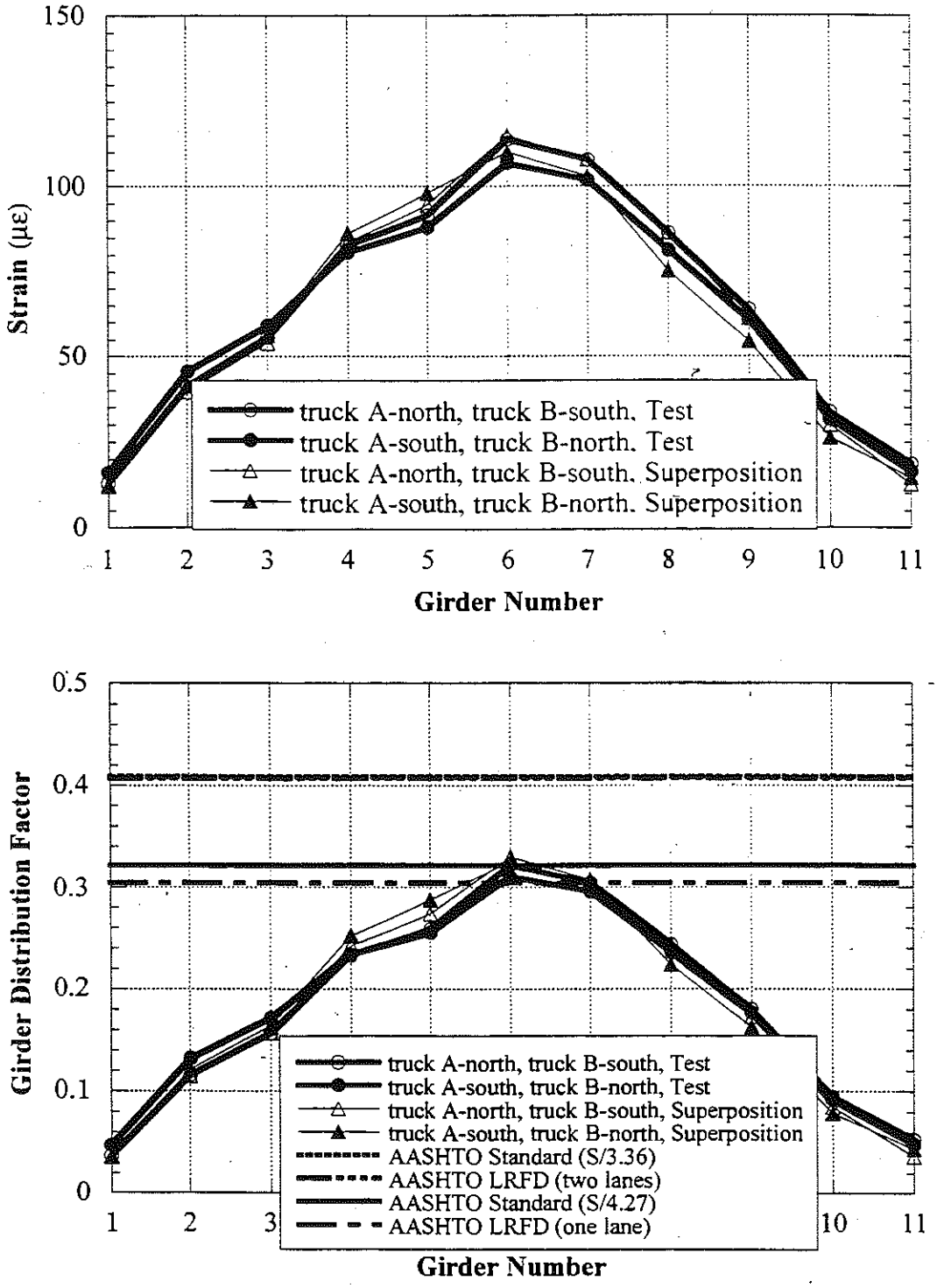

Figure 10.13. Strain and GDF under Side-by-Side Loading at Regular Speed, M46/PR (B01-29041).

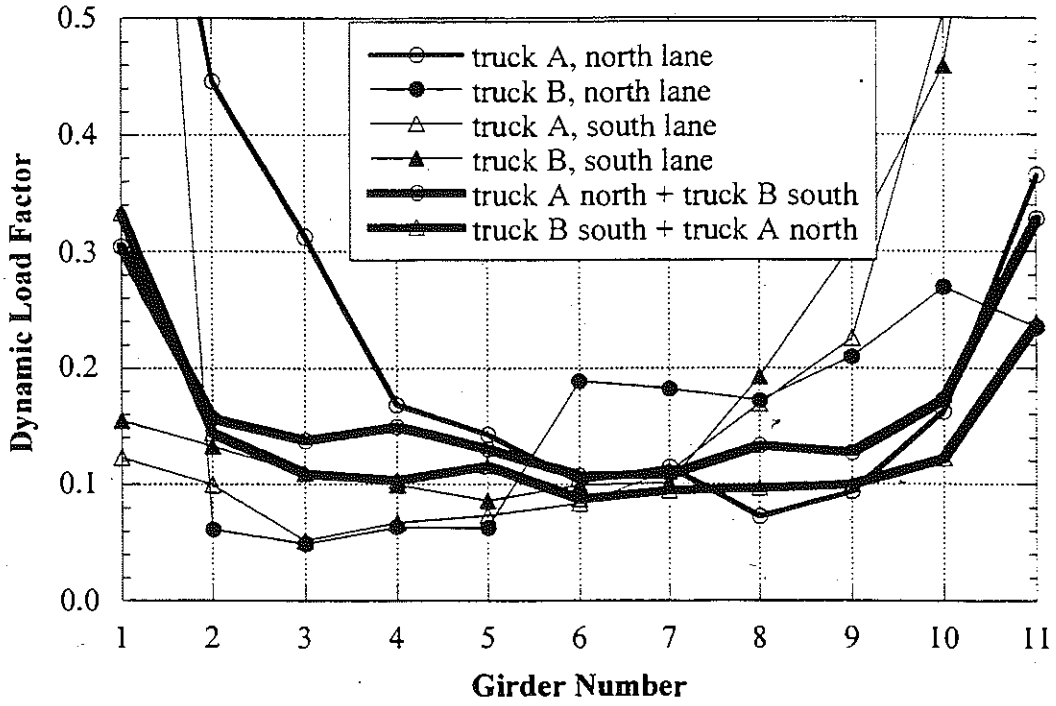

Figure 10.14. Dynamic Load Factors, M46/PR (B01-29041).

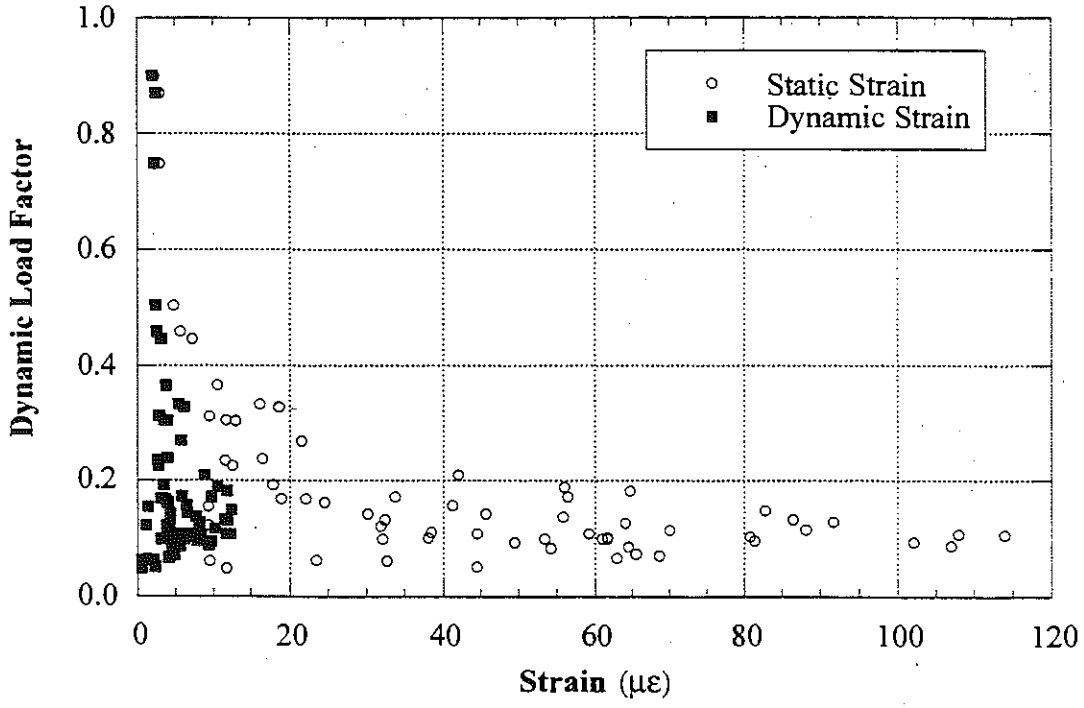

Figure 10.15. Strain vs. Dynamic Load Factors, M46/PR (B01-29041).

Note:

Intentionally left blank

11. Bridge on M-82 over Tamarack Creek, Montcalm County (B01-59041, M82/TC)

11.1 Description

This bridge was built in 1932 and reconstructed in 1961 with salvaged girders. It is located on M-82 over Tamarack Creek in Montcalm County, Michigan. As shown in Figure 11.1, there is one lane in each direction. It has ten steel girders spaced at 1.37 m. It is a three span, simply supported, composite structure, as shown in Figure 11.2. The total bridge length is 43.4 m. The test was performed on the main span. The length of the main span is 26.4 m without skew. It carries average daily traffic (ADT) of 4200. The bridge has a load rating of 979 kN, according to the Michigan Structure Inventory.

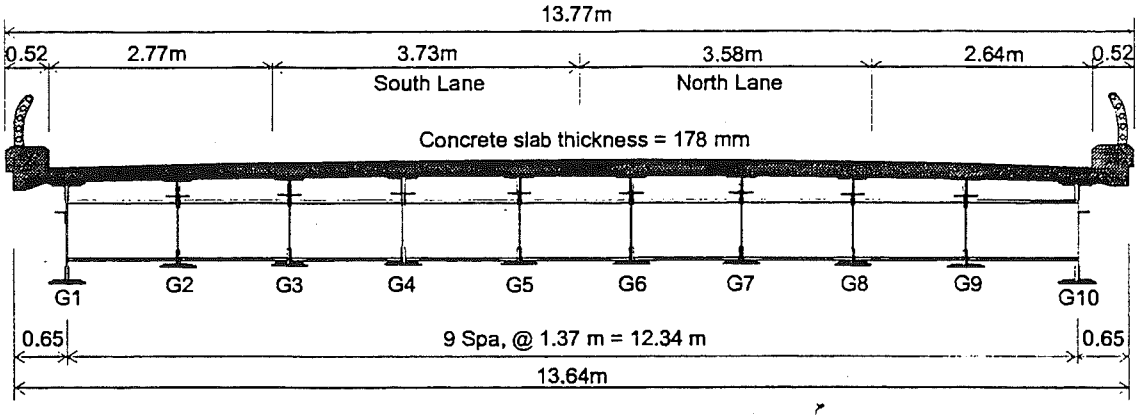

Figure 11.1. Cross-Section of Bridge M82/TC (B01-59041).

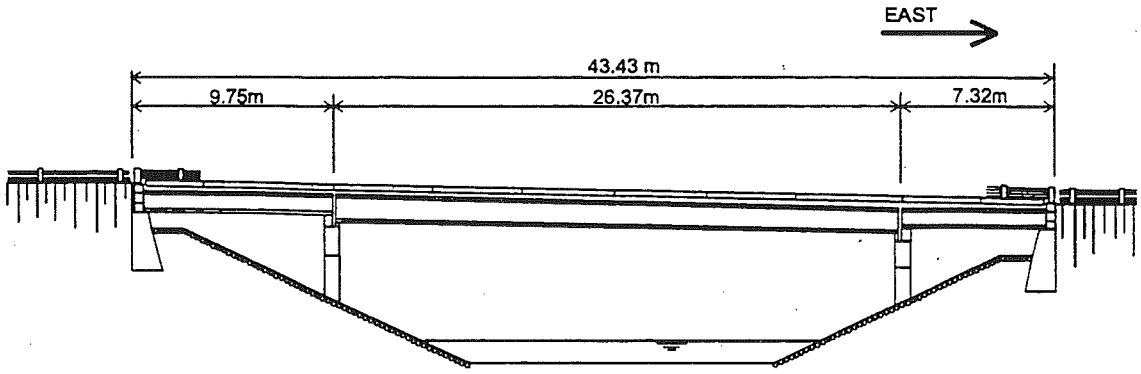

Figure 11.2. Elevation of Bridge M82/TC (B01-59041).

11.2 Instrumentation

Strain transducers were installed on the bottom flanges of girders at midspan and selected support locations (Figure 11.3) of the main span. The reflector for the PSM-R device from Noptel was installed at the girder No. 6 to measure deflection. The installation of equipment and bridge test were both performed on September 21, 1999.

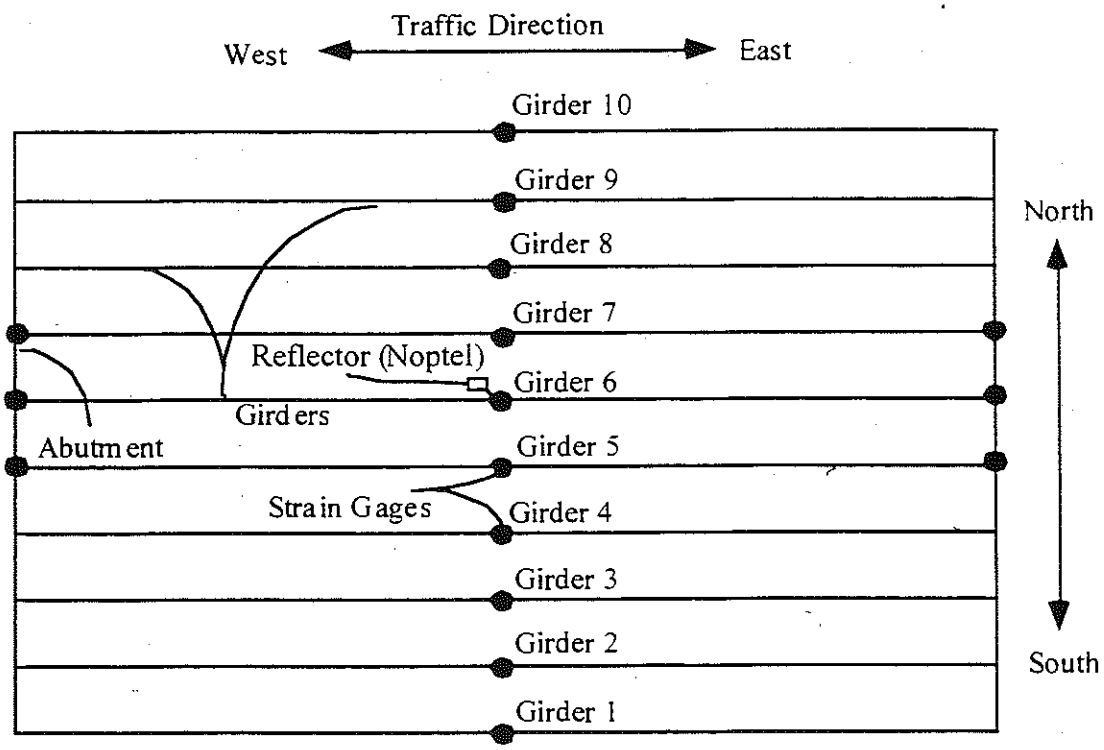

Figure 11.3. Strain Gage Locations in Bridge M82/TC (B01-59041).

11.3 Truck Loads

Strain data necessary to calculate girder distribution and impact factors were taken from midspan transducers. The bridge was loaded with 2 three-unit 11-axle trucks. The gross vehicle weight and the truck axle configurations are shown in Figures 11.4 and 11.5.

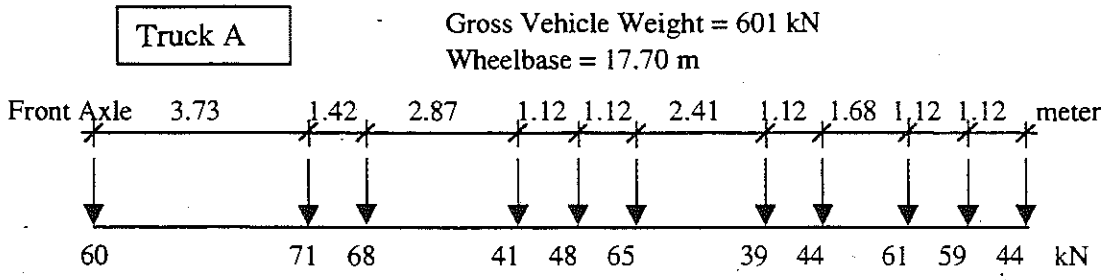

Figure 11.4. Truck A Configuration, Bridge M82/TC (B01-59041).

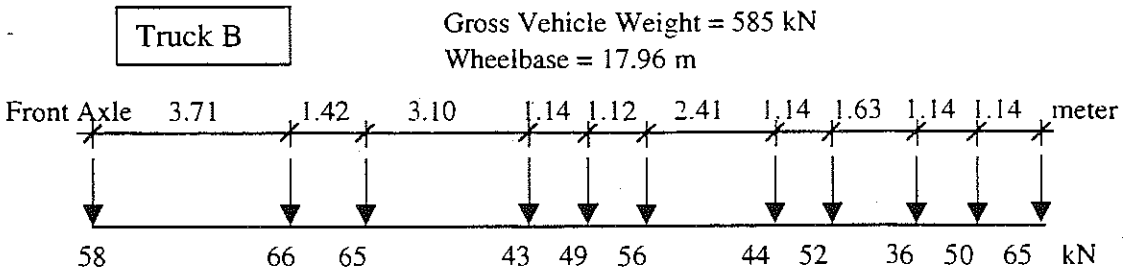

Figure 11.5. Truck B Configuration, Bridge M82/TC (B01-59041).

A total of 16 load cases were considered, as shown in Table 11.1. First each truck was driven by itself at the center of one lane, at crawling speed. Then, the same truck was driven close to the curb. The runs in the center of the lane were repeated at a normal highway speed. The same was repeated for the other lane. Finally, two trucks were driven simultaneously, side-by-side, at crawling speed and normal highway speed. For side-by-side cases, the runs were repeated after the trucks switched lane, i.e. first truck A was in North lane, and B in South lane, then truck A was in South lane, and B in North lane.

Table 11.1. Sequence of Test Runs, Bridge M82/TC (B01-59041).

Run#	Truck	Lane Side	Position in Lane	Truck Speed
1	Truck A	North	Center	Crawling
2	Truck A	North	Curb	Crawling
3	Truck B	North	Center	Crawling
4	Truck B	North	Curb	Crawling
5	Truck B	North	Center	55 km/h
6	Truck A	North	Center	45 km/h
7	Truck A	South	Center	Crawling
8	Truck A	South	Curb	Crawling
9	Truck B	South	Center	Crawling
10	Truck B	South	Curb	Crawling
11	Truck B	South	Center	55 km/h
12	Truck A	South	Center	50 km/h
13	Truck A and B	both	Center	Crawling
14	Truck B and A	both	Center	Crawling
15	Truck A and B	both	Center	55 km/h
16	Truck B and A	both	Center	55 km/h

11.4. Analysis Results

The three-dimensional finite element method (FEM) was applied to investigate the structural behavior of the bridge M82/TC (B01-59041). The concrete slab was modeled with isotrophic, eight node solid elements, with three degrees of freedoms at each node. The girder flanges and web were modeled using three-dimensional, quadrilateral, four node shell elements with six degrees of freedom at each node. The structural effects of the secondary members, such as the sidewalk and parapet, were also taken into account in the finite element analysis models.

Two cases of the boundary conditions were employed in the FEM models. In the first FEM model, it was assumed that the supports could be represented by a hinge at one end and a roller with a hinge at the other end. In the other FEM model, it was assumed that both supports were hinged, with no movement in horizontal direction.

Figure 11.6 illustrates the mesh of the FEM model, and Figure 11.7 shows the deformed shape of the bridge when it is loaded with two trucks side-by-side.

Figure 11.8 shows the results of the finite element analysis for two trucks side-by-side (Run 13). It includes the experimental results and analytical results for the two considered models. The FEM results show that the maximum strain at the most heavily loaded girder is about 130 με, while the maximum strain recorded from the test is about 120 με. In addition, the experimental response lies between the two considered analytical models. This indicates that a partial fixity exists at the supports of the bridge.

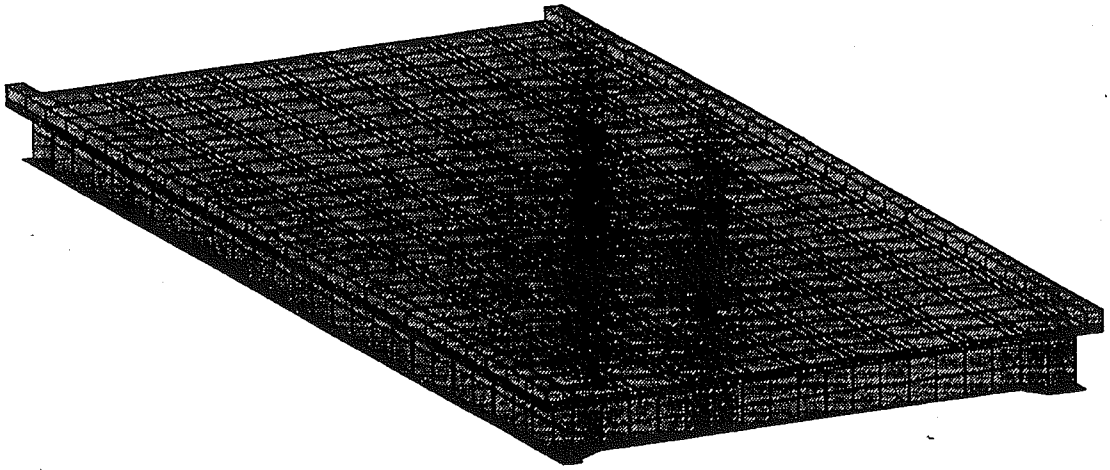

Figure 11.6. The Mesh of the Finite Element Model, M82/TC (B01-59041).

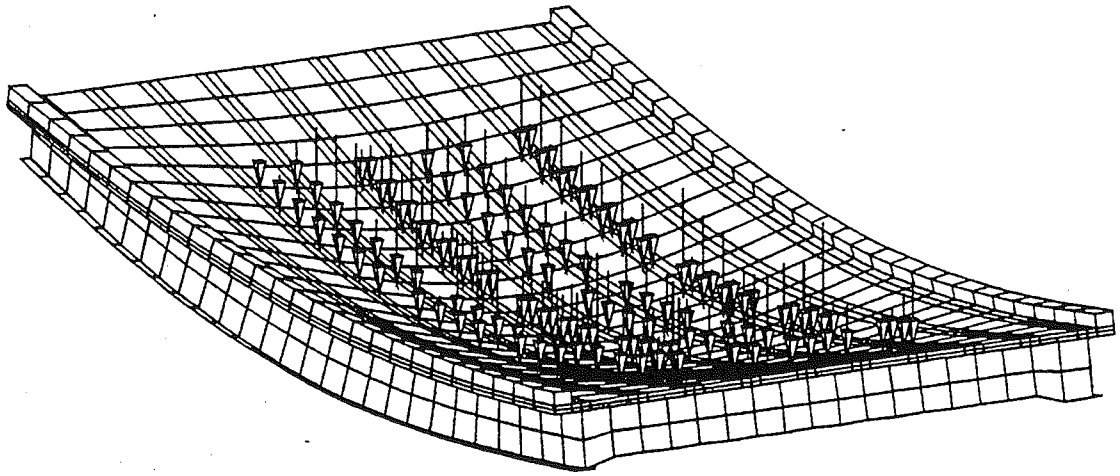

Figure 11.7. Deformed Shape of the Bridge M82/TC (B01-59041) under Two Lane Loading.

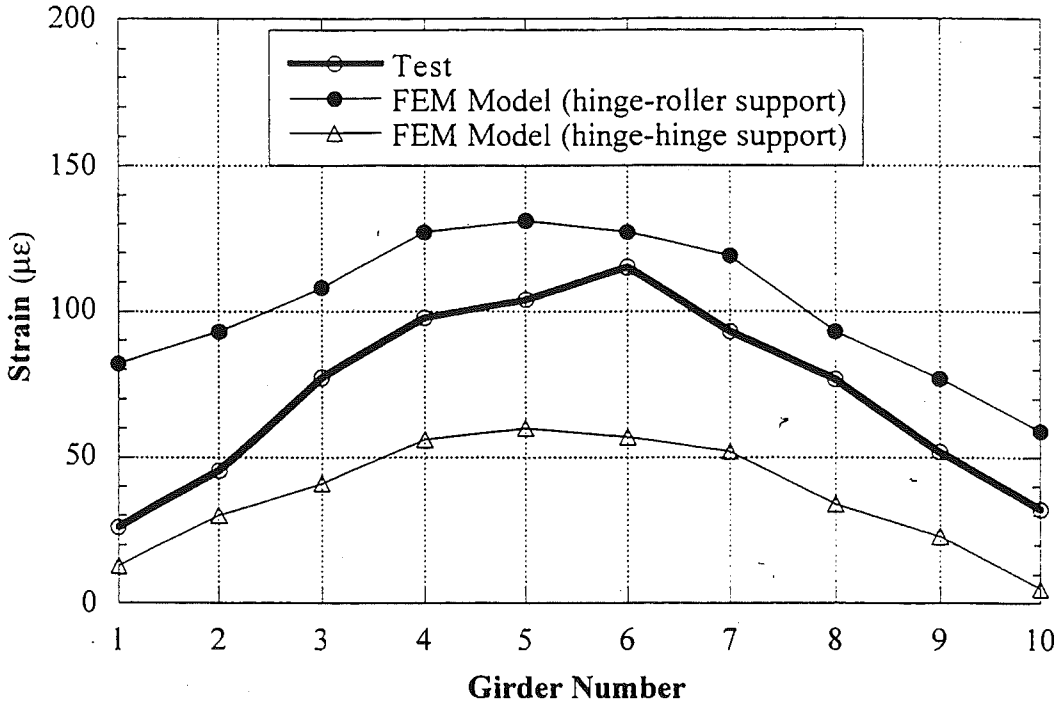

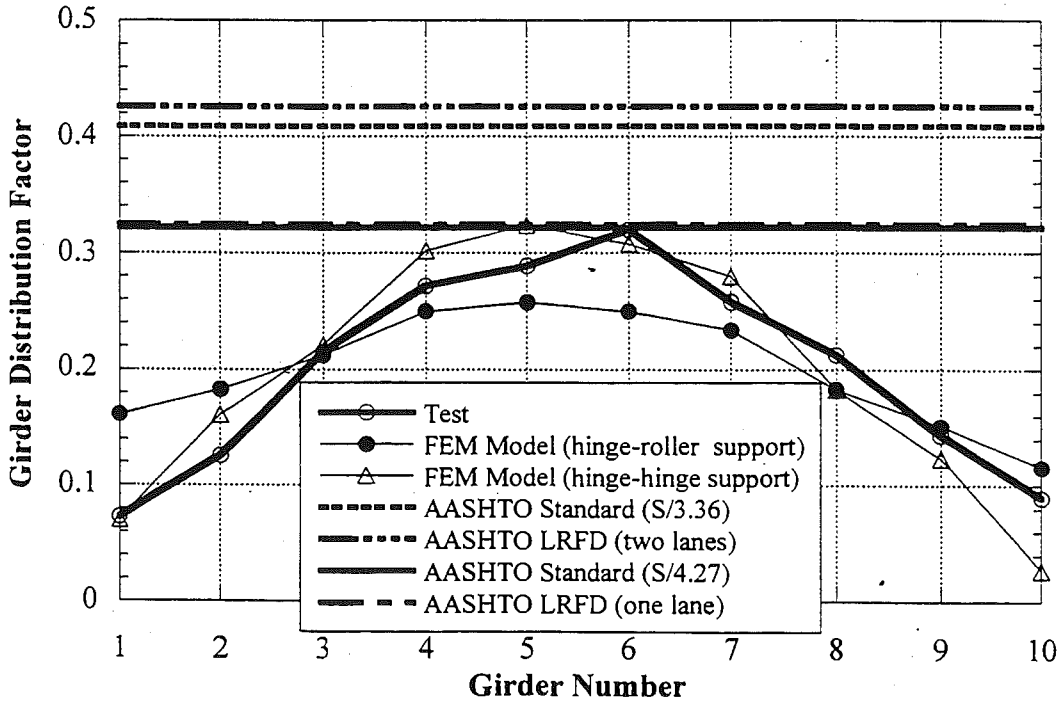

Figure 11.8. Results of the Finite Element Analysis, Truck A-north Truck B-south loading, M82/TC (B01-59041).

11.5. Load Test Results

The resulting strains and GDF's are shown in Figures 11.9 through 11.13. Figures 11.9 to 11.11 present the results of all crawling-speed (static) tests. Figures 11.9 to 11.10 present static strains and GDF's for one truck on the bridge. The maximum strain due to a single truck is about 100 με. This corresponds to about 20 MPa.

Figure 11.11 shows static strains and GDF's from side-by-side static load tests. For two vehicles side-by-side the maximum strain is about 120 με (which corresponds to 24 MPa). The superposition of strains due to a single truck in south and north lanes produces almost the same results as strain due to two trucks side-by-side.

For two trucks side-by-side, the girder distribution factor for girder i is determined using Eq. 4.4. For comparison, GDF are also calculated according to AASHTO Standard Specifications (1996) and AASHTO LRFD Code (1998). Two cases were considered, a single lane loaded, and two lanes loaded. The resulting GDF's are shown in Figures 11.9 through 11.13.

The results indicate that code-specified GDF's are conservative. Also, GDF's specified for a single lane are very close to results from two lane load cases, as shown in Figure 11.11.

Figure 11.12 and 11.13 shows the resulting strain and distribution factors from normal speed tests. There is practically no difference between the crawling speed and normal speed results.

Dynamic load factor (DLF) is defined in section 4.4. In Figure 11.14, DLF's are plotted for all load cases involving normal speed (no dynamic load was measured for crawling speed runs). Large values of DLF in

exterior girders correspond to load cases with a single truck in the opposite lane (resulting in very low static strain).

The relationship between DLF and static and dynamic strains is shown in Figure 11.15. The open circles correspond to static strain, ε_{stat}, and black solid squares correspond to dynamic strain, ε_{dyn}. For each static strain value (open circle), the corresponding dynamic strain is denoted by solid square (the numbers of circles and squares are same). From Figure 11.15 it is clear that the absolute values of dynamic strain do not exceed about 15 με (3 MPa). Two different runs of regular speed side-by-side tests were performed in this bridge test. It was observed that a two truck side-by-side loading caused the dynamic load factor of about 0.06 and 0.135 for the most heavily loaded girder (girder No. 6). However, the value of DLF is overestimated. This is explained in the Section 12.2..

Girder Number 6 was instrumented with remote deflection measurement device manufactured by Noptel. The reflector was installed at midspan. The result is shown in Table 11.2. The maximum deflection recorded during the test is 9.82 mm for girder number 6.

Table 11.2. Maximum deflections measured at the center of Girder 6, M82/TC (B01-59041).

Run #	Horizontal (mm)	Vertical (mm)
1	0.28	5.84
2	0.72	2.54
3	0.34	5.49
4	0.70	2.57
5	NA	NA
6	0.24	5.94
7	-0.50	4.60
8	-0.44	1.34
9	-0.29	4.24
10	-0.40	1.42
11	-0.31	4.15
12	NA	NA
13	-0.18	9.72
14	-0.25	9.82
15	0.17	9.40
16	-0.18	9.72

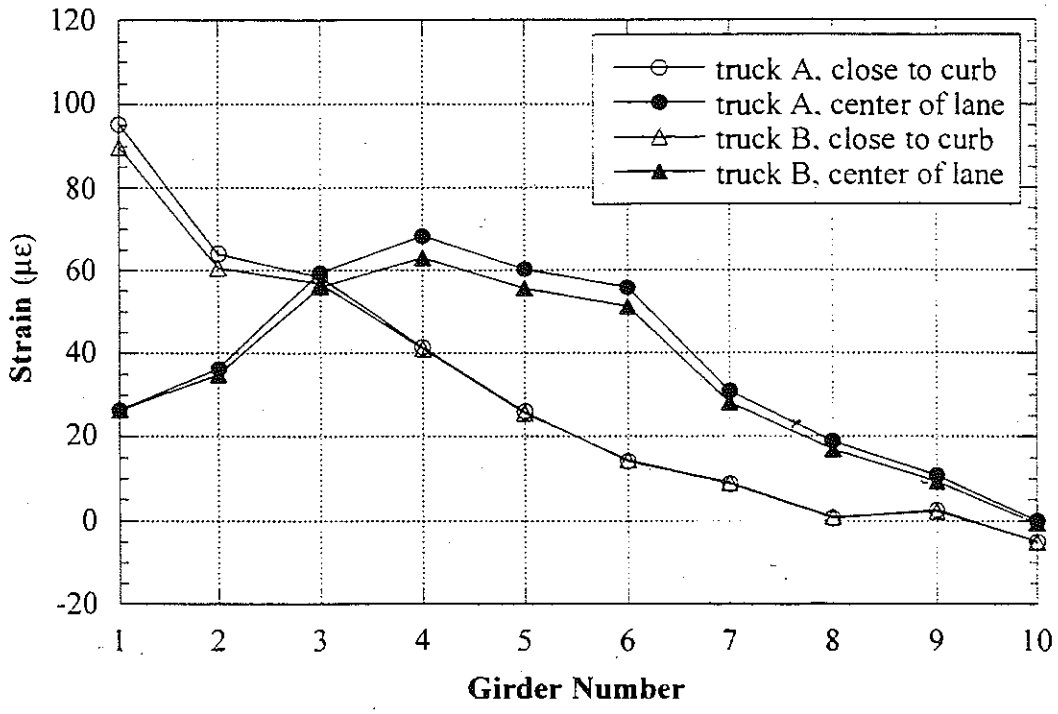

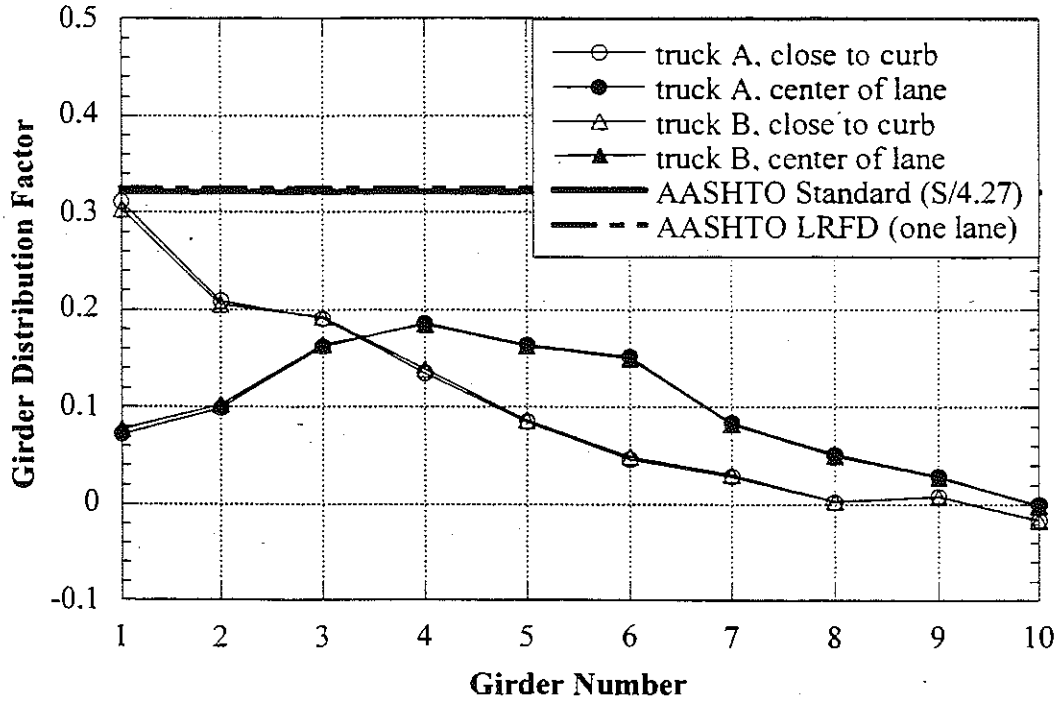

Figure 11.9. South Lane, Crawling Speed, M82/TC (B01-59041).

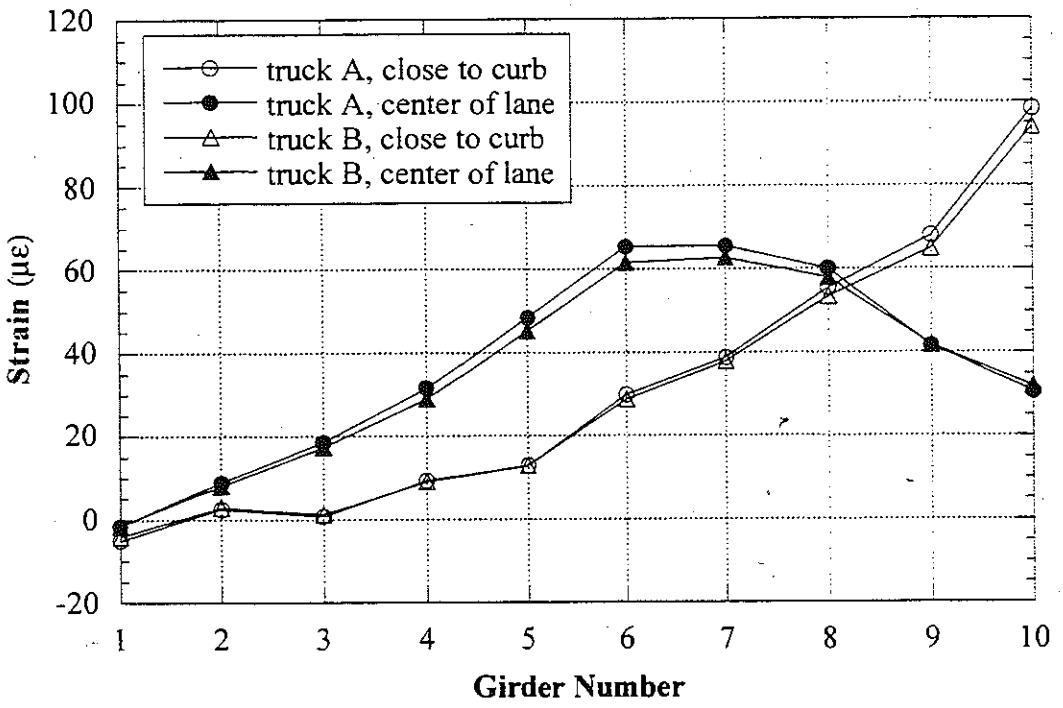

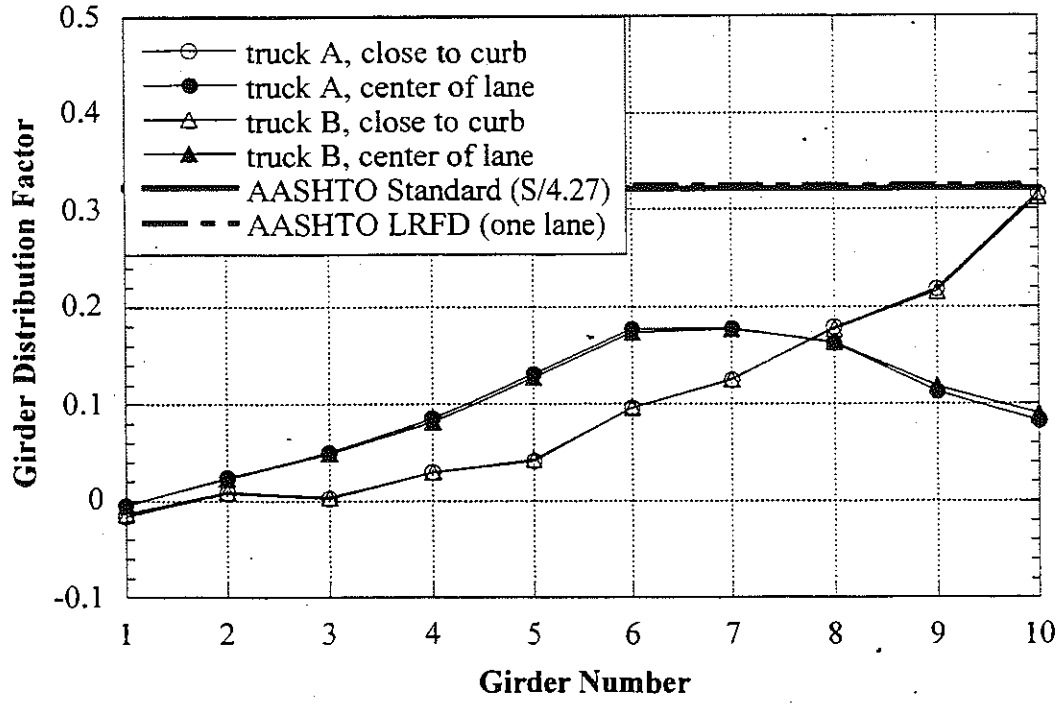

Figure 11.10. North Lane, Crawling Speed, M82/TC (B01-59041).

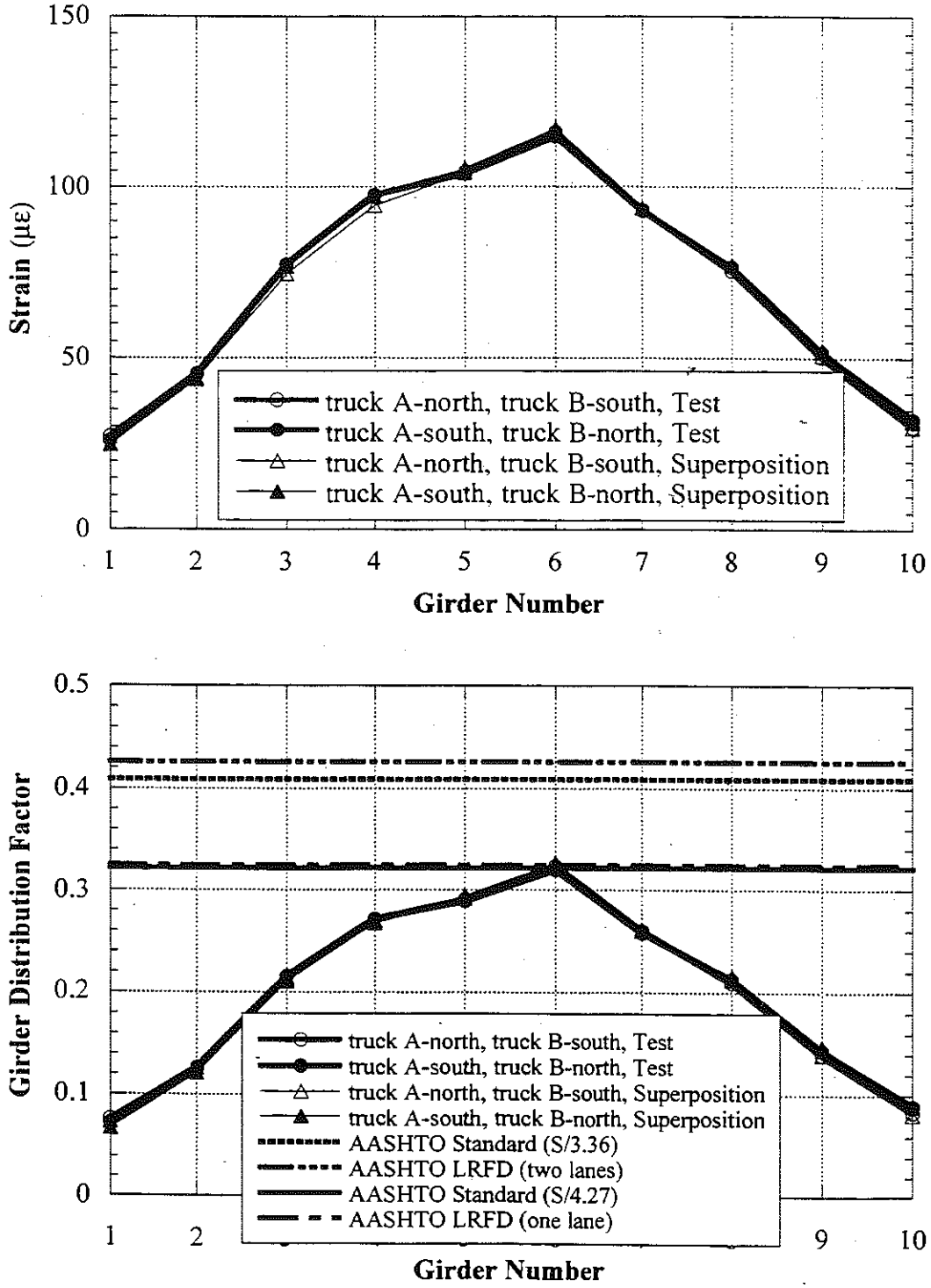

Figure 11.11. Side-by-Side Loading, Center of Lane, Crawling Speed, M82/TC (B01-59041).

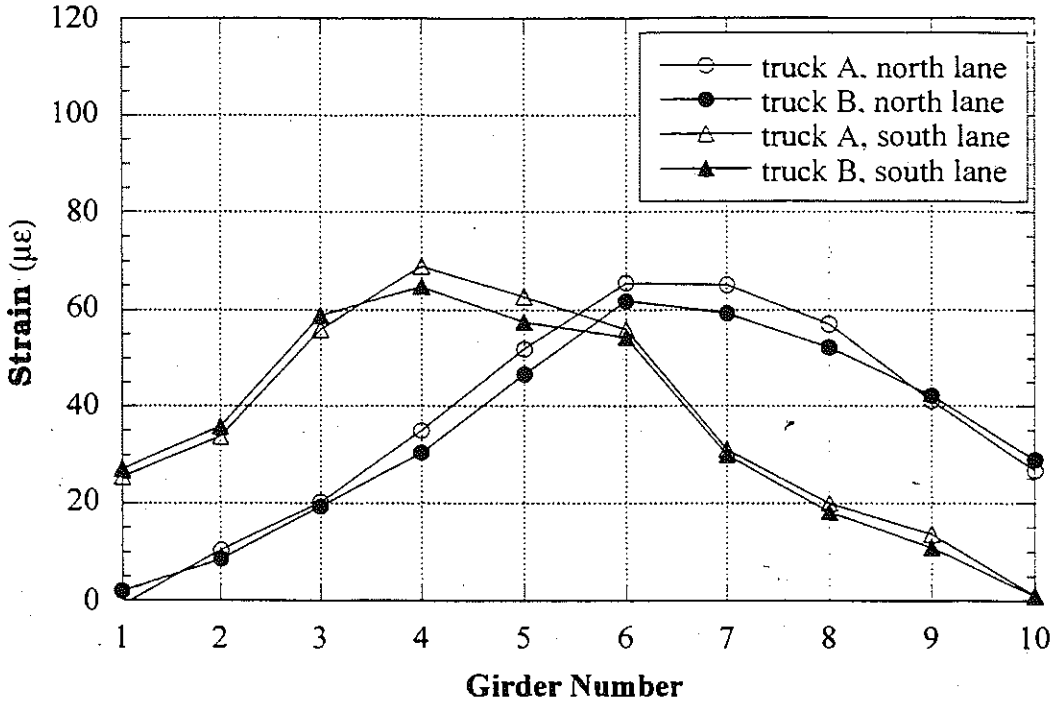

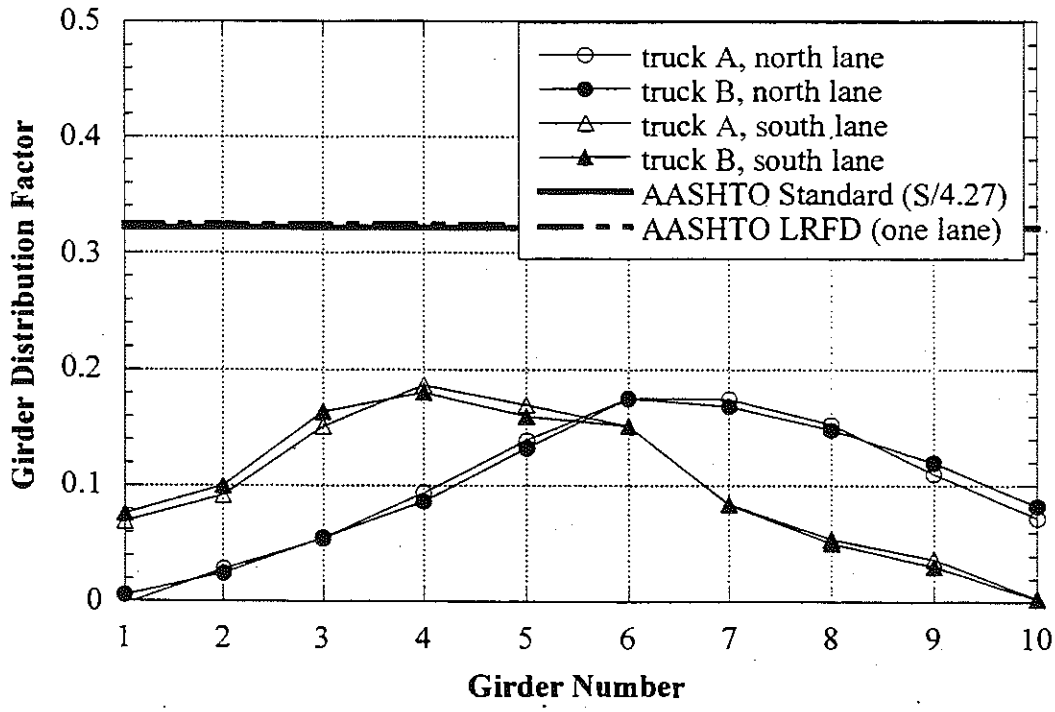

Figure 11.12. Strain and GDF under One Truck Loading at Regular Speed, M82/TC (B01-59041).

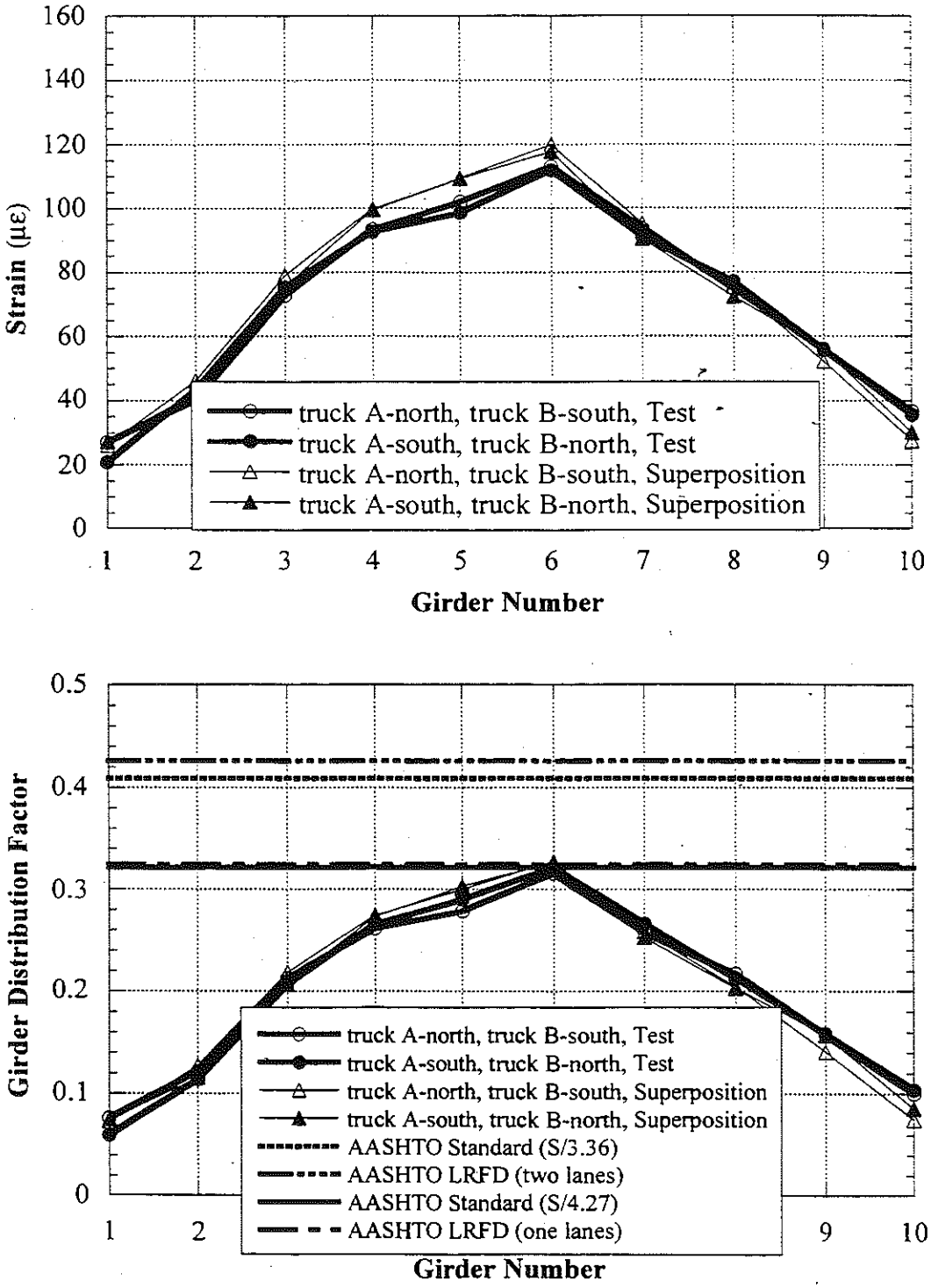

Figure 11.13. Strain and GDF under Side-by-Side Loading at Regular Speed, M82/TC (B01-59041).

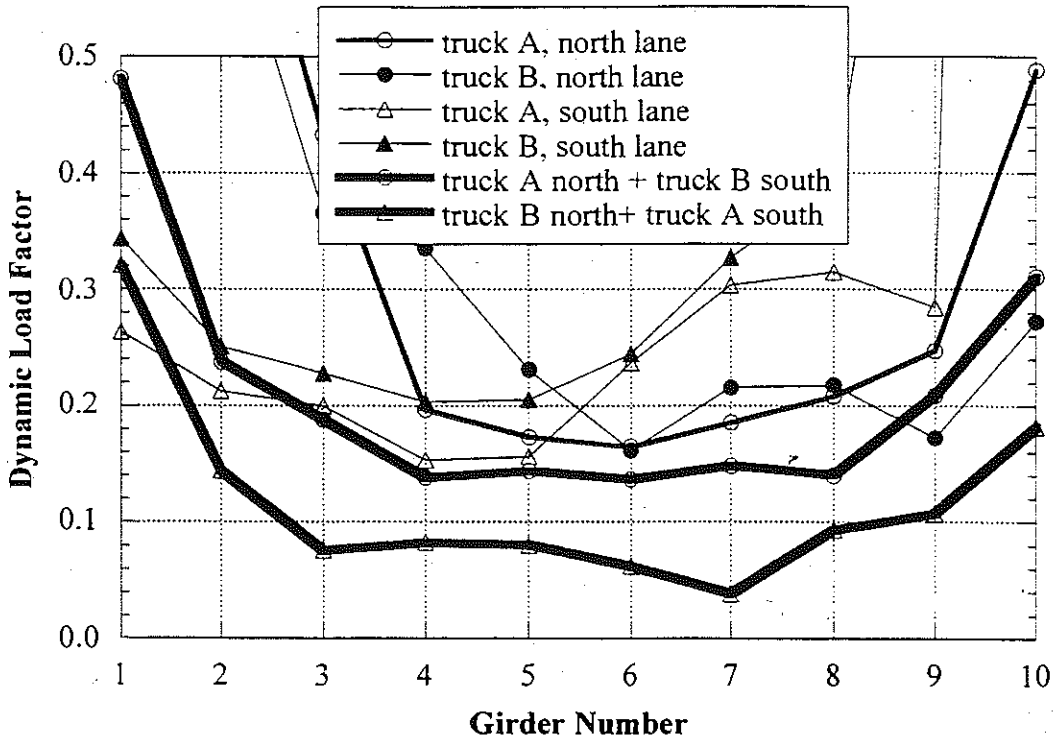

Figure 11.14. Dynamic Load Factors, M82/TC (B01-59041).

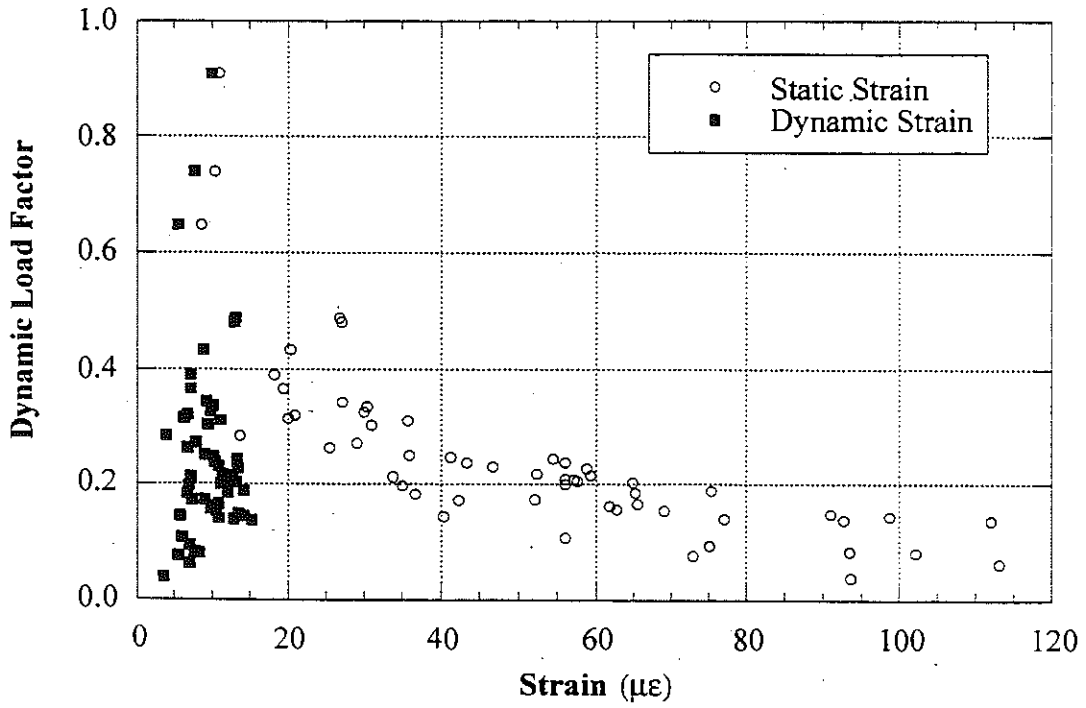

Figure 11.15. Strain vs. Dynamic Load Factors, M82/TC (B01-59041).

Note:

Intentionally left blank

12. Summary and Conclusions

The test program documented in this report covered simply supported, steel girder bridges with spans from 20 to 30 m. The objective of the tests was to verify girder distribution factors (GDF), dynamic load factors (DLF), and load carrying capacity for the bridges selected. In addition, the tests were to check the efficiency of two new equipment systems: wireless transmitters to replace the cables, and an optical deflection measurement device.

12.1. Girder Distribution Factors

Six bridges were instrumented and loaded with heavy 11-axle trucks. The resulting strains are shown in Figures 12.1 to 12.5, for one truck and two trucks side-by-side.

In Figures 12.1 and 12.2, the strains are plotted for one lane loading at crawling speed. Two truck positions are considered for each case: close to the curb and center of the traffic lane. The strains for truck A and B are practically the same, which confirms the repeatability of the results. For a single truck, the maximum strain was recorded in the interior girder, about 230 με. For two trucks side-by-side and crawling speed the strains are shown in Figure 12.3. For two trucks side-by-side, the maximum strain is about 348 με.

Similar results are obtained for the strains measured at the regular speed, as shown in Figures 12.4 and 12.5. This confirms that the speed does not affect the accuracy of the results for GDF's.

The girder distribution factors are summarized in Figures 12.6 to 12.8 at crawling speed and Figures 12.9 and 12.10 for the regular speed.

For a one lane loaded, GDF's observed for interior girders are lower than GDF's specified in the code as shown in Figures 12.6 and 12.7 for crawling speed, and in Figure 12.9 for normal speed. For exterior girders the code specified GDF's are different than for GDF's for interior girders and the test results are not compared to code specified values in this study.

The code specified GDF's are conservative for two trucks side-by-side. As shown in Figure 12.8 and Figure 12.10, the GDF's from the tests are equal or less than the GDF's specified for two lanes loaded by the AASHTO LRFD (1998) and AASHTO Standard (1996). In many cases, even code specified GDF's for one lane loading are sufficient for, or very close to, the test results from the two trucks side-by-side loading.

The absolute values of measured strains are less than 210 με for all the tested bridges except of structure S03-13074 for which it is 348 με. There are two main reasons low strain values:

- Partial fixity of supports. All of the considered bridges, except of structure S03-13074, were designed with simple supports. Yet, the actual supports provide some resistance to horizontal movement and rotation. This is due to collection of debris, corrosion, and counter-balancing effect of weight of structural and non-structural components on the other end of the bearing center (cantilever portion of the girder, concrete diaphragm over the support, portion of the deck slab, portion of the pavement adjacent to the bridge).
- More uniform girder distribution factors. The truck load is distributed among the girders and other components (deck slab, sidewalks, parapet, curbs). The latter are not considered in the design and their contribution to the overall stiffness of the bridge can be about 10%.

The measured strain in structure S03-13074 is larger than in other tested bridges because of different support conditions. Even though this bridge is a statically determinate structure, the girders are continuous over the supports with pin-hangers joints in adjacent spans. Therefore, the effect of partial fixity of the supports is reduced (or even eliminated).

For evaluation of existing steel girder bridges, it is recommended to use AASHTO LRFD (1998) girder distribution factors. For the bridges which have ADTT lower than 1000, GDF's specified for a single lane structures can be used, because of a reduced probability of a simultaneous occurrence of two heavy truck side-by-side. This recommendation is an extension of the previous one, and it applies to spans up to 30m (previous recommendation was based on bridge tests limited to shorter spans).

12.2. Dynamic Load Factors

The dynamic load factors (DLF) obtained from the tests are summarized in Figures 12.11 and 12.12. For a one lane loading, DLF corresponding to the maximum static strain, is about 0.20. For two trucks side-by-side, DLF is less than 0.10 for all the bridges except of bridge B01-59041 for which it is about 0.135. However, in case of the latter bridge, the value of DLF is overestimated. The actual strain vs. time relationship is shown in Figure 12.15. The static strain is calculated by filtering the dynamic effect. The computer procedure and filtering involves some subjective judgement. The computer simulated static strain and manually simulated strain are shown in Figure 12.16. DLF corresponding to the latter is less than 0.10.

In evaluation of existing steel girder bridges, it is recommended to use the DLF = 0.10 for two lane bridges, with both lanes loaded. For a single lane load DLF = 0.20 can be used.

12.3. Finite Element Analysis

Figure 12.13 shows the results of the finite element analysis for two truck side-by-side loading. It includes the experimental results and analytical (FEM) results from the two different models. In the first FEM model, it was assumed that the supports were represented by a hinge at one end and a roller with a hinge at the other end. In the other FEM model, it was assumed that both supports were hinged, with no movement in horizontal direction. The experimental response lies between the two different analytical models. This indicates that the partial fixity exists at the supports of the bridge.

For comparison, the GDF's obtained in field tests as a part of this study, are plotted versus analytical values calculated using AASHTO Standard (1996) and AASHTO LRFD (1998). The results are shown in Figure 12.14 for single truck (one lane loaded) and for two trucks (two lanes loaded).

The maximum measured static strains are compared to calculated strains in Table 12.1 for two trucks side-by-side. The maximum calculated strains were obtained by using (1) the maximum bending moment from 685 kN legal truck load and the GDF's specified in AASHTO Standard (1996), and (2) finite element analysis using the test trucks.

For finite element analysis (FEA) in Table 12.1, three-dimensional finite element analysis was performed. The concrete slab was modeled as an isotrophic, eight node solid element, with three degrees of freedoms at each node. The girder flanges and web were modeled using three-dimensional, quadrilateral, four node shell element with six degrees of freedom at each node. The structural effects of the secondary members,

such as sidewalk and parapet, are also included in the finite element analysis models.

Two cases of the boundary conditions were employed in the FEA models. In the first FEA model, the supports are truly simple, that is, one of the supports is a fixed hinge, and the other one is a roller support. In the other FEA model, both supports are fixed hinges, thereby not allowing the horizontal movement at the supports.

In evaluation of existing steel girder bridges, the available finite element methods (FEM) can provide useful results. The numerical accuracy depends on the number of elements and geometrical configuration of the model. However, the most important consideration is the selection of the boundary conditions. This is also the most difficult task and it requires a good knowledge of site-specific details. The comparison of the analytical and field test results indicates that the actual performance can be modeled accurately by assuming composite action and partial fixity of supports.

12.4. Wireless Transmitters

The research team's experience with using the wireless transmitters is not very good. It took a long time to get them fixed because of many problems (interference, poor connections, range). When finally applied in parallel with the cable-based system, the results were very similar, however, one of the transmitters did not work. The installation time compared to cable-based system is not much shorter. Nevertheless, we are planning to use the wireless transmitters in future tests and try to make further improvements in the system.

12.5. Optical Device for Measurement of Deflection

An important consideration in field testing is the access to the structural components without interfering with traffic. Therefore, we tried to use the optical device by Noptel to remotely measure deflection. For verification, bridges with ID S03-13074 were instrumented with two parallel systems, Noptel device, and LVDT's. Only one Noptel device was available for this project because of the high price. The comparison confirmed that the resulting deflections are very close for both systems. Therefore, the project team intends to purchase additional devices to measure the deflection of several girders simultaneously.

Table 12.1. Comparison of the Strain Values from the test and analysis.

MDOT ID #	Maximum Measured Strain (10^{-6})	Maximum Calculated Strain (10^{-6})			
		AASHTO S/4.27	AASHTO S/3.36	Finite Element Analysis	
				Simple Supports	Restrained Supports
B02-46062	161.8	247.4	314.7	187	76
R01-78054	207.3	305.4	388.9	231	173
B04-77012	96.4	214.1	248.8	153	71
S03-13074	348.3	501.5	638.4	285	150
B01-29041	120.0	338.0	430.0	157	74
B01-59041	116.3	260.4	331.4	131	60

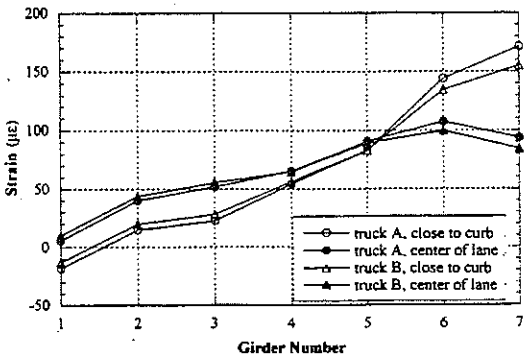

US223/RR (B02-46062)
North Lane Loaded

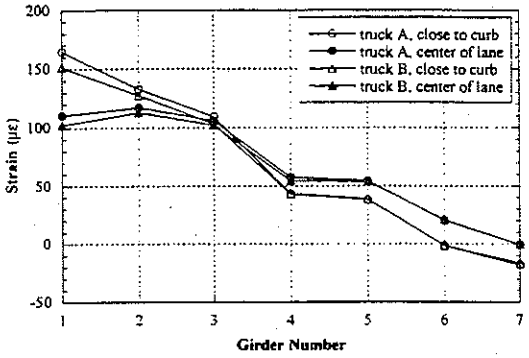

US223/RR (B02-46062)
South Lane Loaded

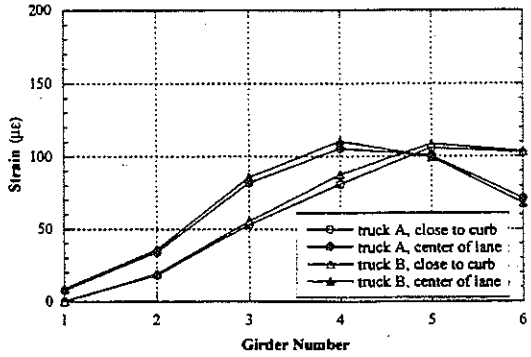

M66/RR (R01-78054)
West Lane Loaded

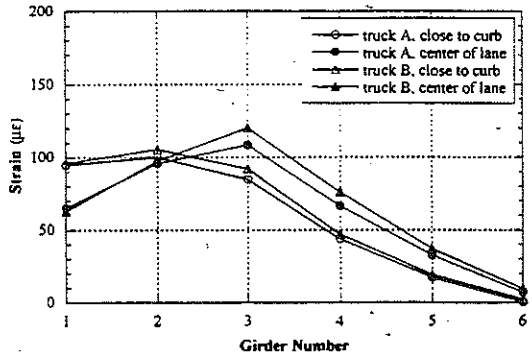

M66/RR (R01-78054)
East Lane Loaded

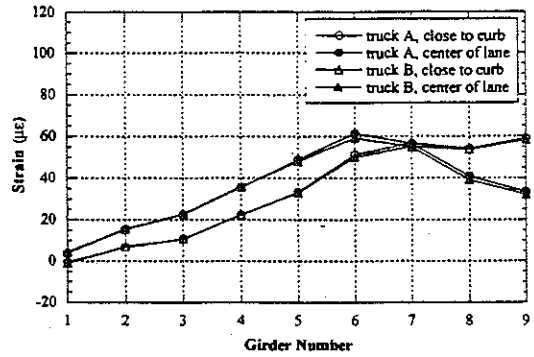

M19/MC (B04-77012)
West Lane Loaded

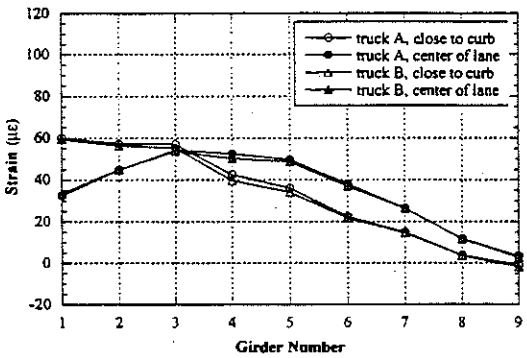

M19/MC (B04-77012)
East Lane Loaded

Figure 12.1. Strains under One Lane Loading at Crawling Speed

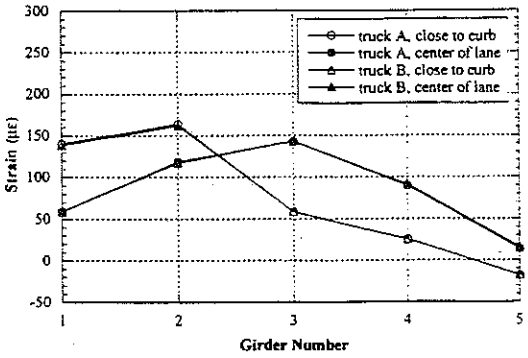

NDN/I69 (S03-13074)
North Lane Loaded

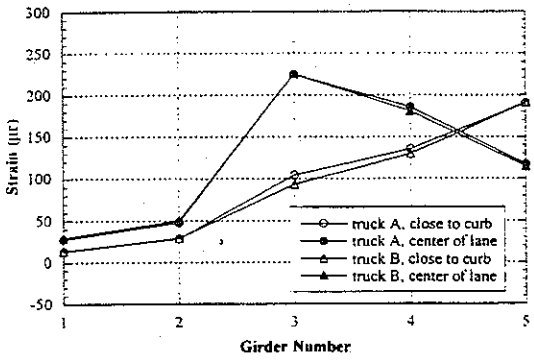

NDN/I69 (S03-13074)
South Lane Loaded

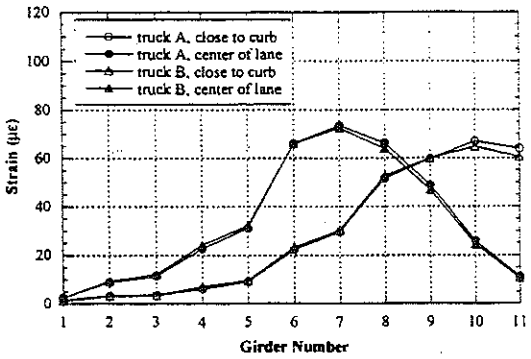

M46/PR (B01-29041)
North Lane Loaded

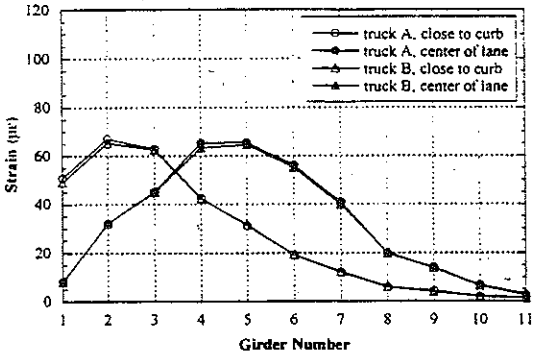

M46/PR (B01-29041)
South Lane Loaded

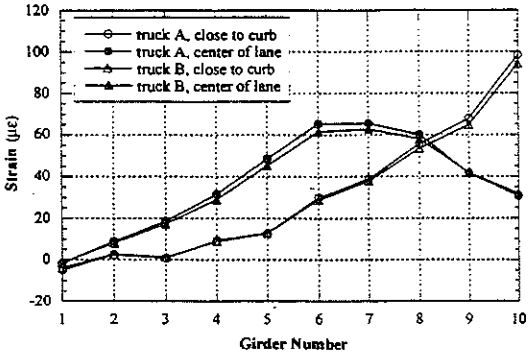

M82/TC (B01-59041)
North Lane Loaded

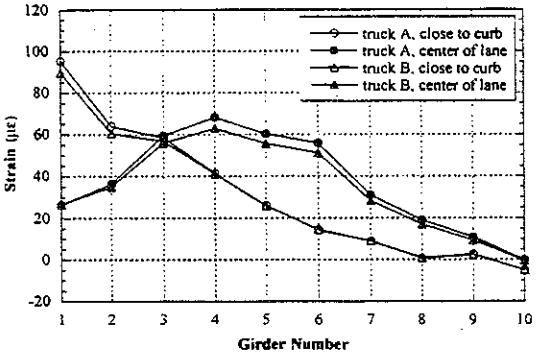

M82/TC (B01-59041)
South Lane Loaded

Figure 12.2. Strains under One Lane Loading at Crawling Speed (Continued).

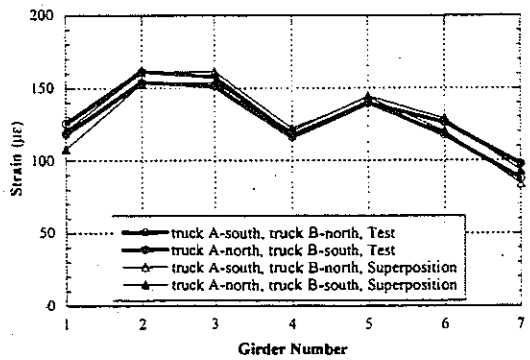

US223/RR (B02-46062)

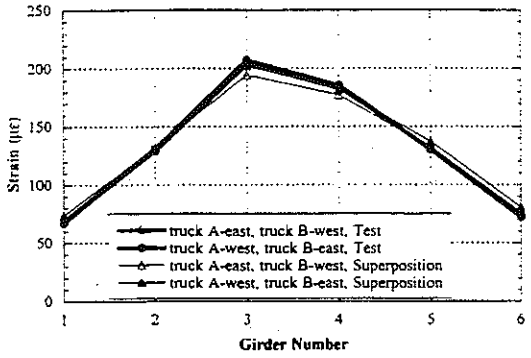

M66/RR (R01-78054)

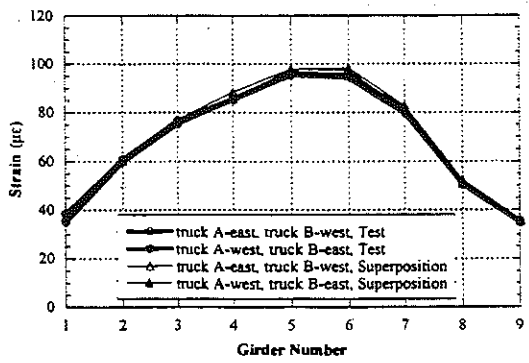

M19/MC (B04-77012)

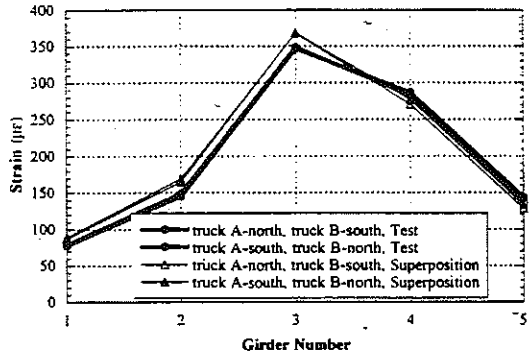

NDN/I69 (S03-13074)

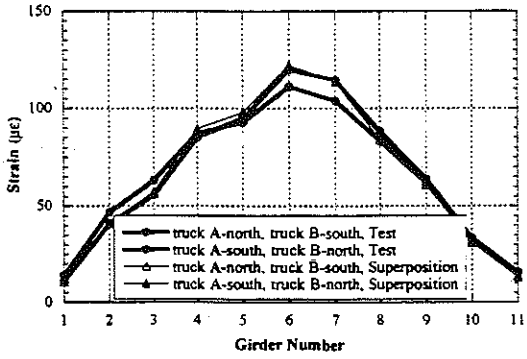

M46/PR (B01-29041)

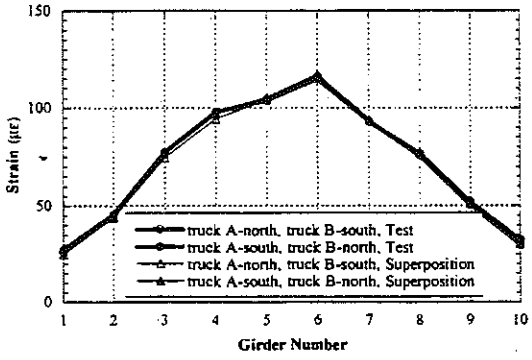

M82/TC (B01-59041)

Figure 12.3. Strains under Side-by-Side Truck Loading at Crawling Speed

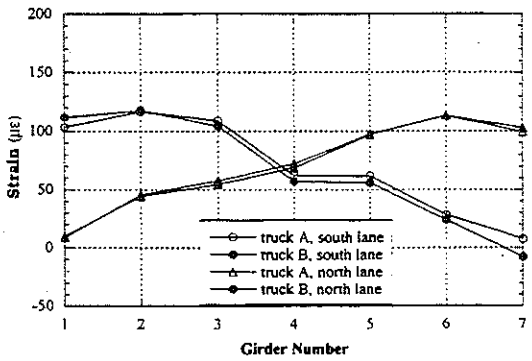

US223/RR (B02-46062)

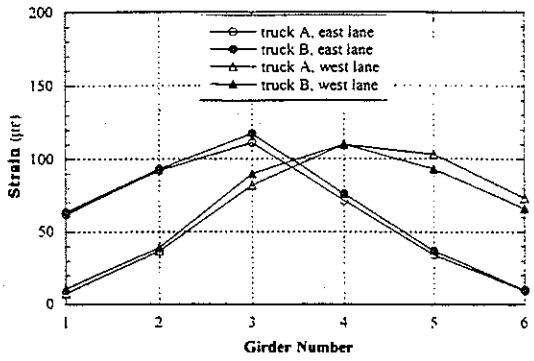

M66/RR (R01-78054)

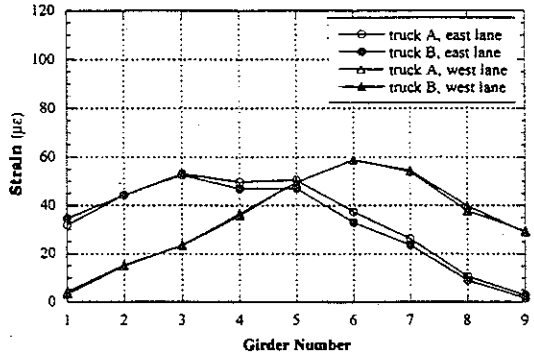

M19/MC (B04-77012)

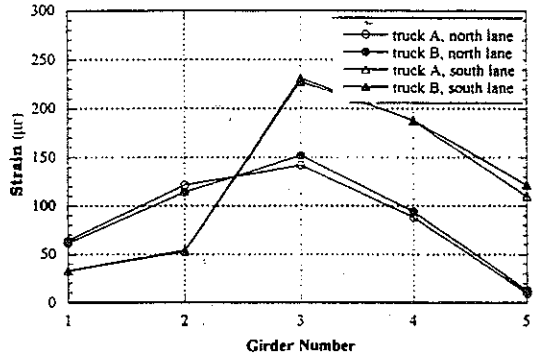

NDN/I69 (S03-13074)

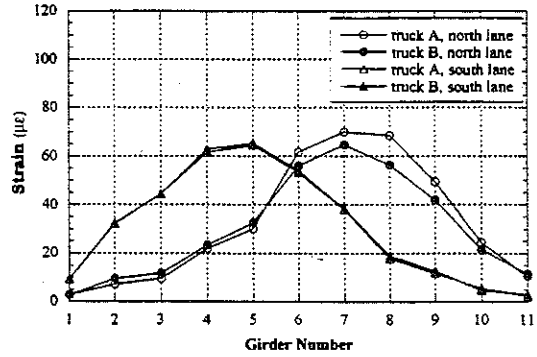

M46/PR (B01-29041)

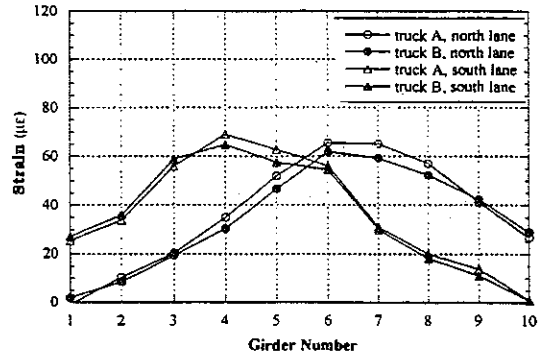

M82/TC (B01-59041)

Figure 12.4. Strains under One Lane Loading at Regular Speed.

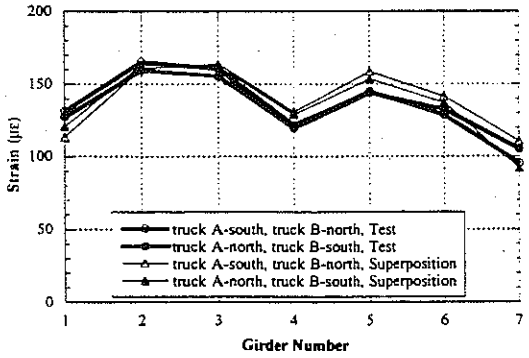

US223/RR (B02-46062)

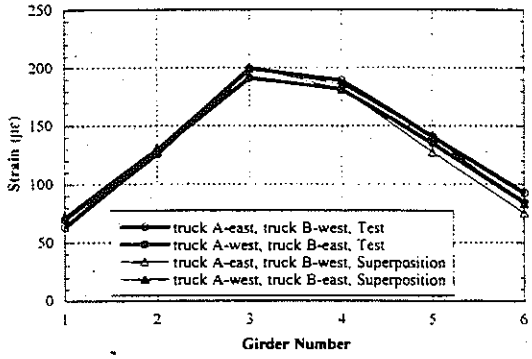

M66/RR (R01-78054)

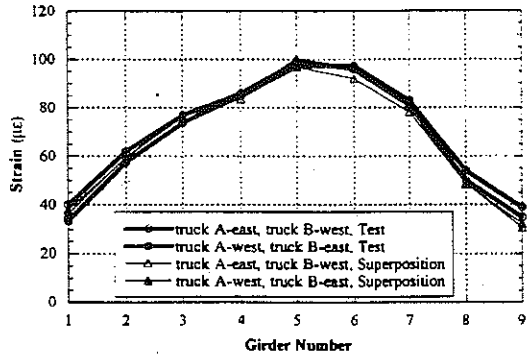

M19/MC (B04-77012)

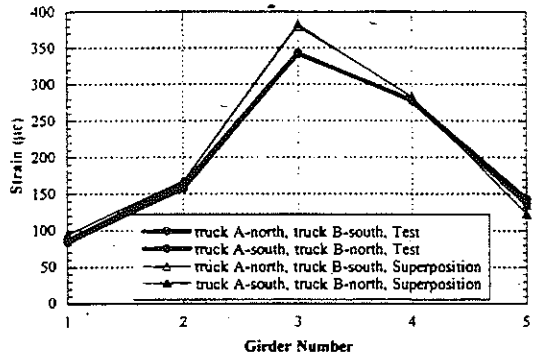

NDN/I69 (S03-13074)

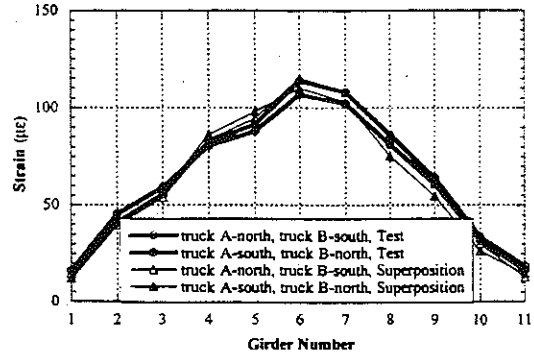

M46/PR (B01-29041)

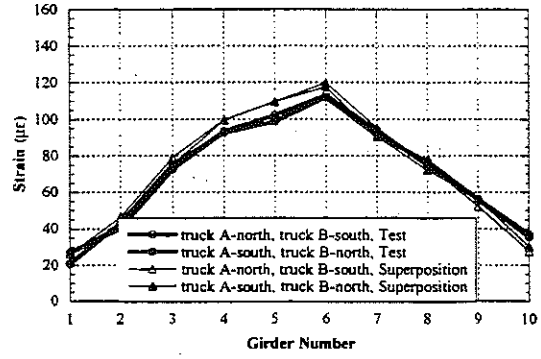

M82/TC (B01-59041)

Figure 12.5. Strains under Side-by-Side Truck Loading at Regular Speed.

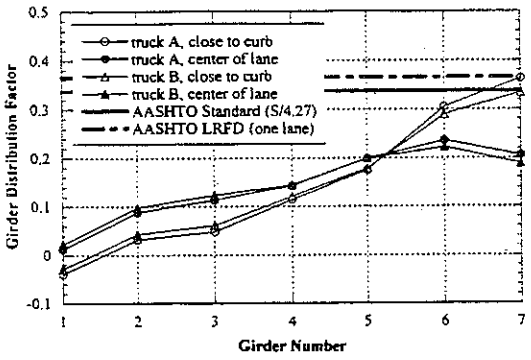

US223/RR (B02-46062)
North Lane Loaded

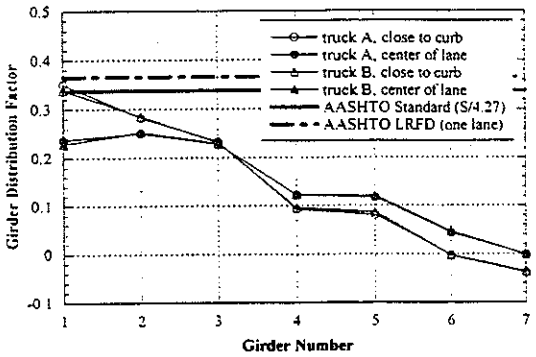

US223/RR (B02-46062)
South Lane Loaded

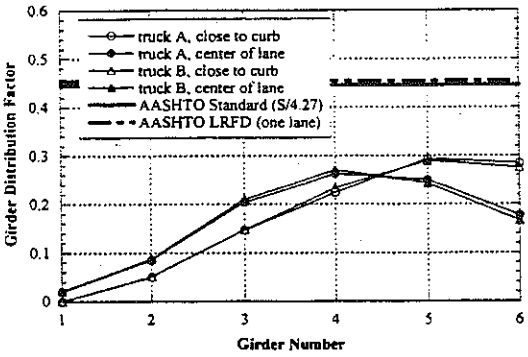

M66/RR (R01-78054)
West Lane Loaded

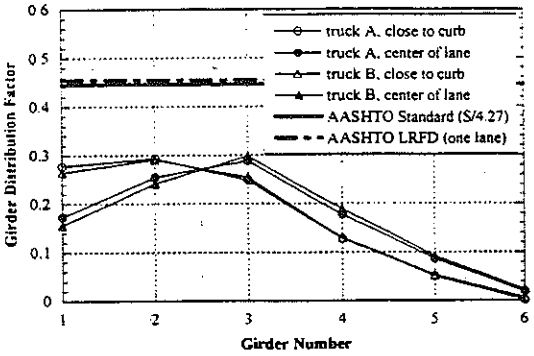

M66/RR (R01-78054)
East Lane Loaded

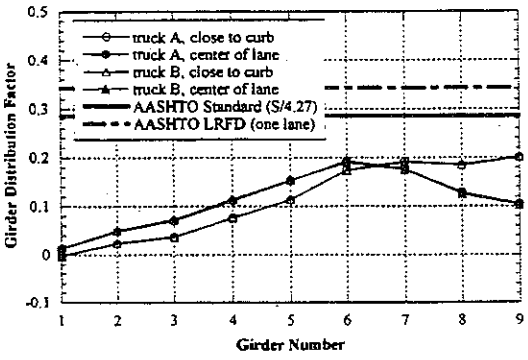

M19/MC (B04-77012)
West Lane Loaded

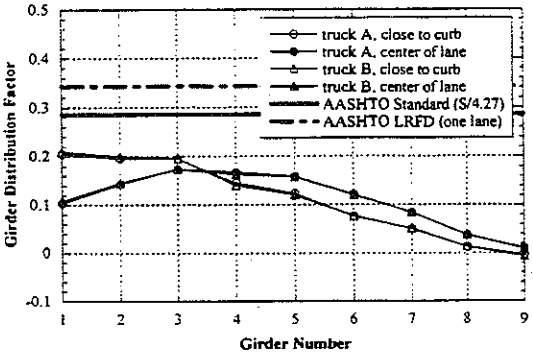

M19/MC (B04-77012)
East Lane Loaded

Figure 12.6. Girder Distribution Factor under One Truck Loading at Crawling Speed.

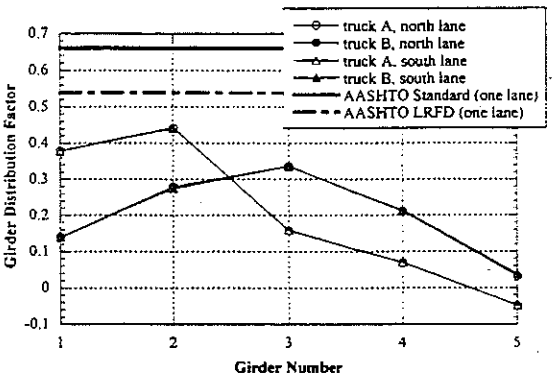

NDN/I69 (S03-13074)
North Lane Loaded

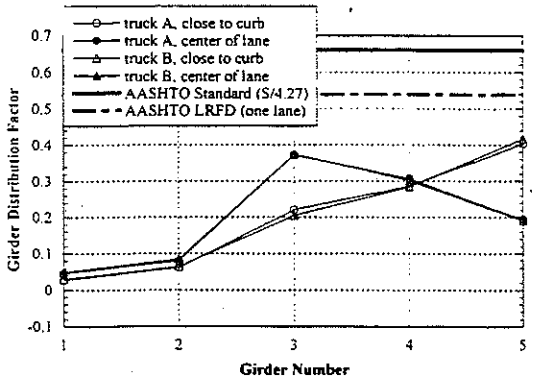

NDN/I69 (S03-13074)
South Lane Loaded

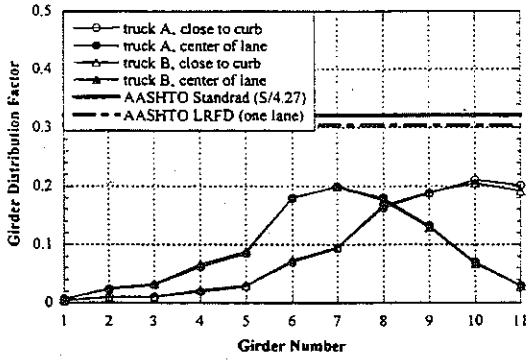

M46/PR (B01-29041)
North Lane Loaded

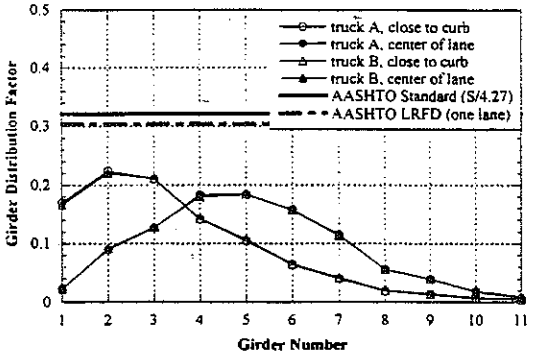

M46/PR (B01-29041)
South Lane Loaded

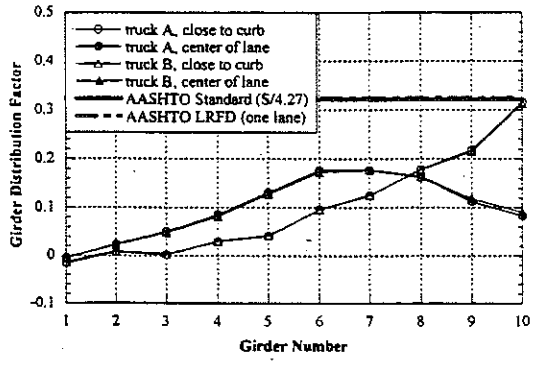

M82/TC (B01-59041)
North Lane Loaded

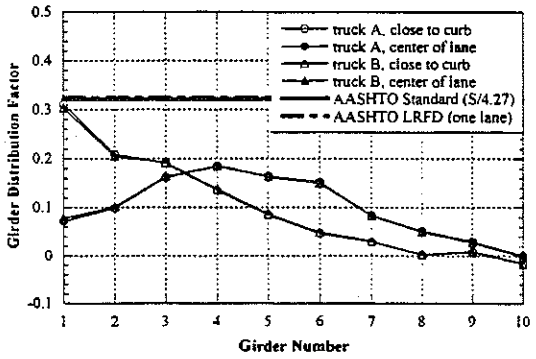

M82/TC (B01-59041)
South Lane Loaded

Figure 12.7. Girder Distribution Factor under One Truck Loading at Crawling Speed (continued).

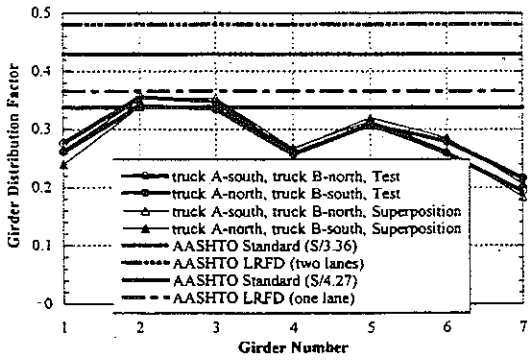

US223/RR (B02-46062)

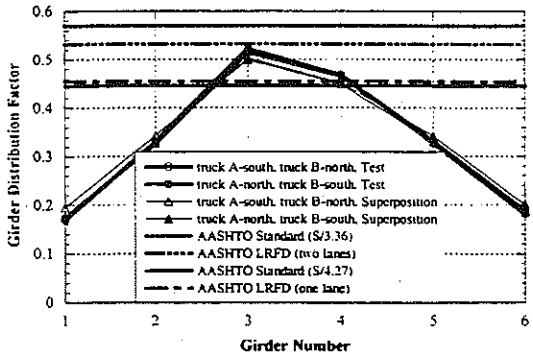

M66/RR (R01-78054)

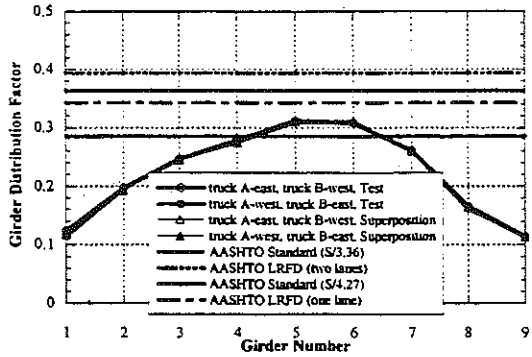

M19/MC (B04-77012)

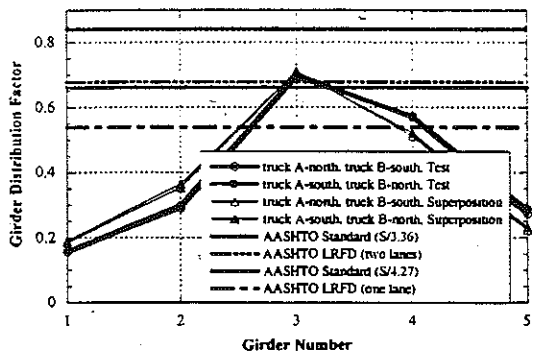

NDN/I69 (S03-13074)

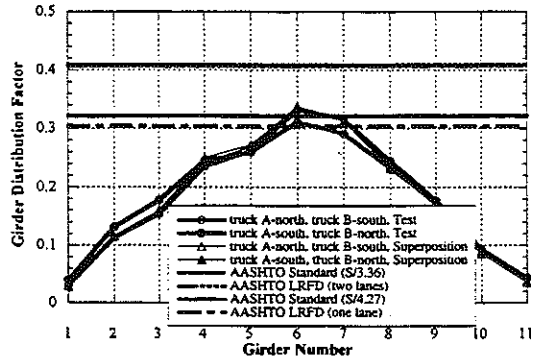

M46/PR (B01-29041)

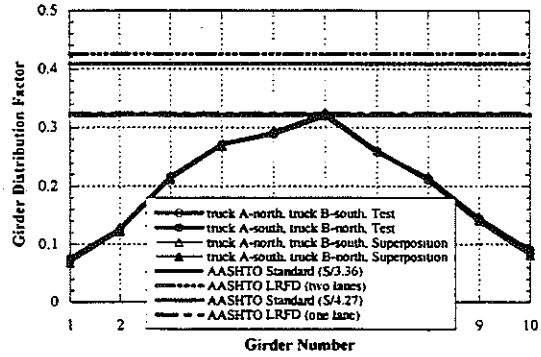

M82/TC (B01-59041)

Figure 12.8. Girder Distribution Factor under Two Truck Side-by-Side Loading at Crawling Speed.

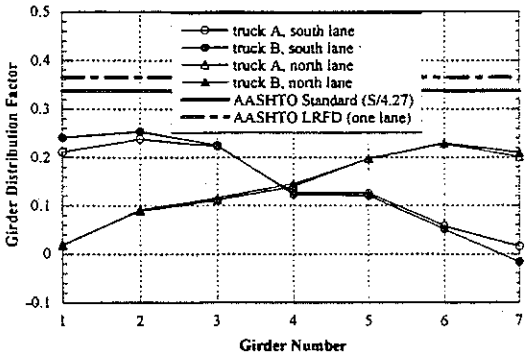

US223/RR (B02-46062)

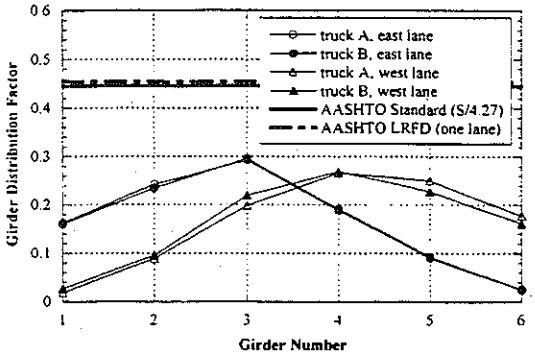

M66/RR (R01-78054)

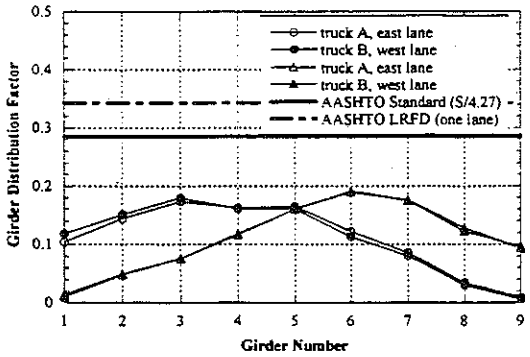

M19/MC (B04-77012)

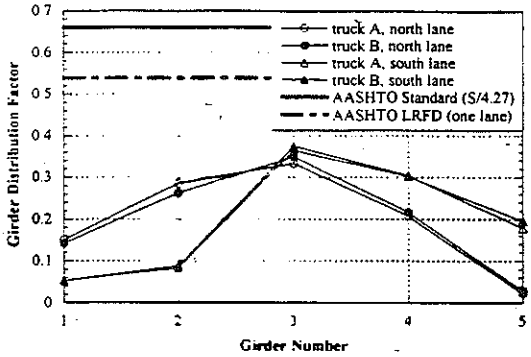

NDN/I69 (S03-13074)

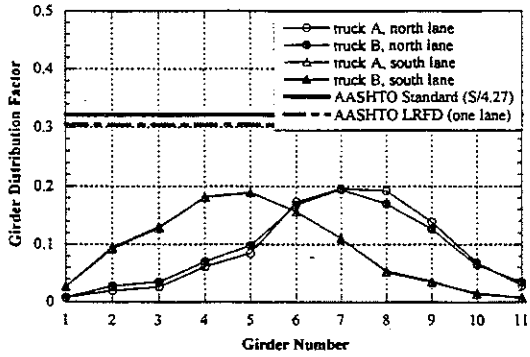

M46/PR (B01-29041)

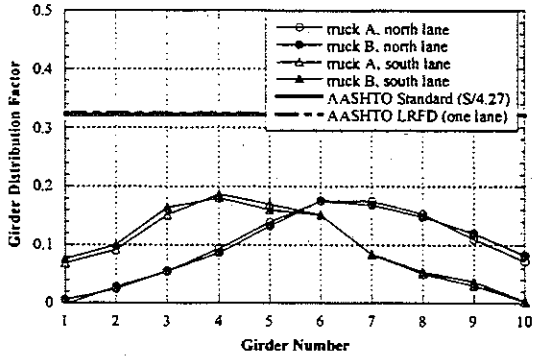

M82/TC (B01-59041)

Figure 12.9. Girder Distribution Factor under One Truck Loading at Regular Speed.

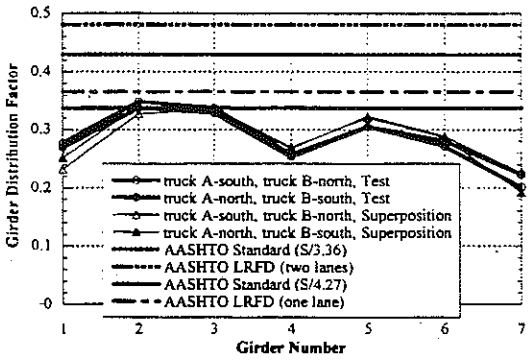

US223/RR (B02-46062)

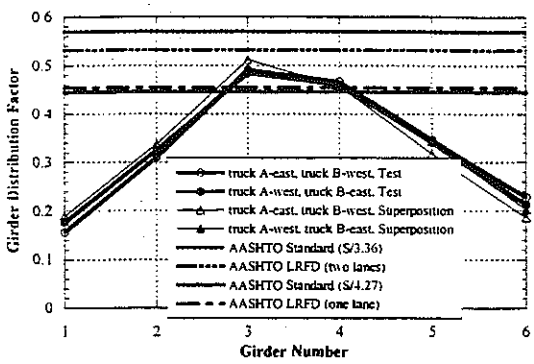

M66/RR (R01-78054)

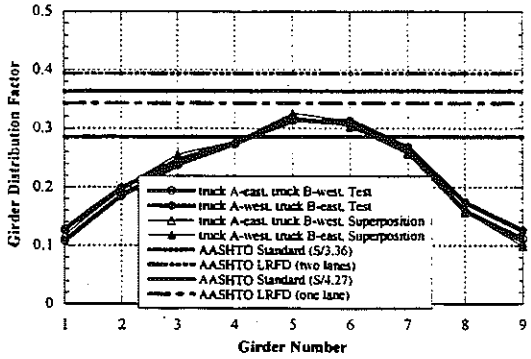

M19/MC (B04-77012)

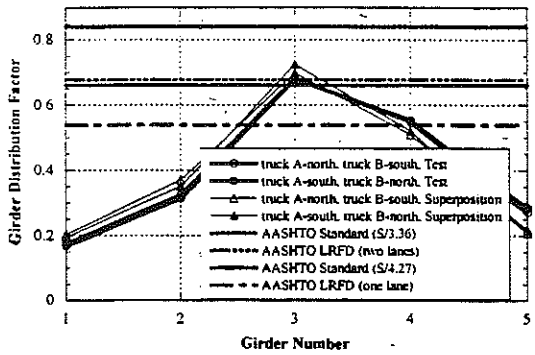

NDN/I69 (S03-13074)

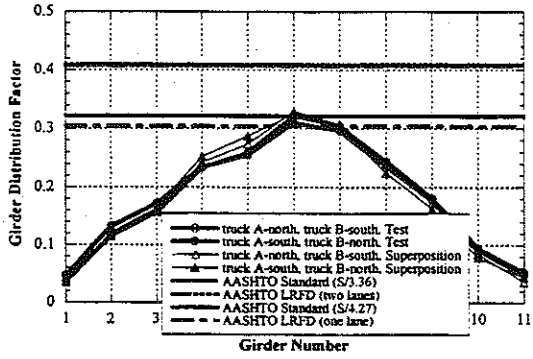

M46/PR (B01-29041)

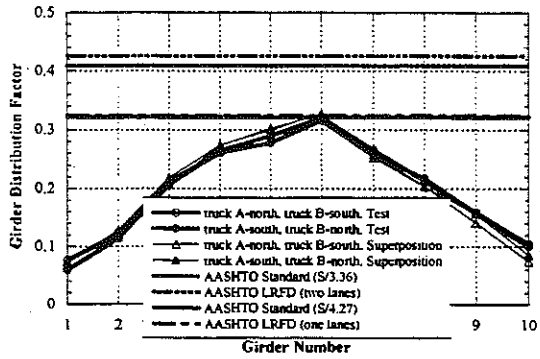

M82/TC (B01-59041)

Figure 12.10. Girder Distribution Factor under Two Truck Side-by-Side Loading at Regular Speed.

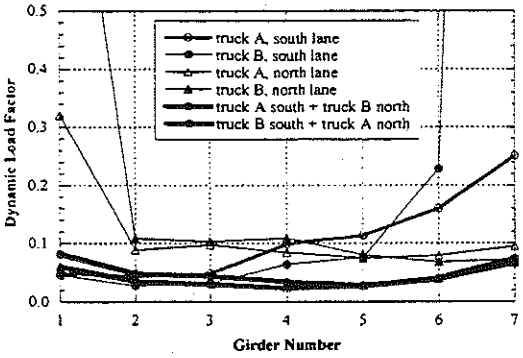

US223/RR (B02-46062)

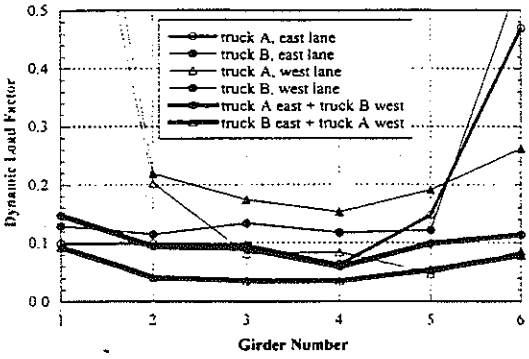

M66/RR (R01-78054)

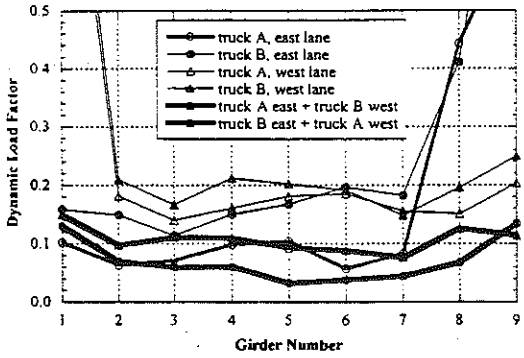

M19/MC (B04-77012)

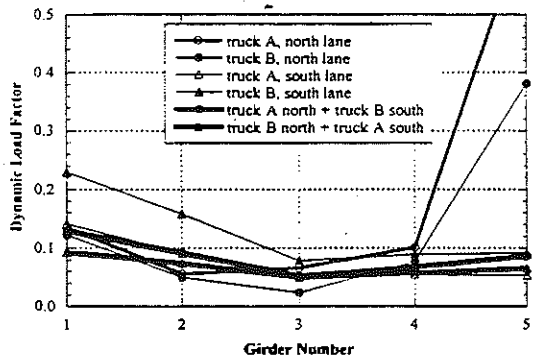

NDN/I69 (S03-13074)

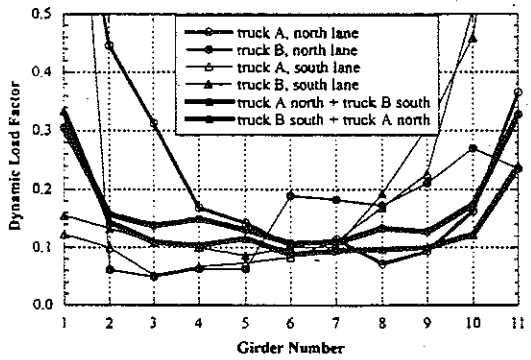

M46/PR (B01-29041)

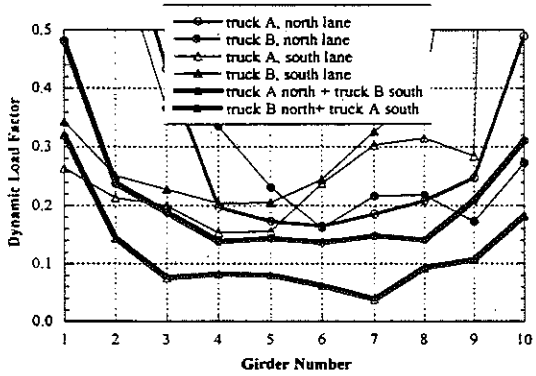

M82/TC (B01-59041)

12.11. Dynamic Load Factor.

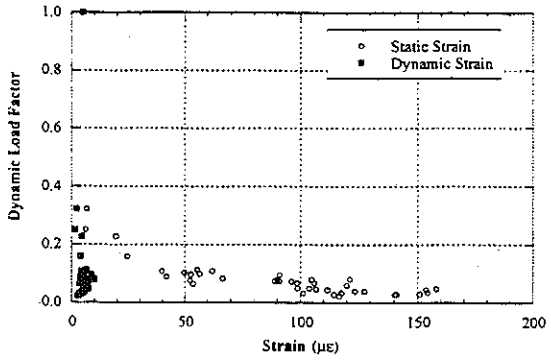

US223/RR (B02-46062)

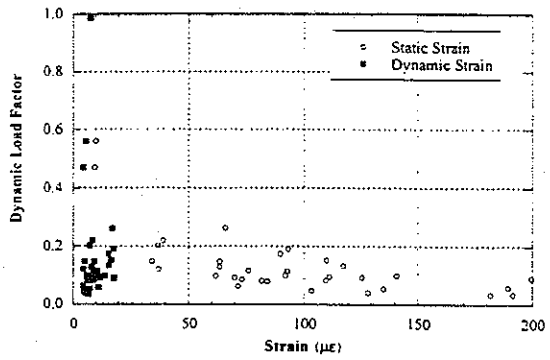

M66/RR (R01-78054)

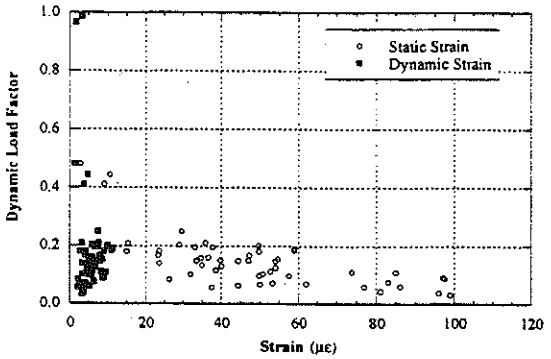

M19/MC (B04-77012)

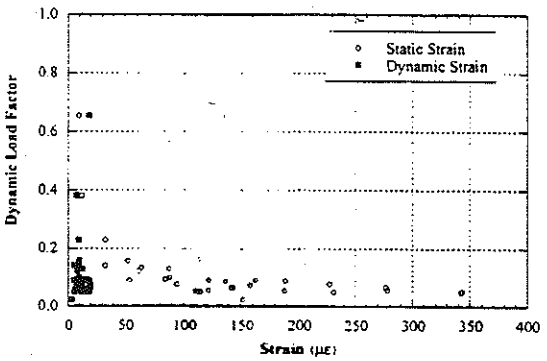

NDN/I69 (S03-13074)

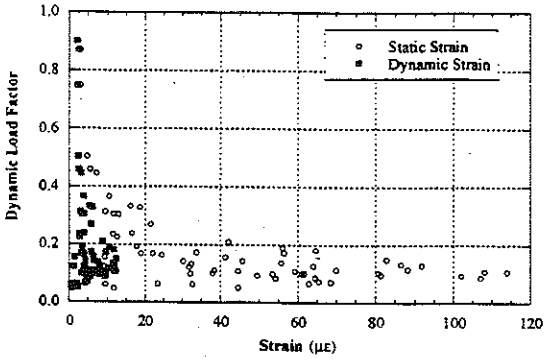

M46/PR (B01-29041)

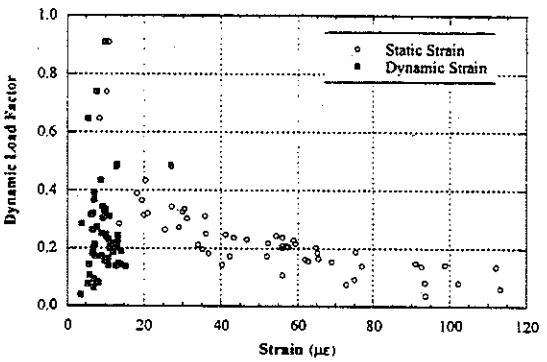

M82/TC (B01-59041)

12.12. Strain Vs. Dynamic Load Factor.

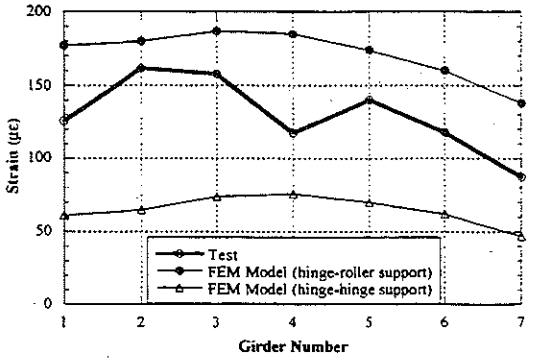

US223/RR (B02-46062)

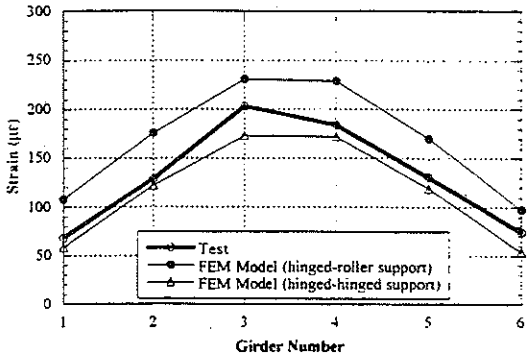

M66/RR (R01-78054)

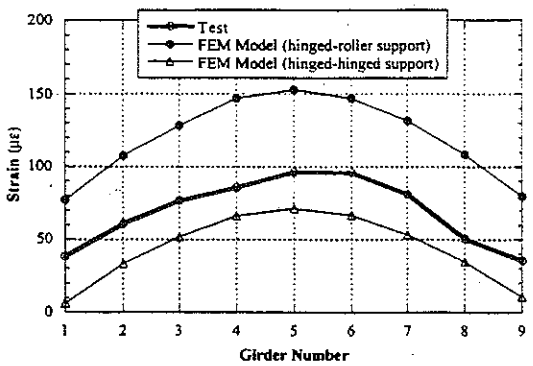

M19/MC (B04-77012)

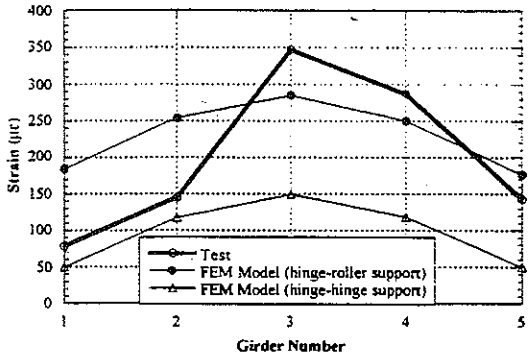

NDN/I69 (S03-13074)

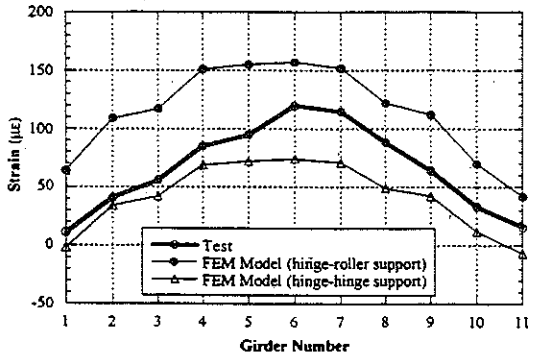

M46/PR (B01-29041)

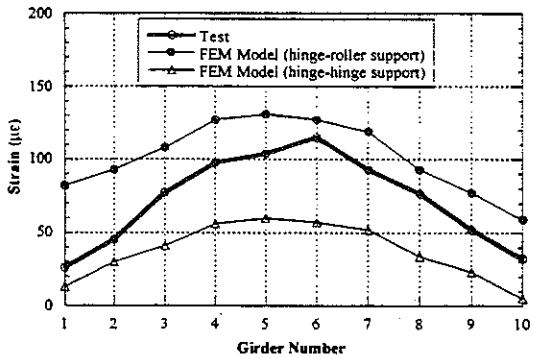

M82/TC (B01-59041)

12.13. Results of the Finite Element Analysis.

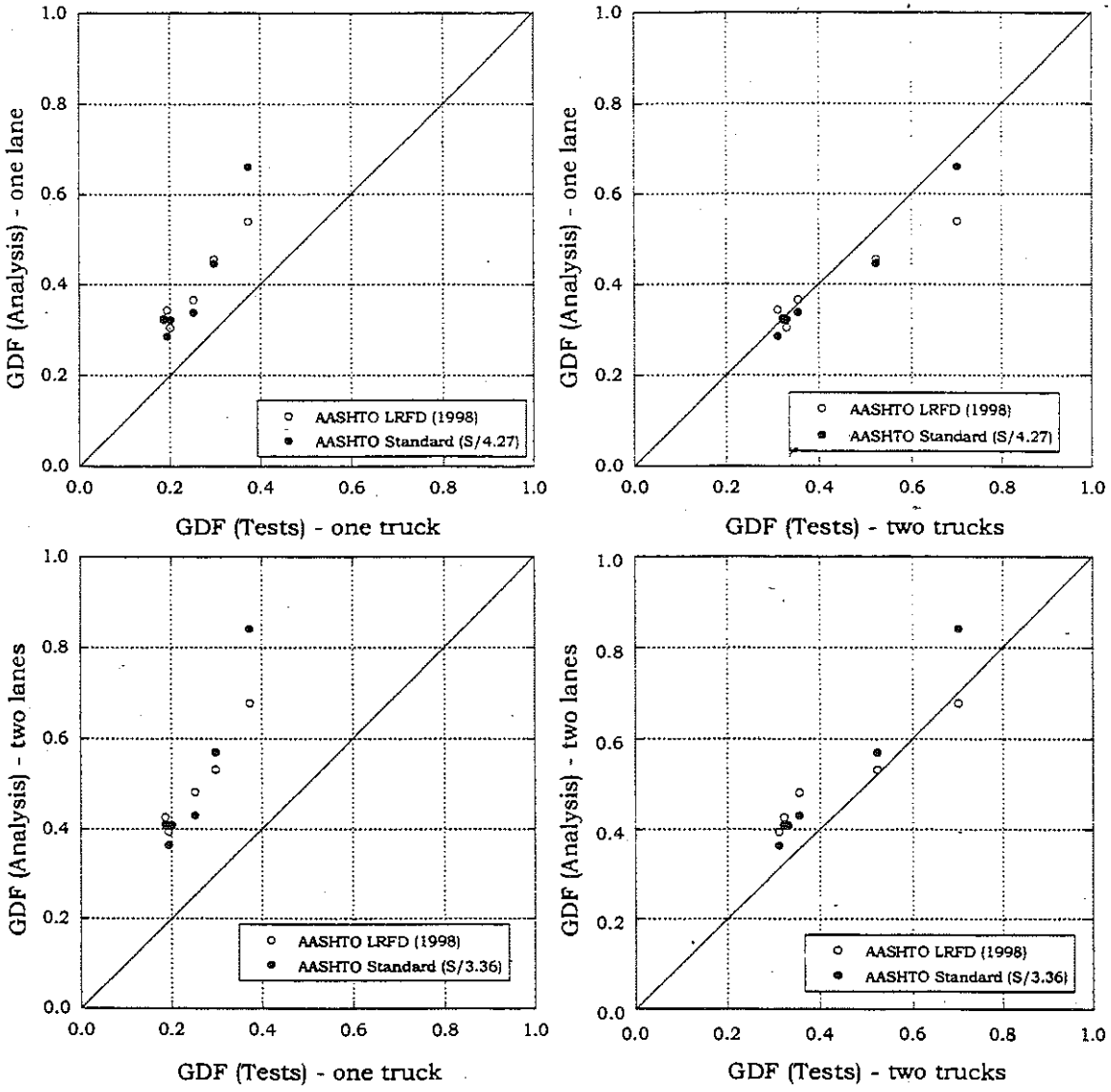

Figure 12.14. GDF (test) Versus GDF (Analysis).

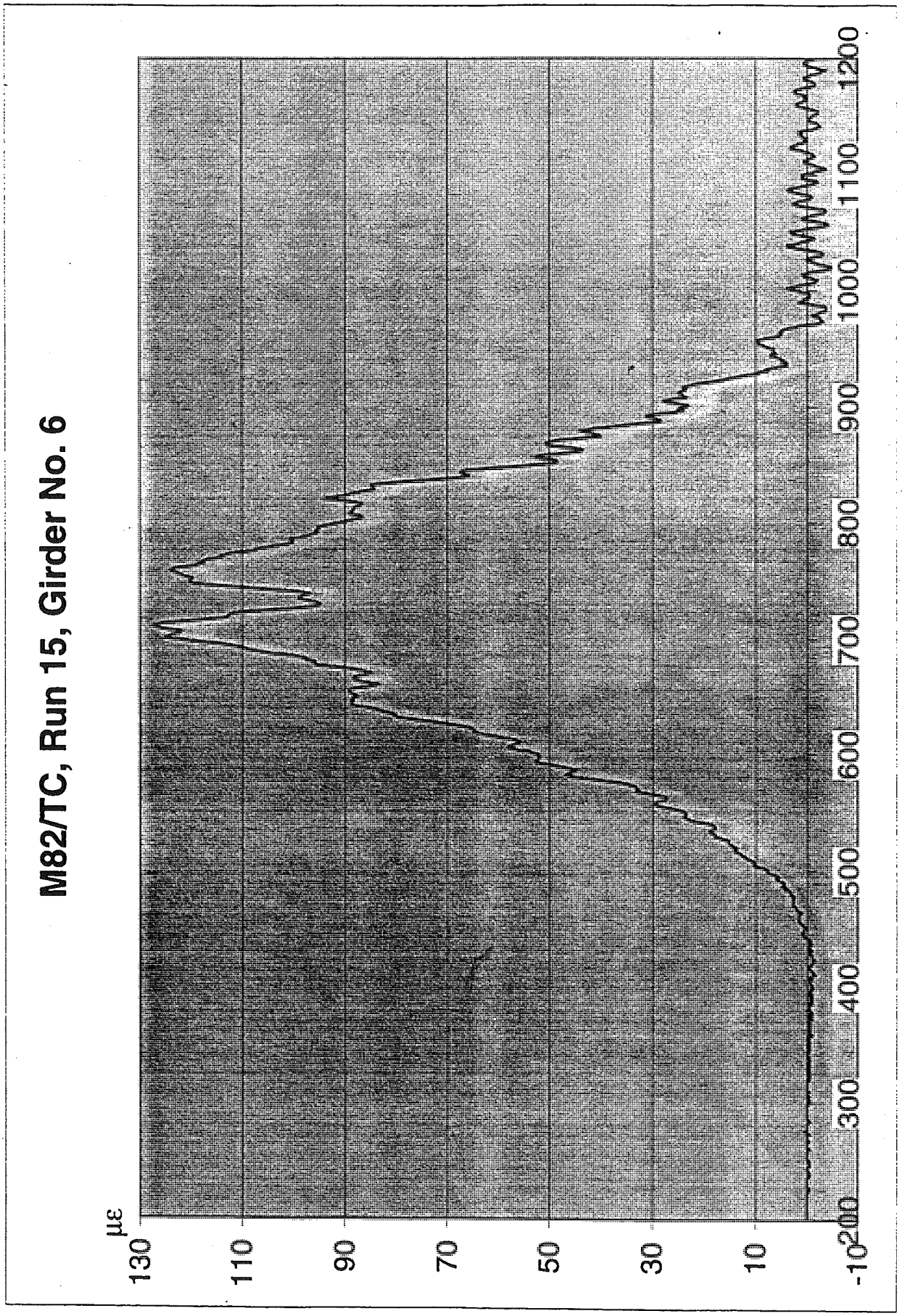
M82/TC, Run 15, Girder No. 6
με
130
110
90
70
50
30
10
-10
200
300
400
500
600
700
800
900
1000
1100
1200

Figure 12.15.

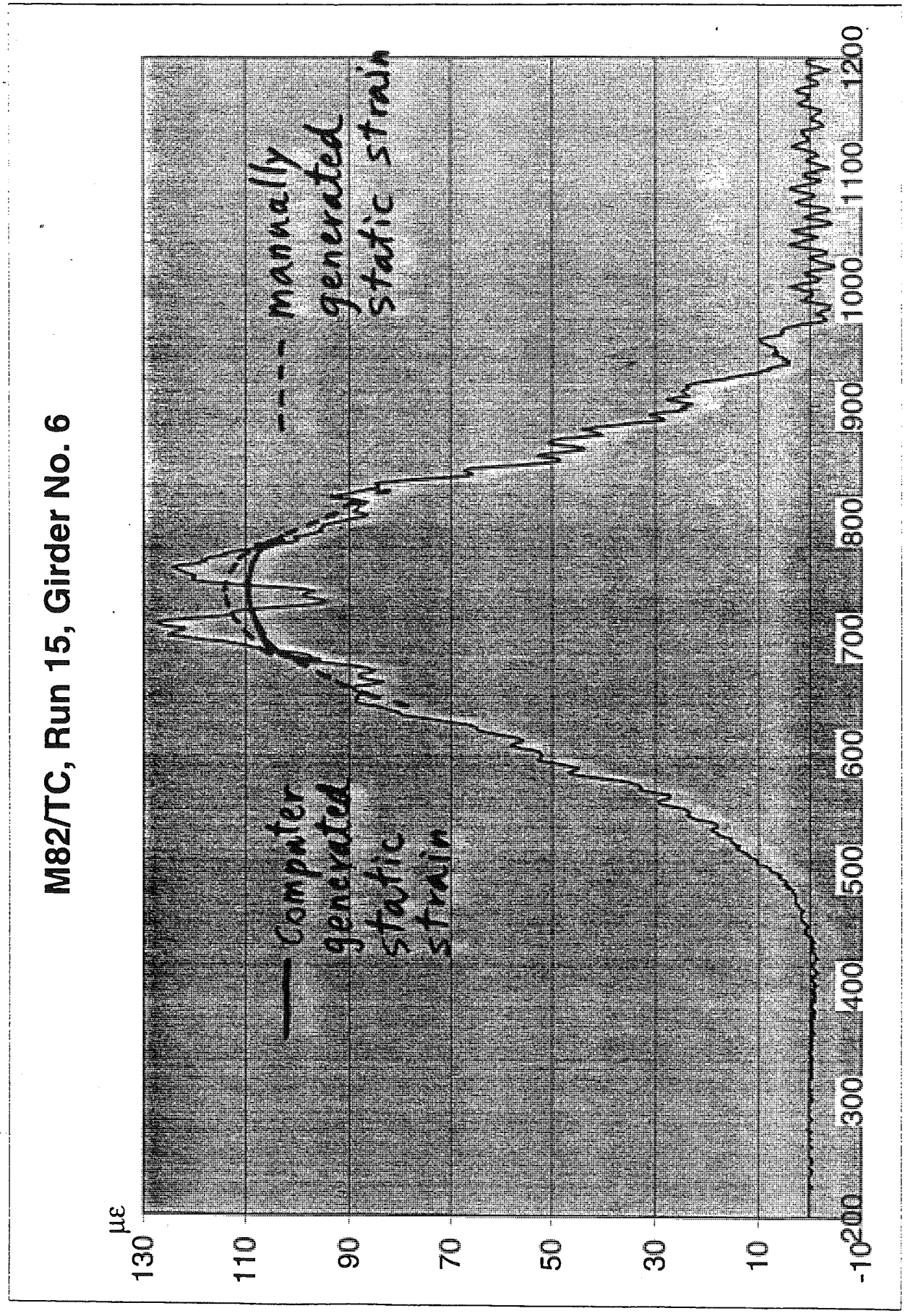
M82/TC, Run 15, Girder No. 6
— Computer generated static strain
---- manually generated static strain
με
130
110
90
70
50
30
10
-10
200
300
400
500
600
700
800
900
1000
1100
1200

Figure 12.16.

13. References

1. AASHTO Standard Specifications for Highway Bridges, American Association of State and Transportation Officials, Washington, DC, 1996.

2. AASHTO LRFD Bridge Design Specifications. American Association of State Highway and Transportation Officials, Washington, D.C., 1998.

3. AASHTO Guide Specifications for Distribution of Loads for Highway Bridges, American Association of State Highway and Transportation Officials, Washington, D.C., 1994.

4. Bakht, B., and Pinjarkar, S.G., "Dynamic Testing of Highway Bridges-A Review." Transportation Research Record 1223, Transportation Research Board, National Research Council, Washington, D.C., pp. 93-100, 1989.

5. Brockenbrough, R.L., "Distribution factors for curved I-girder bridges." Journal of Structural Engineering, ASCE, Vol. 112, No. 5, 1986.

6. Ghosn, M., Moses, F., and Gobieski, J., "Evaluation of Steel Bridges Using In-Service Testing." Transportation Research Record 1072, Transportation Research Board, National Research Council, Washington, D.C., pp. 71-78, 1986.

7. Hays, C.O., Sessions, L.M., and Berry, A.J. (1986), "Further studies on lateral load distribution using FEA." Transportation Research Record 1072, Transportation Research Board, National Research Council, Washington, 1986.

8. Hwang, E.S., and Nowak, A.S., "Simulation of Dynamic Load for Bridges." Journal of Structural Engineering, ASCE, Vol. 117, No.5, pp.1413-1434, July, 1991.

9. Imbsen, R.A., and Nutt, R.V., "Load Distribution Study on Highway Bridge using STRUDL FEA" Proceeding, Conference on Computing in Civil Engineering, ASCE, New York, 1978.

10. Lichtenstein, A. G., Manual for Bridge Rating Through Nondestructive Load Testing, NCHRP Report 12-28(13) A, 1998.

11. Mabsout, M.E., Tarhini, K.M., Frederick, G.R., and Tayar, C. "Finite-Element Analysis of Steel Girder Highway Bridges." Journal of Bridge Engineering. Vol. 2, No 3, August 1997.

12. Nassif, H.H. and Nowak, A.S., "Dynamic Load Spectra for Girder Bridges." Transportation Research Record 1476, Transportation Research Board, National Research Council, Washington, D.C., pp. 69-83, 1995

13. Nowak, A.S., Laman, J.A., and Nassif H., "Effect of Truck Loading on Bridges." Report UMCE 94-22. Department of Civil and Environmental Engineering, University of Michigan, Ann Arbor, 1994

14. Paultre, P., Chaallal, O., and Proulx, J., "Bridge Dynamics and Dynamic Amplification Factors-A Review of Analytical and Experimental Findings." Canadian Journal of Civil Engineering, Vol. 19, pp. 260-278, 1992.

15. Stallings, J.M., and Yoo, C.H., "Tests and Ratings of Short-Span Steel Bridges." Journal of Structural Engineering, ASCE, Vol. 119, No. 7, pp. 2150-2168, July, 1993.

16. Tarhini K.M and Frederick, G. R. 1992. "Wheel load distribution in I-girder highway bridges" Journal of Structural Engineering Vol 118, No 5, pp1285-1294.

17. Zokaie, T., Osterkamp, T.A., and Imbsen, R.A., Distribution of Wheel Loads on Highway Bridges, National Cooperative Highway Research Program Report 12-26, Transportation Research Board, Washington, D.C., 1991.